

INFORMATION TO USERS

This manuscript has been reproduced from the microfilm master. UMI films the text directly from the original or copy submitted. Thus, some thesis and dissertation copies are in typewriter face, while others may be from any type of computer printer.

The quality of this reproduction is dependent upon the quality of the copy submitted. Broken or indistinct print, colored or poor quality illustrations and photographs, print bleedthrough, substandard margins, and improper alignment can adversely affect reproduction.

In the unlikely event that the author did not send UMI a complete manuscript and there are missing pages, these will be noted. Also, if unauthorized copyright material had to be removed, a note will indicate the deletion.

Oversize materials (e.g., maps, drawings, charts) are reproduced by sectioning the original, beginning at the upper left-hand corner and continuing from left to right in equal sections with small overlaps. Each original is also photographed in one exposure and is included in reduced form at the back of the book.

Photographs included in the original manuscript have been reproduced xerographically in this copy. Higher quality 6" x 9" black and white photographic prints are available for any photographs or illustrations appearing in this copy for an additional charge. Contact UMI directly to order.

U·M·I

University Microfilms International
A Bell & Howell Information Company
300 North Zeeb Road, Ann Arbor, MI 48106-1346 USA
313/761-4700 800/521-0600

Order Number 9410175

**Climate, seasonal snow cover and permafrost temperatures in
Alaska north of the Brooks Range**

Zhang, Tingjun, Ph.D.

University of Alaska Fairbanks, 1993

Copyright ©1994 by Zhang, Tingjun. All rights reserved.

U·M·I
300 N. Zeeb Rd.
Ann Arbor, MI 48106

**CLIMATE, SEASONAL SNOW COVER AND PERMAFROST TEMPERATURES
IN ALASKA NORTH OF THE BROOKS RANGE**

**A
THESIS**

**Presented to the Faculty of the University of Alaska
in Partial Fulfillment of the Requirements
for the Degree of**

DOCTOR OF PHILOSOPHY

**By
Tingjun Zhang, B.S., M.S.**


Fairbanks, Alaska


DECEMBER 1993

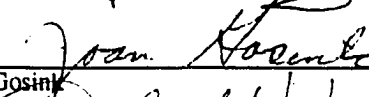
CLIMATE, SEASONAL SNOW COVER AND PERMAFROST TEMPERATURES
IN ALASKA NORTH OF THE BROOKS RANGE

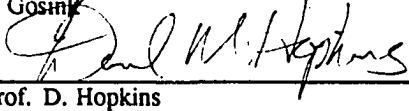
By
Tingjun Zhang


RECOMMENDED:

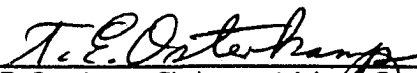

Prof. S. A. Bowling


Prof. D. Goering



Prof. J. Gosink

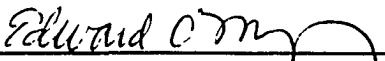

Dist. Prof. D. Hopkins


Prof. G. Weidler


Prof. T. E. Osterkamp, Chairman, Advisory Committee


Prof. R. Keith Crowder, Head, Dept. of Geology and Geophysics

APPROVED: 
Prof. P. B. Reichardt, Dean, College of Natural Sciences


Dr. Edward Murphy, Dean of the Graduate School

22 October 1993
Date

ABSTRACT

Climatological data, active layer and permafrost measurements, and modeling were used to investigate the response of permafrost temperatures to changes in climate in Alaska north of the Brooks Range. Mean annual air temperature (MAAT) from 1987 to 1991 within about 110 km from the Arctic Coast was $-12.4 \pm 0.3^{\circ}\text{C}$, while the mean annual permafrost surface temperature (MAPST) ranged from -9.0°C along the coast to -5.2°C inland. Air temperature changes alone can not explain the permafrost warming from the coast to inland. Measurements show that MAPST are about 3°C to 6°C warmer than MAAT in the region. The interaction of local microrelief and vegetation with snow appears to change the insulating effect of seasonal snow cover and may be the major factor which controls the permafrost temperature during the winter and thus the MAPST. Sensitivity analyses show that for the same MAAT conditions, changes in seasonal snow cover parameters can increase or decrease the MAPST about 7°C . Snowfall was greater during the cold years and less during the warm years and was poorly correlated between stations. These results suggest that the effects of changes in air temperatures on permafrost temperatures historically may also have been modified by changes in snow cover. A numerical model was used to investigate the effect of changes in initial permafrost temperature conditions, MAAT, seasonal snow cover and thermal properties of soils on the permafrost temperatures. Permafrost may have started warming about the same time as the atmosphere did in the late 1800's, and the long term mean surface temperature of the permafrost may have been established prior to this time. Variations in the penetration depth of the warming signal may be related to differences in thermal properties of permafrost. Variations in the magnitude of the permafrost surface warming may be due to the effect of local factors such as soil type, vegetation, microrelief, soil moisture, and seasonal snow cover. The effect of the

interaction of vegetation and snow cover may amplify the signal of temperature change in the permafrost.

TABLE OF CONTENTS

	Page
Abstract	iii
Table of Contents	v
List of Figures	ix
List of Tables	xix
Acknowledgments	xxii
1. Introduction	1
2. Climate and Climatic Change	3
2.1 Introduction	3
2.2 Data Sources and Methods	4
2.3 Surface Climate in Alaska North of the Brooks Range	7
2.3.1 Temperatures	7
2.3.2 Precipitation	13
2.4 Climatic Change	16
2.5 Relation to Permafrost Temperatures	26
2.6 Summary	33
3. Physical and Thermal Properties of the Active Layer and Permafrost	38
3.1 Introduction	38
3.2 Methods	40
3.3 Results and Discussions	43
3.3.1 Physical Properties	44
3.3.2 Apparent Thermal Diffusivity	44
3.4 Summary	58

4. Seasonal Snow Cover and its Influence on the Ground Thermal Regime	62
4.1 Introduction	62
4.2 Data Source and Methods	64
4.3 Seasonal Snow Cover	65
4.3.1 Timing and Duration	65
4.3.2 Evolution of Seasonal Snow Cover	69
4.4 Effect on Ground Thermal Regime	76
4.4.1 Amplitude of Daily Ground Surface Temperature	76
4.4.2 Ground Surface Temperature	78
4.4.3 Permafrost Temperature	81
4.5 Summary	85
5. Modeling the Influence of Snow Cover on the Ground Thermal Regime	90
5.1 Introduction	90
5.2 Model Assumptions	91
5.3 Results	96
5.4 Sensitivity Analysis	100
5.4.1 Timing and Duration	108
5.4.2 Thickness	112
5.4.3 Depth Hoar Layer	112
5.4.4 Accumulation and Melting Processes	118
5.4.5 Amplitude of Mean Annual Air Temperature	120
5.5 Discussion	125
5.6 Summary	132

6. Response of Permafrost Temperature to Changes in Climate	136
6.1 Introduction	136
6.2 Model Assumptions and Data	137
6.3 Modeling Results	142
6.3.1 Effects of Initial Conditions and Air Temperature	142
6.3.2 Effect of Seasonal Snow Cover	153
6.3.3 Effect of Thermal Properties	164
6.4 Application of the Modeling Results to Permafrost Temperature Data	166
6.5 Relation to Climatic Change	174
6.6 Summary	176
7. Summary	180
7.1 Climate and Climatic Change	180
7.2 Physical and Thermal Properties of Soils	182
7.3 Seasonal Snow Cover	183
7.4 Influence of Seasonal Snow Cover on Ground Thermal Regime	185
7.5 Relation of Current Climatic Conditions with Permafrost Temperatures	186
7.6 Calibration of the Numerical Model	187
7.7 Sensitivity Analysis of Ground Thermal Regime to Changes in Snow Cover Parameters	188
7.8 Response of Permafrost Temperature to Changes in Climate	190
Appendix A: Derivation of a Numerical Expression for Uneven Space and Time Intervals	194

Appendix B: Considerations in Determining Thermal Diffusivity from Temperature Time Series Using Numerical Methods	197
B.1 INTRODUCTION	198
B.2 REVIEW OF THEORY	199
B.2.1 Model I	201
B.2.2 Model II	203
B.3 RESULTS AND DISCUSSION	206
B.3.1 Daily Surface Temperature Variations	206
B.3.2 Daily and Seasonal Surface Temperature Variations	210
B.3.3 Climatic Fluctuations and Ground Surface Temperature Variations	211
B.4 APPLICATIONS	213
B.5 SUMMARY	216
B.6 Acknowledgements	220
References	221

LIST OF FIGURES

		Page
Fig. 2.1	Variations of the mean annual air temperature (A); annual amplitude of air temperature (B) with distance from the ocean for the period from 1987 through 1991 for the sites listed in Table 2.1 except Lonely and sites south of Sagwon.	8
Fig. 2.2	Variation of mean monthly air temperature for the period from 1977 through 1988 at Barter Island and Umiat.	10
Fig. 2.3	Seasonal variations of the spatial temperature gradients from the coast, inland for the period from 1987 through 1991 for the sites listed in Table 2.1 except Lonely and sites south of Sagwon.	11
Fig. 2.4	Variations of thaw (A) and freeze (B) index with distance from the coast, inland for the period from 1987 through 1991 for the sites listed in Table 2.1 except Lonely and sites south of Sagwon.	12
Fig. 2.5	Correlation of mean annual air temperatures for the period from 1949 through 1988 between Barrow and Barter Island.	14
Fig. 2.6	Annual precipitation and snowfall (water equivalent) measured by a Wyoming Gauge for the period from 1977 through 1991 at Prudhoe Bay, Sagwon and Toolik River (<i>Soil Conservation Service, 1991</i>)	18
Fig. 2.7	Mean annual air temperature departures from the mean (dashed lines) for (A) Barrow, (B) North American Arctic (<i>Hansen and Lebedeff, 1987</i>), and (C) Arctic as a whole (<i>Hansen and Lebedeff, 1987</i>). Data were smoothed (solid lines) by a low-pass filter with a cut-off frequency of 0.15 year^{-1} .	19
Fig. 2.8	Power spectra for air temperature time series at Barrow for the period from 1921 through 1991 with the length of the prediction error filter (LPEF) equals 23, 35, 47, and 56, corresponding to 33%, 50%, 66% and 80% of the data length of 71 years.	20
Fig. 2.9	Variation of mean annual air temperature, freeze and thaw indices, precipitation and snowfall for the period from 1921 through 1991 at Barrow (dashed lines). These data were smoothed by a low-pass filter with a cut-off frequency of 0.15 year^{-1} (dark solid lines).	21

Fig. 2.10	Power spectra for the freeze index time series for the period from 1921 through 1991 at Barrow with the length of the prediction error filter equals 23, 35, 47, and 56, corresponding to 33%, 50%, 66% and 80% of the data length of 71 years.	22
Fig. 2.11	Power spectra for the thaw index time series for the period from 1921 through 1991 at Barrow with the length of the prediction error filter equals 23, 35, 47, and 56, corresponding to 33%, 50%, 66% and 80% of the data length of 71 years.	23
Fig. 2.12	Departures of mean annual air temperature (A), freeze index (solid line) and thaw index (dashed line) (B) from their long-term means for the period from 1921 through 1991 at Barrow	25
Fig. 2.13	Power spectra for precipitation time series for the period from 1921 through 1991 at Barrow with the length of the prediction error filter equals 23, 35, 47, and 56, corresponding to 33%, 50%, 66% and 80% of the data length of 71 years.	27
Fig. 2.14	Power spectra for snowfall time series for the period from 1921 through 1991 at Barrow with the length of the prediction error filter equals 23, 35, 47, and 56, corresponding to 33%, 50%, 66% and 80% of the data length of 71 years.	28
Fig. 2.15	Deviations of the mean annual air temperature and snowfall from their long-term means at Barrow and Barter Island, smoothed by a low-pass filter with a cut-off frequency of 0.091^{-1} .	29
Fig. 2.16	Mean annual air temperatures (A), mean annual ground surface and permafrost surface temperatures (B) and permafrost thickness (C) along a transect from Prudhoe Bay to Happy Valley. The sites include West Dock, ARCO airfield, Prudhoe Bay, Deadhorse, Franklin Bluffs, Umiat and Happy Valley.	31
Fig. 3.1	Variation of soil temperature measured at depth of 0.022 m, 0.072 m and 0.123 m and apparent thermal diffusivity estimated by (3.1) with $\Delta z_1 = 0.05$ m, $\Delta z_2 = 0.051$ m and $\Delta t = 10$ min. on July 8, 1988 at West Dock, Prudhoe Bay.	47
Fig. 3.2	Variation of soil temperatures at depths of 0.422 m, 0.621 m and 0.722 m with $\Delta t = 1$ day and apparent thermal diffusivity estimated using (3.1) at depth of 0.621 m with $\Delta z_1 = 0.199$ m, $\Delta z_2 = 0.101$ m and $\Delta t = 1$ day for the period from October 5, 1986 through October 4, 1987 at West Dock, Prudhoe Bay. Data used in the calculation were selected as described in the text.	49

- Fig. 3.3 Apparent thermal diffusivity ($m^2 yr^{-1}$) estimated using (3.1) at depth of 0.621 m at selected times for the period from October 5, 1986 through October 4, 1987 at West Dock, Prudhoe Bay. 50
- Fig. 3.4 Apparent thermal diffusivity ($m^2 yr^{-1}$) estimated using (3.1) from soil temperature time series for the period from October 5, 1986 through June 23, 1991 at depth of 0.621 m with $\Delta z_1 = 0.199$ m, $\Delta z_2 = 0.101$ m and $\Delta t = 1$ day at West Dock, Prudhoe Bay. Data used in the calculation were selected as described in the text. 51
- Fig. 3.5 Apparent thermal diffusivity ($m^2 yr^{-1}$) estimated using (3.1) from soil temperature time series for the period from October 10, 1986 through June 23, 1991 at a depth of 0.620 m with $\Delta z_1 = 0.200$ m, $\Delta z_2 = 0.099$ m and $\Delta t = 1$ day at Deadhorse, Prudhoe Bay. Data used in the calculation were selected as described in the text. 52
- Fig. 3.6 Apparent thermal diffusivity estimated using (3.1) from soil temperature time series for the period from November 29, 1986 through June 23, 1991 at a depth of 0.56 m with $\Delta z_1 = 0.098$ m, $\Delta z_2 = 0.201$ m and $\Delta t = 1$ day at Franklin Bluffs site. Data used in the calculation were selected as described in the text. 53
- Fig. 3.7 Soil temperatures (a) and apparent thermal diffusivity (b) estimated using (3.4) from soil temperature profiles with $\Delta z = 1$ m and $\Delta t = 68$ days at depths between 3 and 30 m at West Dock, Prudhoe Bay. 56
- Fig. 3.8 (a) Temperature variation of permafrost below 20 m since 1983 at West Dock, Prudhoe Bay, (b) Apparent thermal diffusivity of permafrost below 20 m estimated using (3.3) from soil temperature profiles with Δz ranging from 3 m to 6 m and Δt ranging from 0.8 years to 1.1 years. Dates of temperature profiles, A — Jun. 17, 1983; B — Aug. 23, 1983; C — Sep. 13, 1984; D — Jul. 1, 1985; E — Aug. 22, 1986; F — Jun. 25, 1987. 57
- Fig. 4.1 First and last day of snow on the ground surface for the period from 1953 through 1991 at Barrow, Alaska. 67
- Fig. 4.2 First and last day of snow on the ground surface for the period from 1957 through 1988 at Barter Island, Alaska. 68
- Fig. 4.3 Average monthly and cumulative snowfall for the period of record from 1921 through 1991 at Barrow, Alaska. 70

Fig. 4.4	Monthly and cumulative snowfall (A) and snow on ground, mean monthly air temperature and approximate snow build-up processes (B) during 1953-1954 at Barrow, Alaska.	72
Fig. 4.5	Approximate snow accumulation and melting processes at Barrow, Alaska.	75
Fig. 4.6	Mean daily air and ground surface temperature (A), the difference between mean daily ground surface and air temperature (B), and variation of daily amplitude of mean ground surface and air temperature (C) from November of 1986 to October of 1987 at Franklin Bluffs in Alaska north of the Brooks Range.	77
Fig. 4.7	The difference between mean monthly ground surface temperatures and air temperatures for the period from 1986 through 1991 at West Dock, Deadhorse and Franklin Bluffs.	79
Fig. 4.8	Difference between measured mean monthly permafrost surface temperatures and air temperatures for the period from 1986 through 1991 at West Dock, Deadhorse and Franklin Bluffs.	82
Fig. 4.9	Mean annual air temperatures and annual maximum thickness of seasonal snow cover at Prudhoe Bay (A) and permafrost temperatures at depths 20 m and 30 m at West Dock (B).	84
Fig. 5.1	Relation between measured mean daily air and ground surface temperatures when snow was not present on the ground for the period from 1986 through 1991 at West Dock, Prudhoe Bay.	93
Fig. 5.2	Measured mean daily air temperature at West Dock (A), measured seasonal snow cover at Deadhorse Airport (B), measured mean daily ground surface temperature (solid line) and calculated values (dashed line) (C) for the period from October of 1986 through July of 1990 at West Dock, Prudhoe Bay. The model was run with the upper boundary set at the ground surface when no snow presented and at snow surface when snow presented.	97
Fig. 5.3	Measured (solid line) and calculated daily active layer temperatures at a depth of 0.12 m below the ground surface with snow cover (i.e., using T_a as the appropriate surface boundary condition) (Case I, dashed line) and without snow cover (using the measured T_g as the surface boundary condition) (Case II, dotted line) for the period from October 5, 1986 to June 23, 1990 at West Dock, Prudhoe Bay	98

Fig. 5.4	Measured (solid line) and calculated daily soil temperatures at a depth of 0.72 m with snow cover (Case I, dashed line) and without snow cover (Case II, dotted line) for the period from October 5, 1986 to June 23, 1990 at West Dock, Prudhoe Bay	99
Fig. 5.5	Measured (square) and calculated (circle) permafrost temperatures with depth on July 13, 1988 at West Dock, Prudhoe Bay, Alaska.	101
Fig. 5.6	Measured (square) and calculated (circle) permafrost temperatures with depth on July 13, 1989 at West Dock, Prudhoe Bay, Alaska.	102
Fig. 5.7	Measured (square) and calculated (circle) permafrost temperatures with depth on July 13, 1990 at West Dock, Prudhoe Bay, Alaska.	103
Fig. 5.8	Computed temperature variations with depth ranging from 0.521 m to 10 m for the period from October 5, 1986 to July 13, 1990 at West Dock, Prudhoe Bay, Alaska.	104
Fig. 5.9	Computed temperature variations with depth ranging from 12 m to 20 m for the period from October 5, 1986 to July 13, 1990 at West Dock, Prudhoe Bay, Alaska.	105
Fig. 5.10	Computed temperature variations with depth varying from 15 m to 50 m for the period from October 5, 1986 to July 13, 1990 at West Dock, Prudhoe Bay, Alaska.	106
Fig. 5.11	Influence of the timing and duration of seasonal snow cover on the ground surface temperature (A) and permafrost temperature (1.0 m below the ground surface) (B) along the Alaskan Arctic Coast. Dashed lines stand for case 1, solid lines for case 2 and dotted lines for case 3 corresponding to the longest, average, and shortest duration, respectively.	109
Fig. 5.12	Influence of the timing and duration of seasonal snow cover on ground temperature along the Alaskan Arctic Coast, dashed line stands for case 1, solid line for case 2, and dotted line for case 3 corresponding to the longest, average, and shortest duration, respectively.	110
Fig. 5.13	Influence of the maximum thickness of the seasonal snow cover on the ground surface temperature (A) and temperature at 1.0 m below the ground surface (B) along the Alaskan Arctic Coast. Dashed lines stand for case 4 ($H_{max} = 15 \text{ cm}$), solid lines for case 6 ($H_{max} = 35 \text{ cm}$), and dotted lines for case 8 ($H_{max} = 50 \text{ cm}$)	113

- Fig. 5.14 Influence of the maximum thickness of the seasonal snow cover on the ground temperature along the Alaskan Arctic Coast. Dotted line for case 4 ($H_{max} = 15 \text{ cm}$), chain-dotted line for case 5 ($H_{max} = 25 \text{ cm}$), solid line for case 6 ($H_{max} = 35 \text{ cm}$), dashed line for case 7 ($H_{max} = 45 \text{ cm}$) and chain-dashed line for case 8 ($H_{max} = 50 \text{ cm}$). 114
- Fig. 5.15 Influence of the depth hoar layer fraction of the total thickness of the seasonal snow cover on temperature at the ground surface (A) and at depth of 1.0 m below the ground surface along the Alaskan Arctic Coast. Dashed lines stand for case 9 ($\phi = 0.0$), solid lines for case 11 ($\phi = 0.20$) and dotted line for case 13 ($\phi = 0.50$) 116
- Fig. 5.16 Influence of the depth hoar layer fraction on temperatures at the ground surface (solid line) and at a depth of 1.0 m below the ground surface (dashed line) along the Alaskan Arctic Coast. 117
- Fig. 5.17 Influence of the accumulation and melting rates of seasonal snow cover on temperatures at the ground surface (A) and at depth of 1.0 m below the ground surface (B) along the Alaskan Arctic Coast. Dashed lines for case 14, solid lines for case 17, dotted lines for case 15, and chain-dashed line for case 16. 119
- Fig. 5.18 Variation of the upper boundary conditions with annual amplitude. Dashed line for $A_o = 16^\circ\text{C}$, solid line for $A_o = 18^\circ\text{C}$, chain-dashed line for $A_o = 20^\circ\text{C}$, and dotted line for $A_o = 22^\circ\text{C}$. 121
- Fig. 5.19 Influence of the annual amplitude of the mean air temperature on the temperatures at the ground surface (A) and at depth of 1.0 m below the ground surface (B). Dashed line for case 18 ($A_o = 16^\circ\text{C}$), solid line for case 19 ($A_o = 18^\circ\text{C}$), chain-dashed line for case 20 ($A_o = 20^\circ\text{C}$), and dotted line for case 21 ($A_o = 22^\circ\text{C}$). 122
- Fig. 5.20 Influence of the annual amplitude of mean annual temperature on the ground thermal temperatures. Dotted line for case 18 ($A_o = 16^\circ\text{C}$), chain-dotted line for ($A_o = 18^\circ\text{C}$), dashed line for case 20 ($A_o = 20^\circ\text{C}$), and solid line for case 21 ($A_o = 22^\circ\text{C}$). 123
- Fig. 5.21 Influence of seasonal snow cover on temperatures at the ground surface (A) and at depth of 1.0 m below the ground surface (B) for two extreme cases as summarized in Table 5.9. Dashed lines stand for case 22 and solid lines for case 23. 126

- Fig. 5.22 Influence of seasonal snow cover on ground temperatures for two extreme cases as summarized in Table 5.9. Dashed line stand for case 22 and solid line for case 23. 127
- Fig. 5.23 Influence of air temperature and seasonal snow cover on temperatures at the ground surface (A) and at depth of 1.0 m below the ground surface (B) along the Arctic Coast (solid line) and inland (dashed line) in Alaska north of the Brooks Range. 129
- Fig. 5.24 Influence of air temperature and seasonal snow cover on ground temperatures along the Arctic coast (solid line) and inland (dashed line) in Alaska north of the Brooks Range. 130
- Fig. 6.1 MAAT from the U. S. Weather Bureau at Barrow (A) and at Barter Island (B). The data in (C) represent the temperature variations obtained by Hansen and Lebedeff (1987) for the North American quadrant of the Arctic. The record average (thin solid lines in A and B) and selected regression lines (thin solid and dashed lines in C) as used by Lachenbruch et al. (1988) are also shown. 139
- Fig. 6.2 Relationship between total annual snowfall and maximum thickness of snow on the ground for the period from 1947 through 1991 at Barrow 141
- Fig. 6.3 Calculated permafrost temperature change in 1985 after removal of the initial linear equilibrium temperature profile, for Prudhoe Bay conditions starting in 1880, using BC1 for the upper boundary condition at the permafrost surface. For case 1 (solid line), the initial equilibrium surface temperature was set at -12°C which was changed in increments of -1°C for case 2 (chain-dotted line), case 3 (dashed line) and case 4 (chain-dashed line). 144
- Fig. 6.4 Assumed initial permafrost temperatures in 1880 after removal of the equilibrium temperatures with depth. The initial permafrost temperatures were generated by equations (2) and (6) of Lachenbruch et al. (1988) with $n = 2$, $t^* = 35$ years (prior to 1880), for case 5, $T_o = 0.0^{\circ}\text{C}$ which was changed in increments of -1°C for case 6, case 7, case 8, and case 9 (here T_o represents D in Lachenbruch's paper). 146
- Fig. 6.5 Calculated permafrost temperature changes with time for the period from 1880 through 1991 at site SB3 near Barrow, using BC3 for the upper boundary conditions at the ground surface. The initial MST was chosen as -12.2°C with $T_o = 0.0^{\circ}\text{C}$ for case 5. 147

- Fig. 6.6 Calculated permafrost temperature changes from the assumed initial conditions in 1923 for the conditions at SB3 near Barrow. BC3 was used for the upper boundary conditions at the ground surface. The long term MST was chosen as -12.2°C with different choice of T_0 as shown. 148
- Fig. 6.7 Calculated permafrost temperature changes from the assumed initial conditions in 1949 for the conditions at SB3 near Barrow. BC3 was used for the upper boundary conditions at the ground surface. The long term MST was chosen as -12.2°C with different choice of T_0 as shown. 149
- Fig. 6.8 Calculated permafrost temperature changes, from the assumed initial conditions, in 1973 for the conditions at SB3 near Barrow. BC3 was used for the upper boundary conditions at the ground surface. The long term MST was chosen as -12.2°C with different choice of T_0 as shown. 150
- Fig. 6.9 Calculated permafrost temperature changes, from the assumed initial conditions, in 1991 for the conditions at SB3 near Barrow. BC3 was used for the upper boundary conditions at the ground surface. The long term MST was chosen as -12.2°C with different choice of T_0 as shown. 151
- Fig. 6.10 Calculated permafrost temperature changes in 1985, for Prudhoe Bay conditions starting in 1880, using BC1 (case 10 dotted line and case 12 dashed line), the single regression line in Figure 6.1C (case 11 chain-dotted line), and the two regression lines in Figure 6.1C (case 13 chain-dashed line), for the upper boundary condition at the permafrost surface. 154
- Fig. 6.11 Calculated permafrost temperature changes at site SB3 near Barrow using BC2 as the upper boundary condition at the ground or snow surface as approximate. The dotted and dashed lines represent the results of case 14 (without snow cover). The chain-dotted and chain-dashed lines represent the results of case 15 (with snow cover). The dark dots are the approximate permafrost temperature changes at site SB3 in 1949 (Lachenbruch et al., 1962). 155

- Fig. 6.12 Calculated permafrost temperature changes at site E near Prudhoe Bay using BC2 as the upper boundary condition at the ground or snow surface as appropriate. The dot and chain-dotted lines are for cases 14 and 16 with no snow cover. The dash and chain-dashed lines for 15 and 17 with snow cover. The dots are the approximate permafrost temperature changes at site E in 1973 (Lachenbruch et al., 1988). 157
- Fig. 6.13 Mean annual air temperature (dashed line) and calculated (case 14) ground surface temperature (dotted line) history for the period from 1923 through 1991 at site SB3 near Barrow. These data were smoothed by a low-pass filter with a cut-off frequency of 0.091 year^{-1} . 159
- Fig. 6.14 Calculated permafrost temperature changes since 1880 for the indicated times at site E near Prudhoe Bay. The maximum thickness of seasonal snow cover was assumed to be 12.7 cm (before 1923) (case 18) and BC3 was used as the upper boundary conditions. The upper boundary was set at the ground or snow surface as appropriate. 162
- Fig. 6.15 Calculated permafrost temperature changes since 1880 for the indicated times at site SB3 near Barrow. The maximum thickness of seasonal snow cover was assumed to be 18.0 cm (before 1923) (case 19) and BC3 was used as the upper boundary condition. The upper boundary was set at the ground or snow surface as appropriate. 163
- Fig. 6.16 Calculated permafrost temperature changes with seasonal snow cover for the period from 1923 through 1991 at site SB3 near Barrow (case 20). The initial long term MST was chosen as -9.2°C , about 3°C warmer than the measured values. All the other conditions are the same as case 17. 165
- Fig. 6.17 Calculated permafrost temperature changes with no seasonal snow cover in 1923 at site SB3 near Barrow. The dashed line represents case 21 with $D=15 \text{ m}^2/\text{yr}$, the chain-dotted line case 22 with $D=25 \text{ m}^2/\text{yr}$, the solid line case 23 with $D = 35 \text{ m}^2/\text{yr}$, the chain-dashed line case 24 with $D = 45 \text{ m}^2/\text{yr}$ and the dotted line case 25 with $D = 55 \text{ m}^2/\text{yr}$. 167

- Fig. 6.18 Calculated permafrost temperature changes with no seasonal snow cover in 1949 at site SB3 near Barrow. The dashed line represents case 21 with $D=15 \text{ m}^2/\text{yr}$, the chain-dotted line case 22 with $D=25 \text{ m}^2/\text{yr}$, the solid line case 23 with $D = 35 \text{ m}^2/\text{yr}$, the chain-dashed line case 24 with $D = 45 \text{ m}^2/\text{yr}$ and the dotted line case 25 with $D = 55 \text{ m}^2/\text{yr}$. 168
- Fig. 6.19 Calculated permafrost temperature changes with no seasonal snow cover in 1973 at site SB3 near Barrow. The dashed line represents case 21 with $D=15 \text{ m}^2/\text{yr}$, the chain-dotted line case 22 with $D=25 \text{ m}^2/\text{yr}$, the solid line case 23 with $D = 35 \text{ m}^2/\text{yr}$, the chain-dashed line case 24 with $D = 45 \text{ m}^2/\text{yr}$ and the dotted line case 25 with $D = 55 \text{ m}^2/\text{yr}$. 169
- Fig. 6.20 Calculated permafrost temperature changes with no seasonal snow cover in 1991 at site SB3 near Barrow. The dashed line represents case 21 with $D=15 \text{ m}^2/\text{yr}$, the chain-dotted line case 22 with $D=25 \text{ m}^2/\text{yr}$, the solid line case 23 with $D = 35 \text{ m}^2/\text{yr}$, the chain-dashed line case 24 with $D = 45 \text{ m}^2/\text{yr}$ and the dotted line case 25 with $D = 55 \text{ m}^2/\text{yr}$. 170
- Fig. B.1 (A) Synthetic temperature time series at three depths for a daily surface temperature wave with a surface amplitude of 4°C , (B) $\Delta_{xx}T$ and $\Delta_t T$ at the central depth of 0.3 m, and (C) a comparison of the calculated values of the thermal diffusivity at the 0.3 m depth with the input value of $25 \text{ m}^2 \text{ yr}^{-1}$. For these calculations, $\Delta x = 0.1 \text{ m}$, $\Delta t = 10 \text{ min}$. 207
- Fig. B.2 Variations of the calculated thermal diffusivity at a depth of 0.3 m for different values of Δx and Δt (A) $\Delta x = 0.01 \text{ m}$ and $\Delta t = 60 \text{ min}$, (B) $\Delta x = 0.10 \text{ m}$ and $\Delta t = 1 \text{ min}$, and (C) $\Delta x = 0.01 \text{ m}$ and $\Delta t = 1 \text{ min}$. 209
- Fig. B.3 (A) Five synthetic temperature profiles for depths below the daily zero temperature variations and, (B), a comparison of the calculated values between models I and II. For these calculations, $A_d = 4^\circ \text{C}$, $\Delta x = 1 \text{ m}$, and $\Delta t = 5 \text{ days}$. 212
- Fig. B.4 (A) Five synthetic temperature profiles, calculated after ten years, for a warming trend of ground surface temperature with a superimposed annual surface temperature wave and, (B) a comparison of the calculated thermal diffusivities from the temperature profiles. For the temperature calculations, $A_y = 16^\circ \text{C}$, $\Delta x = 1 \text{ m}$, and $\Delta t = 1 \text{ year}$, and for the thermal diffusivity calculations, $\Delta x = 4 \text{ m}$ and $\Delta t = 1 \text{ year}$. 214

LIST OF TABLES

		Page
Table 2.1	Summaries for stations and sites in Alaska north of the Brooks Range	5
Table 2.2	Statistical parameters for correlation of mean monthly air temperatures and mean annual air temperatures between Barrow and Barter Island. a and b are correlation constants, r is the correlation coefficient and σ is the standard deviation.	15
Table 2.3	Precipitation and snowfall (water equivalent) at sites north of the Brooks Range	16
Table 2.4	Deviations of Barrow mean monthly air temperatures and the mean annual air temperatures from their means	24
Table 2.5	Values for the mean annual air temperature (MAAT), mean annual ground surface temperature (MAGST) and mean annual permafrost surface temperature (MAPST) for the period from 1987 through 1991 at sites of West Dock, Deadhorse and Franklin Bluffs, from 1985 through 1989 at Toolik Lake and from 1976 through 1979 at Happy Valley and Galbraith. Z is the active layer thickness.	30
Table 2.6	Climatic and permafrost conditions for the sites and periods listed in Table 2.1 in Alaska north of the Brooks Range.	34
Table 3.1	Physical and thermal properties of soil samples taken in June, 1990 in Alaska north of the Brooks Range	45
Table 4.1	Timing and duration of seasonal snow cover at the selected stations and sites P_1 , P_{max} and P_2 represent the average dates and their deviations of first, maximum thickness and last day of snow on ground, respectively, over the period specified for each station or site.	66
Table 4.2	Wind speed during 1953-1954 and 1967-1968 at Barrow	73
Table 4.3	Temperature difference between mean ground surface temperature (MGST) and mean air temperature (MAT)	81
Table 4.4	Measured thermal offset values in near-surface mean annual ground temperatures.	85
Table 5.1	Summary of physical and thermal properties of soils at West Dock	94

Table 5.2	Thermal properties of snow used for modeling	96
Table 5.3	Range of snow cover and air temperature parameters. The coast area includes Barrow, West Dock, Prudhoe Bay, Deadhorse and Barter Island, the Inland area includes Franklin Bluffs, Umiat and Toolik Lake.	107
Table 5.4	Effect of maximum snow thickness (H_{max}) on the ground thermal regime, MAGST represents mean annual ground surface temperature, T_g stands for mean annual temperature at the depth of 1.0 m, and T_{off} for the thermal offset value.	115
Table 5.5	Effect of the depth hoar on the ground thermal regime, ϕ stands for the depth fraction of the depth hoar layer.	115
Table 5.6	Effect of build-up of snow cover on the ground thermal regime	118
Table 5.7	Effect of the amplitude of MAAT (A_o) on the ground thermal regime, L_{ts} stands for the length of thaw season and Z for the active layer thickness. The calculation was conducted under the average snow conditions along the coast.	120
Table 5.8	Summary of calculated results for all cases. ΔT represents the difference of mean annual ground surface temperature from the standard calculations, T_{off} is the thermal offset value.	128
Table 5.9	Summary of input values for two extreme cases	131
Table 6.1	Summary of the calculation conditions, PS represents the permafrost surface, GS the ground surface and SS the snow surface.	143
Table 6.2	Summary of physical and thermal properties of soils at Prudhoe Bay, ρ_b stands for dry bulk density; W for soil water content by mass; D_{th} and D_{fr} for the thawed and frozen soil thermal diffusivities, respectively.	145
Table 6.3	Summary of the physical and thermal properties of soils at Barrow, ρ_b stands for dry bulk density; W soil water content by mass; D_{th} and D_{fr} for the thawed and frozen soil thermal diffusivities, respectively.	145
Table 6.4	Sporadic snowfall data from 1902 through 1923 at Barrow	164
Table 7.1	Climate and Permafrost Conditions in Alaska North of the Brooks Range	181

Table 7.2	Apparent Thermal Diffusivity near Prudhoe Bay	183
Table 7.3	Sensitivity of surface temperature to snow cover parameters	189
Table B.4	Effects of errors, δT , in temperature measurements on $\delta(\Delta_{xx}T)$ and $\delta(\Delta'_{xx}T)$ ($^{\circ}C$)	204
Table B.5	Measurement errors in calculated values of D using models I and II at a depth of 0.3 m for a daily temperature wave with a surface amplitude of $4^{\circ}C$ with $\Delta x = 0.1$ m and $\Delta t = 10$ min.	205
Table B.6	Depths for a daily temperature wave (X_d) and an annual wave (X_y) where the amplitude has been reduced to A_x .	216

ACKNOWLEDGMENTS

It was nothing less than a thrill to finally get this thesis done and send it to the advisory committee. As you may expect, a Ph.D. thesis like this one takes a great deal of work. My thesis is an accumulation of the last five years of research and study in the Geophysical Institute, University of Alaska, Fairbanks.

I would like to take a moment to thank everyone who helped make my Ph.D project possible — I could not have done it without them.

The person most responsible for the inception and the guidance I received throughout my graduate study in the Geophysical Institute is Professor T. E. Osterkamp, my thesis adviser and chairman of my advisory committee. He has not only provided the financial and academic support for my prolonged study, but has also taught me a lot about the way of doing research. He has spent a great deal of time editing and vastly improving my writing since I came here as an international student. His invaluable help is deeply appreciated.

I would like to take this chance to thank the other committee members: Prof. S. A. Bowling, Prof. D. Goering, Prof. J. Gosink, Dist. Prof. D. Hopkins and Prof. G. Wendler for their generous help and encouragement in carry through my Ph.D. project and for the time and effort they put into this thesis. Prof. W. Weeks kindly served as the member of my thesis defense committee on behalf of Prof. J. Gosink. Prof. J. L. Hulseley acted as outside examiner. I would also like to record my gratitude to them. I would like to express my special thanks to Dist. Prof. D. Hopkins for his support and caring for my studies and my family during the last several years.

Thanks are due also to Prof. C. Benson and Dr. M. Sturm for their help and discussions on snow cover in this thesis. I deeply appreciate the help of Dr. L. Goodrich in discussions on the use of his original numerical model and his encouragement of this study. I wish to thank Dr. A. H. Lachenbruch and Dr. R. W. Saltus for their discussions and for providing a computer tape with the climatic data of Hansen and Lebedeff (1987).

A special thanks is expressed to my wife, Chunglan, for her understanding, encouragement and love during my graduate studies. None of the efforts that went into my graduate studies would have been possible without her help and support. Thanks also to my daughter, Yourong, for her love and for giving me marvelous joys after my long hours in school.

This research has been supported by Nation Science Foundation grants DPP91-22928, DPP87-21966, DPP86-19382, Army Research Office grant DAAL03-89-k-0106, and by State of Alaska funds.

CHAPTER 1

Introduction

The objective of this thesis is to link changes in climate to changes in permafrost temperature in Alaska north of the Brooks Range. The first half of this thesis focuses on data analysis and provides the physical background on the influence of air temperature, seasonal snow cover, and the active layer on permafrost temperatures. The second half of this thesis investigates, through numerical modeling, the response of permafrost temperatures to changes in climate.

Chapter 2 provides the climatic background in Alaska north of the Brooks Range, North American quadrant of the Arctic and Arctic as a whole. The present climatic conditions in Alaska north of the Brooks Range were investigated. Climatic change in the past 70 years at Barrow was studied using spectrum analysis and compared for the North American Arctic and the Arctic as a whole. Finally, the relation between current climatic and microclimatic conditions and permafrost temperatures are discussed.

Chapter 3 provides information on the physical and thermal properties of the active layer and permafrost. Some results of field measurements of physical and thermal properties of the active layer and permafrost are presented. A model for determining apparent thermal diffusivity using temperature time series with uneven time and space intervals was derived and used to determine apparent thermal diffusivity in the active layer and permafrost. The results are presented and discussed.

Chapter 4 investigates the development of seasonal snow cover (such as timing, duration, accumulating and melting processes) and its influence on the ground thermal regime (such as the ground surface and permafrost temperatures).

Chapter 5 calibrates Goodrich's model using the measured air and soil temperatures, seasonal snow cover, physical and thermal properties of soils. The model was used to study the response of permafrost temperature to surface temperature change and to investigate the sensitivity of the soil temperature to changes in seasonal snow cover parameters, such as timing and duration, thickness, depth hoar layer, accumulation and melting processes, etc. The model was also be used to study the relation between the current climatic conditions and permafrost temperatures in the region.

Chapter 6 investigates the effects of air temperature, seasonal snow cover, the active layer, initial temperature conditions of the permafrost, and variations of thermal properties of soils on permafrost temperatures. Some of the available information on permafrost temperatures were reviewed. Numerical modeling results are presented showing the effects of using past air temperatures as the boundary condition at the permafrost surface, the ground surface, and the surface of the snow cover when snow cover was present on the ground surface and the ground surface when snow cover was absent. The effects of initial conditions, the presence or absence of a snow cover and changes in thermal properties of soils on permafrost temperatures are discussed.

Chapter 7 summarizes the results obtained in this study and provides some suggestions for future studies.

CHAPTER 2

Climate and Climatic Change

2.1 Introduction

The climate of Alaska north of the Brooks Range is dictated by its latitude, distance from the ocean, physical relief, and the interactions with the regional atmospheric circulation. This is the northernmost region in the state bounded by the Arctic Ocean to the north, the Brooks Range to the south and east, and the Chukchi Sea to the west. The region is north of the Arctic Circle and receives minimal sunlight during the winter period. The topography varies from the Brooks Range (Elevations: east 3000 m, west 900 m) and its foothills to the broad, flat Arctic Coastal Plain.

Climatic conditions and their variations in this region are not well understood due to the sparsity of meteorological stations and discontinuity of the observations. *Hamilton* (1965) briefly summarized the temperature fluctuations and trends in Alaska, which included the Barrow station. *Johnson and Hartman* (1971) show that the climate is affected by marine influence in the summer but not to any great extent in the winter. During the 1970's, a series of cooperative National Weather Service (NWS) observations were undertaken by the Alyeska Pipeline Service Company at most construction camps and by the U. S. Army CRREL at the camps and at remote sites along the Haul Road (*Haugen*, 1982). Most of the observations were taken in the summer months. Observations were stopped after the closing of the camps in 1977 and 1978. Subsequently, data were summarized and analyzed by *Haugen and Brown* (1980), *Walker* (1980), *Haugen* (1982).

The objectives of this chapter are: (i) to analyze the air temperature and precipitation records to help understand the surface climatology; (ii) to investigate climatic change in the past 70 years and to compare its variations to the North American Arctic and the Arctic as a whole; and (iii) to investigate the relation of permafrost temperatures to climatic and microclimatic conditions in the region.

2.2 Data Sources and Methods

The basic data in this analysis were mean monthly air temperatures (MMAT), precipitation, and snowfall for stations and sites listed in Table 2.1. Weather observations have been made by the U. S. National Weather Service at Barrow since 1901 and at Barter Island since 1947. Continuous observations were started in 1921 at Barrow and in 1948 at Barter Island. Observations for the rest of stations and sites listed in Table 2.1 were started later.

Some stations in Table 2.1 were moved from time to time. The Barrow station was located at the Army Radio Building during the period from September, 1920 to December, 1942, then moved about 1 km southwest near the shore of the Chukchi Sea. In order to escape sea ice, the station was moved in February, 1944, about 250 m southeast and farther inland. In April of 1955, the station was again moved about 50 m southeast to the new Quonset Building. Finally in 1966, Barrow station was moved to the present site at the airport. The Barter Island station was originally located at the east end of the Main Camp, 800 m west of the airstrip for the period of September 1947 to December 1956. The station was moved about 1.6 km east to the airport until 1988 when the station was closed. ARCO Airfield station was located about 10 km northeast of Deadhorse airport and operated by ARCO Oil Company for the period from 1970 to 1980. Umiat station was operated by NWS for the period from 1948 to 1953 and for the period from 1977 to present.

Table 2.1 Summaries for stations and sites in Alaska north of the Brooks Range

Stations	Latitude °N	Longitude °W	Elevation m	Period	Distance to the Ocean (km)	Sources
Barrow	71.30	156.78	3.0	1921 – 1991	0.55	NWS ¹
Lonely ²	70.92	153.25	3.1	1975 – 1979	1.0	NWS
West Dock	70.38	148.53	3.0	1987 – 1991	0.3	This study
Barter Island	70.13	143.68	3.1	1948 – 1988	0.03	NWS
ARCO airfield	70.25	148.42	7.0	1970 – 1980	5.6	<i>Brown</i> ³
Prudhoe Bay	70.20	148.46	18.2	1983 – 1991	16.0	NWS
Deadhorse	70.10	148.40	20.0	1987 – 1991	20.0	This Study
Franklin Bluffs	69.72	148.68	131.0	1987 – 1991	71.0	This Study
Umiat	69.37	152.13	81.0	1977 – 1991	111.0	NWS
Sagwon ²	69.33	148.68	131.0	1976 – 1979	116.0	CRREL
Happy Valley ²	69.17	148.83	290.0	1975 – 1979	139.0	NWS
Toolik Lake	68.37	149.17	900.0	1986 – 1988	250.0	<i>Hinzman</i> ⁴
Galbraith ²	68.48	149.48	820.0	1975 – 1979	267.1	NWS

1. U. S. Weather Bureau
2. Data were not continuous during the period of observations
3. Brown et al., 1980
4. Hinzman et al., 1990

Meteorological data were obtained for Barrow, Barter Island and Umiat from Local Climatological Data Annual Summaries (LCDAS) (*National Oceanic and Atmospheric Administration, 1991*), Alaska Climatological Data Annual Summaries (ACDAS) (*National Oceanic and Atmospheric Administration, 1921-1991*). Data for Prudhoe Bay (Deadhorse Airport) for the period from January to August of 1983 and from December of 1985 to March of 1986 were based upon the hourly observed air temperatures on microfiche which was provided by the Alaska Climate Center; data from January 1987 to December 1991 were from ACDAS; the rest were provided by the Alaska Climate Center. The MMAT for West Dock, Deadhorse

and Franklin Bluffs were obtained at remote sites established by Osterkamp (unpublished) in October of 1986 (also see *Zhang, 1989*). The mean annual air temperature (MAAT) for Toolik Lake were from *Hinzman et al. (1991)*. Data for Lonely, Sagwon, Happy Valley and Galbraith were obtained from *Haugen (1982)* and were discontinuous during the period of observation. Air temperature time series used for spectrum analysis for the North American Arctic, and the Arctic as a whole were from *Hansen and Lebedeff (1987)*. Precipitation measured with Wyoming gauges at Prudhoe Bay, Sagwon, and Toolik River were from *Soil Conservation Service (1991)*. Freeze and thaw indices are defined as the number of the cumulative degree-days (the difference between the mean daily temperature and 0°C , either positive or negative) of a year. These indices were based upon the mean daily air temperatures during the period from 1950 to 1980 for Barrow and Barter Island. For the rest of time for Barrow, Barter Island and other sites, the freeze and thaw index were calculated from their MMAT. The error between the two methods was less than 5%.

Power spectrum analyses of the time-series of the MAAT, freeze and thaw index, precipitation and snowfall were carried out by using the Maximum Entropy Spectral Analysis (MESA) method developed by *Burg (1967)* and reviewed by *Ulrych and Bishop (1975)*. MESA is superior to the *Blackman and Tukey (1958)* method based upon autocorrelation. In MESA, the choice of the Length of the Prediction Error Filter (LPEF) is not straightforward. From a study of artificial samples, *Kane (1977, 1979)* suggested that spectra may be obtained for several LPEF and periods up to 1/10th of data length (N) may be searched in the small LPEF plots and larger periods in the larger LPEF plots. In this study, MESA was used for MAAT, freeze and thaw indices, precipitation and snowfall time series at Barrow using LPEF of 23, 35, 47, and 56, corresponding to 33%, 50%, 66% and 80% of the data length (71 years).

2.3 Surface Climate in Alaska North of the Brooks Range

The climate in this region is characterized by long, cold winters and short, cool summers. Temperatures in the region remain below the freezing point through most of the year. December through March are generally the coldest months and July is the warmest month of the year. Precipitation values are extremely low. The Arctic Ocean along the northern coast remains ice-covered for nine months or more per year. Prevailing winds often blow onshore bringing polar air into the region and ice into shore during summer.

2.3.1 Temperatures

Air temperatures in the region are strongly affected by the marine influence. The MAAT at sites within about 100 km south of the Beaufort Sea Coast averaged about $-12.4 \pm 0.3^{\circ}\text{C}$ (Figure 2.1A) for the period from 1987 to 1991, while the annual amplitude of air temperature, defined as half of the difference between the warmest and coldest MMAT, ranges from 16.0°C along the coast to 22.0°C inland (e.g. Umiat as shown in Figure 2.1B). The reduction of the annual amplitude along the coast is due to the colder summer temperatures and relatively warmer winter temperatures compared to inland. Figure 2.2 shows that the MAAT at Barter island and Umiat are the same (-12.3°C) but the annual amplitude of air temperature at Umiat is about 5°C greater than that at Barter Island. Mean monthly air temperature in July is about 12.2°C at Umiat and 4.5°C at Barter Island; while in January, mean monthly air temperature is about -32.1°C at Umiat and -25.5°C at Barter island.

Figure 2.3 shows that variations of MAAT from the coast, inland change seasonally. In January, the spatial temperature gradient from the coast, inland, is negative, with air temperature along the coast about 3 to 6°C higher than inland. During May, the temperature gradient becomes positive, air temperature along the coast is about 2 to 4°C lower than inland

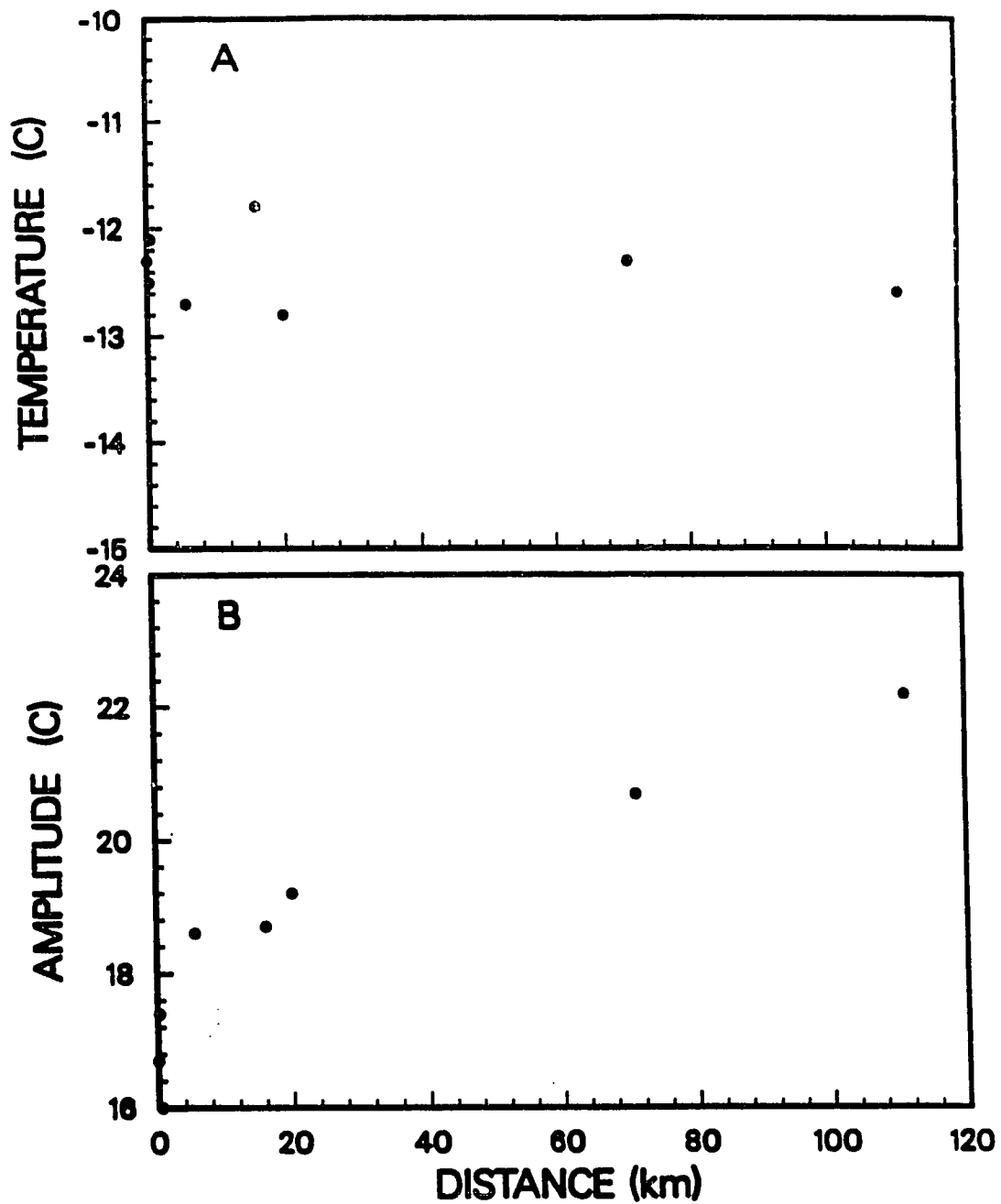


Figure 2.1 Variations of the mean annual air temperature (A); annual amplitude of air temperature (B) with distance from the ocean for the period from 1987 through 1991 for the sites listed in Table 2.1 except Lonely and sites south of Sagwon.

probably because of increased solar radiation on the inland surface during Spring (Bowling, personal communication) and continentality. In July, the temperature gradient becomes greatest, over $6^{\circ}\text{C}/100\text{ km}$. In October, the temperature gradient reverses and becomes negative again, and air temperature is about 3 to 6°C higher along the coast. The magnitude of the temperature gradient is greater during the summer than during the winter, while duration of the positive temperature gradient (from May to September) is shorter than that of negative one (from October to April).

Freeze and thaw indices are a measure of the combined magnitude of temperatures below and above 0°C during a year, respectively. Figure 2.4A shows that the thaw index ranges from about 300°C-day along the coast to about 920°C-day inland, which indicates the thaw season is short and cool along the coast and longer and warmer inland as shown in Figure 2.2. The freeze index (Figure 2.4B) varies from about 4700°C-day along the coast to about 5400°C-day inland, which shows that the freezing season is relatively warmer along the coast and colder inland although the freezing season along the coast is slightly longer than inland (Figure 2.2).

During the summer seasons, the coastal zone experiences more frequent cloudiness and fog, and prevailing northeast winds or sea breezes off the ocean, which keeps average summer air temperatures within a few degrees of freezing (Haugen, 1982). Inland, clear skies are more prevalent, wind directions more variable, and average temperatures higher. During the winter seasons, although the ocean off the western and northern shores of the Alaska is covered with seasonal and multi-year sea ice, the ocean is still a large heat source for the atmosphere. Heat flux from the ocean through sea ice to the atmosphere is much greater than that from the land. For example, under the same air temperature of -20°C with a thickness of sea ice of about 2 m, the typical heat flux from land to the atmosphere is about 6 to 8 W/m^2 , while the heat flux through sea ice to the atmosphere is about 20 W/m^2 , about three times

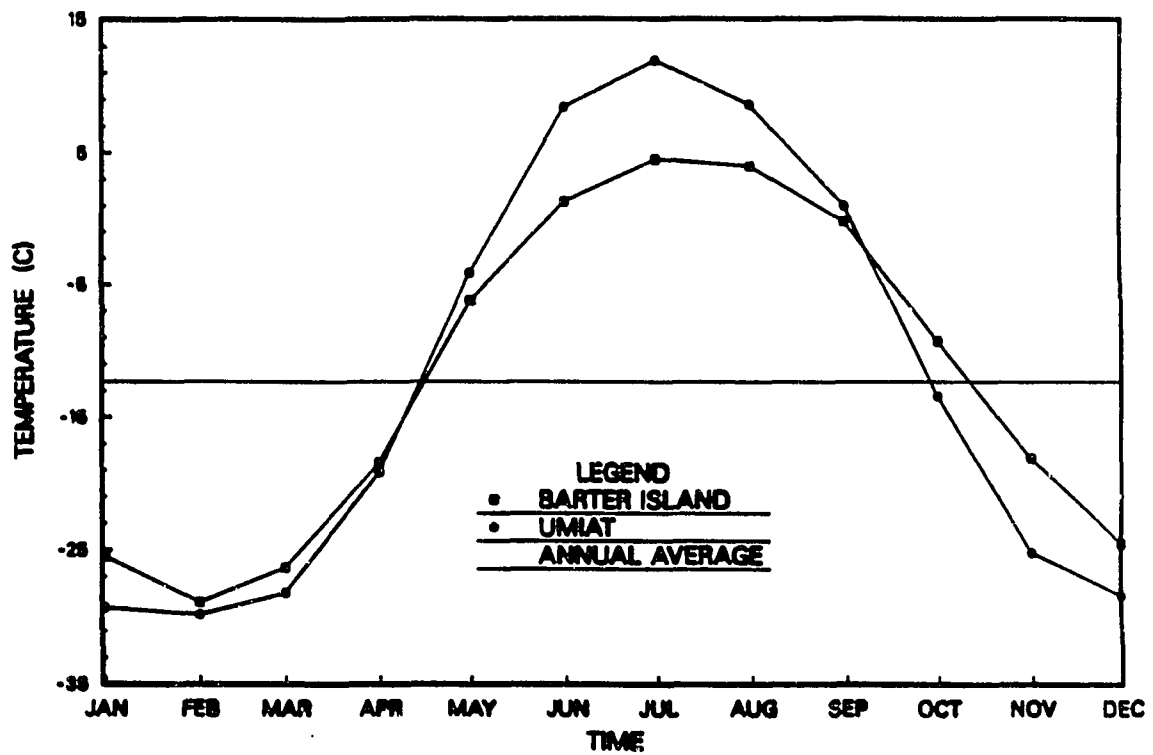


Figure 2.2 Variation of mean monthly air temperature for the period from 1977 through 1988 at Barter Island and Umiat.

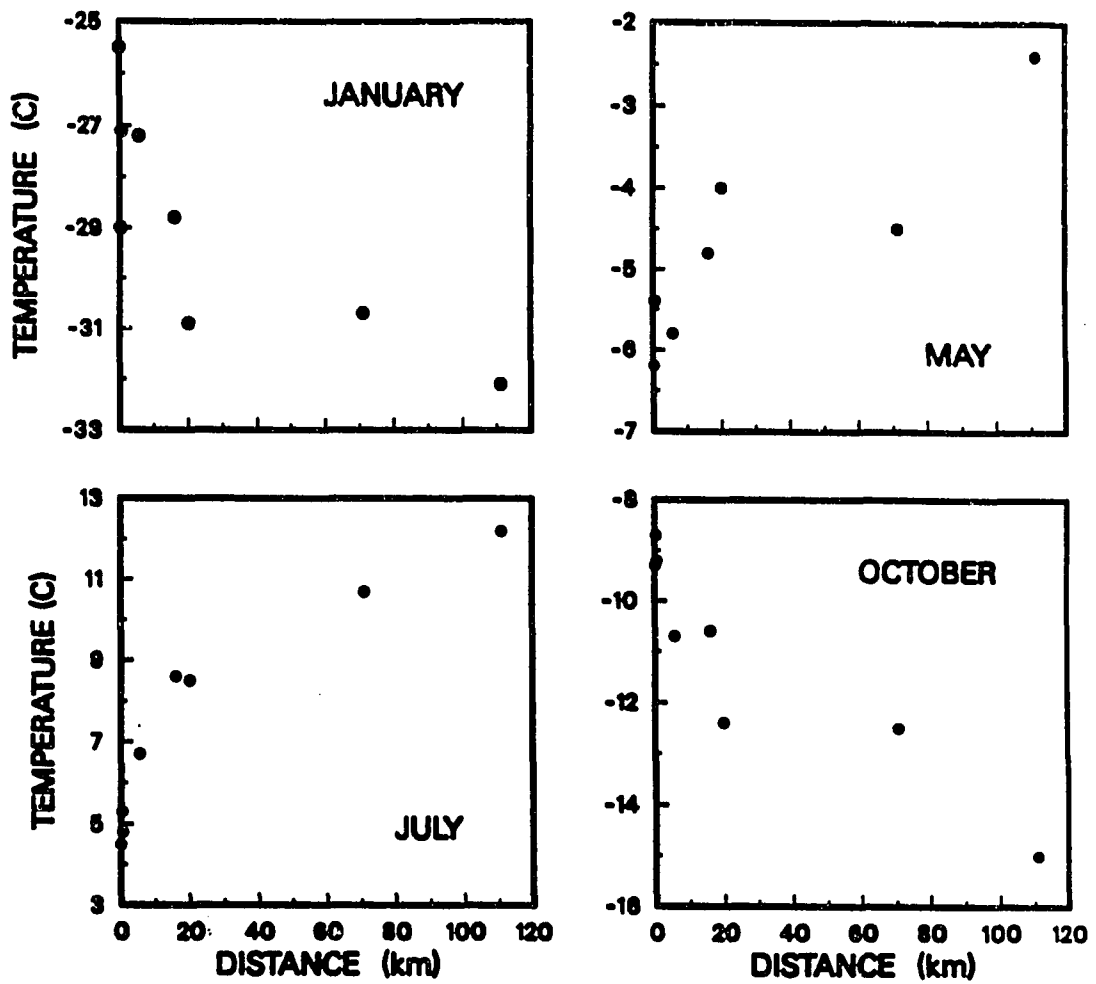


Figure 2.3 Seasonal variations of the spatial temperature gradients from the coast, inland for the period from 1987 through 1991 for the sites listed in Table 2.1 except Lonely and sites south of Sagwon.

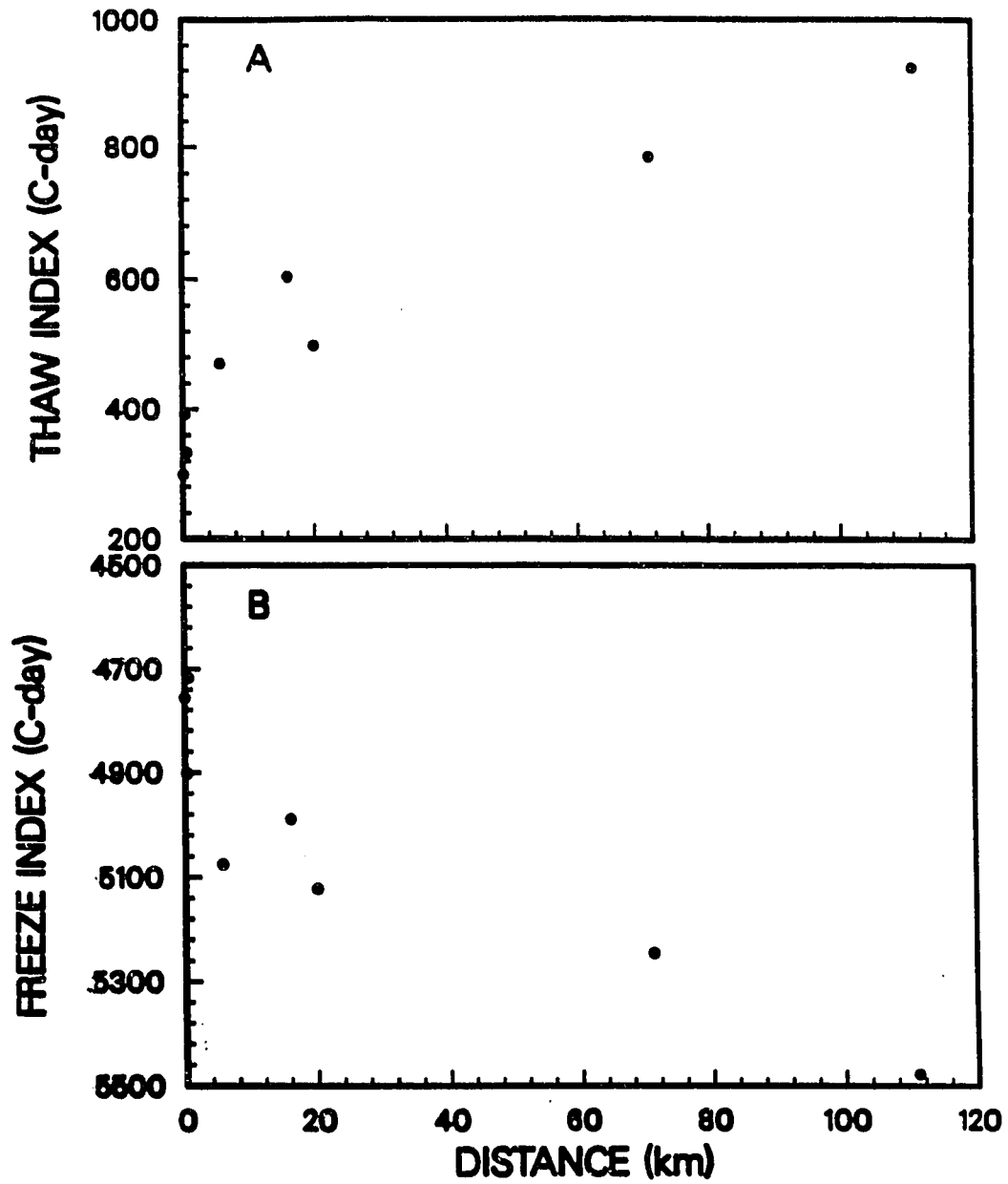


Figure 2.4 Variations of thaw (A) and freeze (B) index with distance from the coast, inland for the period from 1987 through 1991 for the sites listed in Table 2.1 except Lonely and sites south of Sagwon.

greater than that from land. Also, within about 100 km off the shore along the Alaskan Arctic coast, leads may occupy about 10% to 15% of the ocean surface during the later winter, which accounts for about 90% of heat transfer from the ocean to the atmosphere (Weeks, personal communications). As a result, the heat flux from the ocean to the atmosphere during the winter is much greater than from the land, the air along the coast and over the ocean is heated, and the air temperatures are several degrees higher than inland.

The MAAT at Toolik Lake and Galbraith are higher than these along the coast. The major difference is that this area is far away from the ocean (about 230 to 270 km), which reduces the effect of the marine influence and summer temperatures are lower than those inland since the air temperature decreases with increasing elevation. Winter temperatures are higher than those inland and the coast areas due to the effect of winter temperature inversion (up to about 1500 m) (*Bilello, 1966*) since the elevation south of Toolik Lake is over 900 m above sea level.

A correlation analysis of the MAAT and MMAT during the period from 1948 to 1988 between Barrow and Barter Island was conducted using a linear least square method. The empirical equations take the form of $T_b = aT_{bi} + b$, where T_b and T_{bi} are the MAAT at Barrow and Barter Island. Figure 2.5 and Table 2.2 show that the MAAT and MMAT during the winter months are closely linearly correlated between the two stations; while during the summer months (June through September) the correlation is relatively poor.

2.3.2 Precipitation

Table 2.3 summarizes precipitation data from *Soil Conservation Service (1991)*. The 30-year average of these data indicates precipitation ranging from 180 mm for the Coastal Plain to about 640 mm at Atigun Pass. According to *Haugen (1982)*, the 1976-78 record

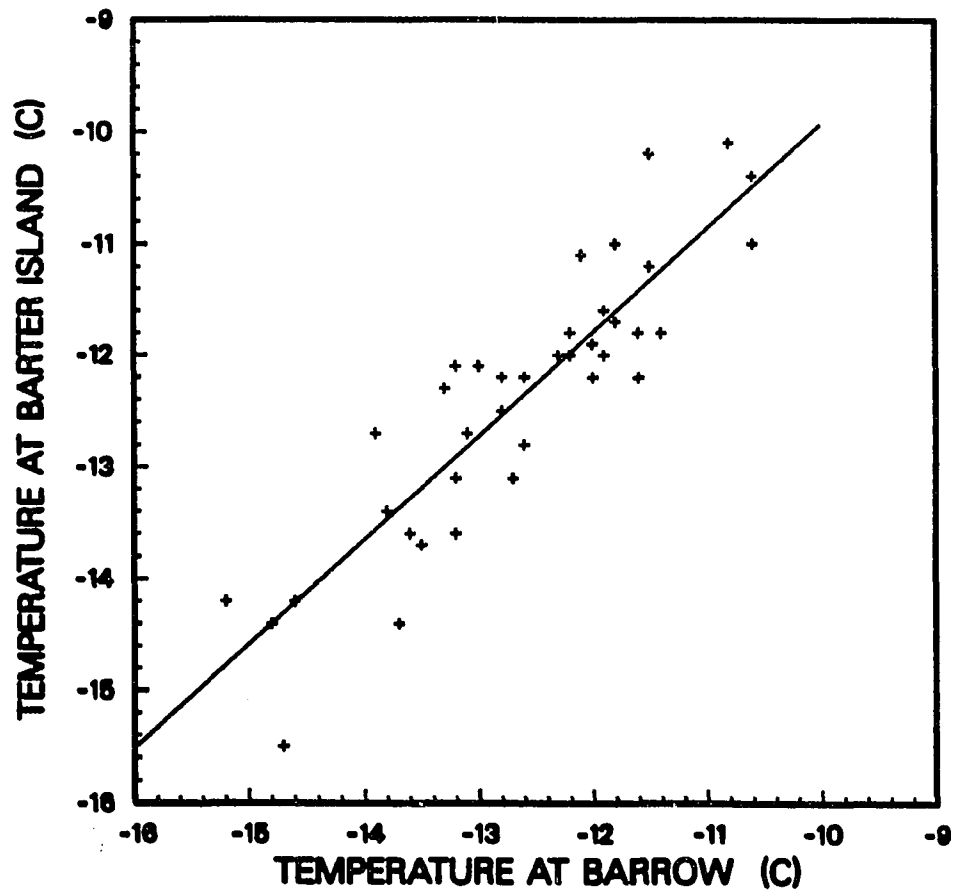


Figure 2.5 Correlation of mean annual air temperatures for the period from 1949 through 1988 between Barrow and Barter Island.

Table 2.2 Statistical parameters for correlation of mean monthly air temperatures and mean annual air temperatures between Barrow and Barter Island. a and b are correlation constants, r is the correlation coefficient and σ is the standard deviation.

Month	Number of Samples	a	b	r	σ
Jan.	40	0.8558	-1.5114	0.96	1.91
Feb.	40	0.7915	-2.9488	0.90	2.93
Mar.	40	0.8049	-2.5991	0.92	1.98
Apr.	40	0.8123	-0.9687	0.90	1.98
May	40	0.6882	4.4723	0.80	1.46
Jun.	40	0.6838	10.0821	0.68	1.21
Jul.	40	0.3324	25.7544	0.35	1.85
Aug.	40	0.2906	26.8797	0.52	3.33
Sep.	40	0.3401	19.8098	0.52	3.25
Oct.	40	0.8581	1.4777	0.82	3.44
Nov.	40	0.8163	-0.4519	0.84	3.73
Dec.	40	0.7099	-3.4457	0.84	3.41
Annual	40	0.9296	-0.6409	0.90	0.56

indicates annual totals ranging from 140 mm (Sagwon) to over 400 mm in the Atigun-Chandalar area. *Haugen* (1982) reported, based upon precipitation data measured by an 8" pan, that the majority of the precipitation received annually is rain inland, whereas about one-half the annual precipitation occurs as rain at Prudhoe Bay and Sagwon. Toward the south, the thaw season becomes longer, and the percentage of rain becomes larger. At Atigun in 1978, the amount of precipitation from May 30 to October 8 accounted for about 74% of total annual value. According to *Walker* (1980), about 35% of the annual precipitation (measured by a Wyoming Gauge) falls in the summer as rain along the coast. According to the weather data at Barrow and Barter Island, in general, snowfall starts in the first decade of September and rainfall starts

at the beginning of June along the coast; inland, snowfall starts a couple of weeks later and rainfall starts a few weeks earlier than along the coast (see Chapter 4). As shown in Table 2.3, more than 60% of the annual precipitation falls as snow in the winter (September through May) along the coast; inland, snowfall accounts about 40 — 50% of annual precipitation. Figure 2.6 shows annual precipitation and snowfall (water equivalent) measured by Wyoming Gauges for the period from 1977 to 1991 at Prudhoe Bay, Sagwon and Toolik River (*Soil Conservation Service, 1991*). It indicates that the snowfall/precipitation ratio decreases inland from the coast.

Table 2.3 Precipitation and snowfall (water equivalent) at sites north of the Brooks Range

Stations	Precipitation (mm)	Snowfall (mm)	S/P Ratio*	Period
Barrow	182.3	113.4	0.64	1921-1991
Barter Island	238.8	144.8	0.61	1949-1988
Prudhoe Bay	213.4	134.7	0.63	1983-1991
Sagwon	228.6	121.7	0.53	1976-1991
Toolik Lake	332.2	129.0	0.39	1976-1991

* — Snowfall/Precipitation Ratio

2.4 Climatic Change

The only weather record of consequence in Alaska north of the Brooks Range is at Barrow where continuous observations began in 1921 (Figure 2.7). For the period of record, the MAAT for Barrow is -12.5°C , shows a warming trend to about 1940, a three and one-half decade long cooling trend to about 1976, followed by a warmer period since then (*Zhang and Osterkamp, 1993a,b*). The instrumental data in other Alaskan stations show a similar pattern

before 1965 (*Hamilton, 1965*) . Most Alaskan Stations warmed suddenly beginning in 1976 and warm winters have been common since then (*Hoffman and Osterkamp, 1986*) .

The MAAT measured at meteorological stations in the northern hemisphere has been increasing since the beginning of recorded data with most of the warming occurring in the period before 1940 (*Ellsaesser, et al., 1986*). *Hansen and Lebedeff (1987)* have shown that, in the northern hemisphere, there was a warming about 0.6°C from 1880 to 1940, a cooling of about 0.3°C from 1940 to 1970, and a warming of about 0.3°C from 1970 to 1987. Warming of the air temperatures in the higher latitudes was significantly greater than at low latitudes and warming in the North American quadrant of the Arctic (Figure 2.6B, *Hansen and Lebedeff, 1987*) was greater than elsewhere. The MAAT increased more than 3.0°C from the mid-1880s to 1940 in this region. However, fragmentary early data suggest significant cooling prior to the mid-1880s such that 25% to about 50% of the subsequent warming may represent a return to earlier levels (*Ellsaesser, et al., 1986*).

The power spectra for the temperature time series (Figure 2.8) show that the MAAT varies with periods of 10 to 11 years and about 50 years at Barrow. This strong signal at 10 to 11 years is the same as the solar cycle. The spectra also show peaks at about 19 to 20 years which is close to the lunar-solar signal of 18.6 years.

Variations of the freeze and thaw indices at Barrow show a pattern similar to the MAAT, i.e., higher MAAT with lower freeze index (Figure 2.9B) and higher thaw index (Figure 2.9C). The average value of the freeze index for the period from 1921 to 1991 was 4835 ± 359 degree-day and for the thaw index 301 ± 107 degree-day. The power spectra show that the freeze index has almost an identical periodicity as the MAAT. The spectra for the thaw index show a similar pattern with MAAT and freeze index for $P \leq 20.0$ years (Figure 2.11). For larger times, the thaw index shows periods of 28.4 and 70.9 years which do not appear in the freeze index.

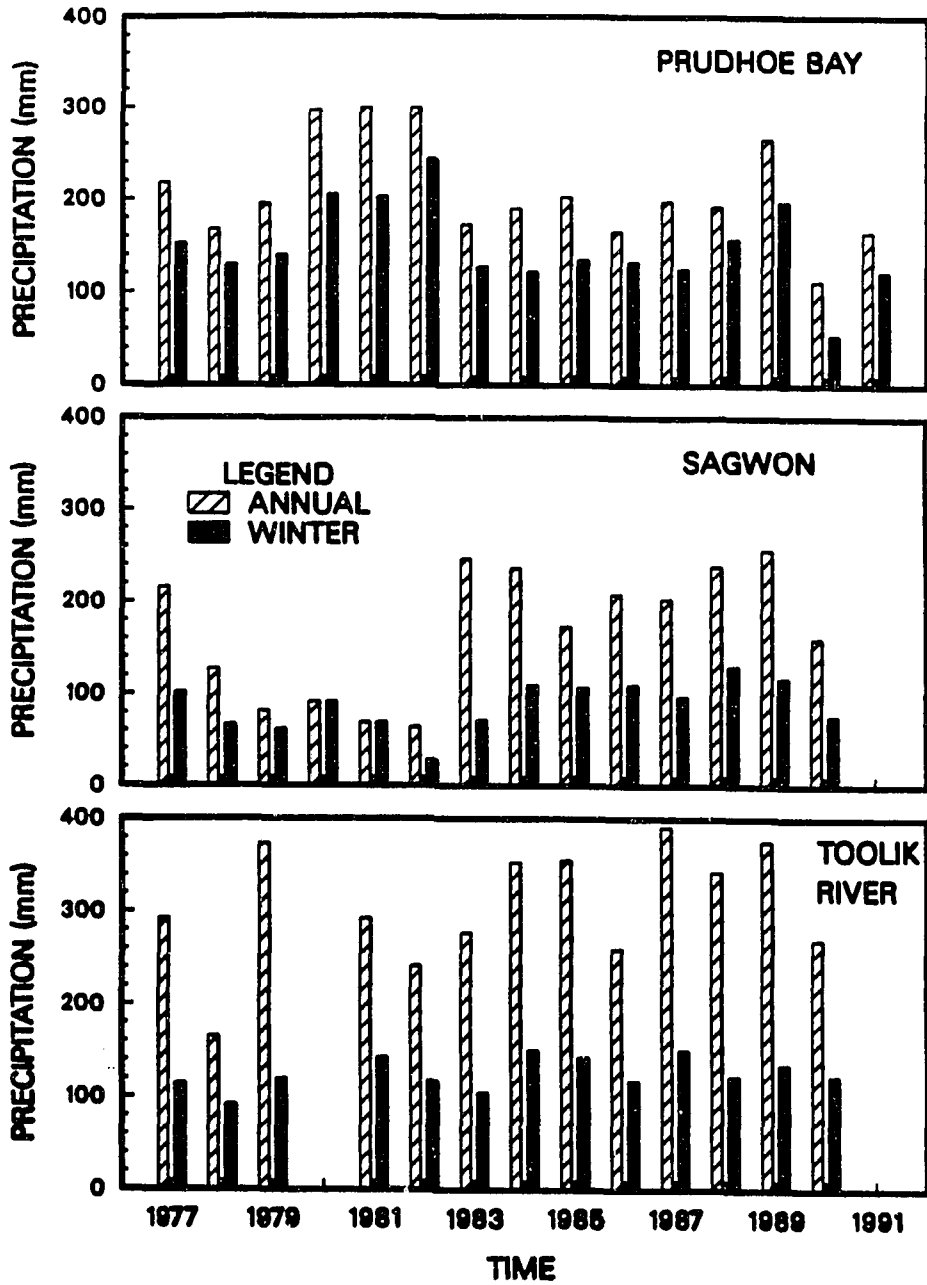


Figure 2.6 Annual precipitation and snowfall (water equivalent) measured by a Wyoming Gauge for the period from 1977 through 1991 at Prudhoe Bay, Sagwon and Toolik River (Soil Conservation Service, 1991)

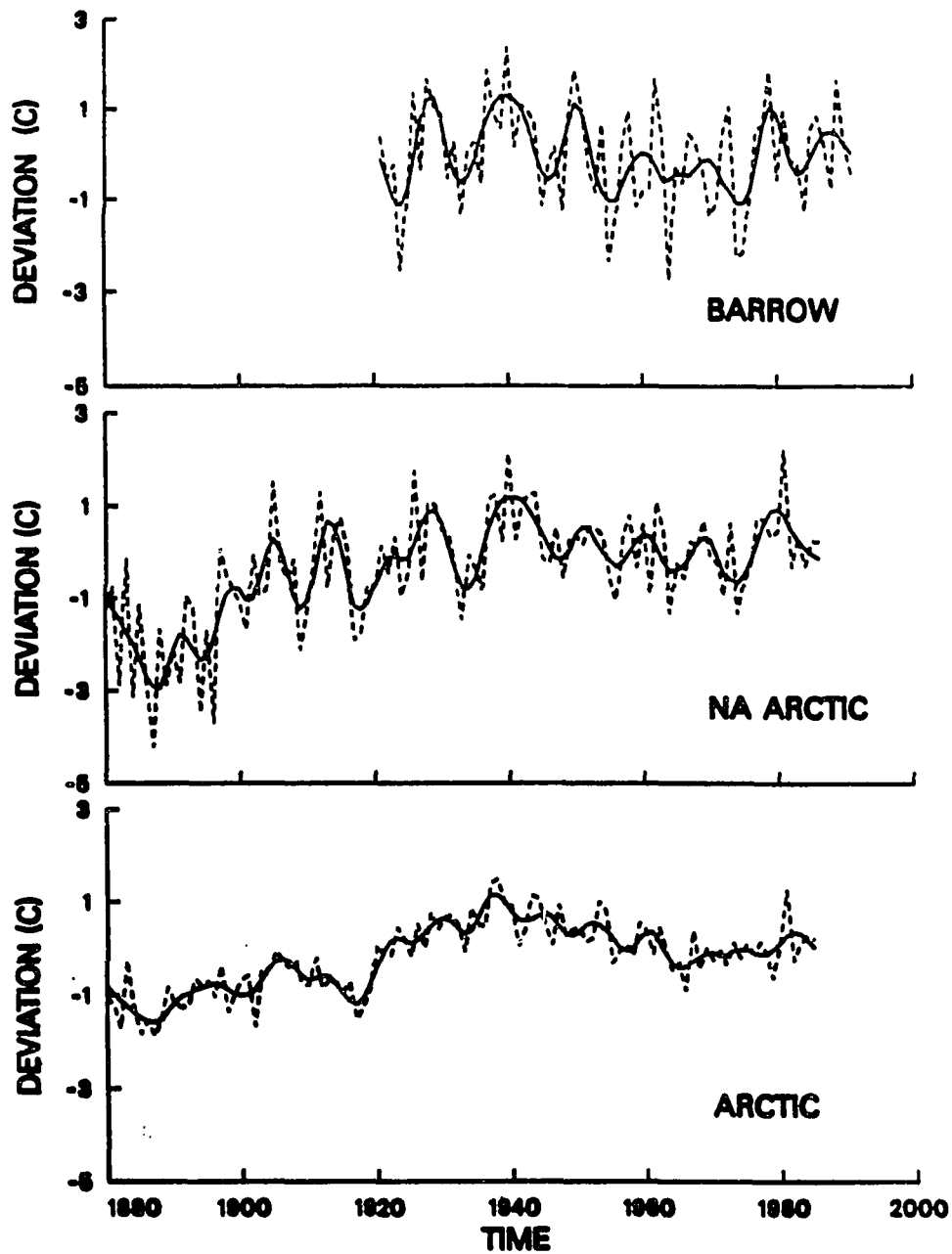


Figure 2.7 Mean annual air temperature departures from the mean (dashed lines) for (A) Barrow, (B) North American Arctic (*Hansen and Lebedeff, 1987*), and (C) Arctic as a whole (*Hansen and Lebedeff, 1987*). Data were smoothed (solid lines) by a low-pass filter with a cut-off frequency of 0.15 year^{-1} .

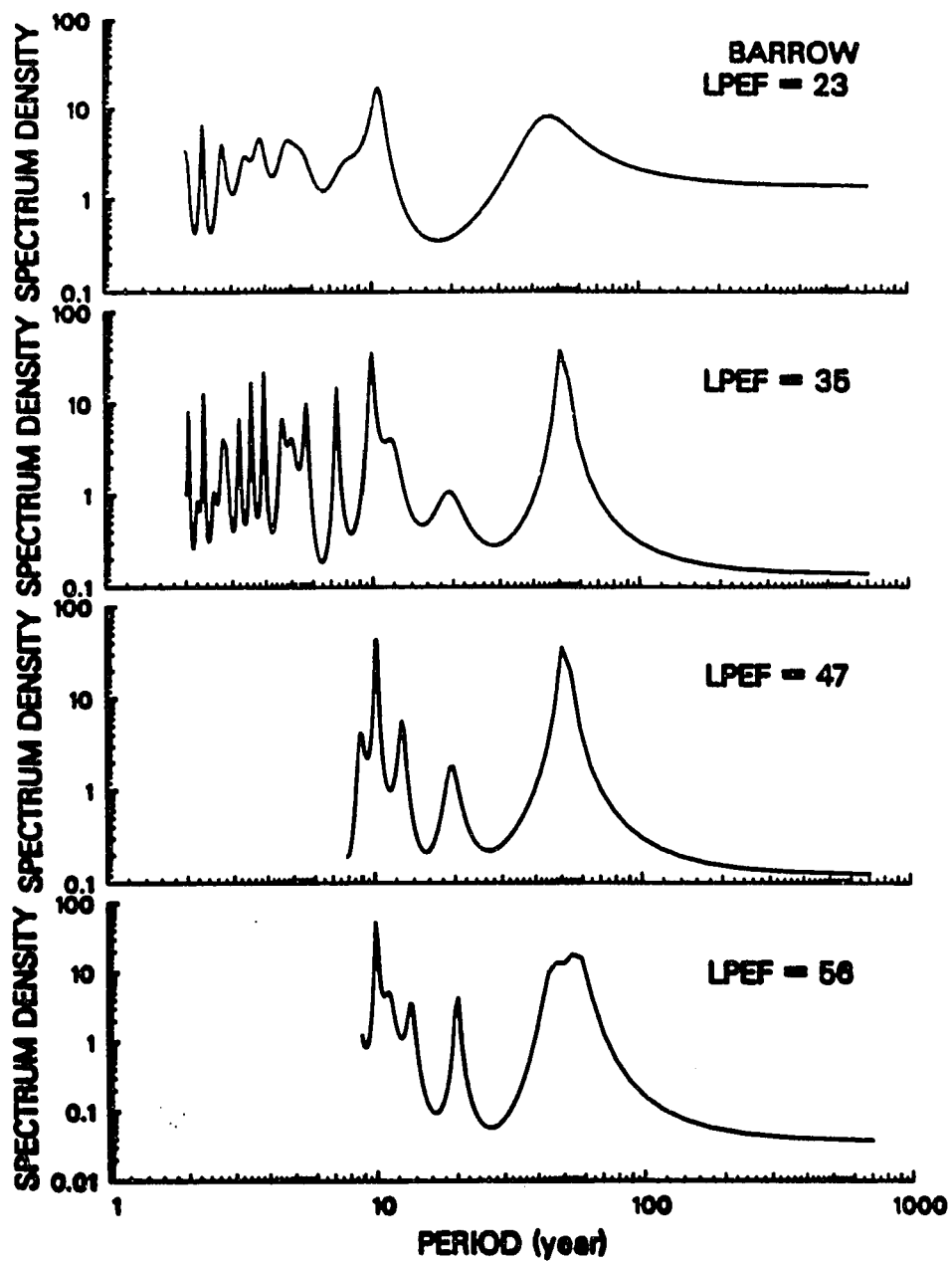


Figure 2.8 Power spectra for air temperature time series at Barrow for the period from 1921 through 1991 with the length of the prediction error filter (LPEF) equals 23, 35, 47, and 56, corresponding to 33%, 50%, 66% and 80% of the data length of 71 years.

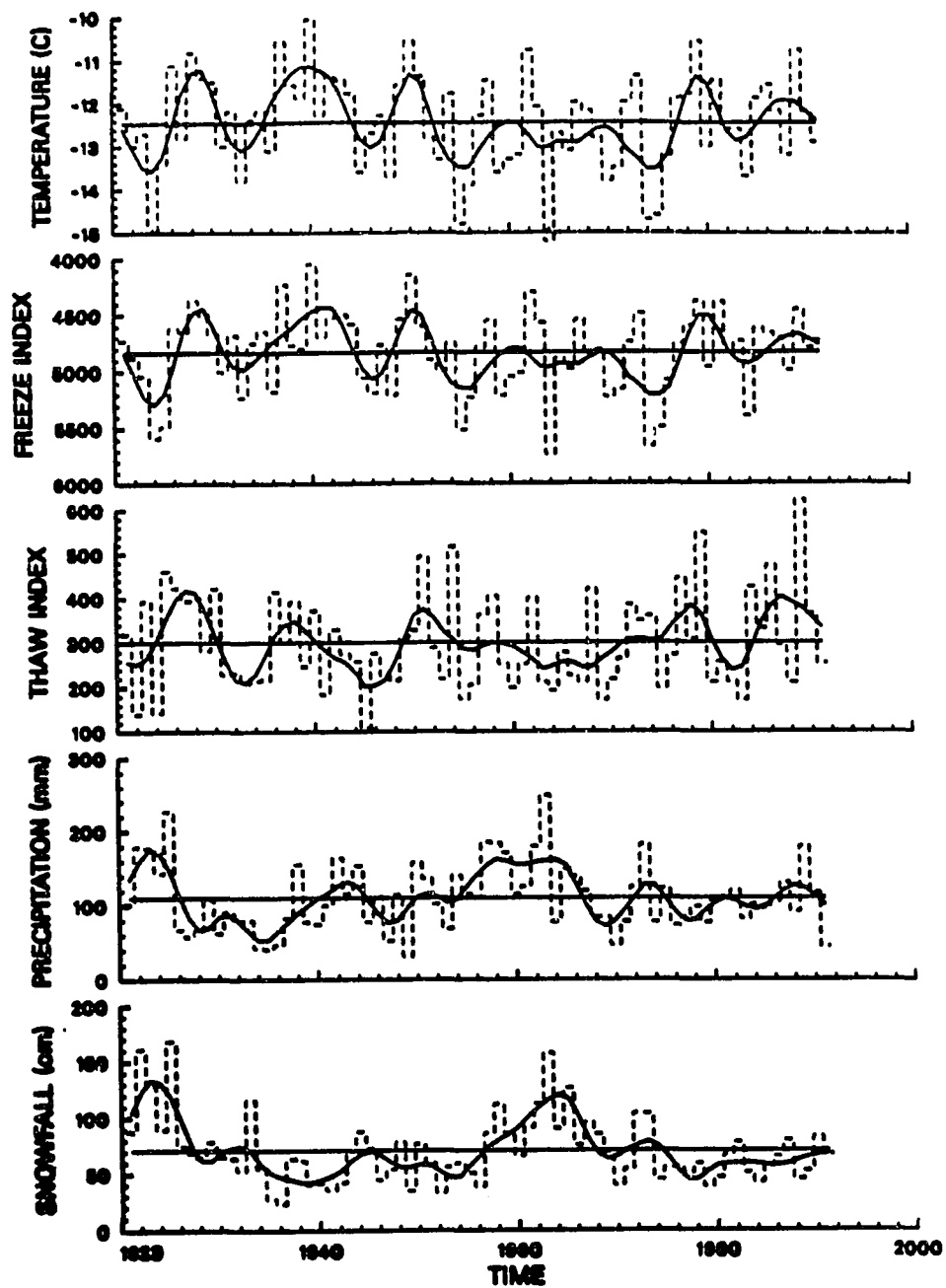


Figure 2.9 Variation of mean annual air temperature, freeze and thaw indices, precipitation and snowfall for the period from 1921 through 1991 at Barrow (dashed lines). These data were smoothed by a low-pass filter with a cut-off frequency of 0.15 year^{-1} (dark solid lines).

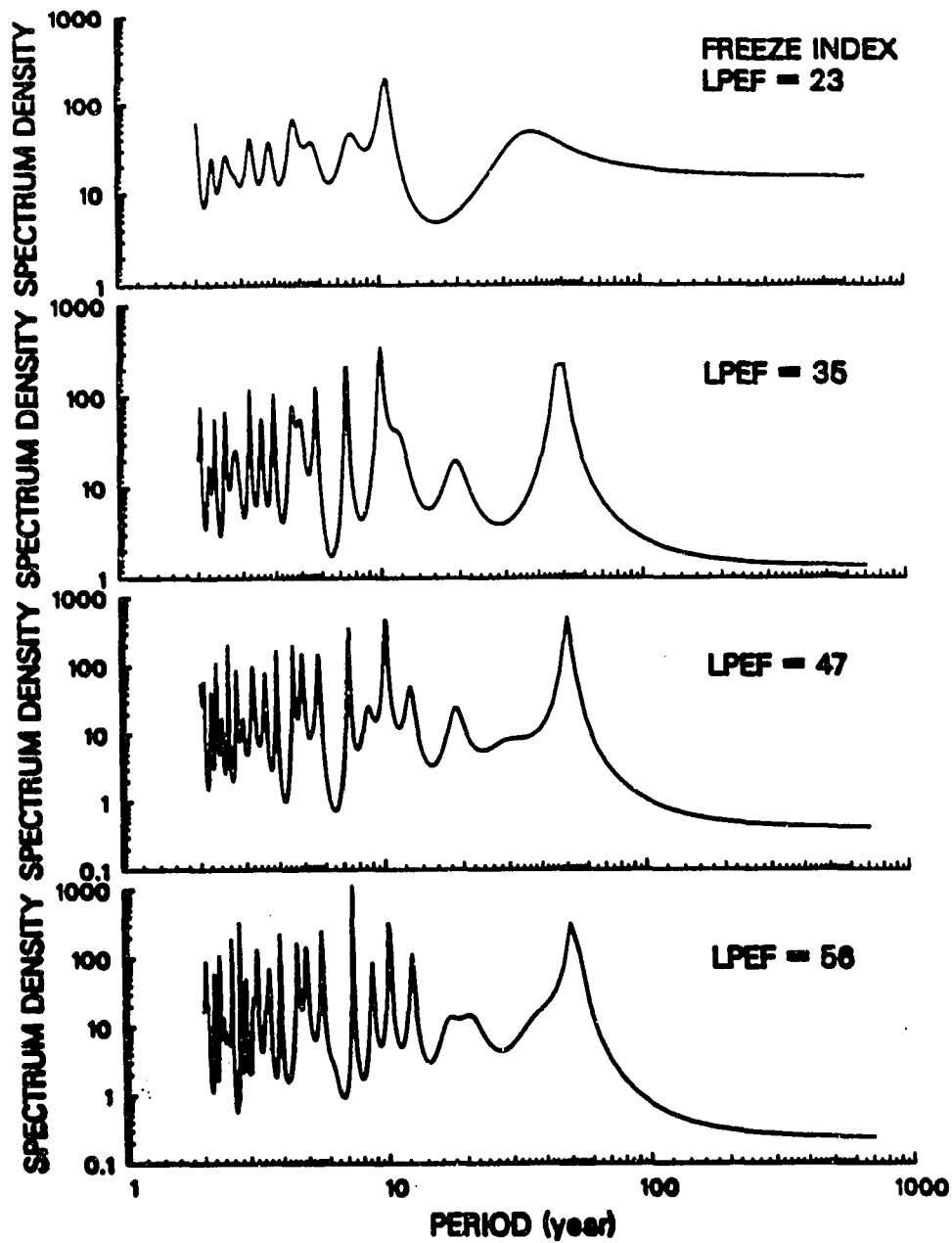


Figure 2.10 Power spectra for the freeze index time series for the period from 1921 through 1991 at Barrow with the length of the prediction error filter equals 23, 35, 47, and 56, corresponding to 33%, 50%, 66% and 80% of the data length of 71 years.

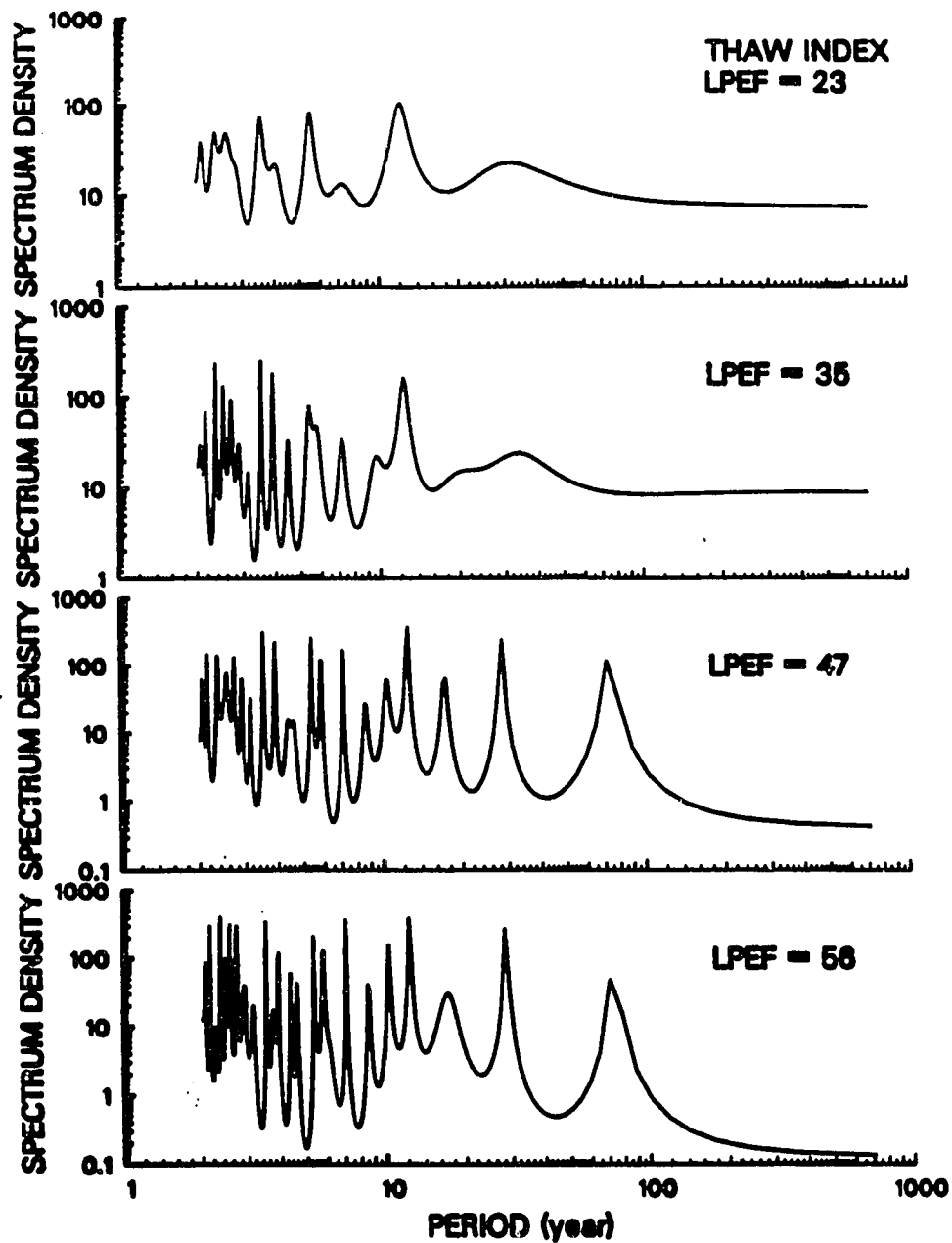


Figure 2.11 Power spectra for the thaw index time series for the period from 1921 through 1991 at Barrow with the length of the prediction error filter equals 23, 35, 47, and 56, corresponding to 33%, 50%, 66% and 80% of the data length of 71 years.

Figure 2.12 shows deviations of MAAT, freeze and thaw indices from their long-term means at Barrow. Clearly, variation of freeze index was over three times greater than that of thaw index. Freeze index was better correlated with the MAAT at Barrow than thaw index. Table 2.4 shows the standard deviations (σ) of monthly air temperature from their long-term means for the period of record at Barrow. For winter time from October through April, the average value of σ is about 3.3°C ; for the summer months from May through September, σ is 1.6°C . Duration of the winter is about two times longer than the summer and the average σ is about two times greater during winter months than during summer months.

These results indicate that changes in MAAT are mainly controlled by the variation of winter temperatures. Colder years have lower winter temperatures and higher freeze index and *vice versa*. The variation of summer temperature is not significant for the variation of the MAAT in this region. This implies that one should be very careful when tree ring data or other proxy, which are related to the summer temperatures, are used to re-construct the mean annual temperature in the Arctic region.

Table 2.4 Deviations of Barrow mean monthly air temperatures and the mean annual air temperatures from their means

	Jan.	Feb.	Mar.	Apr.	May	Jun.	Jul.	Aug.	Sep.	Oct.	Nov.	Dec.	MAAT
Mean	-25.9	-27.9	-26.1	-18.3	- 7.2	1.1	4.1	3.4	-0.9	-9.3	-18.3	-24.1	-12.5
σ	3.9	3.9	2.5	2.8	1.7	1.2	1.3	1.9	1.9	3.2	3.8	3.1	1.1

Precipitation is correlated with snowfall since more than 50% of precipitation falls as snow along the Arctic Coast. The spectral analysis shows that precipitation varies with periods of $P=7.1, 8.2, 10.6, 19.2, 41.7$ and 88.6 years as shown in Figure 2.13. The power spectra show that snowfall changes with periods of $P=6.8, 8.2, 9.9, 13.1, 20.3,$ and 39.4 years (Figure 2.14).

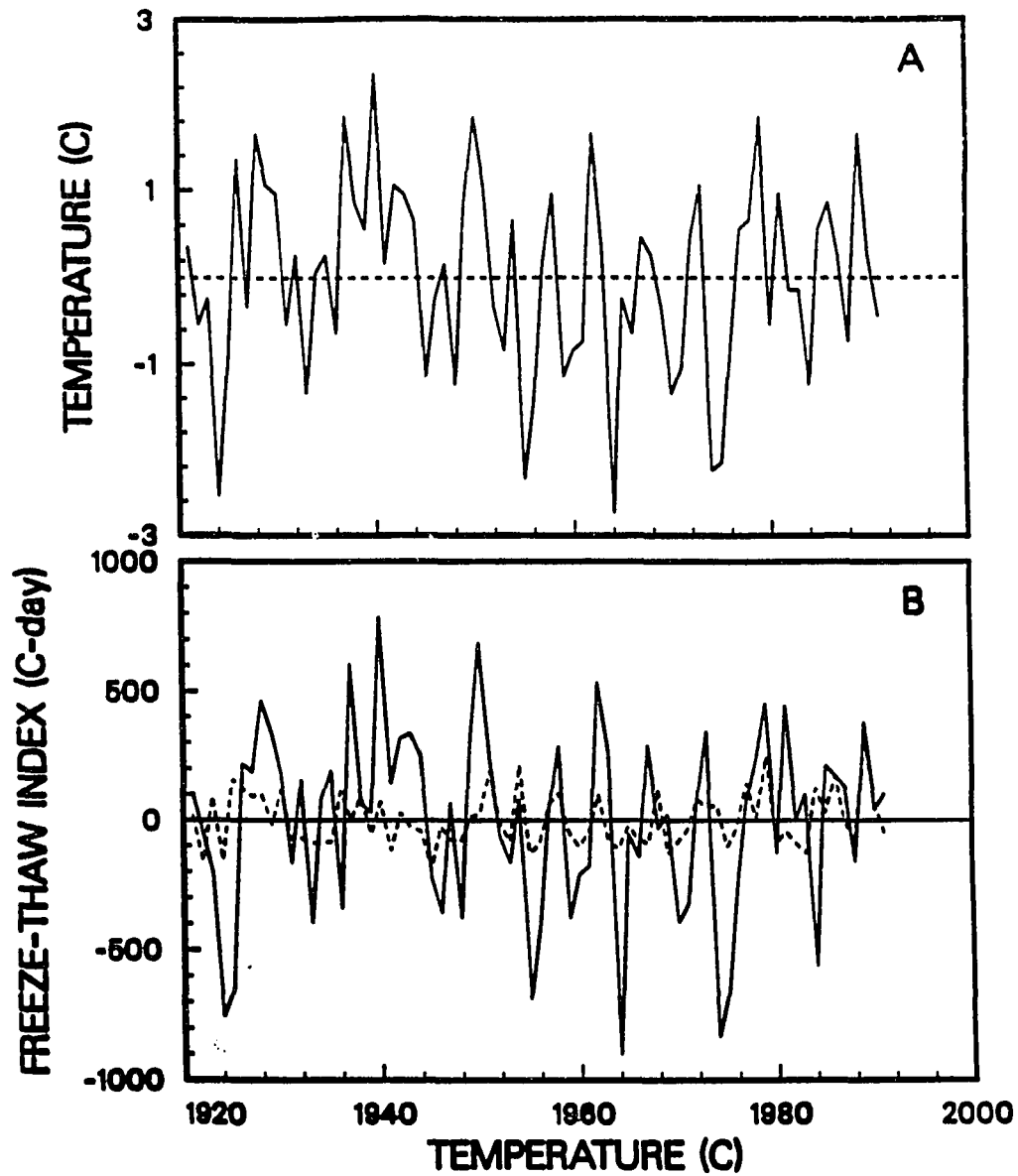


Figure 2.12 Departures of mean annual air temperature (A), freeze index (solid line) and thaw index (dashed line) (B) from their long-term means for the period from 1921 through 1991 at Barrow

Periodic variation of precipitation and snowfall shows a similar pattern except that there is a lack of period at $P=13.1$ years for precipitation and at $P=88.6$ years for snowfall.

Figure 2.15 shows deviations of the MAAT and snowfall from their long-term means at Barrow and Barter Island, smoothed by a low-pass filter with a cut-off frequency of 0.091 year^{-1} . In general, there was a trend with greater snowfall during colder years and less snowfall during warmer years except for a period between the mid-1960's and mid-1970's at Barter Island. This reciprocal relationship between air temperature and snowfall at Barrow also exists in other places in Interior Alaska (Bowling, 1977) and is probably associated with synoptic-scale circulation (Bowling, personal communication).

2.5 Relation to Permafrost Temperatures

Permafrost is associated with a cold climate and is a product of heat exchange between the atmosphere and ground surface. All factors which affect the surface heat balance will influence permafrost temperatures and development. Permafrost temperatures are linked to the temperature at the permafrost table, and to the climate through the active layer, ground surface, intervening vegetation and snow cover. Although the heat flux from the interior of the earth affects the thermal regime of permafrost, annual temperatures at the permafrost surface are mainly controlled by these local factors. For example, the MAAT is nearly constant at about $-12.4 \pm 0.3^\circ\text{C}$ from West Dock to Happy Valley while the mean annual temperature near the permafrost surface (MAPST) is almost 4°C higher (Figure 2.16; Table 2.5).

The length of the thaw season and summer air temperature are major factors that influence permafrost temperatures during the summer. When the active layer develops during the thaw season, the temperature at the upper boundary of permafrost is constrained to the freezing point (close to 0°C) (Lachenbruch, 1962 ; Zhang, 1989; and Zhang, *et al.*, 1991). The

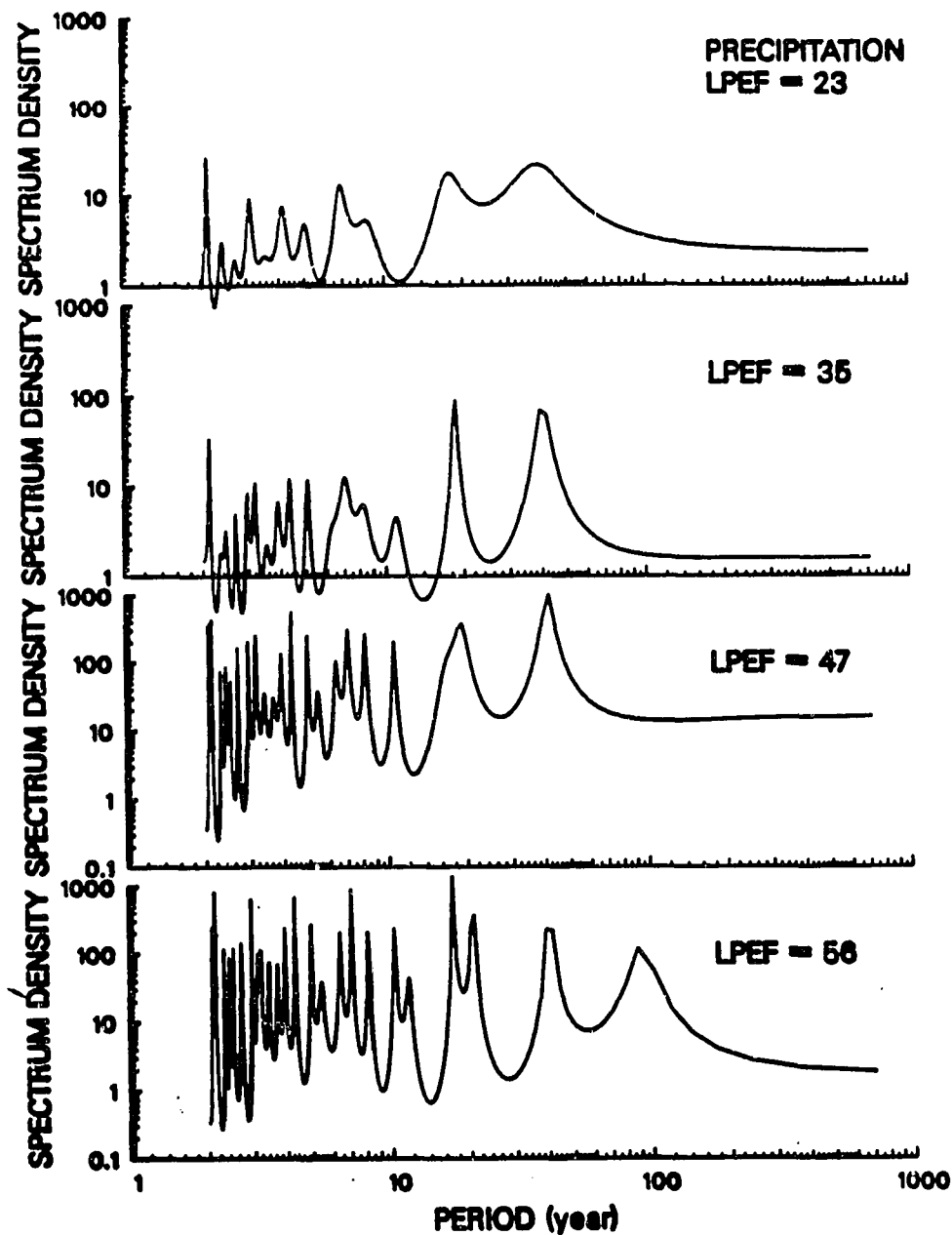


Figure 2.13 Power spectra for precipitation time series for the period from 1921 through 1991 at Barrow with the length of the prediction error filter equals 23, 35, 47, and 56, corresponding to 33%, 50%, 66% and 80% of the data length of 71 years.

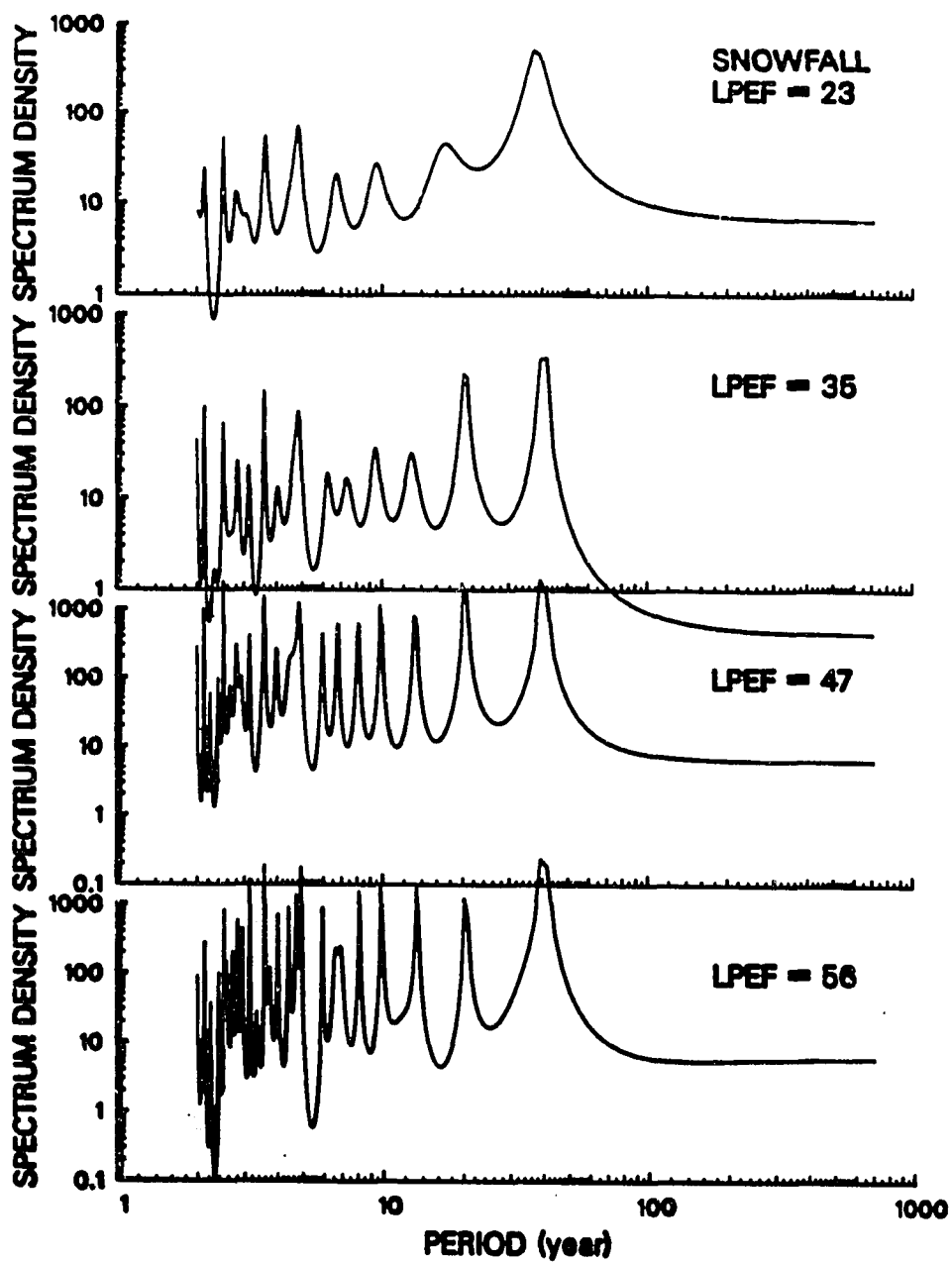


Figure 2.14 Power spectra for snowfall time series for the period from 1921 through 1991 at Barrow with the length of the prediction error filter equals 23, 35, 47, and 56, corresponding to 33%, 50%, 66% and 80% of the data length of 71 years.

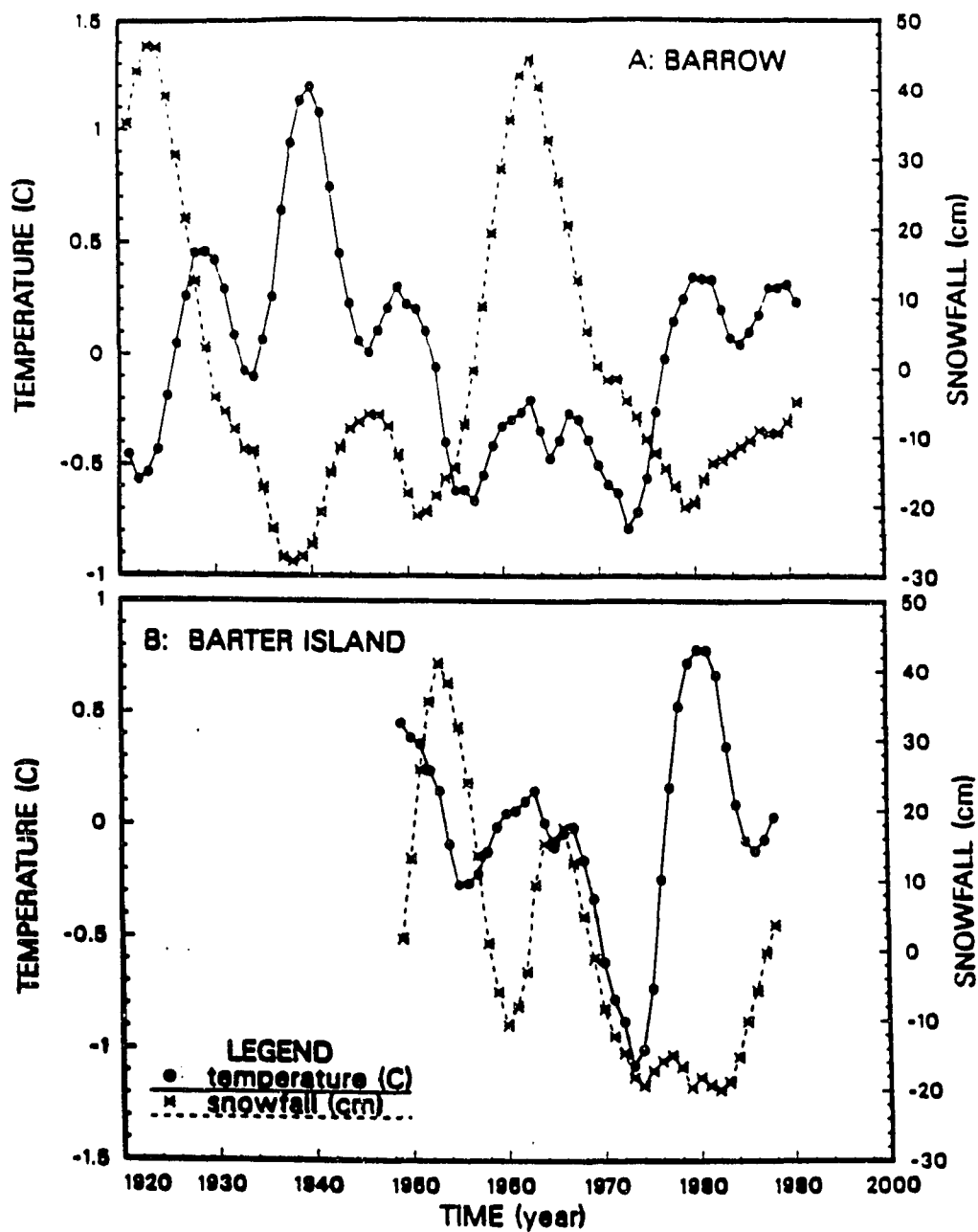


Figure 2.15 Deviations of the mean annual air temperature and snowfall from their long-term means at Barrow and Barter Island, smoothed by a low-pass filter with a cut-off frequency of 0.091^{-1} .

Table 2.5 Values for the mean annual air temperature (MAAT), mean annual ground surface temperature (MAGST) and mean annual permafrost surface temperature (MAPST) for the period from 1987 through 1991 at sites of West Dock, Deadhorse and Franklin Bluffs, from 1985 through 1989 at Toolik Lake and from 1976 through 1979 at Happy Valley and Galbraith. Z is the active layer thickness.

	MAAT	Jan.	July	MAGST	ΔT_1	MAPST	ΔT_2	Z
West Dock	-12.5	-29.0	6.4	-8.3	7.1	-8.8	3.7	0.4-0.6
Deadhorse	-12.8	-30.9	7.5	-7.6	8.9	-8.3	4.7	0.4-0.7
Franklin Bluffs	-12.3	-30.7	10.7	-6.0	10.9	-6.7	5.6	0.6-0.8
Happy Valley	-11.2 ¹	-	-	-	-	-5.2	6.0	
Toolik Lake ²	-7.4	-	-	-	-	-3.1	4.3	
Galbraith	-9.7 ¹	-	-	-	-	-5.8	3.9	

1. Haugen (1982)

2. Hinzman (1991)

thermal regime of the permafrost is linked to its surface boundary condition. The duration of the 0°C phase boundary at the base of the active layer influences the MAPST. Higher summer air temperatures can make a deeper active layer which requires a longer time to freeze during Fall. Table 2.5 indicates that the MAAT in July is about 4°C higher and the active layer is deeper at Franklin Bluffs than at West Dock. The thaw index is about two times greater at Franklin Bluffs than at West Dock. These conditions favour an increase in the MAGST and MAPST inland.

The insulating effect of snow can be a major factor causing changes in permafrost temperatures during the winter. When snow covers the ground surface, it acts as an insulator between the atmosphere and permafrost. ΔT_1 in Table 2.5 is the temperature difference between average monthly air and ground surface temperatures for the period from October through April. ΔT_1 is about 4°C greater at Franklin Bluffs than at West Dock. This indicates that the insulating effect of snow cover during winters is greater inland than along the coast.

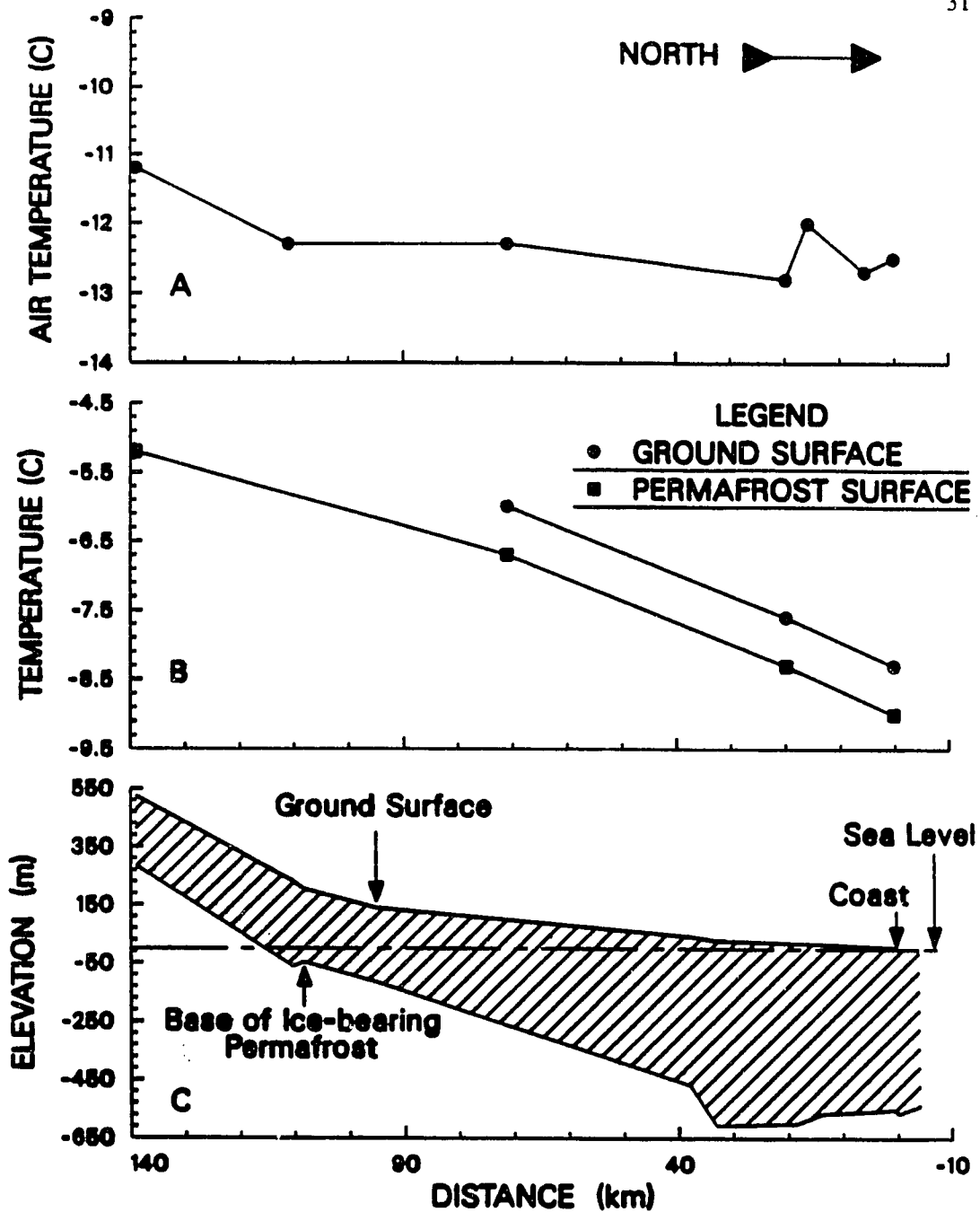


Figure 2.16 Mean annual air temperatures (A), mean annual ground surface and permafrost surface temperatures (B) and permafrost thickness (C) along a transect from Prudhoe Bay to Happy Valley. The sites include West Dock, ARCO airfield, Prudhoe Bay, Deadhorse, Franklin Bluffs, Umiat and Happy Valley.

Variations in the insulating effect of the snow cover during the winter may be due to the combination of microrelief and vegetation with snow cover. Along the coast, the ground surface is mainly occupied by low-center polygons with maximum dimensions ranging from a few meters to tens of meters. Compared to inland areas, the coast has no erect shrubs, no sedge-tussock development and poorly developed moss and lichen communities with a height of about 0.1 m. In this setting, snow can be blown away by strong winds and the insulating effect is reduced. Inland, the ground surface becomes very rough and vegetation changes as a result of increased summer warmth. Shrubs show a particularly dramatic response to the higher summer temperature. At Franklin Bluffs, the willow communities reach heights of about 0.5 to 1.1 m, up to 1.5 m in some protected microsites (*Walker and Webber, 1982*). The flora at Franklin Bluffs is also richer and includes many additional woody plants. Tussocks grow up to 0.45 m tall on the bluffs (*Koranda, 1960*), whereas in the Prudhoe Bay region they rarely exceed 0.2 m. Snow can be held in situ during the early winter against wind thus insulating the ground surface. Field surveys in the spring show that the thickness of the seasonal snow cover is generally greater inland than along the coast (*Hinzman, personal communication, 1993*).

Variations in the thickness of the depth hoar layer can also change the insulating effect of the snow significantly. The structure of the seasonal snow cover consists of a hard, wind-packed layer, overlying a coarse, low density depth hoar layer (*Benson, 1969*). The thickness of the depth hoar layer is up to 50% of the total snow cover thickness and its density ranges from 0.18 to 0.25 g cm⁻³ (*Sturm, personal communication 1993*). The density of the wind slab varies from 0.35 to 0.55 g cm⁻³. The thermal conductivity of depth hoar is about two to four times lower than that of wind slab (*Sturm, 1991*). It is hypothesized that the thickness of the depth hoar layer may be greater inland than along the coast due to the taller vegetation and the deeper active layer which releases more latent heat during freeze up.

It is hypothesized that the combination of microrelief and vegetation with snow cover, greater active layer thickness, and greater depth hoar layer inland increases the insulating effect and the ground surface temperature. ΔT_2 , the temperature difference between MAAT and MAPST as shown in Table 2.5, is greatest inland and reduced along the coast to the north and in the Arctic Foothills to the south.

The thickness of permafrost varies from about 600 m along the coast to about 300 m inland (*Osterkamp and Payne, 1981; Osterkamp et al., 1985*). *Osterkamp et al. (1981, 1985)* concluded that the thinning of the permafrost from the Prudhoe Bay area toward the foothills of the Brooks Range may be the combined result of the change in geological conditions (and therefore thermal conductivity) and the increase in ground surface temperature. Table 2.5 shows that MAPST increases about 4°C from the coast, inland.

2.6 Summary

Table 2.6 summarizes the climatic and permafrost conditions. Air temperatures in Alaska north of the Brooks Range are strongly affected by marine influences. The mean annual air temperature (MAAT) north of Umiat and Franklin Bluffs is about $-12.4 \pm 0.3^{\circ}\text{C}$ and ranges from -11.8°C to -12.8°C , while the annual amplitude of MAAT ranges from 16.0°C along the coast to 22.0°C inland. The reduction of the annual amplitude along the coast is due not only to the lower summer temperatures but also to warmer winter temperatures. The spatial air temperature gradient inland from the coast changes seasonally and the magnitude is greater during the summer (over $6.0^{\circ}\text{C}/100 \text{ km}$ in July) than during the winter (about -3.0 to $-4.0^{\circ}\text{C}/100 \text{ km}$ in January).

The thaw season is short and cool along the coast and longer and warmer inland with the thaw index ranging from about 300 degree-days along the coast to about 920 degree-days

inland. The freeze season is warmer along the coast and colder inland and variations of the freeze index from about 4700 degree-days along the coast to about 5400 degree-days inland.

Table 2.6 Climatic and permafrost conditions for the sites and periods listed in Table 2.1 in Alaska north of the Brooks Range,

	Arctic Foothills	Arctic Inland	Arctic Coast
Distance to the ocean (km)	150 - 300	20 - 150	< 20
Elevation (m)	300 - 900	50 - 400	< 50
Air temperature ($^{\circ}\text{C}$)			
Mean annual	-8.6	-12.4 ± 0.3	-12.4 ± 0.3
Range of mean annual	-8.0 to -9.0	-12.4 to -12.6	-11.8 to -12.8
Annual amplitude	16.8	21.1 ± 0.5	17.5 ± 1.2
Temperature ($^{\circ}\text{C}$)			
Ground surface	-	-6 to -7	-7 to -9
Permafrost surface	-4 to -6	-6 to -8	-8 to -9
Precipitation (mm) ¹			
Snow	186	117	104
Rain	-	113	108
Annual total	324	230	212
Degree-day ($^{\circ}\text{C} - \text{day}$)			
Freeze	3995	5283 ± 74	4930 ± 151
Thaw	800	932 ± 165	420 ± 123
Thaw season (days)	-	128 ± 12	94 ± 11
Thickness of the active layer (m)	-	0.5 - 0.8	0.4 - 0.6
Permafrost thickness (m)	$\sim 250^2$	$\sim 300 - 500^3$	$\sim 600^3$

1 — Soil Conservation Service, 1991

2 — U. S. Geological Survey, 1988

3 — Osterkamp and Payne, 1981

Marine influences on climate change seasonally. During the summer, the ocean is a heat sink for the atmosphere and average summer air temperatures along the coast are within a few degrees of freezing. Inland, clear skies are more prevalent, wind directions are more variable, and average temperatures are higher. During the winter, the Beaufort Sea is covered with sea ice. The heat flux from leads and through the ice to the atmosphere is greater than that from the land so that the ocean acts as a heat source for the atmosphere which keeps the air temperature along the coast a few degrees warmer than inland. This marine influence decreases with distance inland.

Statistical analyses show that air temperature between stations and sites are linearly correlated. The correlation during the winter months (October through May, correlation coefficient ranging from 0.80 to 0.96) is better than during the summer months (June through September, correlation coefficient ranging from 0.52 to 0.68).

Precipitation changes strongly with elevation. This study shows that precipitation ranges from 180 mm for the Coastal Plain to about 640 mm at Atigun Pass which has a shorter record (3 years). Over 60% of precipitation falls in the winter (September through May) as snow, and the rest comes as rain. Those results are consistent with other studies (e.g. *Benson* 1982, *Walker* 1980) which show that about 20 — 30% of precipitation falls as rain along the coast and toward the south around Sagwon, rainfall accounts for about 50%.

The power spectra for air temperature time series at Barrow show that MAAT varies strongly with periods of 10 to 11 years. The MAAT also show periods at $P=7.7$, 9.0, 12.7 and 19.7 years. The period at $P=19.7$ years is close to the lunar-solar signal at $P=18.6$ years.

Variations of freeze and thaw indices at Barrow show a pattern consistent with the MAAT. Power spectra show that the freeze index has similar dominant periodicities as the MAAT at $P=10.1$ and 50.6 years, and also at $P=7.4$, 8.8, 12.7 and 18.7 years. The thaw index agrees very well with the MAAT and freeze index in the region for $P \leq 20$ years. Both the MAAT

and freeze index show a period of 50.6 years but thaw index does not although it has periods of 28.4 and 70.9 years which do not occur in the freeze index.

The spectrum analyses for precipitation shows that the dominant periodicities were 10.6 and 41.7 years for total precipitation and 9.9 and 39.4 years for snowfall. The power spectra also show that precipitation changes with periods of $P=7.1, 8.2, 19.2$ and 88.6 years and snowfall varies with periods of $P=6.8, 8.2, 13.1$ and 20.3 years. Periodic variation of precipitation and snowfall generally shows a similar pattern except that there was a lack of period at $P=13.1$ years for precipitation and at $P=88.6$ years for snowfall.

Departures of the MAAT and freeze and thaw indices from their long-term means at Barrow show that variation of the freeze index is over three times greater than the thaw index. The standard deviation for monthly air temperature from their long-term means is about two times greater during winter months than during summer months. These results indicate that the change of the MAAT is mainly controlled by the variation of winter temperatures. The variation of summer temperature is not significant in the variation of MAAT.

There was a trend with greater snowfall during colder years and smaller snowfall during warmer years.

Although the MAAT is about $-12.4 \pm 0.4^{\circ}\text{C}$ from West Dock to Happy Valley, the mean annual temperature near the permafrost table increases about 4°C . The longer thaw season and higher summer air temperature are major factors in increasing permafrost temperatures inland during the summer. It is hypothesized that the interaction of microrelief and vegetation with snow changes the insulating effect of the seasonal snow cover. Along the coast, the surface is relatively flat with shorter vegetation and snow can be blown away easily which should reduce the insulating effect. Inland, a rough ground surface with taller vegetation such as willows and woody plants, and the presence of tussocks can hold snow in situ earlier and thicker against wind. These conditions are favourable for the development of the depth hoar layer which

increases the insulating effect of the snow cover, and hence the permafrost temperatures. The decrease of permafrost thickness inland from the coast is partly associated with the variation of MAPST which is largely controlled by the above factors.

CHAPTER 3

Physical and Thermal Properties of the Active Layer and Upper Permafrost

3.1 Introduction

The study of the thermal regime of soils in cold regions requires an understanding of the soil properties. For steady-state heat conduction problems, only the thermal conductivity needs to be considered while in the near-surface environment thermal diffusivity becomes the material property of interest. Diffusivity controls the rate of thermal response to transient thermal signals.

All the water in soil and other porous systems does not freeze at the same temperature and the ice content gradually increases as the temperature is lowered (*Lovell 1957; Penner 1970; Williams 1964; Tice et al. 1978*). The relationship between below freezing temperatures and the amount of ice and unfrozen water is peculiar to each soil. Since the volume fractions of ice and unfrozen water in a soil are temperature-dependent, the thermal properties of a soil can change significantly with small changes in temperature below 0°C . The apparent specific heat capacity, C_a , and apparent thermal diffusivity, D , (*Anderson et al., 1973 ; Osterkamp, 1987a*) describe the effects of the continuous phase change.

Various laboratory (*Penner, 1970 ; Hoekstra et al., 1973 ; Penner et al., 1975*) and field (*Goodrich, 1986 ; Nassar and Horton, 1990 ; Persaud and Chang, 1985*) methods have been developed for determining soil thermal properties. These methods often prove unsatisfactory for application to specific problems due to spatial inhomogeneities in the soil or to the presence of non-conductive heat transfer processes and because such methods significantly disturb the

natural conditions of the materials. *McGaw et al.*, (1978) developed a numerical scheme to obtain *in situ* values for D at Barrow from records of soil temperature. The method was employed subsequently by *Nelson et al.* (1985) , *Outcalt and Hinkel* (1989, 1990) , *Zhang* (1989) , and *Hinkel et al.* (1990) . While it appears that good results can be obtained, reported *in situ* values for thermal diffusivity are sometimes unreasonably large, contain zero values, may be negative, and have considerable scatter. *Hinkel et al.* (1990) used synthetic thermal profiles to study the application of this numerical method and showed that large positive and negative values (“spikes”) were a result of the method and occur when the rate of change of temperature gradient becomes small. They attributed other large fluctuations in thermal diffusivity to non-conductive heat flow processes in the active layer. Using synthetic temperature time series, *Zhang and Osterkamp* (see appendix B) investigated the application of numerical methods for determining D in soils. They expanded the usual numerical expression for thermal diffusivity (termed model I) by including higher order terms (model II). Model I produced spikes while model II reduced spikes substantially but model II requires more accurate temperature measurements. *Zhang and Osterkamp* (see appendix B) concluded that selection of values for the space interval (Δx) and time interval (Δt) must take into account the accuracy of the temperature measurements, duration and amplitude of the temperature changes, depth of interest, and the expected values for D.

In this chapter, values of D for the active layer and upper permafrost were obtained from a more complete numerical scheme (*Zhang and Osterkamp*, see Appendix B) with temperature measurements recorded at different frequencies from three sites in Alaska north of the Brooks Range. Dry bulk density and water contents of the active layer and upper permafrost were obtained experimentally both *in situ* and in the laboratory. Thermal conductivity was determined from D and C, and the results were compared with the *in situ* and laboratory measurements.

3.2 Methods

Soil temperatures were measured at different time intervals and with different instrumentation for all three sites. For depths of less than a meter, measurements of soil temperatures started in the Fall, 1986 (Osterkamp, unpublished research) using an automatic data logging system and a string of thermistors. The string consists of nine individually calibrated thermistors mounted securely in a round plastic rod; three of them were placed in the active layer, three at depths bracketing the permafrost table; and three in the permafrost. The maximum and minimum ground surface temperatures and air temperatures (about 1.5 m above the ground surface in a radiation shield) were also measured. The daily air and soil temperatures were recorded on EPROMS by the computer controlled logging system. Accuracy of the individually calibrated temperature probes is much better than 0.1°C . In the Summer of 1988, air, ground surface and soil temperatures for depths less than one meter were measured and recorded at 10 min intervals for one day at the West Dock site. The weather was calm with partly cloudy skies while the ground surface was a little wet but without standing water. For depths below a meter, soil temperatures were logged in a drill hole by a thermistor sensor and cable. The hole was drilled by Osterkamp (unpublished research) during the Spring of 1983 and temperature logging started afterwards and continued one or two times a year until present by Osterkamp (unpublished research) and the author since 1987 when I joined in the project. Sensitivity of the measurements is about a millikelvin and the accuracy is better than $\pm 0.01^{\circ}\text{C}$ under field conditions.

Soil samples were taken during the Summer of 1991 to a depth of about 0.60 m to determine total moisture content, bulk density, thermal properties, and the loss on ignition in the laboratory. The mineral soil samples were oven dried at about 105°C for over 24 hours to determine moisture content. Organic samples were oven dried at about 60°C to constant

weight. Organic samples were also oven burned at about 400°C for over 7 hours to determine the loss on ignition. The moisture contents were also measured using TDR for the thawed layer (Osterkamp, unpublished research). Dry bulk density was determined in the laboratory.

D was determined from the soil temperature time series using a numerical scheme. If the soil temperatures are measured with even space and time intervals, D can be calculated either using the five-point formula applied by *McGaw et al.* (1978), *Nelson et al.* (1985), *Zhang* (1989), *Hinkel et al.* (1990), or *Zhang and Osterkamp* (see appendix B) or the nine-point formula developed by *Zhang and Osterkamp* (see appendix B). In practice, it is very difficult to maintain exact even space and time intervals. Soil temperatures are often measured with uneven space and time intervals. In this case, a new numerical formula was derived to calculate D (see Appendix A). For this study, the soil temperatures were measured for depths less than a meter with uneven space increment and even time increment. D was calculated based upon the equation with uneven space increments Δx_1 , Δx_2 and even time increment Δt ,

$$D = \frac{\Delta x_1 \Delta x_2 (\Delta x_1 + \Delta x_2) (T_i^{j+1} - T_i^{j-1})}{4 \Delta t (\Delta x_1 T_{i+1}^j - (\Delta x_1 + \Delta x_2) T_i^j + \Delta x_2 T_{i-1}^j)} \quad (3.1)$$

and

$$D = \frac{\Delta x_1 \Delta x_2 (\Delta x_1 + \Delta x_2) (T_i^{j+1} - T_i^j)}{2 \Delta t (\Delta x_1 T_{i+1}^j - (\Delta x_1 + \Delta x_2) T_i^j + \Delta x_2 T_{i-1}^j)} \quad (3.2)$$

where the integers i and j reference positions and times for the node of interest, $\Delta x_1 = x_i^j - x_{i-1}^j$, $\Delta x_2 = x_{i+1}^j - x_i^j$, $\Delta t_1 = t_i^j - t_i^{j-1}$, and $\Delta t_2 = t_i^{j+1} - t_i^j$ represent increments of depth and time in the observation mesh. The application of (3.1) requires three temperature

profiles with two time steps and (3.2) requires two temperature profiles with only one time step.

For depths below 1.0 m, soil temperature measurements were uneven spaced in position and time. For different loggings, depths may be off a few centimeters with the space interval of about 1.0 m and the interval between measurement times varied from a few days to a couple of months from year to year. To estimate the values of D , soil temperatures were set at the same depth with an even space interval of 1.0 m using linear interpolation. Values of D for uneven time increment and even space increment were calculated using

$$D = \frac{(\Delta x)^2 ((\Delta t_1)^2 T_i^{j+1} - ((\Delta t_1)^2 - (\Delta t_2)^2) T_i^j - (\Delta t_2)^2 T_i^{j-1})}{\Delta t_1 \Delta t_2 (\Delta t_1 + \Delta t_2) (T_{i+1}^j - 2T_i^j + T_{i-1}^j)}. \quad (3.3)$$

If only two temperature profiles are used, the equation used to estimate D with even space and one time increment becomes (Zhang, 1989 ; Zhang and Osterkamp, see appendix B) ,

$$D = \left(\frac{(\Delta x)^2}{\Delta t} \right) \frac{T_i^{j+1} - T_i^j}{T_{i+1}^j - 2T_i^j + T_{i-1}^j}. \quad (3.4)$$

Thermal conductivities were measured during the Summer of 1991 for the thawed active layer at the field sites using a transient thermal conductivity probe (Osterkamp, unpublished research). A large peat sample with dimension of about $0.30 \times 0.30 \times 0.20$ m near West Dock site was also taken for thermal conductivity measurements in the laboratory for both the thawed and frozen states.

Thermal conductivity K can be determined from D by the relation $K = C_{va} D$ if the apparent volumetric heat capacity C_{va} of the soil is known. C_{va} can be expressed as (Anderson et al., 1983 ; Osterkamp, 1987):

$$C_{va} = \theta_s C_{vs} + \theta_w C_{vw} + \theta_i C_{vi} + \frac{\rho_b \theta_s}{\rho_w \Delta T} \int_{T_1}^{T_2} L_v \left(\frac{\partial w_\mu}{\partial T} \right) dT \quad (3.5)$$

where θ_s , θ_w and θ_i are the volume fraction of soil particles, water and ice content in the soil system, respectively; C_{vs} , C_{vi} and C_{vw} are the volumetric specific heat capacity of soil particles, ice and water, respectively; L_v is the volumetric latent heat in $J m^{-3}$, and ρ_b and ρ_w are the dry bulk density of the soil and the density of unfrozen water in $kg m^{-3}$, respectively. The first three terms on the right hand side of (3.5) are the sum of the specific heat capacities of each constituent, and the last term is the latent heat of phase change when unfrozen water is present. When the soil is in the thawed state, the last two terms in (3.5) vanish and C_v can be determined from the first two terms, neglecting the contribution of any air that may be present. When the soil is in the frozen state and at low temperatures, the unfrozen water content becomes very small and latent heat may be not very significant in the calculation of C_v so that it can be determined from the first three terms. This effect varies with the soil type and occurs generally around $-5^\circ C$ or lower.

Finally, the results of D , C_{va} and K obtained by the proposed method were compared with the results obtained by other methods, such as the amplitude ratio method (Zhang, 1989), an empirical formula (Kersten, 1949), and results of measurements *in situ* and in the laboratory.

3.3 Results and Discussions

3.3.1 Physical Properties

Although soil profiles on the coastal plain can vary significantly in the microscale, the gross topographic contrast is slight, vast areas appear flat, and the soils in general are wet and homogeneous (Everett, 1980). Table 3.1 shows the soil profiles and their physical properties at West Dock, Deadhorse and Franklin Bluffs. The top 20-30 cm of soil consists of live and dead organic materials mixed with wind blown silt. The thickness of the peat layer was thinner at Deadhorse and Franklin Bluffs. The soil was drier and had less organic content at Deadhorse than the other two sites. Below the peat layer was silt with a few organic inclusions.

3.3.2 Apparent Thermal Diffusivity

The apparent thermal diffusivity was estimated using the numerical method (Zhang and Osterkamp, see appendix B) with different space interval Δz (3.1) and (3.2) and time interval Δt (3.3) and (3.4) for depths from a few centimeters to about 40 m.

Active Layer

For depths from the surface to about 0.30 m, soil temperatures were measured and recorded at depths of 2.2 cm, 7.2 cm and 12.3 cm with a time interval of 10 min. at West Dock. The record of temperature measurements started at 11:18 a.m., July 8th, and ended at 10:28 p.m., July 9th, 1988. Soil was in the thawed state, depth of the active layer was about 31.0 cm, and there was no temperature variation from recorded data beyond 31.0 cm at that day. There was a temperature spike after 4 hours of recording at all these depths, at 7.2 cm it was the largest ($> 1^{\circ}C$). The temperatures above and below this depth had an instantaneous response to this event which disappeared at a depth of about 26 cm. This could be the result of non-conductive heat transfer processes. A possible explanation is that when temperature rose at the surface, water vapour moved downward and then condensed at a depth of around 7.2 cm. The release of

Table 3.1 Physical and thermal properties of soil samples taken in June, 1990 in Alaska north of the Brooks Range

Depth (m)	Soil Type	ρ_b (kg/m^3)	w (Lab) (%)	w (TDR) (%)	Δw (%)	LI (%)
West Dock						
0.0 - 0.10	peat	-	319.3	-	-	71.2
0.10 - 0.20	peat	455	150.0	141.0	+6.4	44.84
0.20 - 0.31	peat	371	207.1	-	-	33.93
Deadhorse						
0.0 - 0.12	peat	-	119.0	-	-	15.33
0.12 - 0.23	peat	531	113.0	126.0	+5.6	25.03
0.23 - 0.40	silt	1377	32.5	30.0	+8.3	5.57
0.40 - 0.60	silt	1250	36.0	-	-	-
Franklin Bluffs						
0.0 - 0.08	peat	-	247.3	-	-	53.2
0.08 - 0.20	peat	502	163.9	151.3	+8.3	27.85
0.20 - 0.40	silt	1466	34.0	31.0	+9.7	-

latent heat from condensation would increase the temperature in the surrounding peat. About one hour later, the latent heat dissipated into the media, and the temperature curve gradually became normal.

D was calculated for a depth of 7.2 cm using (3.1) with $\Delta x_1 = 5.0$ cm, $\Delta x_2 = 5.1$ cm and $\Delta t = 10.0$ min (Figure 3.1). The extreme values of D occur around the temperature spike noted above and where the temperature had a maximum for that day at the depth of interest. The effect of this event on D continues for several hours until $t = 600$ min. There were two different sets of values before and after the temperature spike. The average D is

about $3 \text{ m}^2 \text{ yr}^{-1}$ before the temperature spike and about $6.5 \text{ m}^2 \text{ yr}^{-1}$ afterward. The thermal diffusivity obtained by the amplitude ratio method (Zhang, 1989) for depths between 0.0 cm and 12.3 cm is about $12.8 \pm 0.8 \text{ m}^2 \text{ yr}^{-1}$ (Zhang, 1989), much higher than the average value of D obtained by the numerical method.

Depths between 0.4 and 1.0 m

For depths from 0.4 to 1.0 m, soil temperatures were measured and recorded with $\Delta t = 1$ day. Due to the snow insulation, the daily amplitude of ground surface temperature during the winter was often reduced to less than 1°C (see Figure 4.8). Small daily amplitude and low thermal diffusivity in the peat layer reduces the depth of daily temperature variation to around 0.4 m in this region. Thus, D can be estimated from soil temperature time series measured below 0.4 m for a recording interval around 1 day or longer.

Figure 3.2 shows soil temperatures and the calculated D at a depth of 62.1 cm from October of 1986 to October of 1987 at West Dock, Prudhoe Bay. Equation (3.1) was used and all temperature data were used for which the magnitude of the denominator of (3.1) was less than 0.3°C . D varied from 12.5 to $-2.5 \text{ m}^2 \text{ yr}^{-1}$. This variation in D (Fig. 3.2 B and C) is mainly due to frequent changes in temperature over a relatively short time. Figure 3.3 shows a few sets of temperature profiles used for calculating D , where circle stands for time t_i^j , triangle for t_i^{j+1} and square for t_i^{j-1} . At $t_i^j = 54$ days in Figure 3.3(A), three temperature profiles showed a continuous cooling trend and were almost "parallel". This indicates that the heat flow is in one direction. When $t_i^j = 60$ days, the first two profiles show a cooling trend while the third one shows a warming trend. This reduces the rate of temperature change and the temperature gradients at the nodes involved, resulting in a decrease of D as shown in Figure 3.3(B). When $t_i^j = 99$ days, the situation gets worse and negative values of D appear (cf. Zhang and Osterkamp, see appendix B). Figure 3.3(D) and (E) show a continuous warming

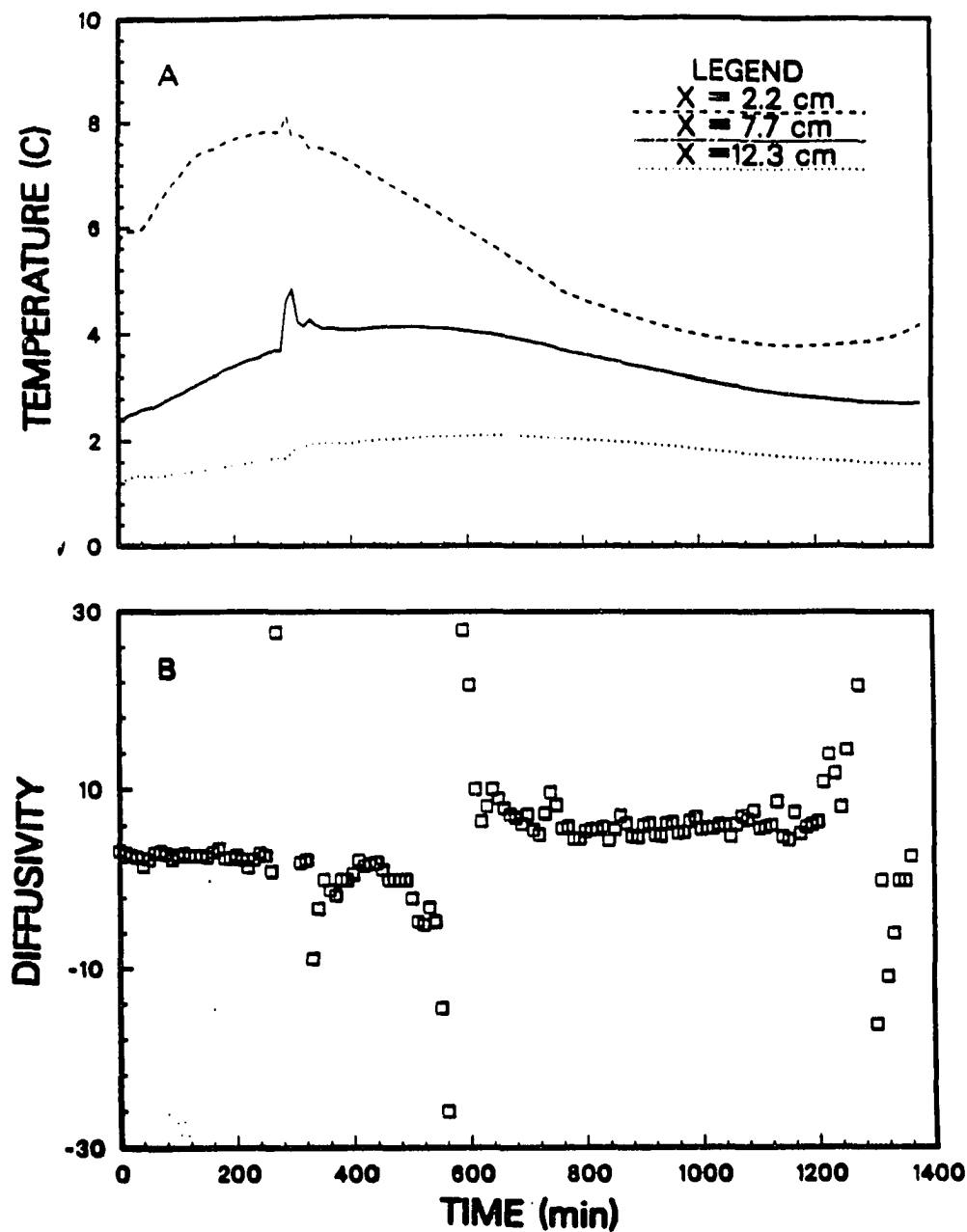


Figure 3.1 Variation of soil temperature measured at depth of 0.022 m, 0.072 m and 0.123 m and apparent thermal diffusivity estimated by (3.1) with $\Delta x_1 = 0.05$ m, $\Delta x_2 = 0.051$ m and $\Delta t = 10$ min. on July 8, 1988 at West Dock, Prudhoe Bay.

trend with low D values. This may be due to a non-conductive process in the soil such as latent heat and water movement in the frozen soil.

D was estimated by the above procedures from soil temperature time series for the period from October 1986 to June 1991 at West Dock, Deadhorse and Franklin Bluffs. Soil temperatures were measured and recorded at depths of 42.0 cm, 62.0 cm and 71.9 cm with $\Delta x_1 = 20.0$ cm, $\Delta x_2 = 9.9$ cm and $\Delta t = 1$ day for the calculation of D at the Deadhorse site. At Franklin Bluffs, D was calculated at a depth of 55.8 cm with $\Delta x_1 = 9.8$ cm, $\Delta x_2 = 20.1$ m and $\Delta t = 1$ day. D was calculated by (3.1) for data where the magnitude of the denominator of (3.1) was greater than 0.5°C . Values of D were calculated when the temperature profiles (at least three) showed a continuous cooling or warming trend as shown in Figure 3.3A. Figures 3.4, 3.5 and 3.6 show the results at West Dock, Deadhorse and Franklin Bluffs, respectively.

Values of D show a strong temperature dependence at all three sites which may be associated with the movement of unfrozen water and/or the temperature dependence of unfrozen water content in the active layer and upper permafrost. When the permafrost temperature approaches the freezing temperature, C_{va} becomes large due to the latent heat effect as shown by Osterkamp (1987) which reduces the value of D (Figures 3.4, 3.5 and 3.6). For an assumed value of θ_u characteristic of Fairbanks silt, values for D calculated from the relation $D = K/C$ (eg, Osterkamp, 1987) are graphed in Figures 3.5 and 3.6. These calculated D are in reasonable agreement with the data.

The characteristics of the variation in D at West Dock are different from the variations at Deadhorse and Franklin Bluffs. The range of temperature over which D is temperature dependent at West Dock is wider (from about -0.6°C to about -8.0°C) than at Deadhorse (from about 0°C to -4°C) and at Franklin Bluffs (from about 0°C to -3°C). The average value of D at West Dock for $T < -8^\circ\text{C}$ is about $7.7 \pm 2.5 \text{ m}^2 \text{ yr}^{-1}$, about $20.0 \pm 2.0 \text{ m}^2 \text{ yr}^{-1}$ at Deadhorse for $T < -4^\circ\text{C}$ and about $27.0 \pm 3.0 \text{ m}^2 \text{ yr}^{-1}$ for $T < -3^\circ\text{C}$ at Franklin

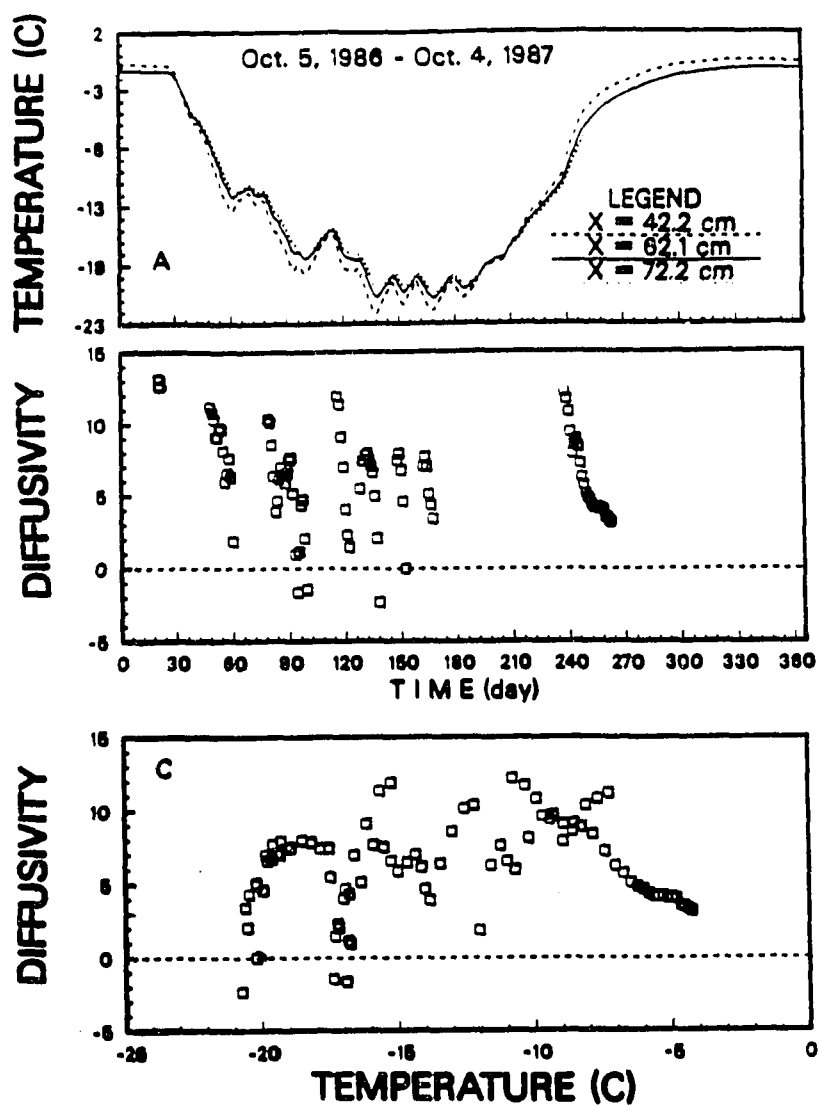


Figure 3.2 Variation of soil temperatures at depths of 0.422 m, 0.621 m and 0.722 m with $\Delta t = 1$ day and apparent thermal diffusivity estimated using (3.1) at depth of 0.621 m with $\Delta x_1 = 0.199$ m, $\Delta x_2 = 0.101$ m and $\Delta t = 1$ day for the period from October 5, 1986 through October 4, 1987 at West Dock, Prudhoe Bay. Data used in the calculation were selected as described in the text.

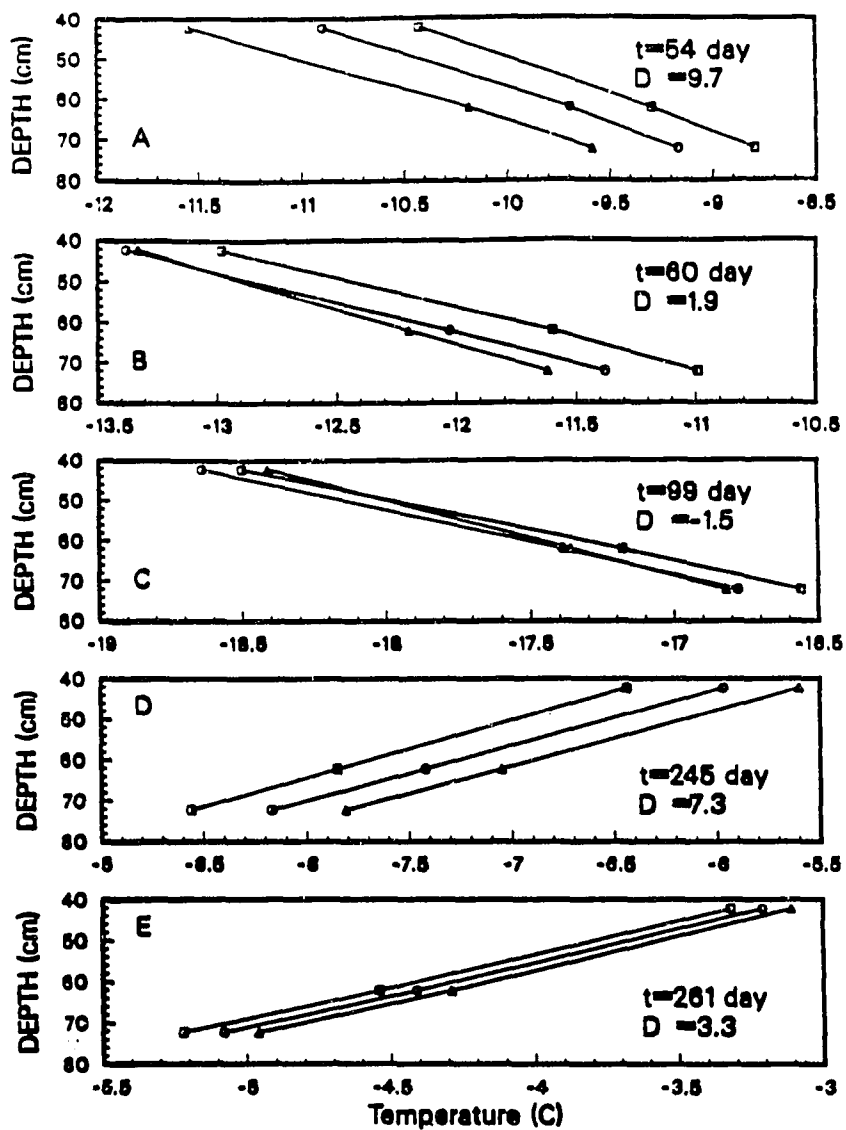


Figure 3.3 Apparent thermal diffusivity ($m^2 yr^{-1}$) estimated using (3.1) at depth of 0.621 m at selected times for the period from October 5, 1986 through October 4, 1987 at West Dock, Prudhoe Bay.

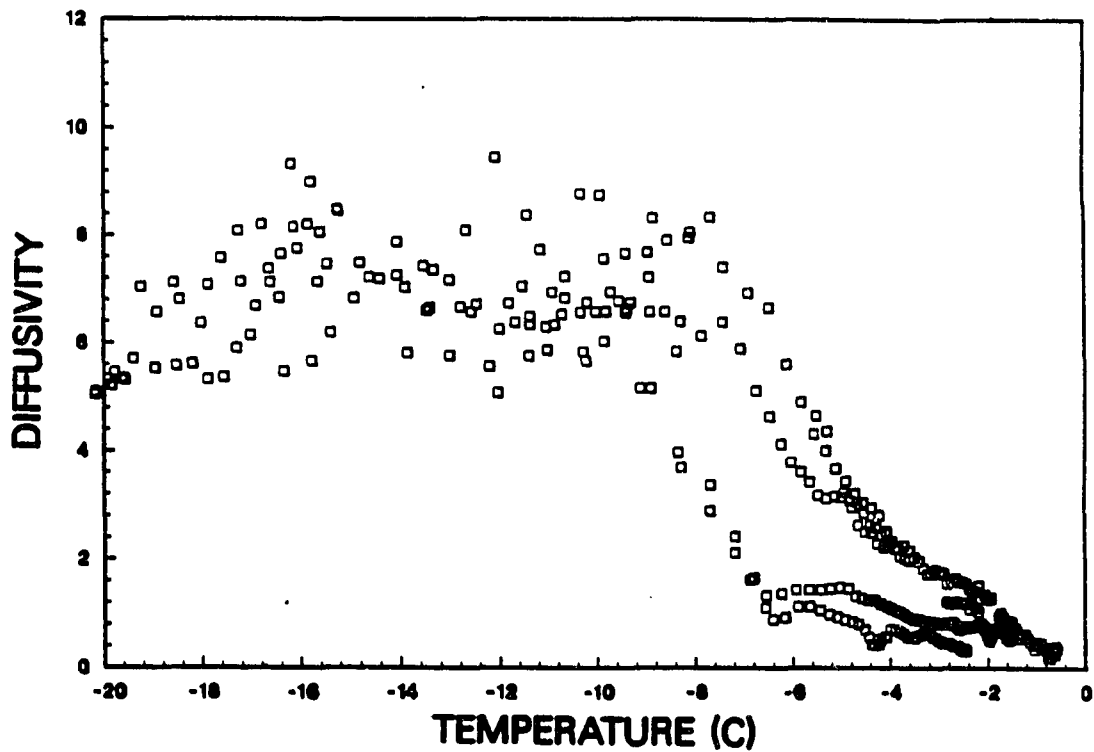


Figure 3.4 Apparent thermal diffusivity ($m^2 yr^{-1}$) estimated using (3.1) from soil temperature time series for the period from October 5, 1986 through June 23, 1991 at depth of 0.621 m with $\Delta x_1 = 0.199$ m, $\Delta x_2 = 0.101$ m and $\Delta t = 1$ day at West Dock, Prudhoe Bay. Data used in the calculation were selected as described in the text.

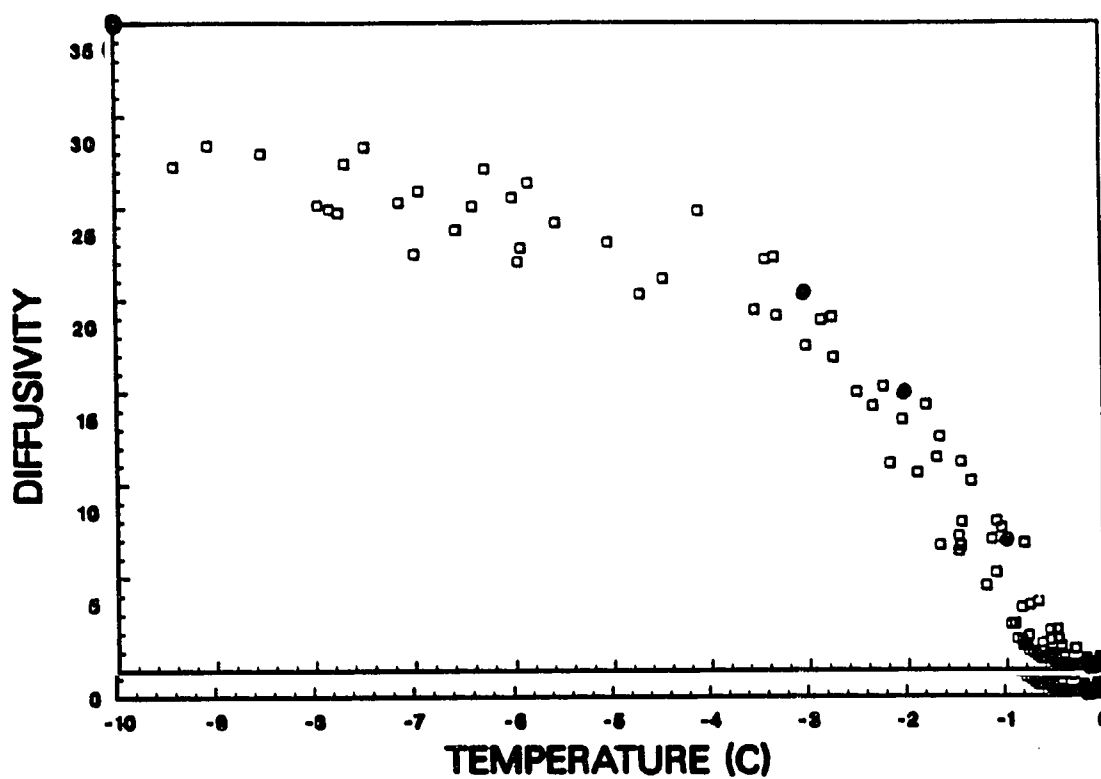


Figure 3.5 Apparent thermal diffusivity ($m^2 yr^{-1}$) estimated using (3.1) from soil temperature time series for the period from October 10, 1986 through June 23, 1991 at a depth of 0.620 m with $\Delta z_1 = 0.200$ m, $\Delta z_2 = 0.099$ m and $\Delta t = 1$ day at Deadhorse, Prudhoe Bay. Data used in the calculation were selected as described in the text.

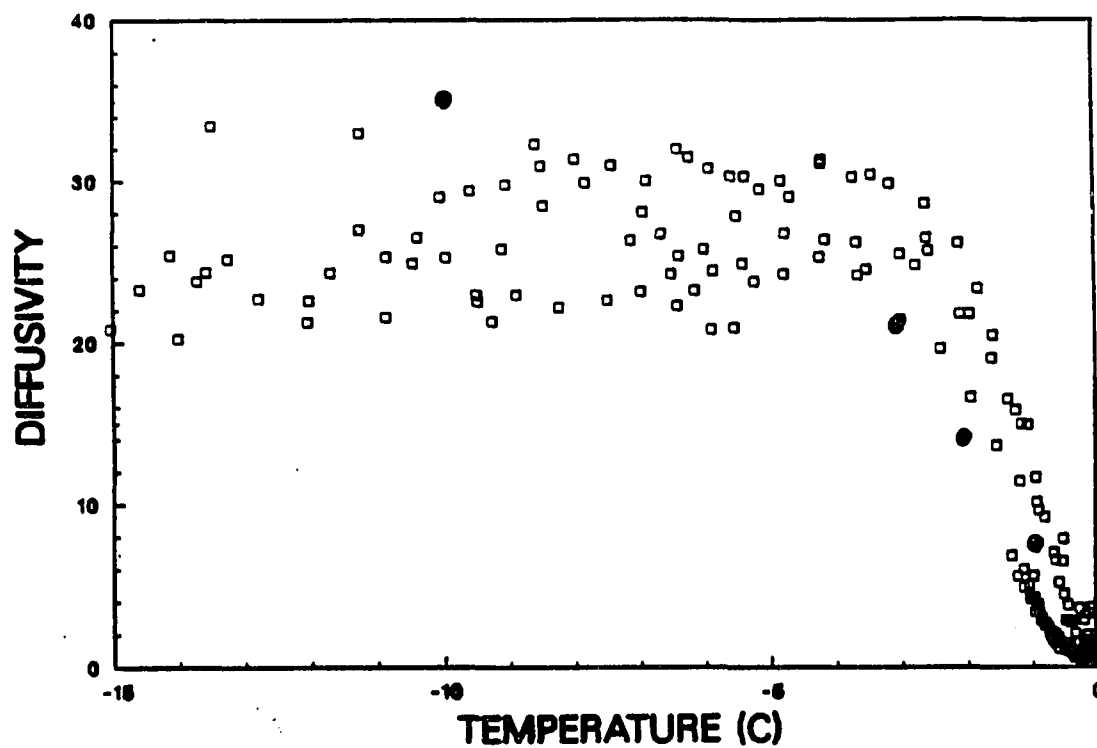


Figure 3.6 Apparent thermal diffusivity estimated using (3.1) from soil temperature time series for the period from November 29, 1986 through June 23, 1991 at a depth of 0.56 m with $\Delta x_1 = 0.098$ m, $\Delta x_2 = 0.201$ m and $\Delta t = 1$ day at Franklin Bluffs site. Data used in the calculation were selected as described in the text.

Bluffs. This indicates that the soil at West Dock site (about 300 m away from the ocean) is peat. It is also possible that there is a higher salt content than soils at Deadhorse and Franklin Bluffs. Measurements (Osterkamp, unpublished research) show that salt content at West Dock is about 15 times greater than that of normal ground water. The presence of a thicker peat layer at West Dock could also play an important role.

Another noteworthy feature of the data shown in Figures 3.4, 3.5 and 3.6 is that there is a difference in D during the cooling and warming of the upper permafrost. At West Dock the difference is very significant. The values of D during warming are less than those during cooling, particularly at West Dock. Rapid cooling of the upper permafrost occurs just after the active layer (about 0.3 to 0.4 m in thickness) freezes and usually lasts a month. The warming process occurs during the spring and lasts about two months as shown in Figure 2.2. The difference in D indicates that there may be a difference in the rate of change of unfrozen water content (Zhang, 1989). The higher value of D during cooling than during warming for a given temperature seems to imply that permafrost has a smaller rate of change of unfrozen water content during cooling than during warming. Soil temperature data show that the rate of temperature change with time during the cooling process is much greater than during warming (Figure 2.2). Laboratory experiments of Tice et al. (1988) show that there is a slight difference in unfrozen water content during cooling and warming at a given temperature in laboratory but not enough of a difference to explain these results.

Another potential explanation for the difference in D is the unequal water movement in the frozen ground during cooling and warming of the upper permafrost. Unequal water movement in the frozen ground has been reported by many investigators (Cheng, 1982, 1983; MacKay, 1984). Unfrozen water in the frozen ground can move in the direction along which the ground temperature decreases in response to an imposed thermal gradient. During the freeze-back of the active layer, water moves to the upper (downwards freezing zone) and lower (upwards

freezing zone) parts of the active layer, the last part to freeze loses water in a closed system (MacKay, 1984). After the freeze-up of the active layer, water can move upwards from the upper permafrost to the active layer but there is a very limited amount of water available for migration due to the cold temperatures. By contrast, the downward movement of water in the summer thaw periods takes place in an open system, because water in the thawed layer can be replenished by rain, snowmelt, and groundwater flow. Therefore, during the cooling processes of the upper permafrost in the early winter, D may be relatively greater due to the limited amount of water movement. In this case, the contribution of the latent heat to the apparent heat capacity is very limited. By way of contrast, during warming processes of the upper permafrost, water moves downwards to the upper permafrost and then refreezes, the latent heat released will increase the apparent heat capacity which results in a decrease in D .

Depth below 1.0 m

For depths below a meter, soil temperatures have been obtained one or two times a year by the thermistor sensor and cable system since 1983. Before 1987 when the author joined in this project, temperature data were obtained by Osterkamp (unpublished research). Since the temperature was not logged at the same depth each time, soil temperature was set at the same depth with an even space interval (1.0 m) using linear interpolation.

For depths within the annual temperature variation X_y , two temperature profiles were used for the calculation with $\Delta t = 68$ days and $\Delta x = 1.0$ m. D was estimated using (3.4). The criterion for the calculation was that the magnitude of the denominator of (3.4) was greater than 0.03°C . Figure 3.7 shows (a) temperature profiles and (b) the results of the calculation. For depths from 3.0 to 6.0 m, D ranges from 36 ± 2 to $42 \pm 3 \text{ m}^2 \text{ yr}^{-1}$ and the average value is about $40 \pm 3 \text{ m}^2 \text{ yr}^{-1}$. For depths from 14.0 to 25.0 m, D ranges from 42 ± 3 to $48 \pm 3 \text{ m}^2 \text{ yr}^{-1}$ with an average $44 \pm 3 \text{ m}^2 \text{ yr}^{-1}$.

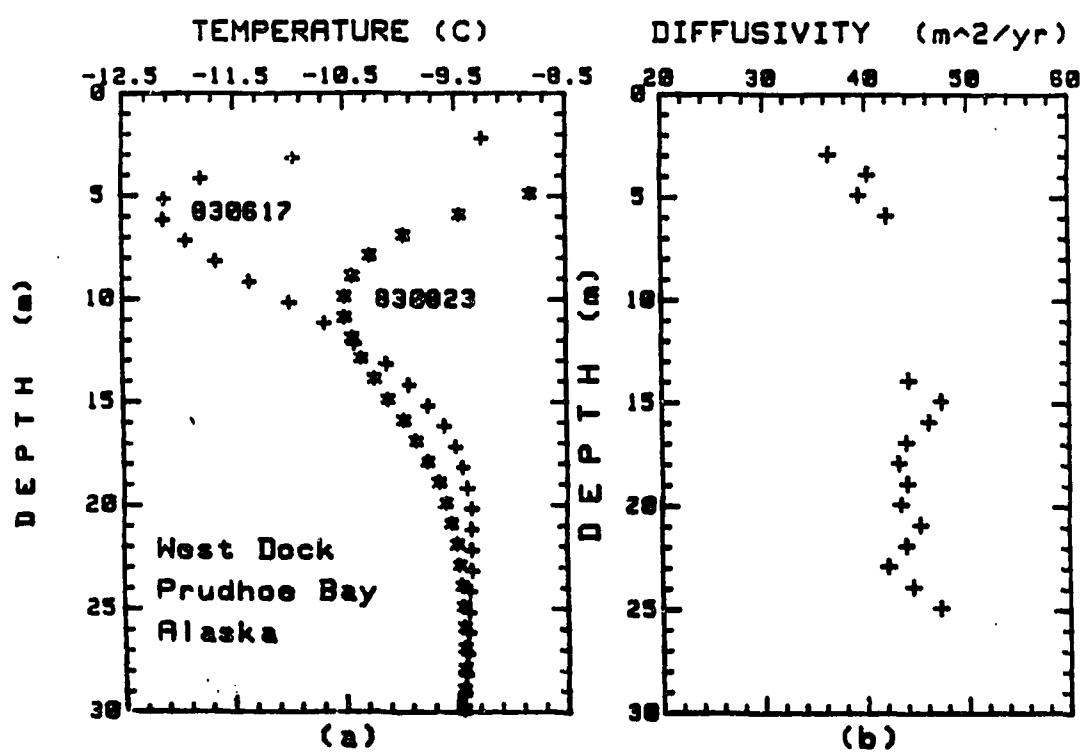


Figure 3.7 Soil temperatures (a) and apparent thermal diffusivity (b) estimated using (3.4) from soil temperature profiles with $\Delta x = 1$ m and $\Delta t = 68$ days at depths between 3 and 30 m at West Dock, Prudhoe Bay.

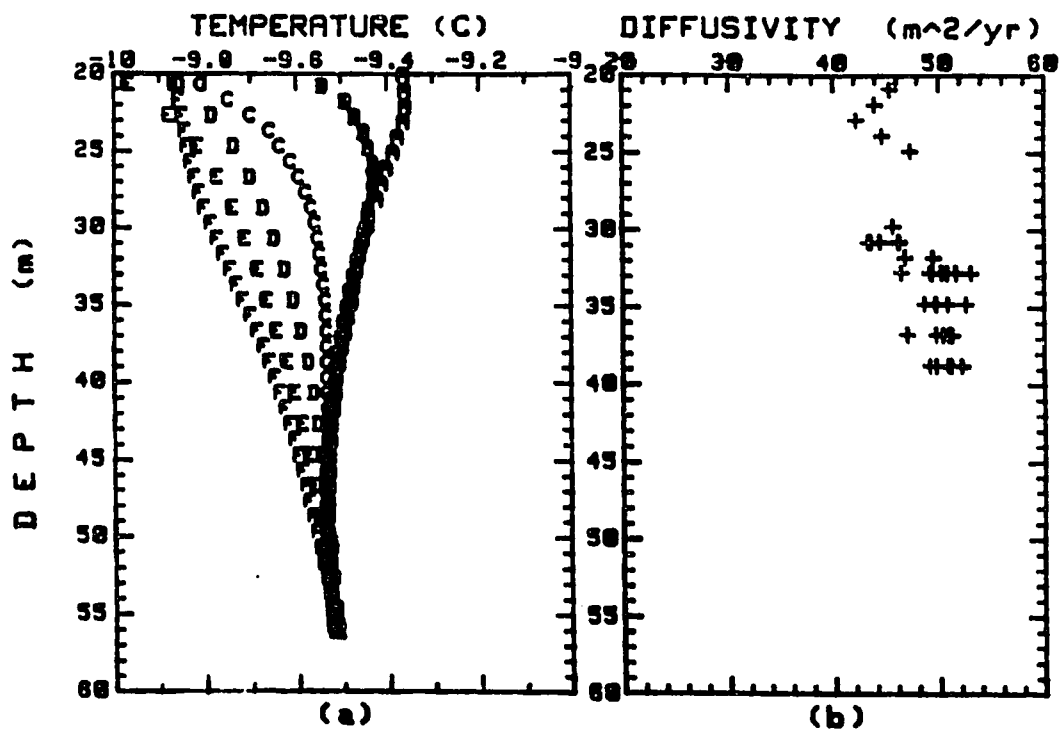


Figure 3.8 (a) Temperature variation of permafrost below 20 m since 1983 at West Dock, Prudhoe Bay. (b) Apparent thermal diffusivity of permafrost below 20 m estimated using (3.3) from soil temperature profiles with Δz ranging from 3 m to 6 m and Δt ranging from 0.8 years to 1.1 years. Dates of temperature profiles, A — Jun. 17, 1983; B — Aug. 23, 1983; C — Sep. 13, 1984; D — Jul. 1, 1985; E — Aug. 22, 1986; F — Jun. 25, 1987.

For depths below 30 m, the time interval varied from 0.80 to 1.10 years and the corresponding space interval from 3.0 to 6.0 m, depending upon the temperature difference between the two consecutive temperature measurements. D was estimated using (3.3) and selected temperature profiles with temperature data where the magnitude of the denominator of (3.3) was greater than 0.03°C . Figure 3.8 shows (a) the temperature variation of permafrost below 20 m since 1983 and (b) the results of the calculation for D based upon three temperature measurements ((3.3) was used). Figure 3.8 (b) shows some variation of D at the same depth. This variation may be produced by variable Δx and Δt , or it may be the result of the errors in the method. D varies from 45 ± 3 to $53 \pm 4 \text{ m}^2 \text{ yr}^{-1}$ and the average value is about $49 \pm 4 \text{ m}^2 \text{ yr}^{-1}$. For depths below 40 m, the temperature variation is so small that the method is not applicable.

3.4 Summary

Soil samples were taken during the summer of 1991 to a depth of about 0.60 m to determine total moisture content, bulk density and the loss on ignition for three sites. It was found that the top 0.2 m to 0.3 m of the soils consists of live and dead organic materials mixed with wind blown silt. The soil was drier and had less organic content at Deadhorse site than the other two sites. There is silt below the peat layer with a few organic inclusions. Dry bulk density of the mineral soils ranges from 1350 kg/m^3 to about 1500 kg/m^3 . The soil moisture was also measured by the TDR method (Osterkamp, unpublished research) *in situ* and the results were consistent with the measurements in the laboratory, with the maximum percent difference less than 10%.

The apparent thermal diffusivity of the active layer and upper permafrost was determined from soil temperature time series using a numerical scheme (Zhang and Osterkamp, see also

Appendix A) . Since in practice, it is very difficult to maintain an exact even space increment (Δx) and even time increment (Δt) for soil temperature measurements, an equation with uneven space increments Δx_1 , Δx_2 and even time increment Δt and an equation with even space increment Δx and uneven time increments Δt_1 and Δt_2 was derived for the purpose of estimating the values of D. In some cases, soil temperatures at whole number depths were obtained using linear interpolation.

Soil temperatures were measured and recorded at depths of 2.2 cm, 7.2 cm, and 12.3 cm with a time interval of 10 min. D was estimated using uneven space increments $\Delta x_1 = 5.0$ cm, $\Delta x_2 = 5.1$ cm and even time increment $\Delta t = 10$ min. There were two distinct values for D at about $3 \text{ m}^2/\text{yr}$ and about $6.5 \pm 3.5 \text{ m}^2/\text{yr}$. Using the same temperature data, the thermal diffusivity obtained by the amplitude ratio method (Zhang, 1989) for the layer between 0.0 m and 0.123 m is about $12.8 \pm 0.8 \text{ m}^2/\text{yr}$, much higher than the average value of D obtained by the numerical method.

For depths between 0.4 m and 1.0 m, D was determined with $\Delta t = 1$ day since the daily amplitude of ground surface temperature was often reduced to less than 1°C due to the insulating effect of snow cover. At West Dock, soil temperatures were measured at depths of 0.422 m, 0.621 m and 0.722 m and apparent thermal diffusivity was estimated with uneven space increments $\Delta x_1 = 0.199$ m and $\Delta x_2 = 0.101$ m. Initial results showed considerable scatter with a range from 12.5 to $-2.5 \text{ m}^2/\text{yr}$. More reliable values can be obtained if the three temperature profiles show a continuous cooling or warming trend which gives a larger rate of temperature change with time and larger temperature gradients. Crossover of the temperature profiles reduce the rate of temperature change and temperature gradients at nodes involved, resulting in a decrease of D.

D was estimated by the above procedures with uneven space increments and even time increment at West Dock, Deadhorse and Franklin Bluffs. D shows a strong temperature

dependence at the three sites. The temperature dependence of D is thought to be associated with the presence, temperature dependence, and movement of unfrozen water in the active layer and upper permafrost. The range of temperature dependence of D at West Dock was larger (from -0.6°C to -8.0°C) than at Deadhorse (from about 0°C to -4°C) and at Franklin Bluffs (from about 0°C to -3°C). The average value of D at West Dock for ($T < -8^{\circ}\text{C}$) is about $7.7 \pm 2.5 \text{ m}^2/\text{yr}$; about $28 \pm 3 \text{ m}^2/\text{yr}$ at Deadhorse ($T < -3^{\circ}\text{C}$) and about $29 \pm 3 \text{ m}^2/\text{yr}$ at Franklin Bluffs for ($T < -4.0^{\circ}\text{C}$). This indicates that soils at West Dock site (about 300 m away from the ocean) may be different (e.g. peat) and have a higher salt content than soils at the other two sites.

Another noteworthy feature shows that the values of D during warming of permafrost are less than during cooling. It may indicate that there is a larger difference in the rate of change of unfrozen water content during cooling and warming processes (Zhang, 1989). Soil temperature data show that the rate of temperature change with time during the cooling process is much greater than during the warming process. Tice *et al.* (1988) showed that there is only a slight difference in unfrozen water content during cooling and warming at a given temperature which can not explain the observations. A possible explanation for the difference in D may be the unequal water movement during the cooling and warming processes of the upper permafrost. During the cooling processes after the freeze-up of the active layer, water movement upwards from the upper permafrost to the active layer may be very limited due to its cold temperatures; while the downwards movement of water in the summer thaw periods takes place in an open system at warmer temperatures. This movement of the water from the thawed layer during warming to the upper permafrost where it may refreeze would release latent heat increasing the apparent heat capacity which results in a decrease in D .

For depths below a meter, soil temperature was measured with uneven space and time intervals at different levels. However, the displacement from each logging and uneven space

increment is only a few centimeters compared with the 1 m increment. The soil temperature was set at the same level using linear interpolation. D was estimated with Δz ranging from 1.0 m to about 6.0 m, and Δt ranging from 2 months to 1.1 years, depending upon the temperature difference between the two consecutive temperature measurements. D was estimated with selected data and the more reliable values were chosen when $\Delta_{zz}T \geq 0.03^\circ \text{C}$. For depths from 3.0 to 25.0 m, the average D ranges from $36 \pm 2 \text{ m}^2/\text{yr}$ to $44 \pm 3 \text{ m}^2/\text{yr}$. For depths from 30 m to about 40 m, the average D varies from $45 \pm 3 \text{ m}^2/\text{yr}$ to about $53 \pm 4 \text{ m}^2/\text{yr}$.

CHAPTER 4

Seasonal Snow Cover and its Influence on the Ground Thermal Regime

4.1 Introduction

Heat exchange between the land surface and the atmosphere is driven by climate and modified by local environmental factors including seasonal snow cover which experiences large fluctuations spatially and temporally. The thermal properties of snow introduce competing effects with air temperature and significantly influence the ground thermal regime. The higher surface albedo causes a reduction in the absorbed solar energy and results in a cooling of the ground. On the other hand, due to its low thermal conductivity, snow acts as an insulator and, as it is present only during the cold portion of the year, it can raise the MAGST by several degrees above the ambient MAAT.

The insulating effect of seasonal snow cover on the ground thermal regime, especially on the thermal regime of permafrost in cold regions, is well-known. *Lachenbruch* (1959) presented a simplified analytical solution with constant thermal properties to investigate the influence of snow cover on the ground surface temperature and annual amplitude. *Mackay et al.* (1975) carried out field measurements of the influence of snow on ground surface temperatures at a depth of 0.90 m during 1968-1973 in Garry Island, N. W. T. Their results show that snow-ground interface temperature varies significantly from site to site within a few hundred meters due to the thickness variations of the snow cover. *Smith* (1975) studied the variations in ground thermal regime over a small area in the east-central part of the Mackenzie Delta, Northwest Territories. The results show that snow cover is a permafrost-controlling

factor in that area; where accumulations are greatest a talik formed due to the insulating effect of deep snow. *Goodrich* (1976, 1982, 1983) developed a numerical thermal model which included snow cover and allowed a detailed study of the effect of snow cover on long-term, periodic, steady-state equilibrium ground temperatures. *Zhang et al.* (1985) found that due to the snow insulating effect, the lower limit of permafrost in the Altai Mountains is a few hundred meters higher than the lower limit in the other alpine permafrost regions in the Northern Hemisphere.

Snow studies in Alaska north of the Brooks Range include snow measurements and redistribution (*Black*, 1954 ; *Wendler*, 1974, 1978 ; *Benson*, 1982); physical and thermal properties (*Benson*, 1982 ; *Liston*, 1986 ; *Sturm*, 1991); heat and mass transfer in seasonal snow cover (*Sturm*, 1992); snow hydrology (*Dingman et al.*, 1980 ; *Hinzman*, 1991); and snow as a possible indicator of climatic change (*Foster*, 1989 ; *Dutton and Endres*, 1991 ; *Foster et al.*, 1991).

Influence of the seasonal snow cover on heat balance at the ground surface is another major subject in this area. *Weller et al.* (1972) provided the details of the tundra microclimate changes in the heat balance during snowmelt in the Barrow area, showing dramatic changes in the heat balance during this period when surface conditions were changing very rapidly. Yearly variations of surface albedo allow description of four distinct seasons: winter stationary, spring transitional, summer stationary, and autumn transitional (*Maykut and Church*, 1973). *Weller and Holmgren* (1974) conducted complete energy balance studies of the snow/tundra surface during different times of the year and found six periods with distinctly different energy balance characteristics which all related to the presence or absence and conditions of the seasonal snow cover. A concise summary of climate, snow cover, microclimate, and hydrology of the Barrow area is provided by *Dingman et al.*, (1980) .

Influence of the seasonal snow cover on the ground thermal regime could have a significant effect on the development of the active layer and permafrost temperatures. *Outcalt et al. (1975)* conducted a computer simulation of the snowmelt and soil thermal regime at Barrow. However, very little work has been done since then.

In this chapter, the development of seasonal snow cover (such as timing, duration, snowmelt) and its influence on the ground thermal regime (such as the ground surface and permafrost temperatures) are investigated.

4.2 Data Source and Methods

Air, ground surface, and soil temperatures from the surface to about 60 m depth were measured at different time intervals and with different instrumentation at West Dock, Deadhorse and Franklin Bluffs (see Chapter 2 and 3 for details). Snow data in this region were from various sources. Annual precipitation was measured with a Wyoming Gauge at Prudhoe Bay starting in the 1976-1977 hydrological year (Soil Conservation Service, 1991). The measurements were conducted in the first week of the month and continue until present (*Clagett, personal communication*). Precipitation, snowfall and snow on ground were also reported at the meteorological stations at Barrow, Barter Island, Prudhoe Bay, Umiat, and Fairbanks (*Local Meteorological Data, 1991*).

The date when the seasonal snow cover first becomes established in the autumn and finally disappears in the spring is of particular interest for climatic change and permafrost studies. For sites at West Dock, Deadhorse and Franklin Bluffs, the beginning and ending of seasonal snow cover were determined by the sharp change in the daily amplitude of ground surface temperature (see Chapter 4.3.2 for details). For stations at Barrow, Barter Island, Prudhoe Bay, Umiat and Fairbanks, the date of seasonal snow cover appearance or disappearance was

given as the day when a trace of snow can be observed in the autumn or can no longer be observed in the spring at the reporting station. The results obtained by these two methods at Prudhoe Bay are very consistent.

4.3 Seasonal Snow Cover

Snow is a feature that responds rapidly to changing climate, and a given climate forcing may influence the snow cover differently in different geographic regions in its magnitude, timing, and evolution. The length of the seasonal snow cover affects the annual surface albedo, which in turn impacts the energy balance of an area. Changes in the magnitude, timing and evolution processes of seasonal snow cover can provide different feedbacks to the climate system, and thus influence the ground thermal regime differently. The systematic study of snowfall and seasonal snow cover may provide a better understanding of interactions between the atmosphere and the ground thermal regime.

4.3.1 Timing and Duration

The seasonal snow cover lasts for eight to nine months. *Benson (1982)* divided the year into nine "winter months", September through May, when all precipitation was assumed to fall as snow and three "summer months", June through August when all precipitation was assumed to fall as rain, estimated by the relative amount of snow and rain represented by raw data at Barrow and Barter Island. The "winter" can be reduced to eight months, about from the middle of September through middle of May, near Sagwon and Toolik Lake. Table 4.1 shows the timing and duration of seasonal snow cover at the selected stations and sites. The first day snow on ground varies from late August to early October; while the date of seasonal snow cover disappearance in the spring can be about three weeks earlier inland than along

the coast during the period of record. Length of the snow free period increases inland from the coast which may be due to the air temperature variations from the coast to inland. Mean monthly air temperature in April is $-17.6^{\circ} \pm 2.1^{\circ}$ C for stations from the coast to inland. The maximum daily air temperature is below 0° C which keeps snow from melting, although the solar radiation increases and penetrates into the snowpack but it may be still very limited for snow melting. As the spring progresses, increases in the air temperature inland are much faster than along the coast. In May, mean air temperature inland is over 3° C higher than along the coast and in June it is over 7° C. The snow melts faster and disappears earlier inland than along the coast as shown in Table 4.1.

Table 4.1 Timing and duration of seasonal snow cover at the selected stations and sites P_1 , P_{max} and P_2 represent the average dates and their deviations of first, maximum thickness and last day of snow on ground, respectively, over the period specified for each station or site.

Stations	P_1	P_{max}	P_2	Snow free (day)	period
Barrow	Sep. 20 \pm 10	Apr. 25 \pm 12	Jun. 17 \pm 10	95 \pm 13	1947-1991
West Dock	Sep. 14 \pm 9	-	Jun. 6 \pm 12	102 \pm 18	1986-1991
Barter Island	Sep. 23 \pm 8	Apr. 28 \pm 27	Jun. 16 \pm 8	100 \pm 16	1957-1988
Deadhorse airport	Sep. 6 \pm 14	-	May 28 \pm 14	102 \pm 18	1986-1991
Deadhorse	Sep. 10 \pm 15	-	May 24 \pm 17	111 \pm 11	1986-1991
Franklin Bluffs	Sep. 26 \pm 18	-	May 25 \pm 9	117 \pm 13	1986-1991
Umiat	Oct. 2 \pm 6	Apr. 23 \pm 7	May 22 \pm 8	133 \pm 11	1978-1991
Fairbanks	Oct. 10 \pm 13	Feb. 24 \pm 23	Apr. 29 \pm 9	164 \pm 11	1950-1991

Figures 4.1 and 4.2 show the first and last day of snow on the ground for the period from 1957 through 1991 at Barrow and for the period from 1957 through 1988 at Barter Island. The date when seasonal snow cover first becomes established at both stations shows a relatively constant time over the period. However, for Barrow, there has been a trend towards earlier

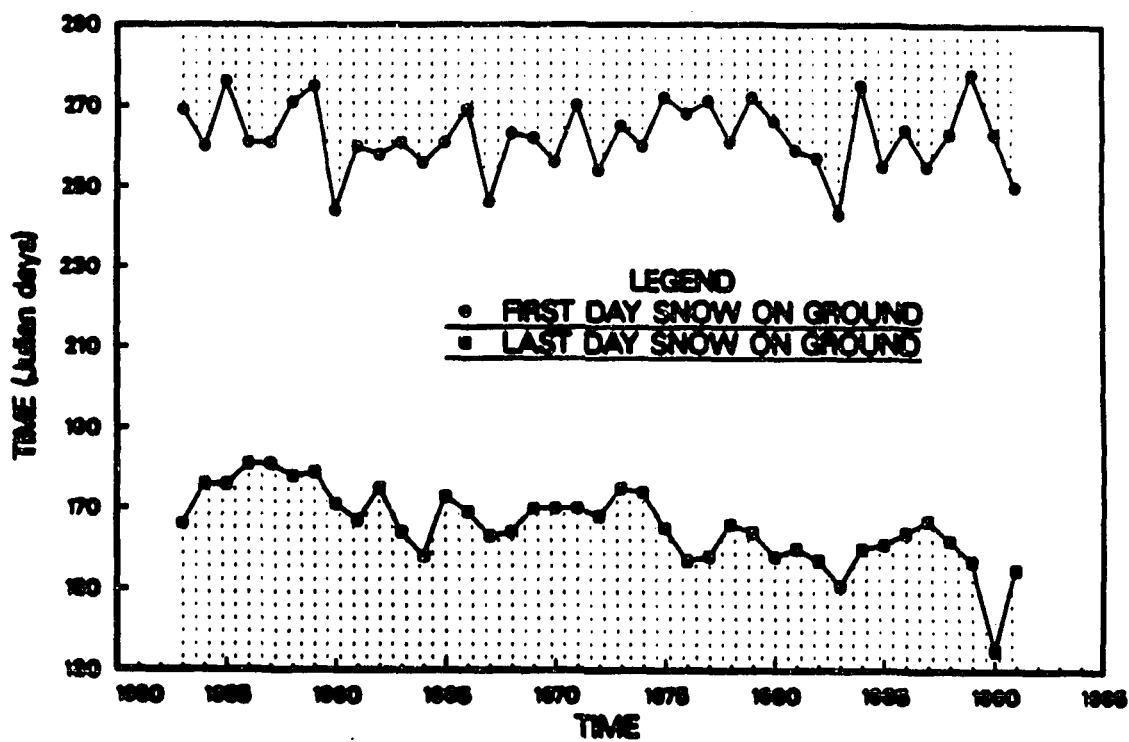


Figure 4.1 First and last day of snow on the ground surface for the period from 1953 through 1991 at Barrow, Alaska.

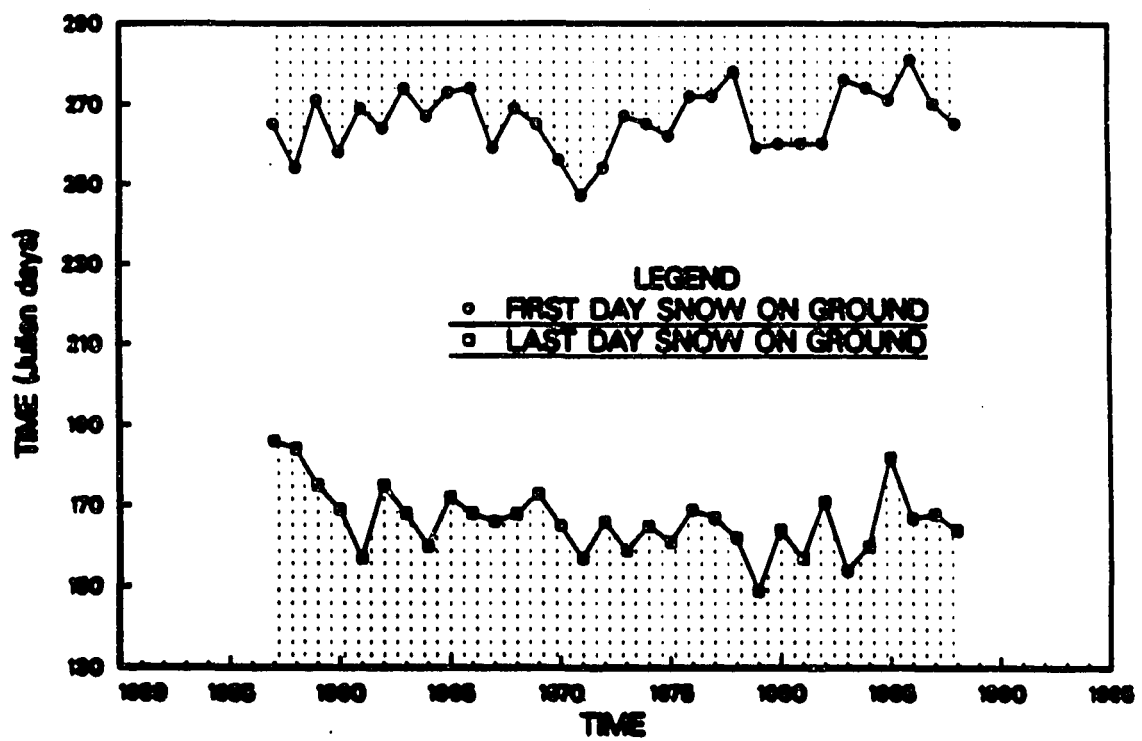


Figure 4.2 First and last day of snow on the ground surface for the period from 1957 through 1988 at Barter Island, Alaska.

snowmelt since about 1953 as reported by *Foster (1989)* and *Foster et al. (1991)*. This trend is not very obvious at Barter Island over the period from 1957 to 1988. *Dutton and Endres (1991)* determined the date of snowmelt near Barrow from radiometric *in situ* measurements of the tundra solar albedo. Their results show that there is no significant trend in the date of snowmelt near Barrow. They believe that *Foster et al. (1991)* results are not typical, but rather a result of urbanization at Barrow.

4.3.2 Evolution of Seasonal Snow Cover

The development of the seasonal snow cover is influenced by the magnitude, timing and duration of snowfall, low temperatures, blowing snow, existence of permafrost, local microrelief, and snow metamorphism. The pattern of seasonal snow cover development depends strongly upon the magnitude and timing of snowfall. Figure 4.3 shows the average monthly and cumulative snowfall at Barrow over the period of record. Snowfall occurs all year along the coast. During the summer (June through August), snowfall is relatively small, less than 10% of the annual total. The maximum monthly snowfall occurs in October and more than 50% of the annual snowfall occurs in September through November. The amount of snowfall from December through May is relatively low and evenly distributed. This pattern is similar to that at Barter Island.

Figure 4.4 shows monthly, cumulative snowfall and snow on the ground and monthly air temperatures for the period from July 1, 1953 to June 30, 1954 at Barrow. Snowfall started in August but the continuous snow cover began in late September. There were two peaks of monthly snowfall at November of 1953 and January of 1954, and two major step increases in thickness of snow on ground. After January, 1954, the thickness of snow cover continued to

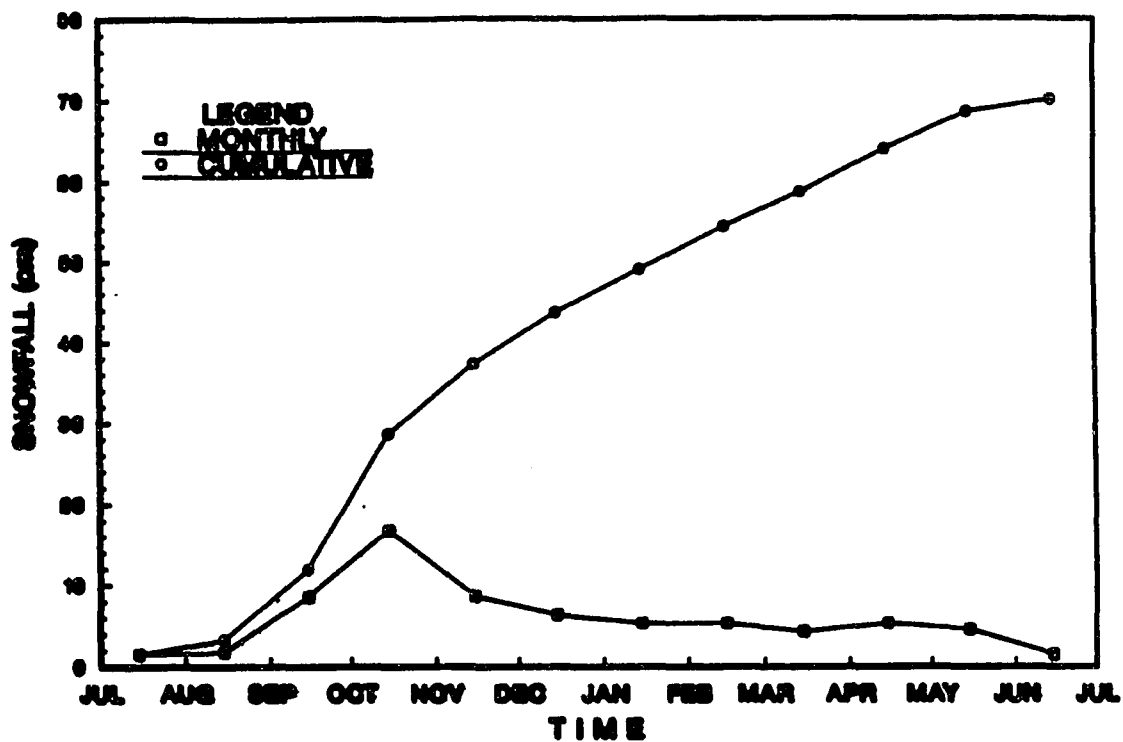


Figure 4.3 Average monthly and cumulative snowfall for the period of record from 1921 through 1991 at Barrow, Alaska.

increase at a relatively lower rate. The snow built to a thickness of over 20 cm within the first one and half months, about 50% of its maximum thickness during 1953-1954.

Wind conditions (wind speed and direction) determine the structure and thickness variations of the seasonal snow cover from place to place (*Wendler, 1978*). *Wendler (1978)* compared blowing snow and snow precipitation relationships at Barrow and Barter Island and found that winds from the east and west were frequently associated with blowing snow at those stations. Barter Island was found to receive more snow than Barrow, with most of Barter Island snowfall occurring with west winds and Barrow snowfall occurring with east winds.

Billelo (1969) obtained an empirical correlation formula between seasonal snow pack density and seasonal mean wind speed. *Goodrich (1976)* reported the initial wind speed for blowing snow is about 4 *m/sec*; Table 4.2 shows the average and maximum monthly wind speed for periods from July 1953 to June 1954 and from July 1967 to June 1968 at Barrow. The average monthly wind speed for these two years was about 4.5 *m/sec* and 4.8 *m/sec*, with the maximum ranging from about 10 *m/sec* to about 25 *m/sec*. These wind conditions have a significant effect on snow redistribution in the Arctic tundra regions. After the establishment of the initial snow cover, the surface roughness is reduced significantly and permits more effective snow drifting. Snow is deposited in drift traps and, as winter progresses, the surface microrelief becomes more and more subdued. Although fresh snow continues to accumulate throughout the winter, the steady winds constantly reshape the pattern of the seasonal snow cover (*Dingman, 1980*). Across the smoothed surface, barchan dunes form and move during storm periods. *Sturm (personal communication, 1993)* noted that the thickness of the seasonal snow cover can vary about 50% to over 100% within a few meters in the Prudhoe Bay region. Our field survey in Spring of 1993 near Barrow showed a similar pattern.

After the seasonal snow cover reaches its maximum thickness around late April, it starts to decrease. The seasonal snow cover completely disappears in the middle of June along

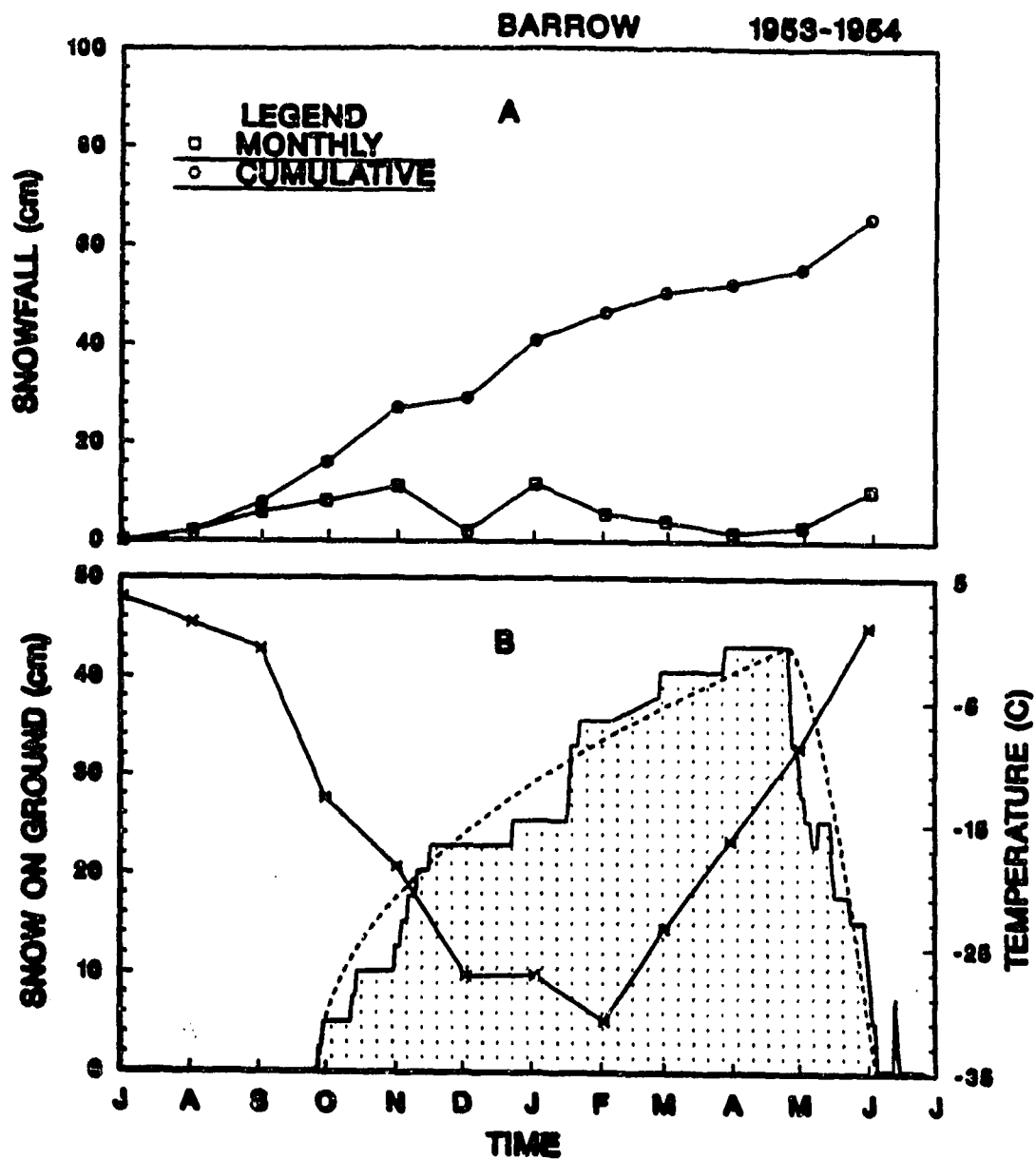


Figure 4.4 Monthly and cumulative snowfall (A) and snow on ground, mean monthly air temperature and approximate snow build-up processes (B) during 1953-1954 at Barrow, Alaska.

Table 4.2 Wind speed during 1953-1954 and 1967-1968 at Barrow

	Jan	Feb	Mar	Apr	May	Jun	Jul	Aug	Sep	Oct	Nov	Dec	Ann.
1953 — 1954													
Mean	4.8	5.2	5.4	6.3	4.1	4.6	4.6	5.2	4.8	3.7	4.6	5.5	4.9
Max.	17.6	13.1	25.2	15.8	13.1	18.0	19.4	14.0	15.3	10.8	10.8	13.5	19.4
1967 — 1968													
Mean	4.3	5.1	5.8	4.5	5.2	4.2	5.0	3.5	4.1	3.9	5.4	3.7	4.9
Max.	10.8	13.1	15.8	11.3	11.7	14.9	17.6	13.1	11.7	11.3	17.6	8.1	17.6

the coast and in late May inland. Generally, it takes 40 to 50 days for the disappearance of seasonal snow cover along the coast and about 30 days inland as shown in Table 4.1. This is probably because the surface receives more solar radiation and air temperature increases faster inland than along the coast during Spring.

Although the evolution of seasonal snow cover is a complicated process and affected by many factors, it can be approximated by

$$H_s(t) = \begin{cases} 0 & 0 \leq t \leq P_1 \\ A H_{max} & P_1 \leq t \leq P_2 \\ (1 - B) H_{max} & P_2 \leq t \leq P_3 \\ 0 & P_3 \leq t \leq P \end{cases} \quad (4.1)$$

where H_s is thickness of seasonal snow cover in meters at time, t , in days, P_1 is the first day of steady seasonal snow cover on the ground, P_2 is the time at which snow thickness reaches its maximum, H_{max} in m, P_3 is the last day of a steady seasonal snow cover on ground, and

$$A = \left(\frac{t - P_1}{P_2 - P_1} \right)^{n/2}$$

$$B = \left(\frac{t - P_2}{P_3 - P_2} \right)^{n/2}$$

where n is a positive integer.

In (4.1), the time periods $0 \leq t \leq P_1$ and $P_3 \leq t \leq P$ are generally snow free, where $P=365$ days starts at July 1. During these periods, snow may stay on the ground for a few hours or a few days. The time period $P_1 \leq t \leq P_2$ is for the accumulating processes and $P_2 \leq t \leq P_3$ for the melting processes. The accumulating and melting processes vary with the choice of n . Figure 4.5 shows a few possible combinations by varying n . As shown in Figure 4.4, $n = 1$ for $P_1 \leq t \leq P_2$ and $n = 3$ for $P_2 \leq t \leq P_3$ would give a best fit to data.

Generally, the evolution of the seasonal snow cover throughout the winter is a continuous process. From the beginning when the steady snow cover is established through November when the active layer freezes completely, the thickness of the seasonal snow cover increases rapidly and has a relatively low density. At this stage, the temperature gradients are greatest and the depth hoar may start to form. From December through the middle decade of April, the maximum thickness of the seasonal snow cover is reached, the rate of snow thickness increases are relatively low, depth hoar and wind slab are well developed, and some fresh snow may exist on the top of the wind slab. As the air temperature increases, snow starts to melt in late April or early May.

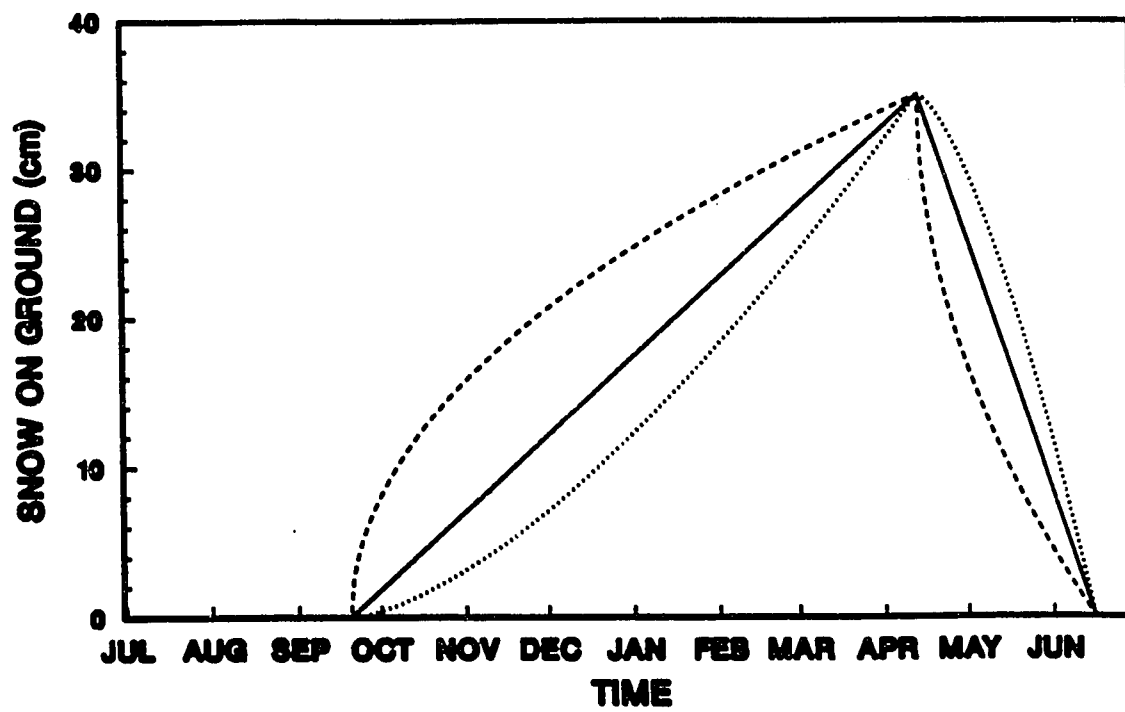


Figure 4.5 Approximate snow accumulation and melting processes at Barrow, Alaska.

4.4 Effect on Ground Thermal Regime

Seasonal snow cover acts as an insulating layer between the atmosphere and ground surface and changes in timing, duration, accumulation and melting processes, thickness, structure, and physical and thermal properties would have significant effects on the ground thermal regime. Seasonal snow cover reduces the amplitude of daily surface temperature and the amount of heat exchange between the atmosphere and ground surface, thus indirectly increasing ground surface temperature by several degrees.

4.4.1 Amplitude of Daily Ground Surface Temperature

The amplitude of daily temperature is defined as $A_d = (T_{max} - T_{min})/2$. Acting as a filter, snow cover can reduce the amplitude of daily ground surface temperature by five to over 10 times compared with the amplitude of daily air temperature as shown in Figure 4.6C. During the winter when the seasonal snow cover exists, the amplitude of daily air temperature varies from 2° C to 6° C, while the amplitude of daily ground surface temperature underneath snow ranges from 0.1° C to about 1° C. During the summer, the amplitudes of both daily air and ground surface temperature are of the same magnitude (Figure 4.6C). There is a sharp change in the amplitude of daily ground surface temperature at the date when snow disappears in the spring and at the date when snow cover first becomes established in the Autumn. This sharp change in the amplitude can provide some evidence about the presence or absence of seasonal snow cover on the ground surface. Table 4.1 shows that the date when the ground surface is snow free as determined by the change in the daily surface amplitude is consistent with the date measured at the reporting stations when a trace (snow thickness is less than 1.0 inch) was observed.

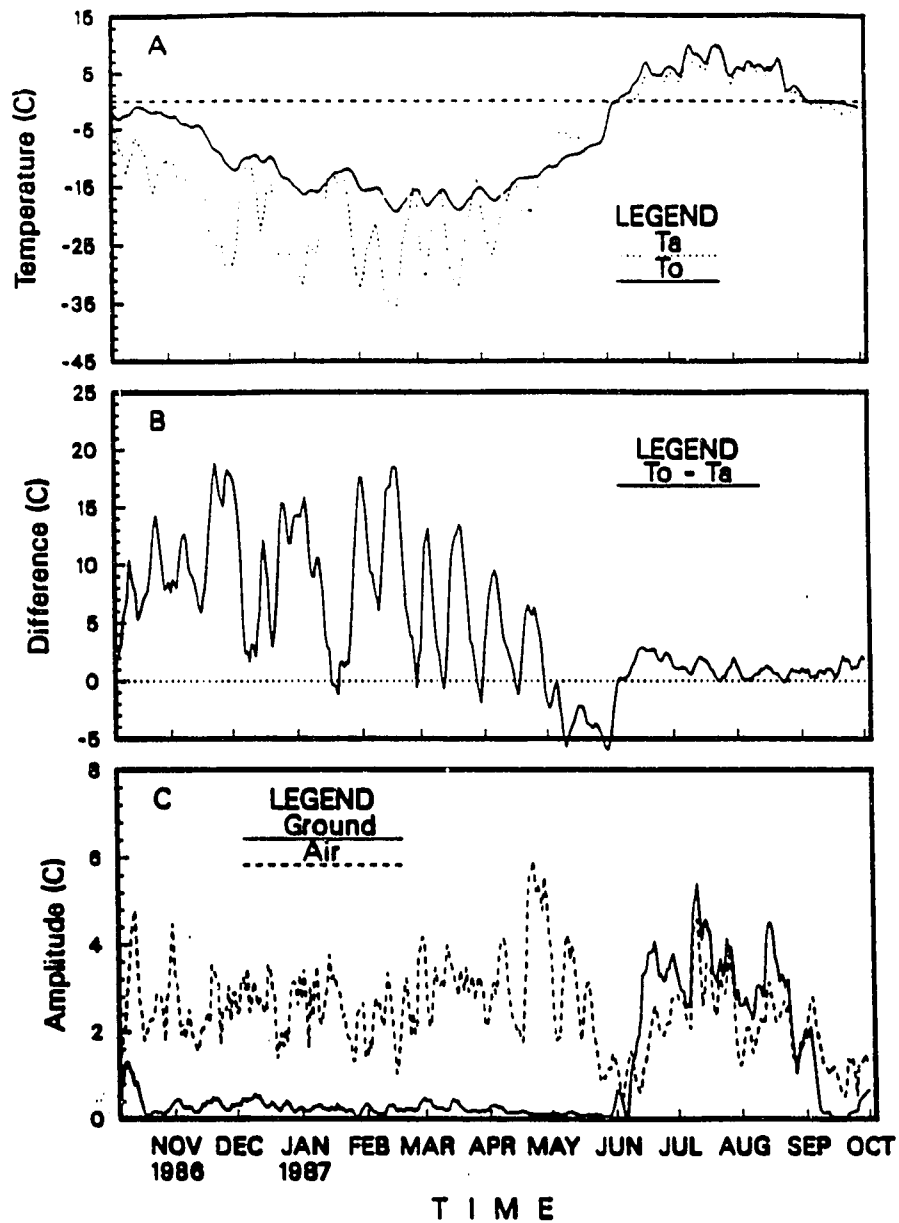


Figure 4.6 Mean daily air and ground surface temperature (A), the difference between mean daily ground surface and air temperature (B), and variation of daily amplitude of mean ground surface and air temperature (C) from November of 1986 to October of 1987 at Franklin Bluffs in Alaska north of the Brooks Range.

4.4.2 Ground Surface Temperature

At different times of the year, the net effect of the seasonal snow cover on the ground surface temperature is different. During the snow free period, in the event of snowfall, the instantaneous snow cover on the ground, usually lasts a few hours to a few days, may cool the ground surface and reduce the difference, ΔT_{ga} , between daily ground surface temperature and air temperature. The average value of ΔT_{ga} for summer (snow free) over five years measured at West Dock, Deadhorse and Franklin Bluffs was about 1.3° C as shown in Figure 4.7.

After the establishment of continuous seasonal snow cover on the ground surface, ΔT_{ga} increases. As the winter progresses, ΔT_{ga} becomes greater. ΔT_{ga} in November is always the greatest every year at the three sites. The air temperature can cool rapidly to -15° C or even lower than -20° C in a few days, while the surface temperature may stay near -5° C until November when the active layer freezes up (Figure 4.6A). This is because the latent heat released from the active layer “warms” the ground surface (*Sturm, 1989*) and seasonal snow cover with low density reduces the loss of heat from the surface to the atmosphere due to its low thermal conductivity. At this stage, the temperature gradients within the seasonal snow cover are greatest which is a favourable condition for formation of depth hoar which enhances the insulating effect of snow due to its low density.

During the middle of winter (December through February) when the seasonal snow cover becomes thicker and the active layer freezes up, the daily ground surface temperature sometimes can be 10° C higher than the daily air temperatures, the highest value recorded was 35° C in the winter of 1988 at Franklin Bluffs. In the meantime, the ground surface temperature could be lower than air temperature during a storm when air temperature increases by 10° to 15° C in a few days. This can be seen from Figure 4.6B where the daily ΔT_{ga} was close to 0° C or negative. In this case, seasonal snow cover decreases the heat flux from the atmosphere into

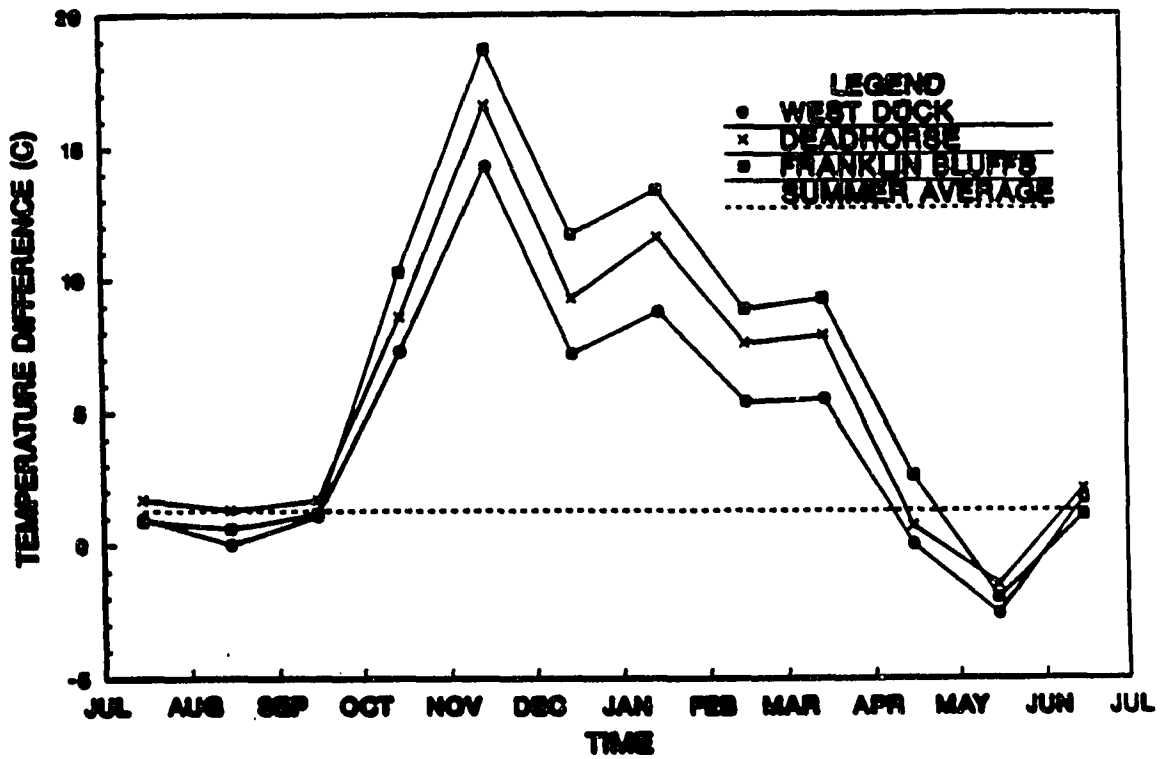


Figure 4.7 The difference between mean monthly ground surface temperatures and air temperatures for the period from 1986 through 1991 at West Dock, Deadhorse and Franklin Bluffs.

ground. As a whole, the difference between MMGST and MMAT is less than the difference in November.

In April, when seasonal snow cover reaches its maximum thickness, ΔT_{ga} decreases to the summer average value when the ground is generally snow free as shown in Figure 4.7. The incoming shortwave solar radiation and air temperature increase steadily in spring, while the response of the surface temperature to this increase is very slow, thus ΔT_{ga} decreases substantially. As the melting season progresses, air temperature increases much faster than the ground surface temperature as shown in Figure 4.6A. During May, the average daily (Figure 4.6A and 4.6B) and monthly (Figure 4.7) air temperatures are a few degrees higher than the ground surface temperatures and ΔT_{ga} is negative. When snow melts at the top layer, the temperature gradient across the snowpack changes to near isothermal conditions. The ground surface and soil temperature also rose steeply during this period. As shown in Figure 4.6A, surface temperature increased about 10° C within a few days. Seasonal snow cover cools the ground surface in May. This cooling effect continues in early June until the seasonal snow cover is completely removed. After the disappearance of the seasonal snow cover, the surface temperature increases substantially (Figure 4.6A), as a whole, ΔT_{ga} in June is very close to the summer average value of ΔT_{ga} as shown in Figure 4.7.

On seasonal and annual bases, seasonal snow cover can increase the ground surface temperature by several degrees as shown in Table 4.3. The average value for ΔT_{ga} during winter is about 5° C to 8° C higher than during snow free period. If there were no snow on the ground and $\Delta T_{ga} = 1.3^{\circ}$ C all year, the seasonal snow cover would increase MAGST by 3° C to 6° C.

Table 4.3 Temperature difference between mean ground surface temperature (MGST) and mean air temperature (MAT)

Stations	1986-87	1987-88	1988-89	1989-90	1990-91	Average
Winter (with snow cover)						
West Dock	5.60	4.47	7.32	6.03	5.65	5.81
Deadhorse	8.30	5.26	12.9	6.90	13.5	8.58
Franklin Bluffs	9.66	6.70	11.40	8.02	13.40	9.38
Summer (snow free)						
West Dock	1.43	1.79	-0.34	2.48	-	1.34
Deadhorse	1.03	2.04	-	1.70	-	1.59
Franklin Bluffs	1.36	0.83	0.06	1.40	-	0.91
Annual						
West Dock	3.9	4.3	4.6	4.4	-	4.3
Deadhorse	5.8	5.0	-	4.0	-	4.9
Franklin Bluffs	6.8	5.9	6.8	8.8	-	7.0

MAT — Mean air temperature in ° C

MGST — Mean ground surface temperature in ° C

4.4.3 Permafrost Temperature

Permafrost temperatures are linked to the temperature at the permafrost table, and to the climate through the active layer, ground surface, intervening vegetation and seasonal snow cover. Figure 4.8 shows the difference, ΔT_{pa} , between mean monthly permafrost surface temperatures and air temperatures over 5 years at West Dock, Deadhorse and Franklin Bluffs. ΔT_{pa} is defined as $\Delta T_{pa} = \bar{T}_{pf} - \bar{T}_a$, where \bar{T}_{pf} is mean monthly temperature at the permafrost surface with depths ranging from 0.4 m at West Dock to 0.6 m at Franklin Bluffs. Variation of

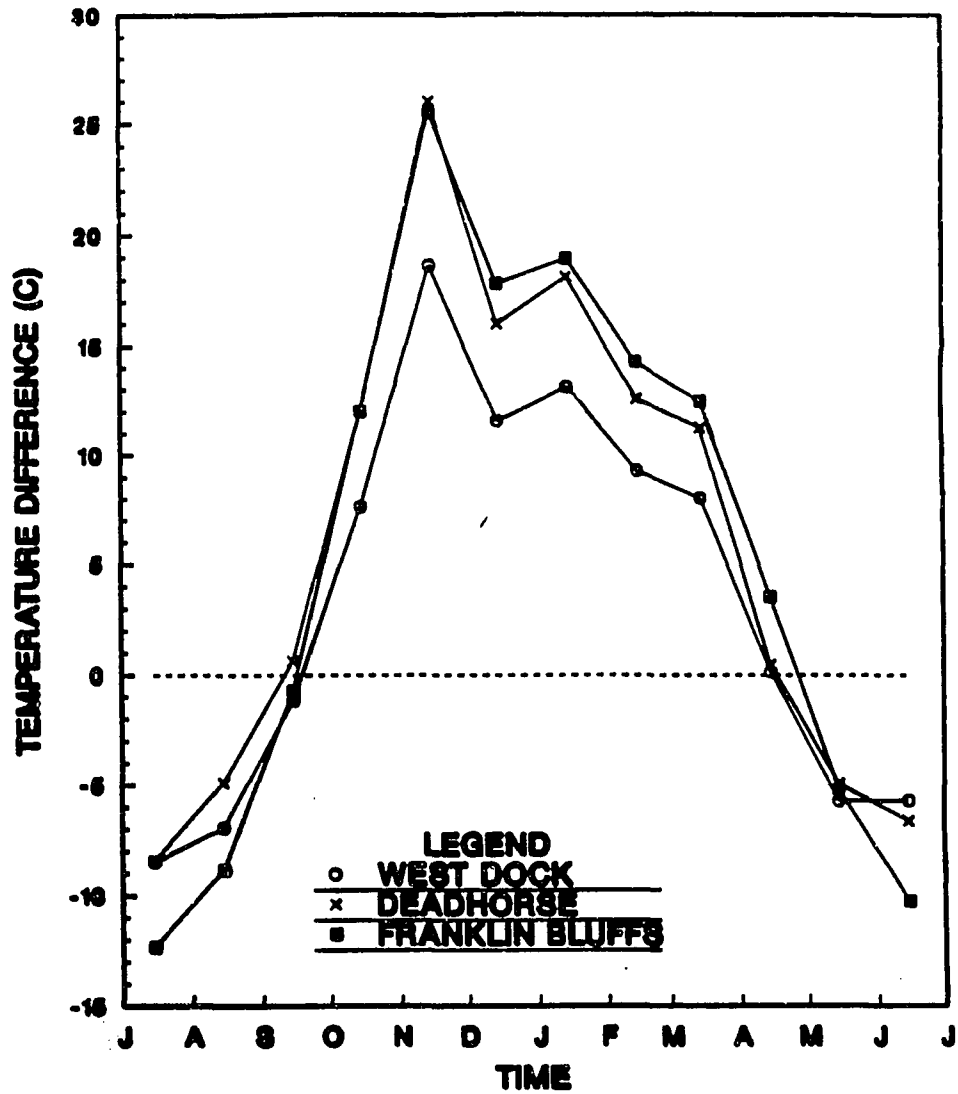


Figure 4.8 Difference between measured mean monthly permafrost surface temperatures and air temperatures for the period from 1986 through 1991 at West Dock, Deadhorse and Franklin Bluffs.

ΔT_{pa} over a year follows a pattern similar to ΔT_{ga} . From May to August, ΔT_{pa} is negative since temperature near the permafrost surface can not rise above 0° C. The magnitude of ΔT_{pa} is about a few degrees greater from October through March than ΔT_{ga} . ΔT_{pa} is close to 0° C in September and April as shown in Figure 4.8.

Figure 4.9 shows MAAT at West Dock, annual maximum thickness of seasonal snow cover at Prudhoe Bay, and permafrost temperature at 20 and 30 m at West Dock (Osterkamp, unpublished data) since 1983. Average air temperature over the period of record was about -12.0° C and average maximum thickness of snow on ground was about 12 cm. From 1983 to 1985, average air temperature was lower than -12.0° C with very thin snow cover (less than 10 cm). This is a very favourable condition for permafrost cooling. Figure 4.9B indicates permafrost temperatures decreased about 0.5° C from 1983 to 1985 at 20 m. For the period from 1985 to 1988, the average air temperature was almost the same as before, but the thickness of snow increased more than 100%, which increased the insulating effect. The cooling decreased more slowly and then warming started. In 1989, the higher air temperature and thick snow cover were favourable conditions for warming permafrost. Temperatures at the 30 m depth shows a similar pattern as at 20 m but with a reduced magnitude of variation and two to three years of phase lag. However, the insulating effect of the seasonal snow cover is controlled by many factors such as timing, duration, structure, accumulating processes, etc. Air temperature alone can not drive the changes in permafrost temperature shown in Figure 4.9.

Another important feature is that variations in seasonal snow cover can influence the thermal offset in near-surface mean annual ground temperatures significantly. Thermal offset, as defined by *Goodrich* (1982), is the difference between MAGST and MAPST. Table 4.4 shows the values of the thermal offset measured at West Dock and Franklin Bluffs. The thermal offset value ranges from 0.3° C to about 1.8° C over four years of measurements at

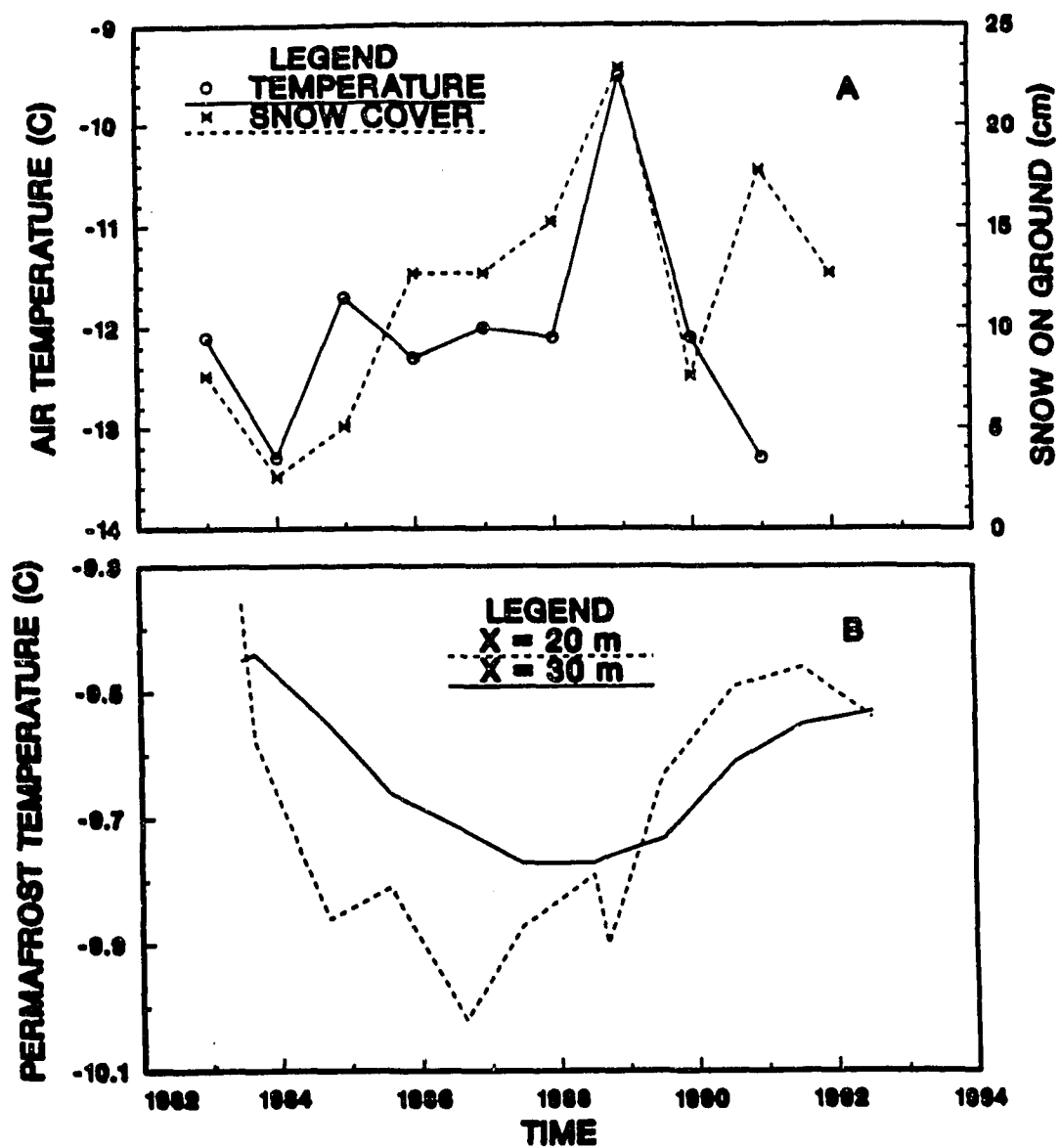


Figure 4.9 Mean annual air temperatures and annual maximum thickness of seasonal snow cover at Prudhoe Bay (A) and permafrost temperatures at depths 20 m and 30 m at West Dock (B).

two sites. The value of thermal offset is greatest with heavy snowfall and more snow on ground during the year of 1988-1989; by contrast, the value of the thermal offset is smallest with light snowfall and less snow on ground during the year of 1989-1990. The thermal offset is affected by many factors, such as the ratio of K_f/K_t , length of thaw season, thickness of the active layer and seasonal snow cover. In conjunction with the reduced heat flux resulting from the overlying insulating snow cover, latent heat released by the underlying active layer is sufficient to maintain the snow-ground interface temperature at relatively high values throughout the entire freeze-back period, which results in an increase in MAGST. The effectiveness of this mechanism is enhanced if the thawed active layer persists beyond the time of minimum air temperatures. Early snowfall and snow accumulation on the ground surface can make the thawed active layer persist longer and produce greater thermal offset values; by contrast, late snowfall and thin snow cover accelerate the freeze-up processes which reduces the thermal offset value.

Table 4.4 Measured thermal offset values in near-surface mean annual ground temperatures.

Stations	1986-87	1987-88	1988-89	1989-90	Average
West Dock	0.8	0.8	1.8	0.3	0.9
Franklin Bluffs	1.0	1.0	1.8	0.3	1.0

4.5 Summary

The seasonal snow cover in Alaska North of the Brooks Range lasts about eight to nine months. The first day of the snow on the ground varies from early September to early October. By late April, maximum thickness of seasonal snow cover is reached. The date when seasonal

snow cover disappears ranges from late May inland to the middle of June along the coast. The length of the snow free period inland from the coast. This is because increase in the air temperature inland is much faster in the spring than along the coast, which results in early snowmelt inland.

The date when the seasonal snow cover first becomes established shows a relatively constant time over the period of record; while, for Barrow, there has been a trend towards earlier snowmelt since about 1953. This trend is not very obvious at Barter Island (1957-1988) and at Umiat (1978-1991). The early snowmelt at Barrow may be related to the local development and population expansion.

The development of seasonal snow cover is controlled by many factors, such as the magnitude, timing and duration of snowfall, low temperatures, blowing snow, existence of permafrost, vegetation, local microrelief and snow metamorphism. Summer snowfall is relatively small, less than 10% of the annual total. Summer snow only lasts a few hours or a few days on the ground. The maximum monthly snowfall occurs in October and more than 50% of the annual snowfall occurs in September through November when the thickness of seasonal snow cover increases rapidly.

It takes 40 to 50 days for the disappearance of seasonal snow cover along the coast and about 30 days inland.

The evolution of seasonal snow cover can be approximated by

$$H_s(t) = \begin{cases} 0 & 0 \leq t \leq P_1 \\ (A) H_{max} & P_1 \leq t \leq P_2 \\ (1 - B) H_{max} & P_2 \leq t \leq P_3 \\ 0 & P_3 \leq t \leq P \end{cases} \quad (4.1)$$

where H_s is thickness of seasonal snow cover in m at time t in day, P_1 is the first day of steady seasonal snow cover on ground, P_2 is time at which snow thickness is maximum H_{max}

in m, P_3 is last day of steady seasonal snow cover on ground, n is a positive integer and

$$A = \left(\frac{t - P_1}{P_2 - P_1} \right)^{n/2}$$

$$B = \left(\frac{t - P_2}{P_3 - P_2} \right)^{n/2}$$

In (4.1), the time periods $0 \leq t \leq P_1$ and $P_3 \leq t \leq P$ are generally snow free, where $P=365$ days started at July 1. During these periods, snow may stay on ground for a few hours or a few days. The time period $P_1 \leq t \leq P_2$ is for the accumulating processes and $P_2 \leq t \leq P_3$ for the melting processes. The accumulating and melting processes vary with the choice of n ; $n = 1$ for $P_1 \leq t \leq P_2$ and $n = 3$ for $P_2 \leq t \leq P_3$ would give a best fit to data.

There is a sharp change in the amplitude of daily ground surface temperature at the date when snow disappears in the spring and at the date when snow cover first becomes established in autumn. This sharp change in the amplitude can provide some evidence about the presence or absence of the seasonal snow cover on the ground surface. The date for presence or absence of snow on the ground determined by a change in daily surface amplitude is consistent with the date measured at the reporting stations when a trace (snow thickness is less than 2.5 cm) is observed.

Snow on the ground (a few hours or a few days) during the summer cools the ground surface and reduces the difference, ΔT_{ga} , between daily ground surface and air temperature due to its high albedo and snowmelt. The average value of ΔT_{ga} for summer is about 1.3°C for the period from 1986 through 1991.

After the establishment of a continuous seasonal snow cover on the ground surface, ΔT_{ga} increases. ΔT_{ga} reaches its maximum value in November due to the rapid decrease of air

temperature, low density of snow and release of latent heat from the active layer. At this stage, the temperature gradient across the snowpack is greatest which is a favourable condition for formation of the depth hoar layer, which enhances the insulating effect of snow due to its low density.

During the middle of winter (December through March) when the seasonal snow cover becomes thicker and the active layer has frozen, ΔT_{ga} is mainly driven by air temperature changes. In general, ΔT_{ga} varies from a few degrees to about 10° C. An extreme value of $\Delta T_{ga} = 35^{\circ}$ C was recorded in the winter of 1988 at Franklin Bluffs. In a storm event, air temperatures may increase rapidly ΔT_{ga} can be reduced to 0° C or becomes negative, that is, the snow cools the surface. As a whole, the average monthly ΔT_{ga} is less than that in November.

When the thickness of the seasonal snow cover reaches its maximum value in late April, ΔT_{ga} decreases to the average summer value. This is because air temperature increases steadily in Spring, while the response of surface temperature to this increase is very retarded by the snow. During May, air temperature can be a few degrees higher than the ground surface temperature and ΔT_{ga} becomes negative. This cooling effect continues in early June until the seasonal snow cover is completely removed. After the disappearance of seasonal snow cover, the surface temperature increases substantially. as a whole, ΔT_{ga} in June is very close to the summer average value ΔT_{ga} .

Seasonal snow cover can raise the seasonal and mean annual ground surface temperature by several degrees. The average value of ΔT_{ga} during winter is about 5° C to 8° C higher than that during the snow free period. Seasonal snow cover can increase the mean annual ground surface temperature by at least 3° C to 6° C.

The response of the near surface permafrost temperatures to air temperatures follows a pattern similar to ΔT_{ga} . The difference, ΔT_{pa} , between the permafrost surface and air

temperature from May to August is negative and the magnitude of ΔT_{pa} is greater from October to March than ΔT_{pa} .

Permafrost temperatures at deep levels shows a cooling trend from 1983 to 1987 and then warming again until 1992. Over the same time period, average air temperature was about -12.0°C and average maximum thickness of snow on the ground was about 12 cm. Cold air temperature (below -12.0°C) and thin snow cover (less than average) during the early years of record are responsible for the permafrost cooling. Higher air temperature and thicker snow cover after 1987 may have caused the warming of the permafrost. Obviously, changes in air temperature alone can not drive the change in permafrost temperature although the insulating effect of seasonal snow cover is controlled by many factors such as timing, duration, structure, and accumulating processes.

Thermal offset in near-surface mean annual ground temperature at West Dock and Franklin Bluffs ranged from 0.3°C to 1.8°C over four years of measurements. The value of thermal offset was greatest with heavy snowfall and thick snow on the ground during the year of 1988-1989; by contrast, the value is smallest with light snowfall and less snow on the ground during the year of 1989-1990. This is probably because early and thick snow on ground can make the thawed active layer persist longer and the thermal offset value becomes greater; while late and thin snow cover accelerate the freeze-up processes which reduce the thermal offset value.

CHAPTER 5

Modeling the Influence of Snow Cover on the Ground Thermal Regime

5.1 Introduction

The purpose for studying the relationship between permafrost development and climatic change includes the determination of the past ground surface temperature or heat balance at the ground surface and investigation of heat flow in the permafrost. Although the driving force for heat and mass exchange between the atmosphere and permafrost is climate, all factors which affect the surface heat balance modify the magnitude of heat and mass flow. Snow cover is a good insulator since it is present only during the cold period of the annual temperature cycle, the net effect over a year is to increase MAGST, often by several degrees. Peat near the ground surface, in general, cools permafrost since the ratio of $k_t/k_f < 1$ and winter is longer than summer in the cold regions. Vegetation may play a complicated role in development of the active layer during the summer and of the depth hoar layer of the seasonal snow cover during the winter. Therefore, in the whole system, there are several physically distinct domains, i.e., the atmosphere, vegetation and peat layer, seasonal snow cover, the active layer, and permafrost. Each is governed by different physical processes.

Nakano and Brown (1972) developed a numerical model to investigate the soil thermal regime at Barrow, Alaska. The upper boundary was set at the base of living plants with the boundary condition represented by measured temperatures. Their calculated results show good agreement with field measurements. *Outcalt et al. (1975)* investigated the effect of snowmelt on the soil thermal regime through the numerical simulation. *Ng and Miller (1977)* studied the

influence of tundra vegetation on soil temperatures. *Goodrich* (1976,1978,1982) conducted a numerical simulation of the influence of seasonal snow cover on the ground thermal regime using a one-dimensional finite difference model. The results show that seasonal snow cover can increase the MAGST by several degrees.

The objectives of this chapter are first, to calibrate *Goodrich's* model using measured air and soil temperatures, seasonal snow cover, physical and thermal properties of soils; then, to study the response of permafrost temperature to surface temperature change; and to investigate the sensitivity of the soil temperature to seasonal snow cover parameters, such as timing and duration, thickness, depth hoar layer, accumulation and melting processes, and amplitude of MAAT.

5.2 Model Assumptions

A finite difference model for one-dimensional heat flow with phase change (*Goodrich, 1976, 1977, 1982*) was used to investigate the effects of air temperature, seasonal snow cover and the active layer on permafrost temperatures. The upper boundary was set at the snow surface when seasonal snow cover was present and was represented by the measured daily mean air temperatures from October 5, 1986 to June 23, 1991 at West Dock, Prudhoe Bay. When snow was not present, the boundary was set at the base of the living plant layer with the surface temperature represented by

$$T_s = A(T_a + 6.0)^B - 6.0 \quad (5.1)$$

where T_s is the daily mean ground surface temperature in °C, T_a is the daily mean air temperature in °C, A and B are constants, with $A = 2.627$ and $B = 0.6325$. Equation (5.1) was obtained by correlating the measured daily mean air temperature with the ground

surface temperature when the ground surface was snow free at West Dock (Figure 5.1); with a correlation coefficient of 0.91 and standard deviation of $0.6^{\circ}C$. The boundary condition at depth was represented by a constant geothermal heat flux (0.0565 W m^{-2}). The lower boundary was located at 150 m which is deep enough to ensure no significant effect on temperatures in the first 50 m below the ground surface.

The one-dimensional freezing or thawing problem with latent heat release (+) or absorption (-) at a fixed temperature is described by the conditions

$$k_f \frac{\partial T}{\partial x} \Big|_z - k_t \frac{\partial T}{\partial x} \Big|_z = (\pm) L_v \frac{dz}{dt} \quad (5.2)$$

and

$$T(z, t) = T_f = \text{constant} \quad (5.3)$$

at the moving interface. The heat conduction equation

$$\frac{\partial}{\partial t}(C_v \cdot T) = \frac{\partial}{\partial x} \left(k \frac{\partial T}{\partial x} \right) \quad (5.4)$$

applies in the frozen and unfrozen regions on either side of the moving phase boundary, due account being taken of differences in thermal properties. The initial condition is given as

$$T(x, 0) = T_i(x) \quad (5.5)$$

and

$$\lim_{x \rightarrow \infty} T(x, t) = T_i(x) \quad (5.6)$$

where k_f and k_t are the thermal conductivities of frozen and thawed soils, respectively, in $\text{W m}^{-1} \text{K}^{-1}$, T is temperature in $^{\circ}C$, x is distance in m , z is the interface position, C_v is

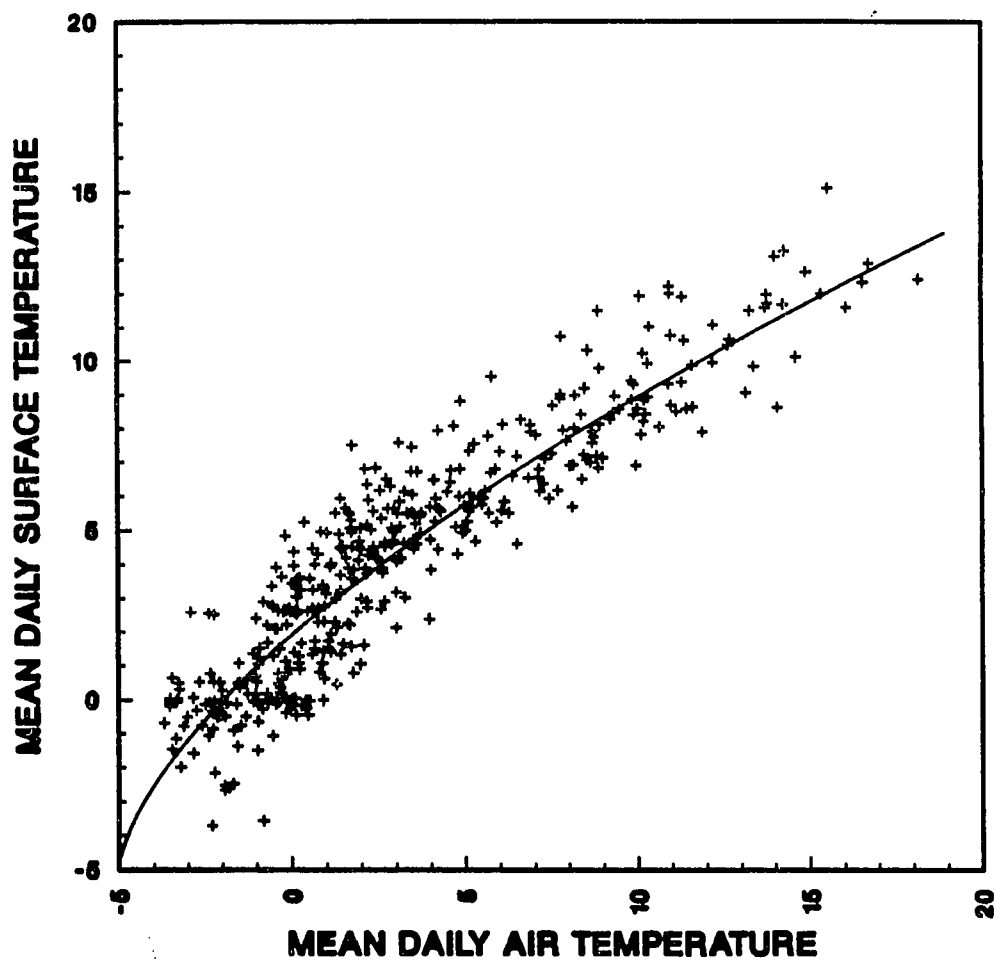


Figure 5.1 Relation between measured mean daily air and ground surface temperatures when snow was not present on the ground for the period from 1986 through 1991 at West Dock, Prudhoe Bay.

volumetric heat capacity in $MJm^{-3}K^{-1}$, L_v is volumetric latent heat in MJ/m^{-3} and t is time. In this study, the soil was represented as a layered system. Thermal properties of soil in a single layer were constant but could vary from one layer to another with distinct frozen and thawed values. For the peat layer and mineral soils in the active layer and the upper permafrost, physical and thermal properties were obtained from *Zhang* (1989) and Chapter 3 in this thesis. For depths below 50 m, material properties were obtained from *Lachenbruch et al.* (1982). Table 5.1 summarizes the physical and thermal properties of soils used in the calculations. No attempt was made to account for the variations in soil thermal properties accompanying changes in temperature and moisture content at shallow depths. Latent heat release or absorption accompanying soil freezing and thawing was included, assuming that the phase change took place completely at the freezing point ($0^\circ C$).

Table 5.1 Summary of physical and thermal properties of soils at West Dock

Depth (m)	Soil Type	ρ_b (kg/m^3)	W (%)	D_{th} (m^2/yr)	D_{fr} (m^2/yr)
0.0-0.35	peat	330	380	7	30
0.35-2.0	silt	1200	37	18	32
2.0-30.0	sand	1400	31		45
30.0-150.0	gravel	1620	24		55

The initial condition $T_i(x)$ was generated by equations (2) and (6) of *Lachenbruch et al.* (1988) with $n = 2$, $t^* = 71$ years (starting in 1915), $T_o = 2.9^\circ C$. The analytical solution (see *Lachenbruch et al.*, 1988) was fitted to the permafrost temperature data by the least square method to about 60 m. Then, the resulting equation was used to predict the temperature profile (in 1986) to a depth of 150 m.

The thickness of seasonal snow cover was measured by the National Weather Service near Deadhorse airport for the same period of the soil temperature measurements in this region.

During March of 1993, a field survey of the seasonal snow cover was conducted near Barrow. Five cross sections of seasonal snow cover (each a few meters in length) were investigated. One of them was snow cover on sea ice, which had almost no depth hoar present, and the rest were on the Arctic tundra. The thickness of the depth hoar layer was a few centimeters while the thickness of seasonal snow cover varied from 20 to 50 cm on a sandy ground surface, usually near the shore of little ponds. On the surface where vegetation was well developed (with height ranging from 10 to 15 cm), the depth hoar was about 15 to 20 cm in thickness when the seasonal snow cover was about 20 to 30 cm. One of the cross-sections shows that the thickness of seasonal snow cover was about 20 cm with the depth hoar layer about 12 to 15 cm. The thickness of seasonal snow cover and the depth hoar layer varied significantly within a few meters.

The effective thermal conductivity of the depth hoar layer for Fairbanks snow (*Sturm and Johnson, 1992*) ranges from 0.026 to 0.105, with an average value of 0.063 W/mK . For the purpose of this study, the effective thermal conductivity for the seasonal snow cover was estimated by using a series heat conduction model with

$$k_s = \frac{k_{dh}k_{wp}}{\phi k_{wp} + (1 - \phi)k_{dh}} \quad (5.7)$$

where k_s is the effective thermal conductivity of the seasonal snow cover, ϕ is the depth fraction of the depth hoar layer, and k_{wp} and k_{dh} are thermal conductivities of the wind-packed and depth hoar layer, respectively. Physical and thermal properties for snow used in the calculations are listed in Table 5.1.

Table 5.2 Thermal properties of snow used for modeling

Items	Values	Unit
ρ_{wp}	0.35	(g/cm^3)
ρ_{dh}	0.18	(g/cm^3)
k_{wp}	0.70	(W/mK)
k_{dh}	0.10	(W/mK)
C_{wp}	0.73	($MJ/m^3 K$)
C_{dh}	0.38	($MJ/m^3 K$)
ϕ	0.30	(%)

All calculations were conducted with $\Delta t = 1$ day and Δx ranged from 0.02 m in the seasonal snow cover and near the ground surface to about 5.0 m near the lower boundary.

5.3 Results

The model was run for two different cases. Case I had the upper boundary set at the snow surface when snow was present on the ground and at the ground surface when there was no snow. The boundary conditions were represented by the measured daily mean air temperature data at West Dock, Prudhoe Bay when snow was present and by (5.1) when there was no snow. Figure 5.2 shows the input daily mean air temperature (A), thickness of seasonal snow cover (B) and the measured (solid line) and computed (dashed line) daily mean ground surface temperature (C). The results show good agreement between the measured and computed values.

Case II had the upper boundary set at the ground surface with the boundary conditions represented by the measured daily mean ground surface temperatures. Figures 5.3 and 5.4 show the comparison between the measured and computed values at depths of 0.12 m (in the active layer) and 0.72 m (in permafrost). In general, the computed daily ground temperatures both in the active layer and permafrost using Case II provide better agreement with the measured data

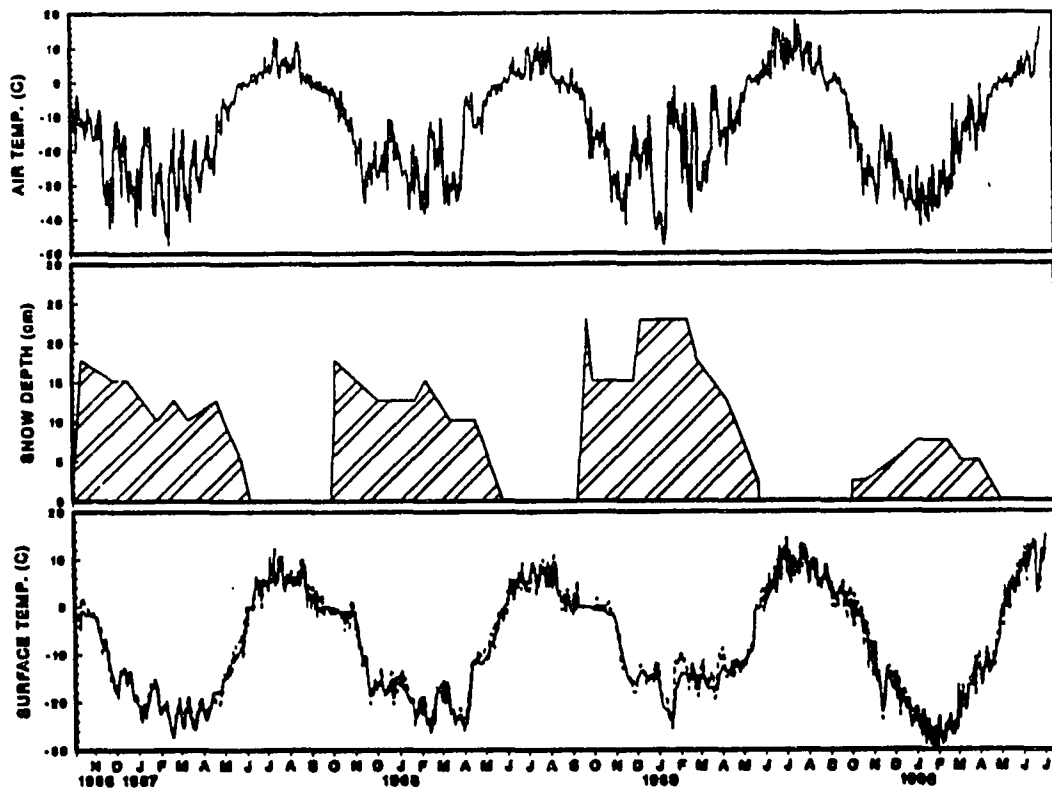


Figure 5.2 Measured mean daily air temperature at West Dock (A), measured seasonal snow cover at Deadhorse Airport (B), measured mean daily ground surface temperature (solid line) and calculated values (dashed line) (C) for the period from October of 1986 through July of 1990 at West Dock, Prudhoe Bay. The model was run with the upper boundary set at the ground surface when no snow presented and at snow surface when snow presented.

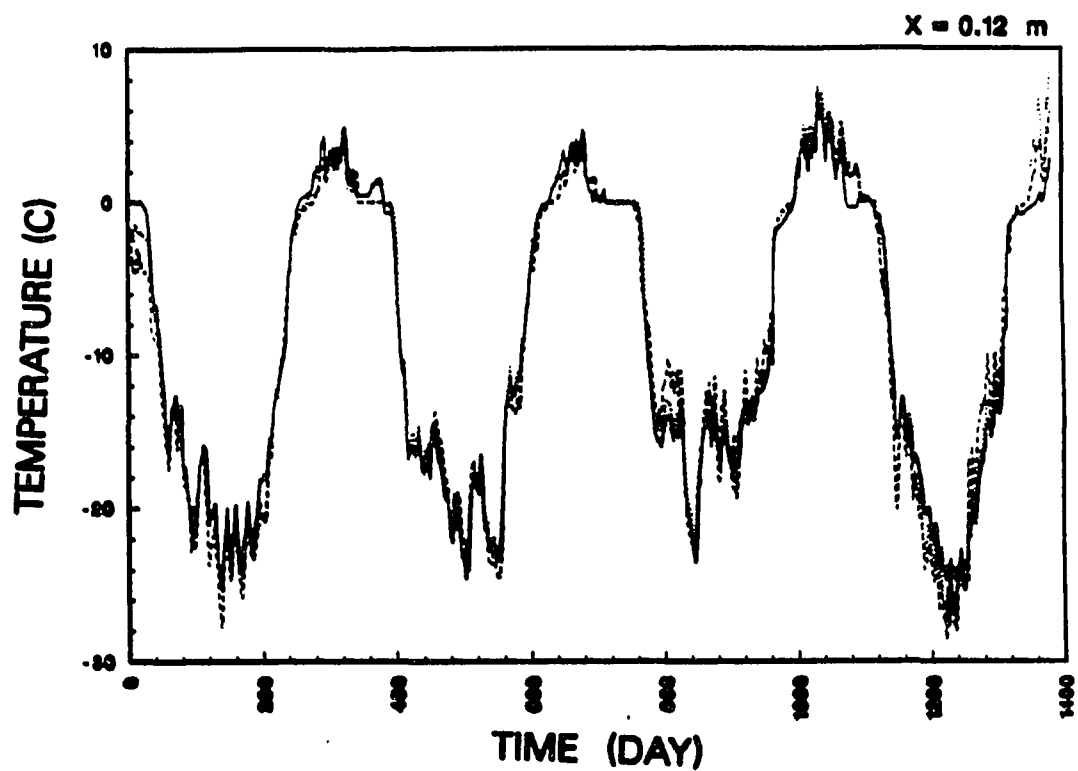


Figure 5.3 Measured (solid line) and calculated daily active layer temperatures at a depth of 0.12 m below the ground surface with snow cover (i.e., using T_a as the appropriate surface boundary condition) (Case I, dashed line) and without snow cover (using the measured T_g as the surface boundary condition) (Case II, dotted line) for the period from October 5, 1986 to June 23, 1990 at West Dock, Prudhoe Bay

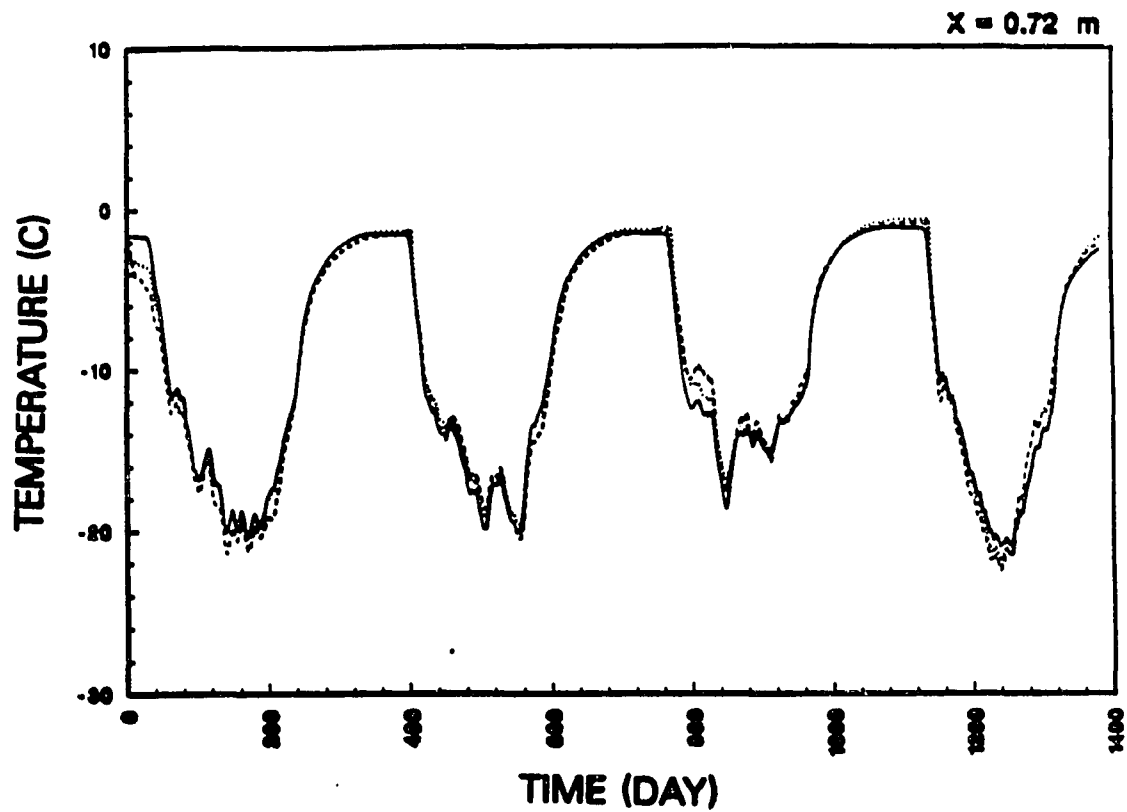


Figure 5.4 Measured (solid line) and calculated daily soil temperatures at a depth of 0.72 m with snow cover (Case I, dashed line) and without snow cover (Case II, dotted line) for the period from October 5, 1986 to June 23, 1990 at West Dock, Prudhoe Bay

than the computed results using Case I. This is simply due to errors produced by modeling the effect of the seasonal snow cover on the ground surface temperatures with daily mean air temperature. As shown in Figure 5.4, there are, at times, significant differences between computed and measured temperatures in the upper permafrost.

Figures 5.5, 5.6 and 5.7 computed by case I indicate an excellent agreement, except for the upper 2 m, between the measured and computed ground temperatures with depth. The maximum difference between the measured and computed values is within 0.2°C .

Figures 5.8, 5.9 and 5.10 illustrate the simulated results of temperature variations at depth using the calibrated numerical model. It clearly shows that the step or truncated sinusoidal temperature variation at or near the permafrost surface approaches a sinusoidal function with depth as illustrated by Zhang (1989) and Zhang et al. (1991). The amplitude of temperature variation decreased with depth and at a depth of about 30 m, the annual harmonic temperature wave almost disappeared, leaving the longer term temperature variation with time. From Figure 5.8, it can be seen that the permafrost temperature increases with time as shown in Figure 4.9. However, from Figure 5.10, the temperature at a depth 30 m shows a cooling trend until about 550 days from the start. This indicates the cooling period before 1986 as shown in Figure 4.9. At a depth of 50 m, temperature variations become very small.

5.4 Sensitivity Analysis

The seasonal snow cover, in general, can increase the annual ground surface temperature by several degrees. However, variation in timing and duration, thickness, accumulation and melting processes, structure, density and thermal properties have a significant influence on the insulating effect of the seasonal snow cover (*Goodrich, 1982*).

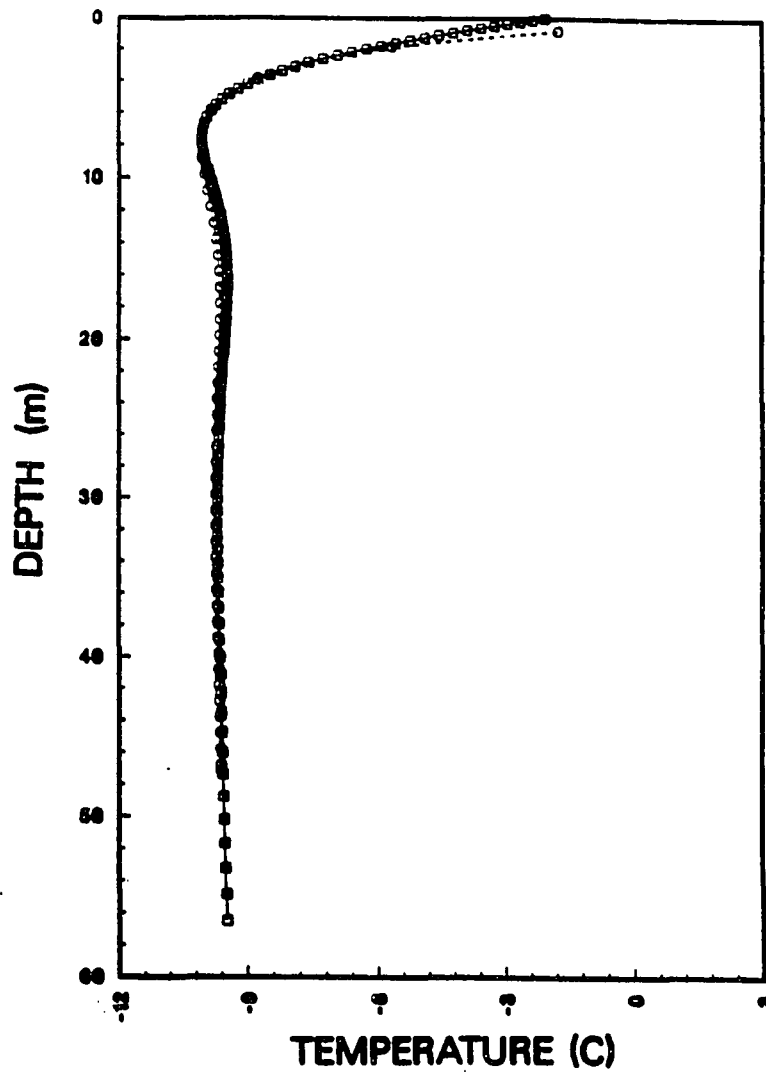


Figure 5.5 Measured (square) and predicted (circle) permafrost temperatures with depth on July 13, 1988 at West Dock, Prudhoe Bay, Alaska.

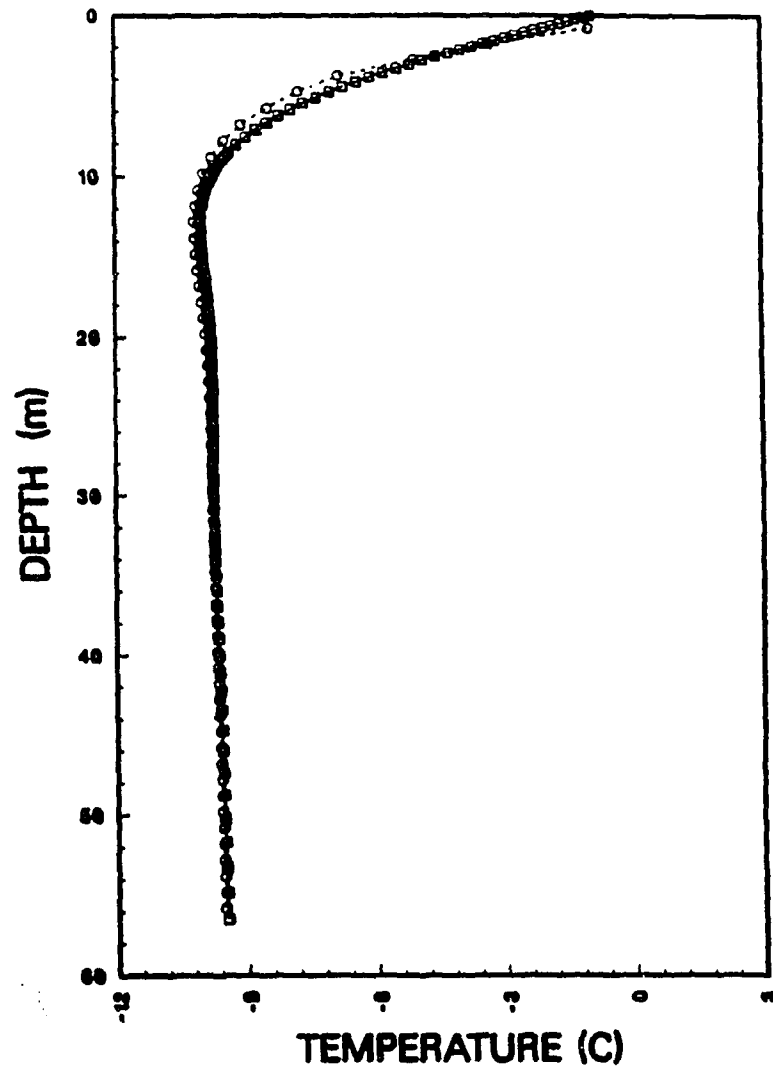


Figure 8.6 Measured (square) and predicted (circle) permafrost temperatures with depth on July 13, 1989 at West Dock, Prudhoe Bay, Alaska.

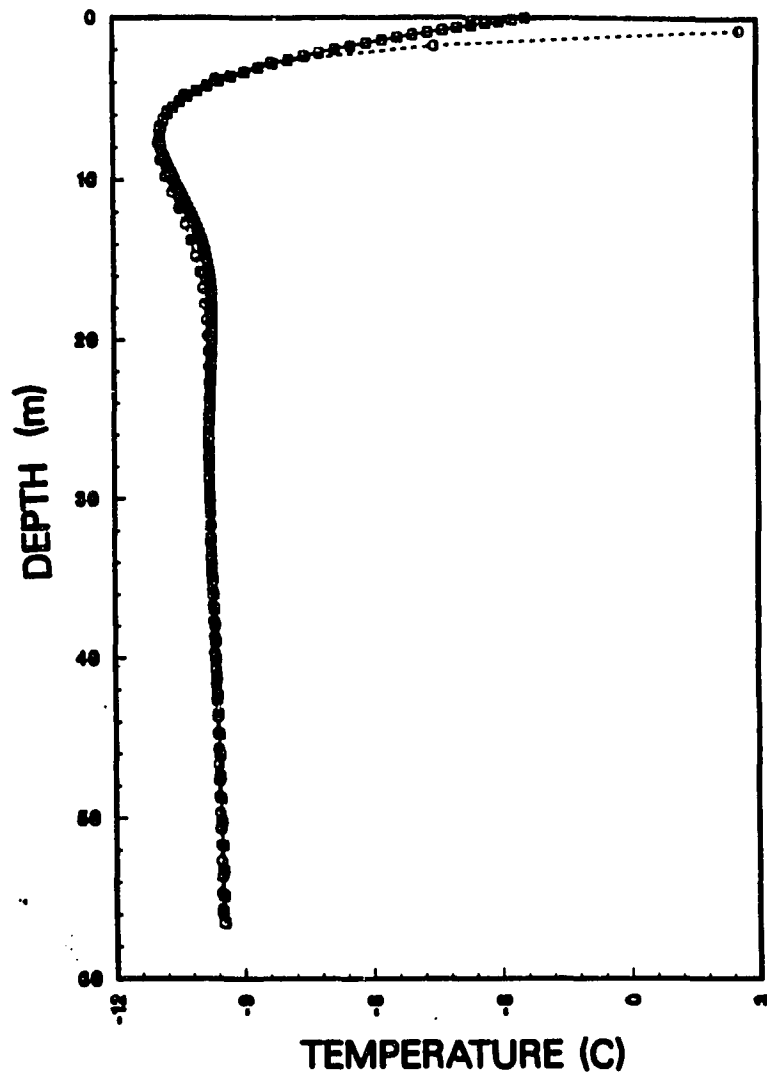


Figure 5.7 Measured (square) and predicted (circle) permafrost temperatures with depth on July 13, 1990 at West Dock, Prudhoe Bay, Alaska.

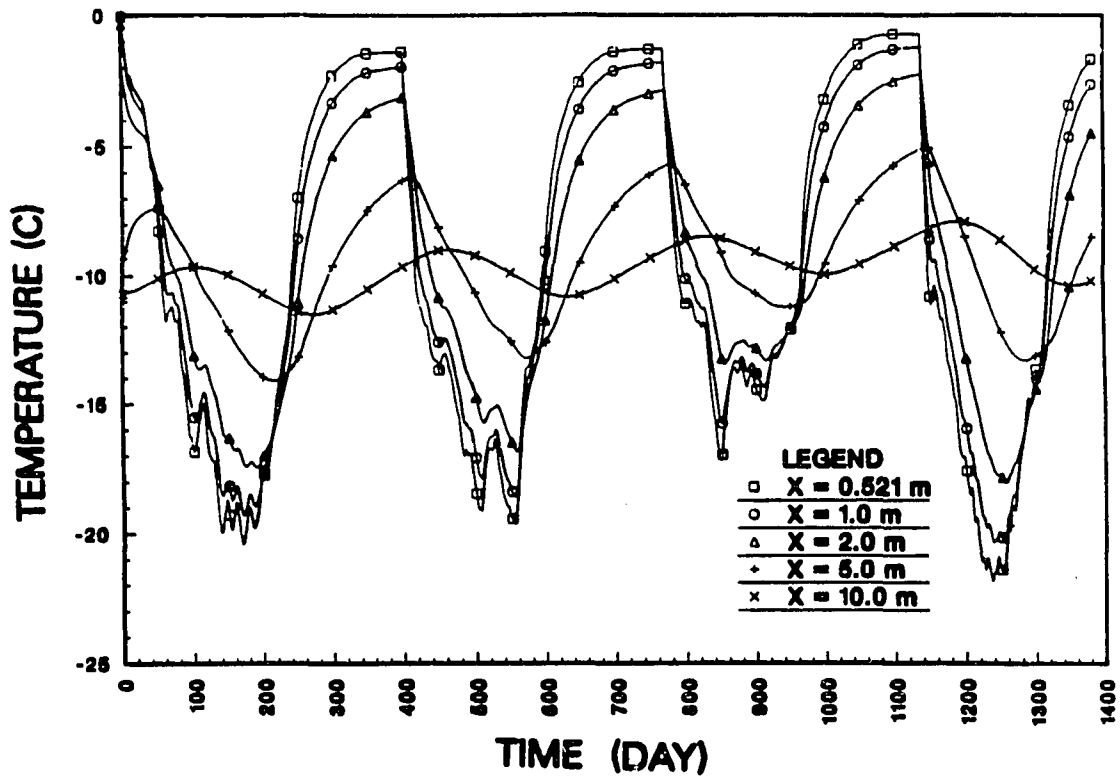


Figure 5.8 Computed temperature variations with depth ranging from 0.521 m to 10 m for the period from October 5, 1986 to July 13, 1990 at West Dock, Prudhoe Bay, Alaska.

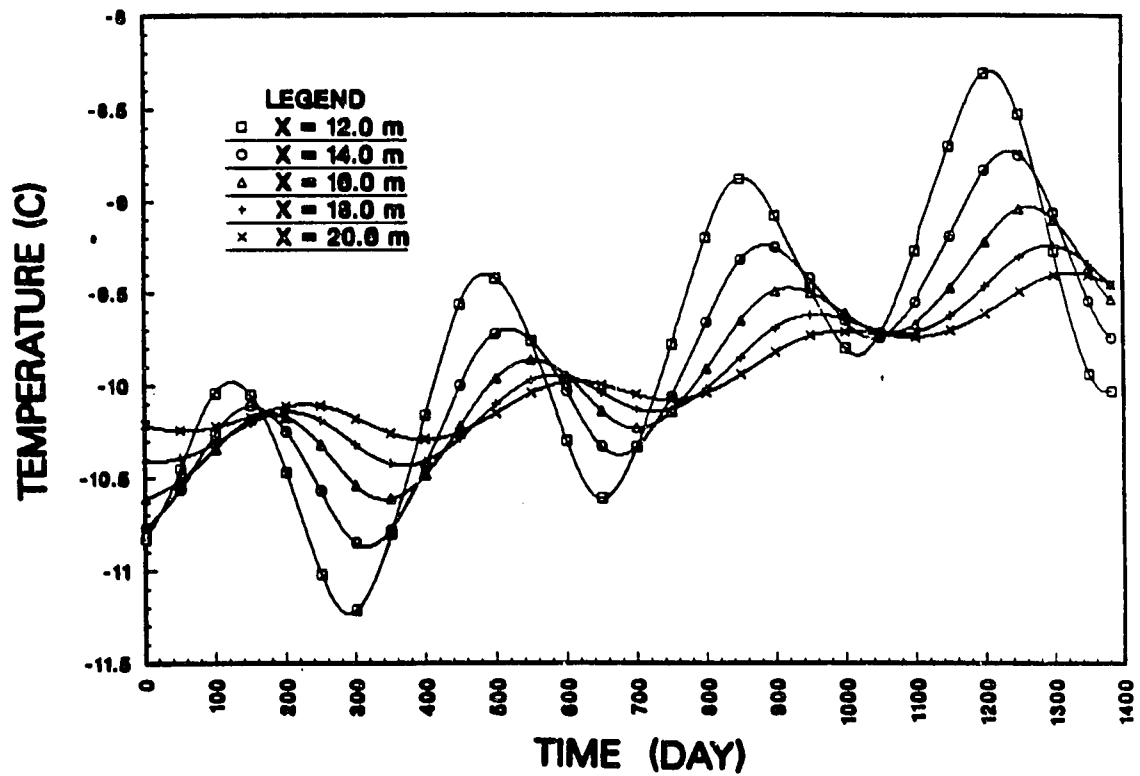


Figure 5.9 Computed temperature variations with depth ranging from 12 m to 20 m for the period from October 5, 1986 to July 13, 1990 at West Dock, Prudhoe Bay, Alaska.

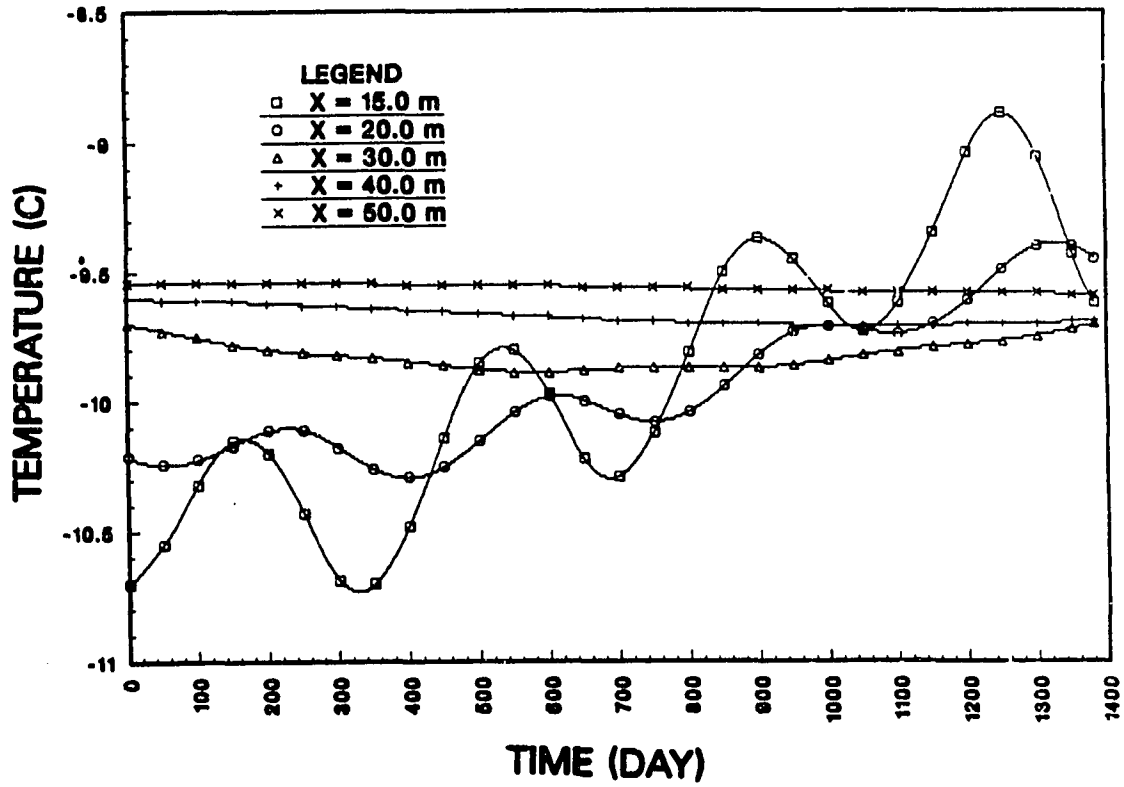


Figure 5.10 Computed temperature variations with depth varying from 15 m to 50 m for the period from October 5, 1986 to July 13, 1990 at West Dock, Prudhoe Bay, Alaska.

A few cases were computed to investigate the sensitivity of the thermal regime of the active layer and permafrost to changes in seasonal snow cover parameters. Equation (4.1) was used to simulate the evolution of seasonal snow cover in Alaska North of the Brooks Range. Air temperature variations were approximated by

$$T_d = T_o + A_o \cos[\omega(t + \alpha)] \quad (5.12)$$

where T_d is the daily mean air temperature, T_o is mean annual air temperature, A_o is the annual amplitude of mean air temperature, $\omega = 2\pi/P$, $P = 365$ days, t is time in days and α is phase lag in days. Table 5.3 summarizes the range of seasonal snow cover and temperature parameters along the coast and inland.

Table 5.3 Range of snow cover and air temperature parameters. The coast area includes Barrow, West Dock, Prudhoe Bay, Deadhorse and Barter Island, the Inland area includes Franklin Bluffs, Umiat and Toolik Lake.

Items	<i>Coast</i>	<i>Inland</i>	Unit
P_1	77 ± 11	91 ± 12	(day)
P_2	299 ± 12	297 ± 12	(day)
P_3	348 ± 10	328 ± 10	(day)
H_{max}	35 ± 25	44 ± 25	(cm)
ϕ	0.0 – 50	0.0 – 50	(%)
T_o	-12.3 ± 0.4	-12.3 ± 0.4	(°C)
A_o	16 ± 2	22 ± 2	(°C)
α	32	26	(day)

Standard reference parameters for seasonal snow cover and air temperature along the coast were chosen to be: $P_1 = 77$ days (September 15, starting from July 1), $P_2 = 299$ (April 15), $P_3 = 348$ (June 13), $H_{max} = 35$ cm, $\phi = 30\%$, $T_o = -12.3^\circ\text{C}$, $A_o = 16^\circ\text{C}$ and $\alpha = 32$ days. All of the following cases were based upon these standard parameters with

only one of them varied each time to study their influence on the thermal regime. Material properties used in the calculations were the same as cases in the previous section. A linear initial subsurface temperature condition was applied and the final stated results were obtained when the changes of mean annual temperature at $x = 1.0$ m was less than 0.01°C from the previous year. The final results include: (a) MAGST, T_s , (b) MAGT, T_g at a depth of one meter under the ground surface, (c) thermal offset values $\Delta T = T_g - T_s$, (d) daily ground surface temperature, starting from July 1, during the snow-free periods (daily ground surface temperature was obtained from (5.1); when snow cover was present, the curve represents the computed snow-ground interface temperature) and finally, (e) daily ground temperature at a depth of one meter under the ground surface, starting from July 1.

5.4.1 Timing and Duration

Three cases were computed on the influence of the timing and duration of the seasonal snow cover on the ground thermal regime, assuming the other conditions are constant. For case 1, the seasonal snow cover started September 4 and ended June 23 with a duration of 292 days, which was the longest observed duration of seasonal snow cover at Barrow. For case 2, the snow cover started on September 15 and ended on June 13 with a duration of 271 days, which was the average duration for snow cover (the standard case). For case 3, the ground surface was covered by snow from September 26 to June 3, about 250 days, which was the shortest observed duration of snow cover. The accumulation of seasonal snow cover was described by equation 4.1 with $n = 1$ for the period $P_1 \leq t \leq P_2$ and with $n = 3$ for the period $P_2 \leq t \leq P_3$, with $\phi = 0.3$.

Figures 5.11 and 5.12 show the results for cases 1, 2 and 3, respectively. Early snow cover (case 1) keeps the ground from freezing and maintains the surface temperature near 0°C for

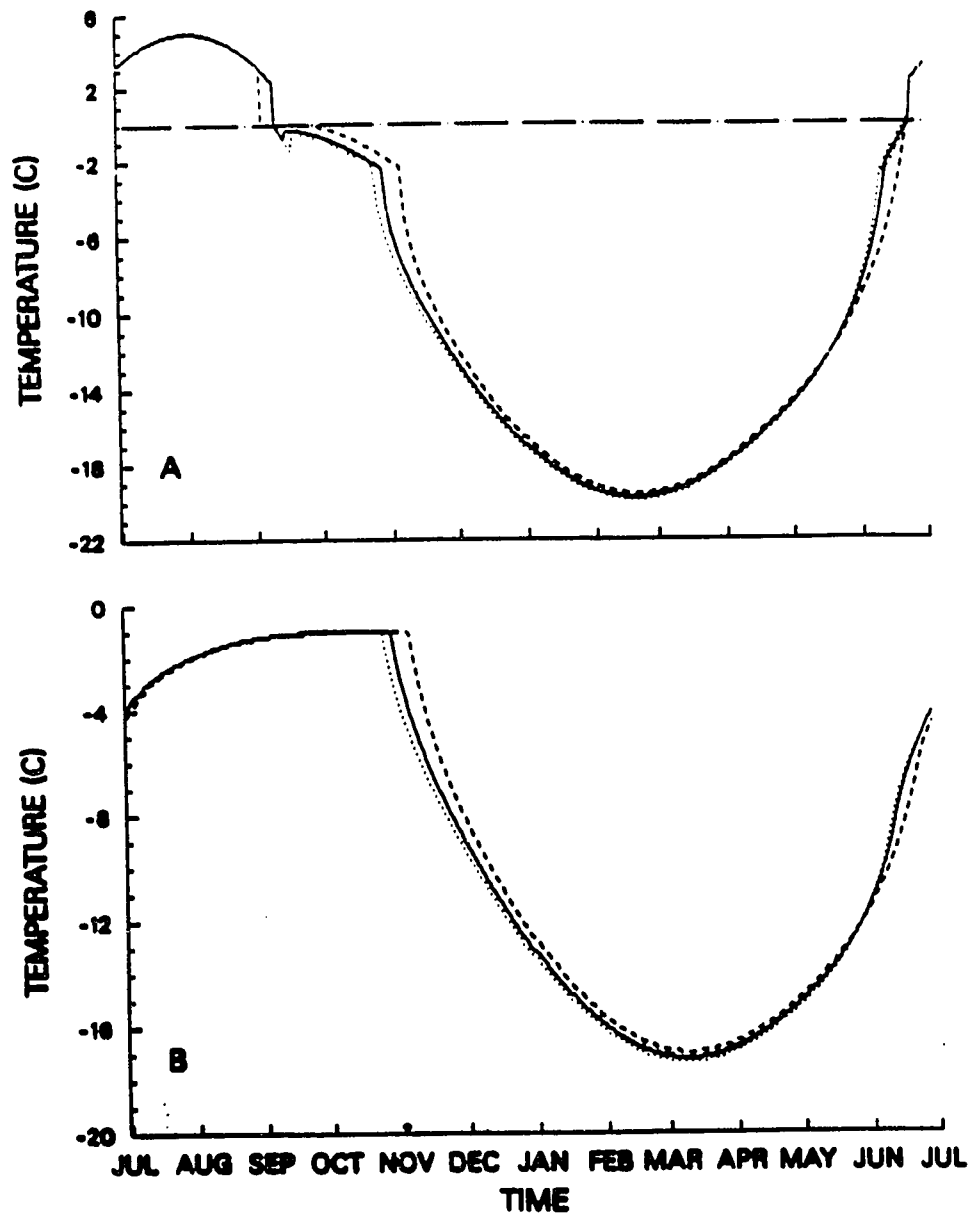


Figure 5.11 Influence of the timing and duration of seasonal snow cover on the ground surface temperature (A) and permafrost temperature (1.0 m below the ground surface) (B) along the Alaskan Arctic Coast. Dashed lines stand for case 1, solid lines for case 2 and dotted lines for case 3 corresponding to the longest, average, and shortest duration, respectively.

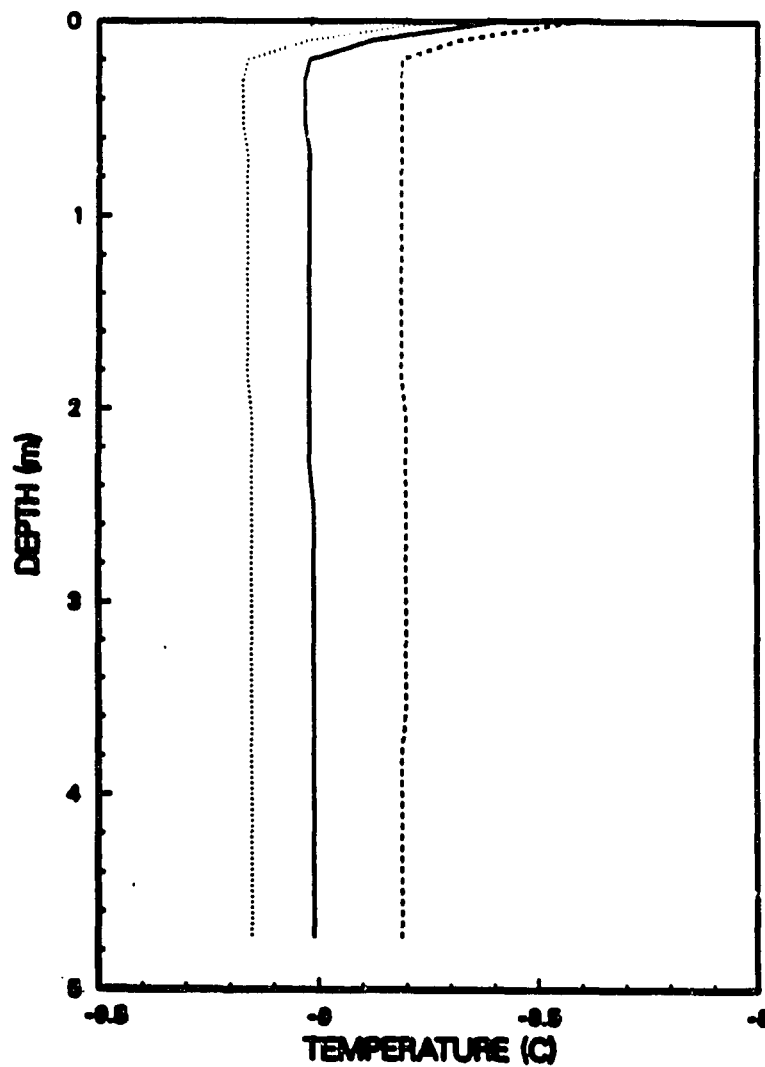


Figure 5.12 Influence of the timing and duration of seasonal snow cover on ground temperature along the Alaskan Arctic Coast, dashed line stands for case 1, solid line for case 2, and dotted line for case 3 corresponding to the longest, average, and shortest duration, respectively.

about two weeks longer compared with the results from the standard case (case 2). Late snow cover (case 3) allows ground freezing before snowfall. The surface temperature falls below -1.0°C before the snow covers the ground surface. As soon as snow cover is established on the ground surface, it acts as an insulator and decreases the heat flux to the atmosphere. The surface temperature increases to near 0°C as shown in Figure 5.11 (case 2 and case 3). The sharp turn of the temperature curves in Figure 5.11 indicates the freeze up of the active layer near the beginning of November. The early snow cover on the ground provides more insulating effect, thus the active layer remains unfrozen (case 1) and temperature at the ground surface and at a depth of one meter increases compared with later snow on ground (case 2 and case 3). As winter progresses, the temperature difference among three cases decreases. However, later snow disappearance (case 1) on the ground in Spring delays the warming of the ground temperatures since latent heat for melting snow is a heat sink. For the same H_{max} , the longest observed duration of snow cover increases the ground temperatures about 0.35°C compared to the shortest observed duration (Fig. 5.12).

Another noteworthy feature is the curvature of the mean annual temperature profile within the active layer. The term "thermal offset" is used to indicate the difference between the MAGT at the bottom of the active layer and that at the ground surface, as reported by *Goodrich* (1976, 1978, 1982), *Burn and Smith* (1988) and as noted in Chapter 4. In permafrost regions, the magnitude of the thermal offset is determined by the ground surface temperature conditions, the ratio of frozen to thawed soil conductivity, the length of thaw season and by the depth of the active layer. As shown in Figure 5.12, the thermal offset value is about -0.4°C and the effect of timing and duration on the thermal offset is not significant between the three cases.

5.4.2 Thickness

A few cases were computed using the same conditions as the standard case except varying the maximum thickness, H_{max} , in (4.1). Table 5.4 summarizes the variable H_{max} and some calculated results. Generally, temperatures at the ground surface and the depth of one meter under the surface increase as the maximum thickness of seasonal snow cover increases as shown in Figures 5.13 and 5.14. Case 4 with $H_{max} = 15$ cm (dashed line in Figure 5.13) indicates the coldest case and the active layer freezes up about 13 days earlier than the standard case (case 2). Case 8 with $H_{max} = 50$ cm (dotted line in Figure 5.13) shows the warmest case the active layer freezes up about 10 days later than the standard case. During the spring, the effect of the variable H_{max} on the ground thermal regime is not very significant although case 4 was a little warmer than the standard case. The rate of MAGST increase with the increase of H_{max} is around $0.1^{\circ}C/cm$ as shown in Figure 5.14 but this rate decreases with increasing H_{max} . For $H_{max} = 50$ cm, the rate is about $0.09^{\circ}C/cm$. The thermal offset value increases slowly with H_{max} and ranges from $0.39^{\circ}C$ for case 4 to $0.45^{\circ}C$ for case 8. The increase of the thermal offset value with H_{max} is due to later freeze-up and longer duration of the thawed state for the active layer in late fall.

5.4.3 Depth Hoar Layer

The seasonal snow cover in Alaska North of the Brooks Range consists of two distinct layers: a wind-packed layer and a depth hoar layer (*Benson and Sturm, 1993*). Generally, the wind-packed layer has higher density with relatively higher thermal conductivity while the depth hoar layer has low density with lower thermal conductivity. The thickness of the depth hoar layer ranges from 0% to over 50% of the total thickness of seasonal snow cover. The variation in thickness of the depth hoar layer has a significant effect on the ground thermal

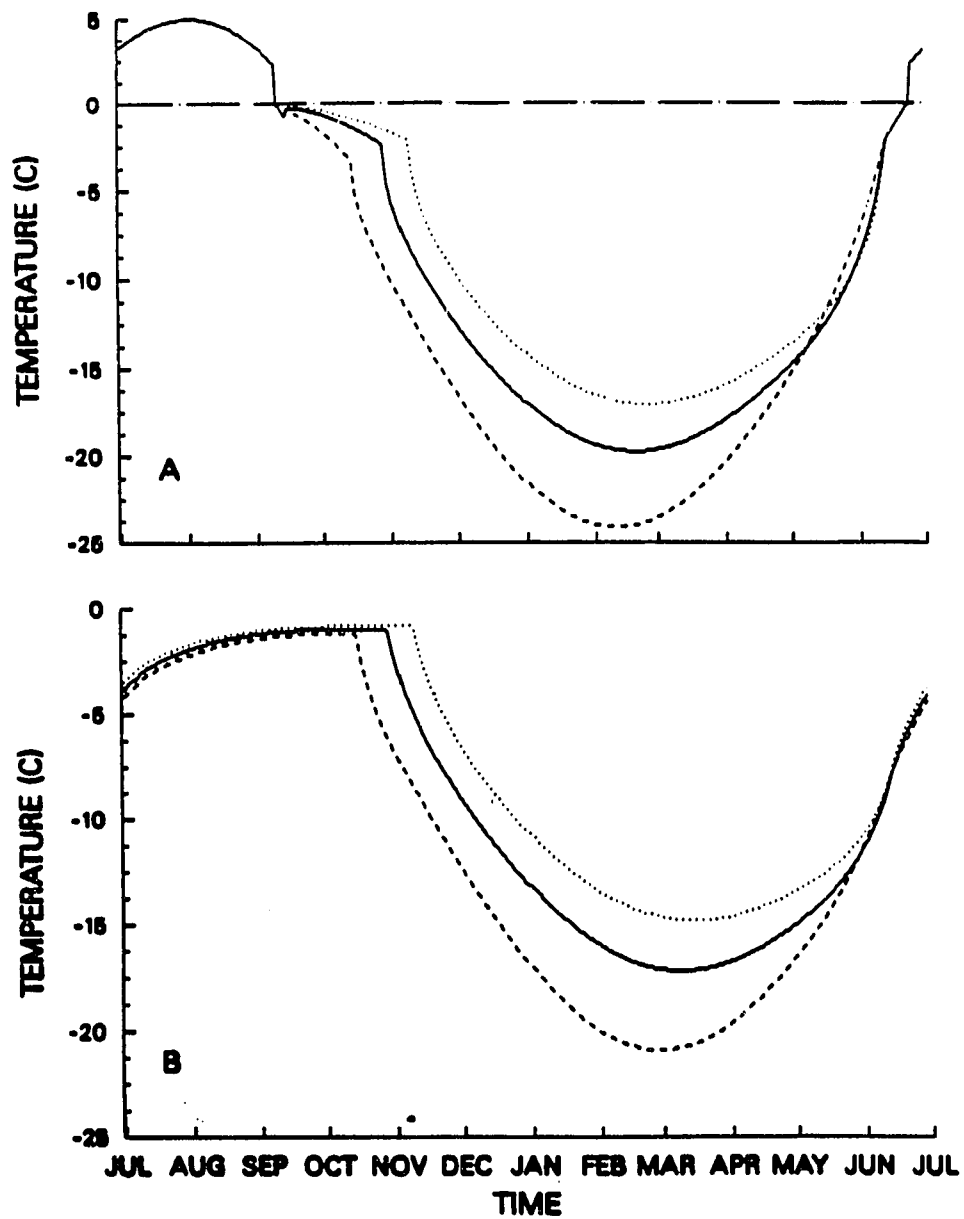


Figure 5.13 Influence of the maximum thickness of the seasonal snow cover on the ground surface temperature (A) and temperature at 1.0 m below the ground surface (B) along the Alaskan Arctic Coast. Dashed lines stand for case 4 ($H_{max} = 15 \text{ cm}$), solid lines for case 6 ($H_{max} = 35 \text{ cm}$), and dotted lines for case 8 ($H_{max} = 50 \text{ cm}$)

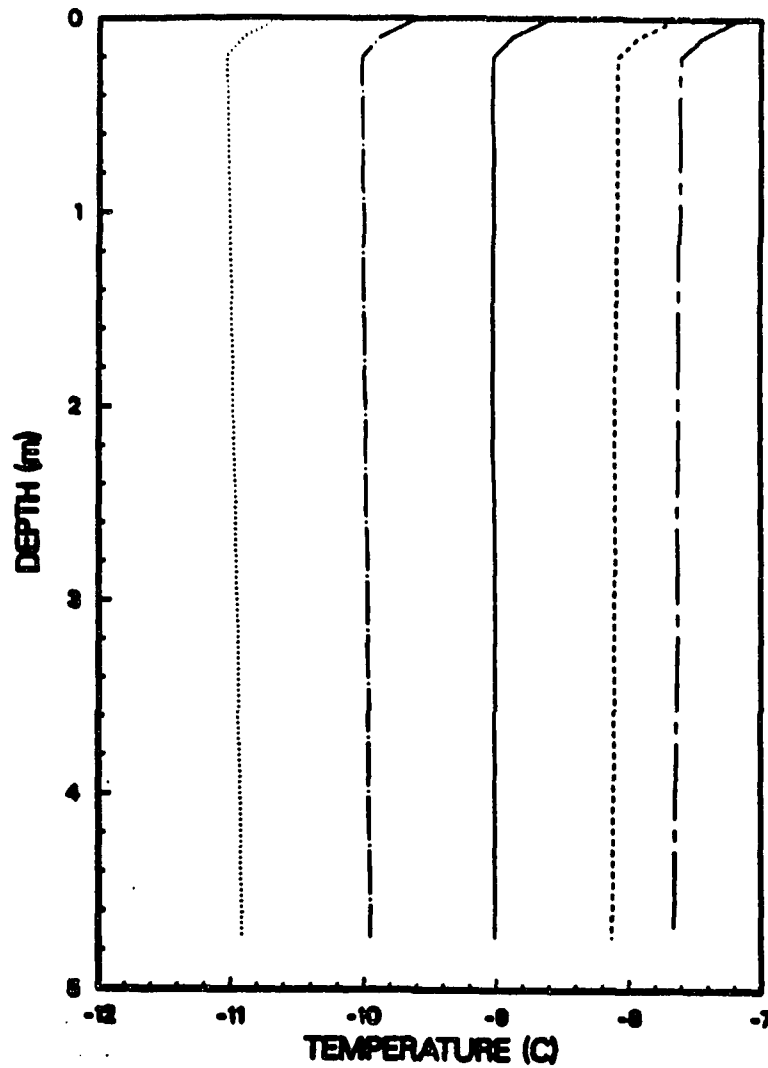


Figure 5.14 Influence of the maximum thickness of the seasonal snow cover on the ground temperature along the Alaskan Arctic Coast. Dotted line for case 4 ($H_{max} = 15 \text{ cm}$), chain-dotted line for case 5 ($H_{max} = 25 \text{ cm}$), solid line for case 6 ($H_{max} = 35 \text{ cm}$), dashed line for case 7 ($H_{max} = 45 \text{ cm}$) and chain-dashed line for case 8 ($H_{max} = 50 \text{ cm}$).

Table 5.4 Effect of maximum snow thickness (H_{max}) on the ground thermal regime, MAGST represents mean annual ground surface temperature, T_g stands for mean annual temperature at the depth of 1.0 m, and T_{off} for the thermal offset value.

Cases	H_{max} (cm)	MAGST (°C)	T_g (°C)	T_{off} (°C)
4	15	-10.62	-11.01	-0.39
5	25	-9.59	-10.00	-0.41
6	35	-8.59	-9.02	-0.43
7	45	-7.64	-8.09	-0.45
8	50	-7.17	-7.62	-0.45

regime. A few cases were computed by varying the depth fraction ϕ of the depth hoar layer to investigate its effect on the ground thermal regime (Table 5.5).

Table 5.5 Effect of the depth hoar on the ground thermal regime, ϕ stands for the depth fraction of the depth hoar layer.

Cases	ϕ	T_s (°C)	T_g (°C)	T_{off} (°C)
9	0.0	-10.72	-11.11	-0.39
10	0.1	-9.86	-10.27	-0.41
11	0.2	-9.01	-9.43	-0.42
12	0.4	-7.41	-8.62	-0.45
13	0.5	-6.62	-7.07	-0.45

Generally, both MAGST (T_s) and mean annual temperature at a depth of 1.0 m increased with increasing ϕ . The results for case 9 with $\phi = 0$ (dashed line in figure 5.15) shows the coldest case compared with case 10 for $\phi = 0.20$ (solid line in Figure 5.15) and case 11 for $\phi = 0.50$ (dotted line in Figure 5.15). It takes about one month longer to freeze-up the active layer with $\phi = 0.50$ (case 11) than without the depth hoar layer (case 9). The maximum daily

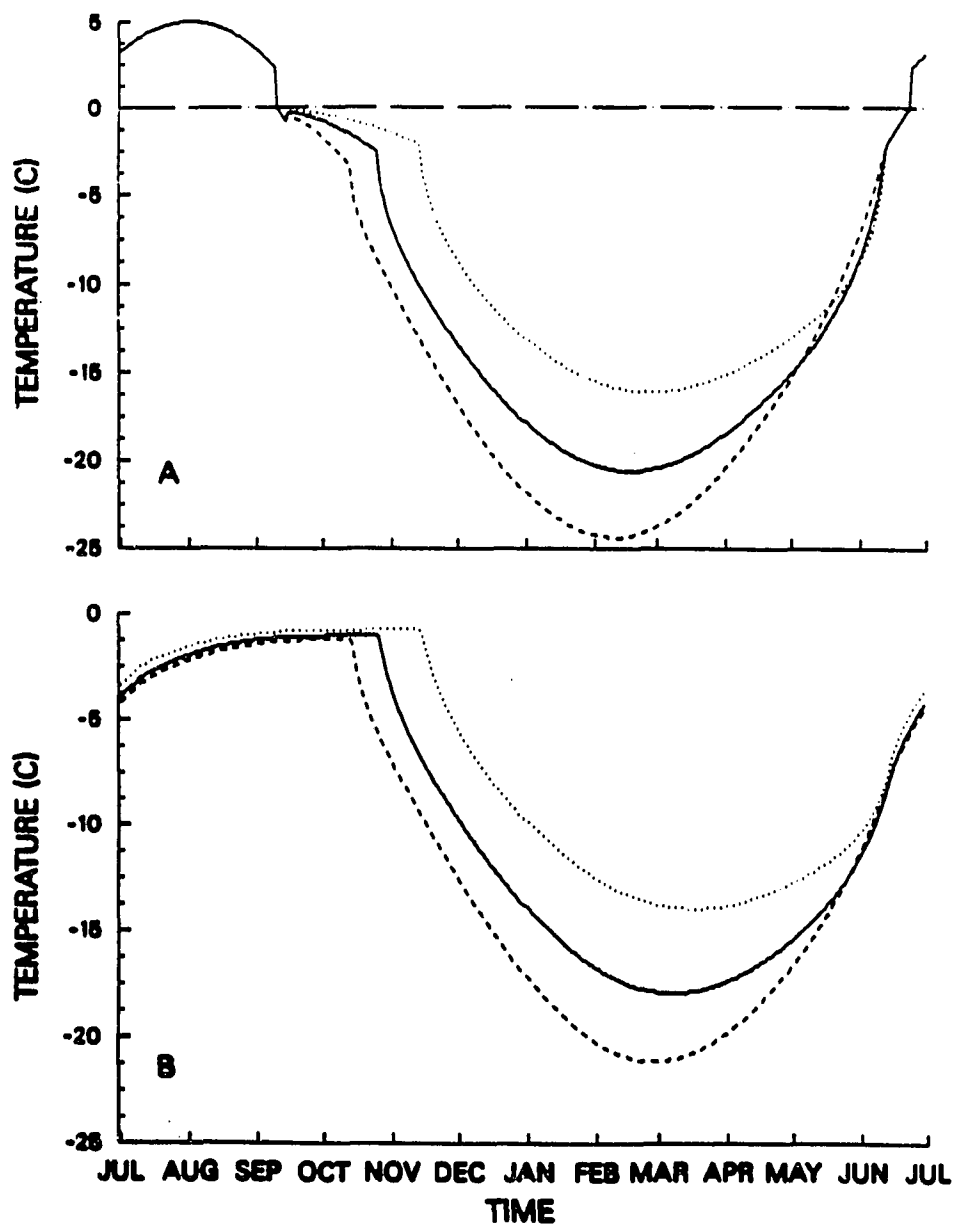


Figure 5.15 Influence of the depth hoar layer fraction of the total thickness of the seasonal snow cover on temperature at the ground surface (A) and at depth of 1.0 m below the ground surface along the Alaskan Arctic Coast. Dashed lines stand for case 9 ($\phi = 0.0$), solid lines for case 11 ($\phi = 0.20$) and dotted line for case 13 ($\phi = 0.50$)

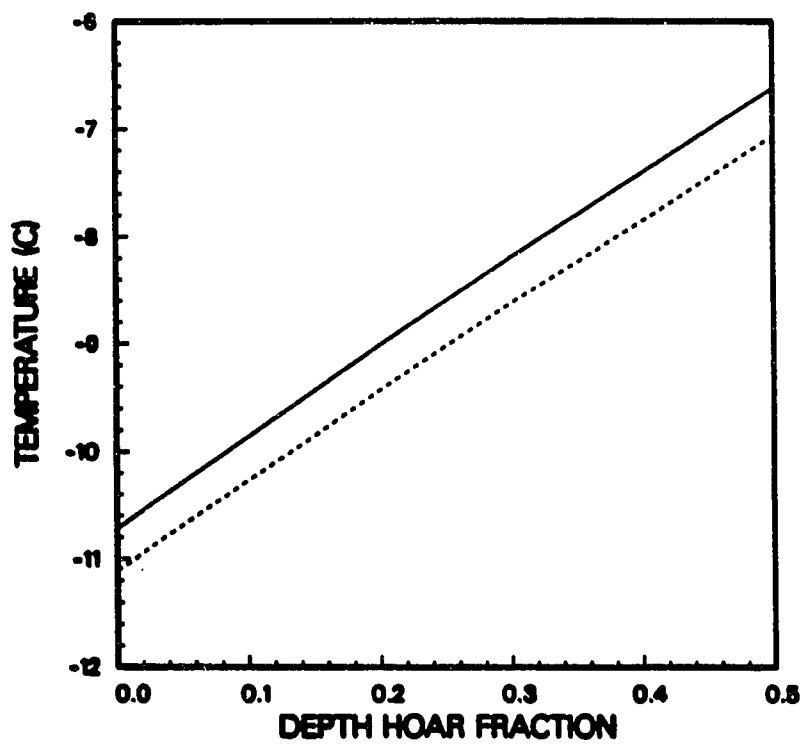


Figure 5.16 Influence of the depth hoar layer fraction on temperatures at the ground surface (solid line) and at a depth of 1.0 m below the ground surface (dashed line) along the Alaskan Arctic Coast.

temperature difference between case 9 and case 11 is over 6°C during the mid-winter. Figure 5.16 shows that MAGST (solid line) and mean annual temperature at a depth of one meter under the ground surface (dashed line) increases with increasing ϕ . The depth hoar layer (with $\phi = 0.50$) can increase MAGST and MAGT by over 4°C . The thermal offset value increases slowly with ϕ , ranging from -0.39°C for $\phi = 0.0$ to -0.45°C for $\phi = 0.50$. This is simply due to the longer thawed state of the active layer.

5.4.4 Accumulation and Melting Processes

The accumulation and melting processes of the seasonal snow cover also play an important role in the insulation effect of the ground thermal regime. As described in Chapter 4, the accumulation and melting processes of snow can be described by (4.1). Four cases were computed by varying n in (4.1) (see Table 5.6) to investigate the response of the ground thermal regime.

Table 5.6 Effect of build-up of snow cover on the ground thermal regime

Cases	$P_1 \leq t \leq P_2$	$P_2 \leq t \leq P_3$	T_s $^{\circ}\text{C}$	T_g $^{\circ}\text{C}$
14	$n = 1$	$n = 1$	-9.50	-9.76
15	$n = 2$	$n = 2$	-10.87	-11.08
16	$n = 3$	$n = 3$	-11.59	-11.79
17	$n = 1$	$n = 3$	-9.68	-9.92

Results for case 14 through case 17 are shown in Figure 5.17. Thicker snow cover in early winter (case 14, dashed line in Figure 5.17) provides the most insulating effect on the ground thermal regime; while thinner snow cover (case 16, chain dashed line in Figure 5.17) indicates the least insulating effect. Thicker snow cover in early winter (case 14) can also

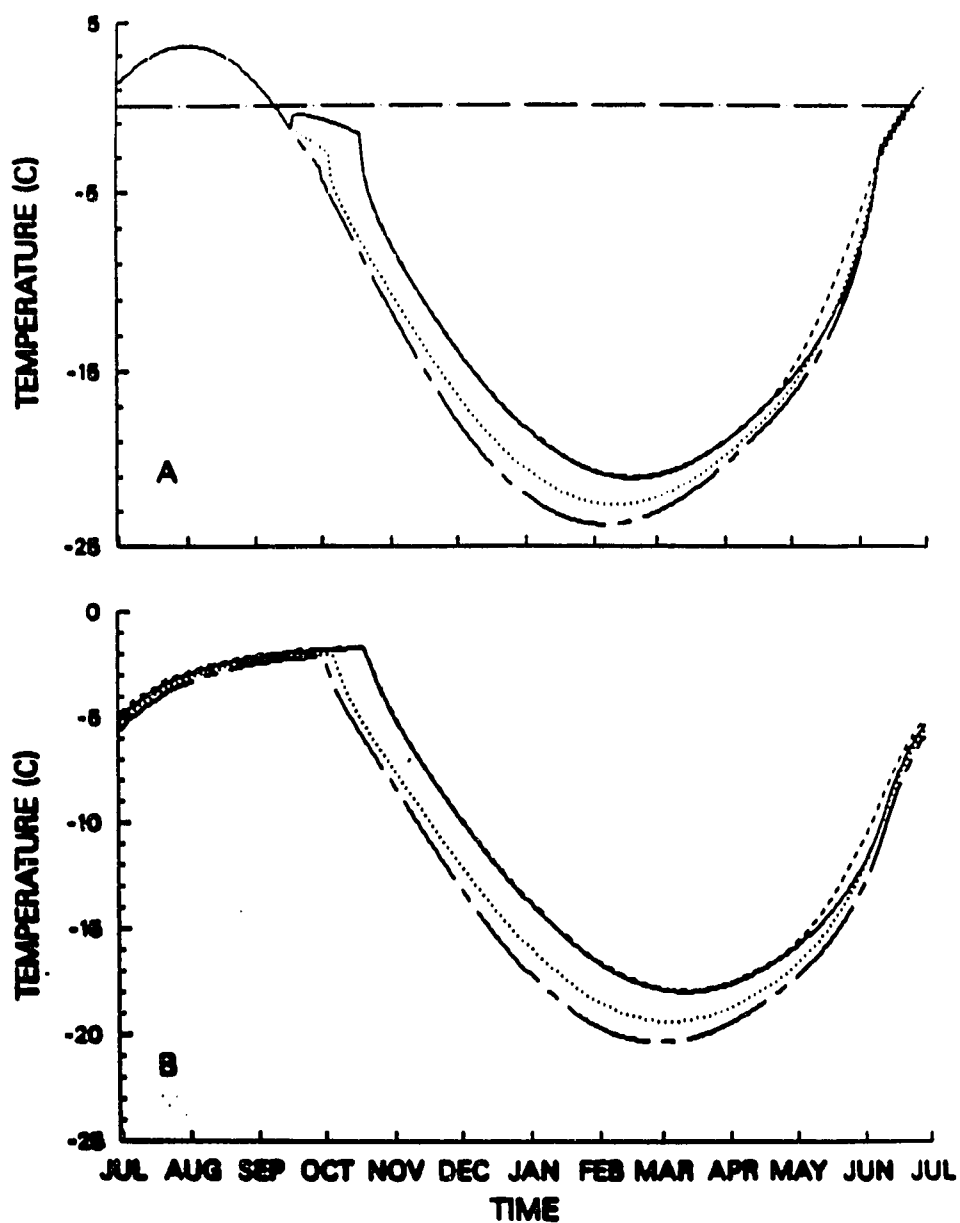


Figure 5.17 Influence of the accumulation and melting rates of seasonal snow cover on temperatures at the ground surface (A) and at depth of 1.0 m below the ground surface (B) along the Alaskan Arctic Coast. Dashed lines for case 14, solid lines for case 17, dotted lines for case 15, and chain-dashed line for case 16.

make the active layer freeze up about one month later and increase MAGST and MAGT about 2°C compared with the thinner snow cover (case 16). The effect of snow melting processes on the ground thermal regime is reduced significantly compared with the accumulation processes. The effect of different snow melting processes in the late spring (e.g. $n=1$, $n=2$, and $n=3$) on MAGST and MAGT is reduced significantly compared with the effect of different snow accumulation processes in the late Fall. For $n=1$, MAGST and MAGT increase slightly faster during Spring than for $n=2$ and $n=3$ as shown in Figure 5.17. In general, $n = 1$ is a favorable melting processes for warming the ground and $n = 3$ is the least favorable condition.

5.4.5 Amplitude of Mean Annual Air Temperature

An amplitude variation of MAAT can have a significant effect on the ground thermal regime. Four cases were computed by varying the annual surface temperature amplitude A_o to study the response of the ground thermal regime with the snow conditions along the coast. Table 5.7 summarizes the input values for A_o and some results.

Table 5.7 Effect of the amplitude of MAAT (A_o) on the ground thermal regime, L_{ts} stands for the length of thaw season and Z for the active layer thickness. The calculation was conducted under the average snow conditions along the coast.

Cases	A_o ($^{\circ}\text{C}$)	MAGST ($^{\circ}\text{C}$)	T_g ($^{\circ}\text{C}$)	T_{off} ($^{\circ}\text{C}$)	L_{ts} (day)	Z (cm)
18	16	-9.56	-9.81	-0.25	79	22
19	18	-8.46	-8.92	-0.46	95	32
20	20	-8.06	-8.73	-0.67	105	40
21	22	-8.12	-9.00	-0.88	113	45

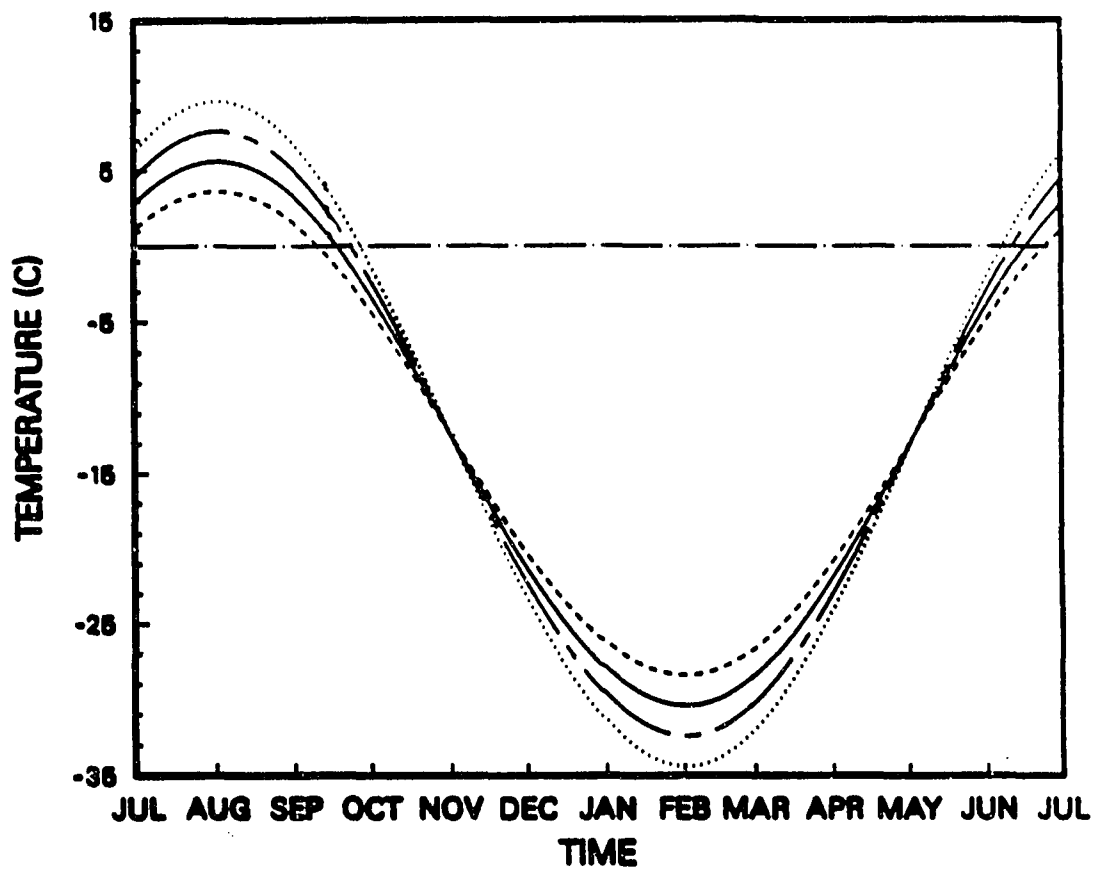


Figure 5.18 Variation of the upper boundary conditions with annual amplitude. Dashed line for $A_o = 16^\circ\text{C}$, solid line for $A_o = 18^\circ\text{C}$, chain-dashed line for $A_o = 20^\circ\text{C}$, and dotted line for $A_o = 22^\circ\text{C}$.

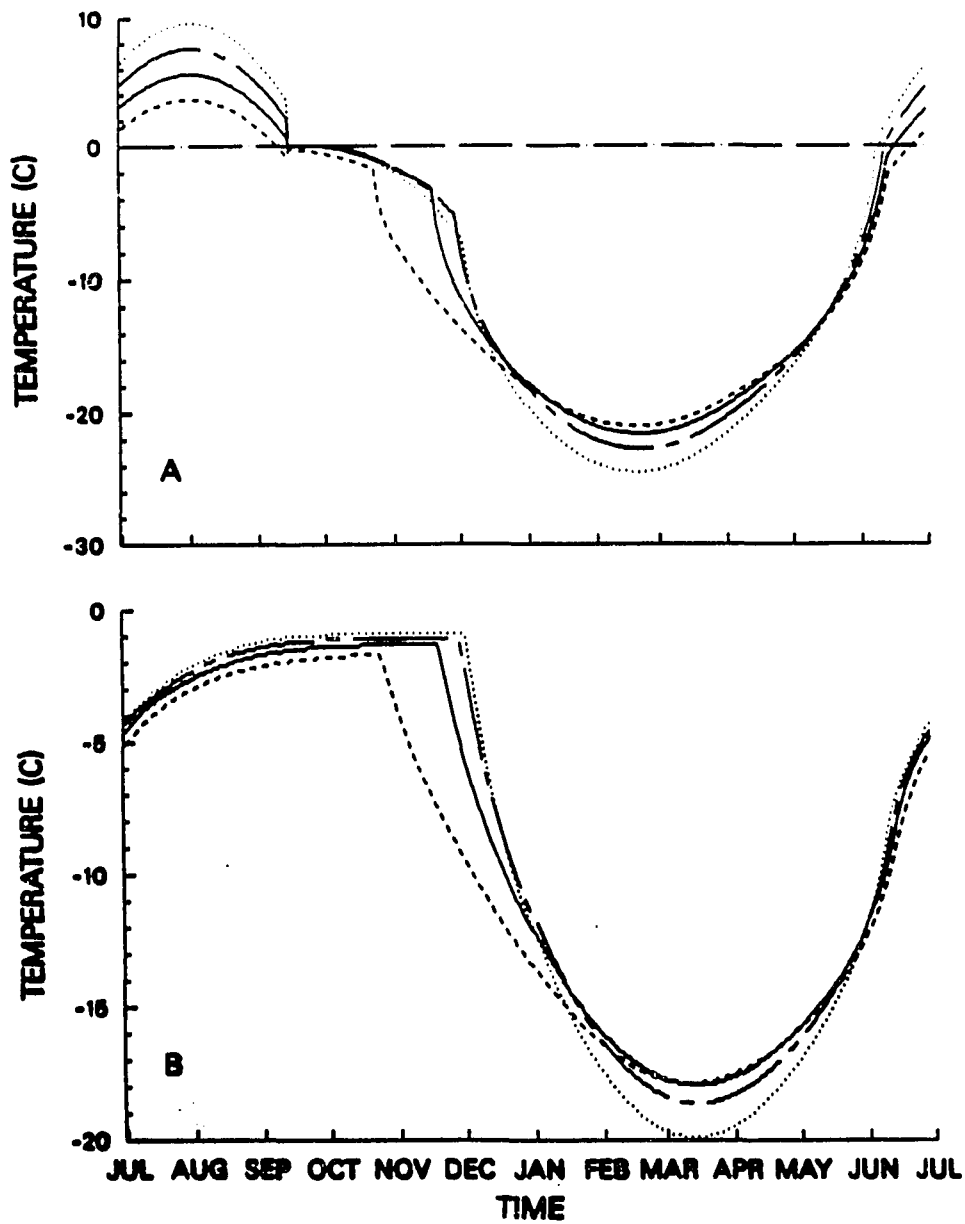


Figure 5.19 Influence of the annual amplitude of the mean air temperature on the temperatures at the ground surface (A) and at depth of 1.0 m below the ground surface (B). Dashed line for case 18 ($A_o = 16^\circ C$), solid line for case 19 ($A_o = 18^\circ C$), chain-dashed line for case 20 ($A_o = 20^\circ C$), and dotted line for case 21 ($A_o = 22^\circ C$).

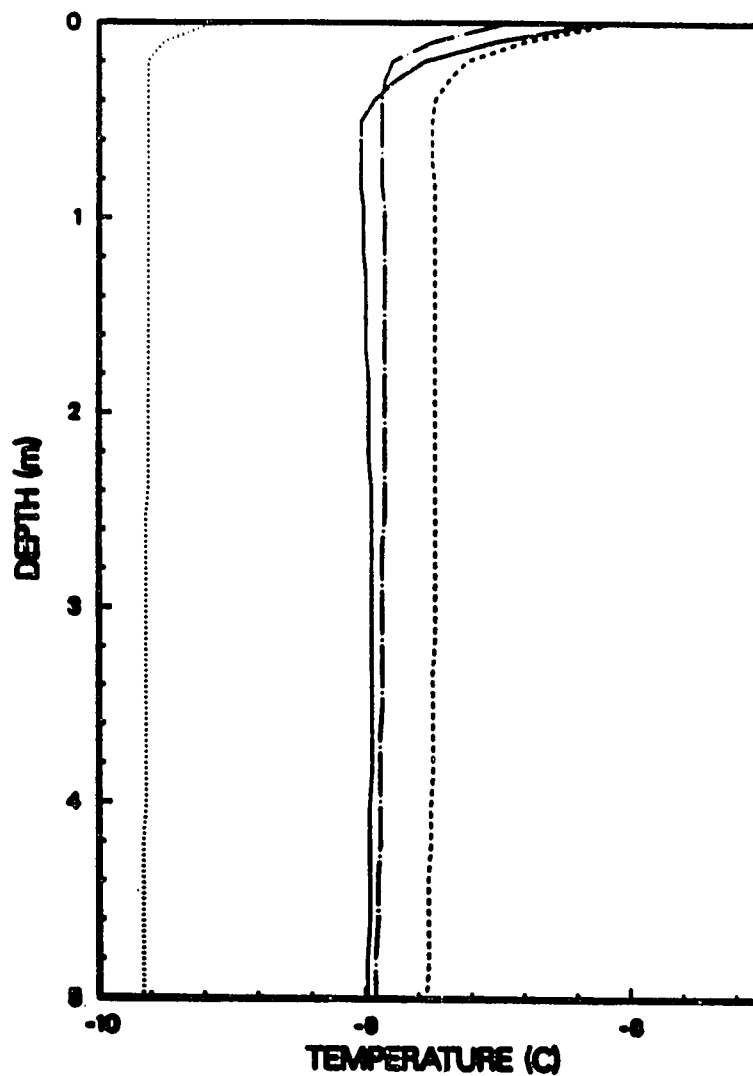


Figure 5.20 Influence of the annual amplitude of mean annual temperature on the ground thermal temperatures. Dotted line for case 18 ($A_o = 16^\circ C$), chain-dotted line for ($A_o = 18^\circ C$), dashed line for case 20 ($A_o = 20^\circ C$), and solid line for case 21 ($A_o = 22^\circ C$).

As shown in Figures 5.18 and 5.19, smaller A_o results in a short and cold summer and a longer and relatively “warm” winter; while larger A_o would have a relatively longer and warmer summer and a colder winter both at the ground surface and in permafrost (one meter under the ground surface). The difference between the dates of the active layer freeze-up decreases as A_o increases. The active layer freezes up about a month earlier for $A_o = 16^\circ C$ than for $A_o = 18^\circ C$; and only about three days earlier for $A_o = 20^\circ C$ than for $A_o = 22^\circ C$ as shown in Figure 5.19. This may be related to the variation in the active layer thickness and the freezing rate with A_o . First of all, the variation of the length of the thaw season with A_o is nonlinear as shown in Table 5.6. The thaw season is about 16 days shorter for $A_o = 16^\circ C$ than for $A_o = 18^\circ C$; while only 8 days shorter for $A_o = 20^\circ C$ than for $A_o = 22^\circ C$. The variation of the active layer thickness with the length of the thaw season is not linear either, as stated by the Stefan problem (Lunardini, 1988). As a result, the rate of the thickness increase of the active layer with A_o is reduced substantially. On the other hand, the cooling and freezing rates in later fall and early winter increase considerably as A_o increases. The larger difference between the dates of the active layer freeze-up for $A_o = 16^\circ C$ and for $A_o = 18^\circ C$ may be also related with the variation of the physical and thermal properties within the active layer. The soil profile consists of about 0.3 m peat layer with a water content of about 300% by mass at the top, then mineral soil with a water content of about 31% by mass is underneath the peat layer. The higher water content in the peat layer requires a considerable amount of latent heat to freeze the active layer.

Figure 5.18 shows that minimum temperatures occur in early February on the snow surface, and the difference between minimum temperature values with A_o is equal. Due to the effect of the seasonal snow cover and the active layer, minimum temperatures occur at the middle of February at the ground surface and at the middle of March in permafrost. In other words, minimum temperatures at the ground surface and at depth of one meter below the

ground surface lag about over one week and over one month with minimum temperature at the snow surface. The difference of minimum temperature between $A_o = 16^\circ C$ and $A_o = 22^\circ C$ at the snow surface is $8^\circ C$, it is reduced to $4^\circ C$ at the ground surface and to $2^\circ C$ at depth of one meter below the ground surface as shown in Figures 5.18 and 5.19.

The magnitude of the thermal offset increases with A_o due to the increase of the active layer thickness and the length of thaw season as shown in Table 5.6.

The influence of the amplitude of MAAT on the ground temperature is complicated by the effect of seasonal snow cover and the active layer. *Lachenbruch* (1959) reported the effect of seasonal snow cover in warming the ground is increased if the surface temperature amplitude is increased. *Goodrich* (1976, 1978, 1982) made some calculations by increasing the surface temperature amplitude from $15^\circ C$ to $17^\circ C$ and results show the mean annual temperature increases about $0.5^\circ C$. However, this is not always true to the same extent when the surface temperature amplitude increases. As indicated in Figure 5.20 and Table 5.6, the ground temperature increases as A_o increases from $16^\circ C$ to $18^\circ C$; while the ground temperature decreases about a few tenths degree as A_o increases from $20^\circ C$ to $22^\circ C$.

5.5 Discussion

Table 5.1 summarizes the seasonal snow cover conditions in Alaska North of the Brooks Range. As shown in the above section, 21 cases were computed to investigate the effect of changes in seasonal snow cover parameters on the ground thermal regime. Table 5.8 summarizes the calculated results for all cases and all the results are compared with the standard case (case 2) along the Alaskan Arctic Coast. ΔT in Table 5.8 represents the difference of MAGST from the standard calculations.

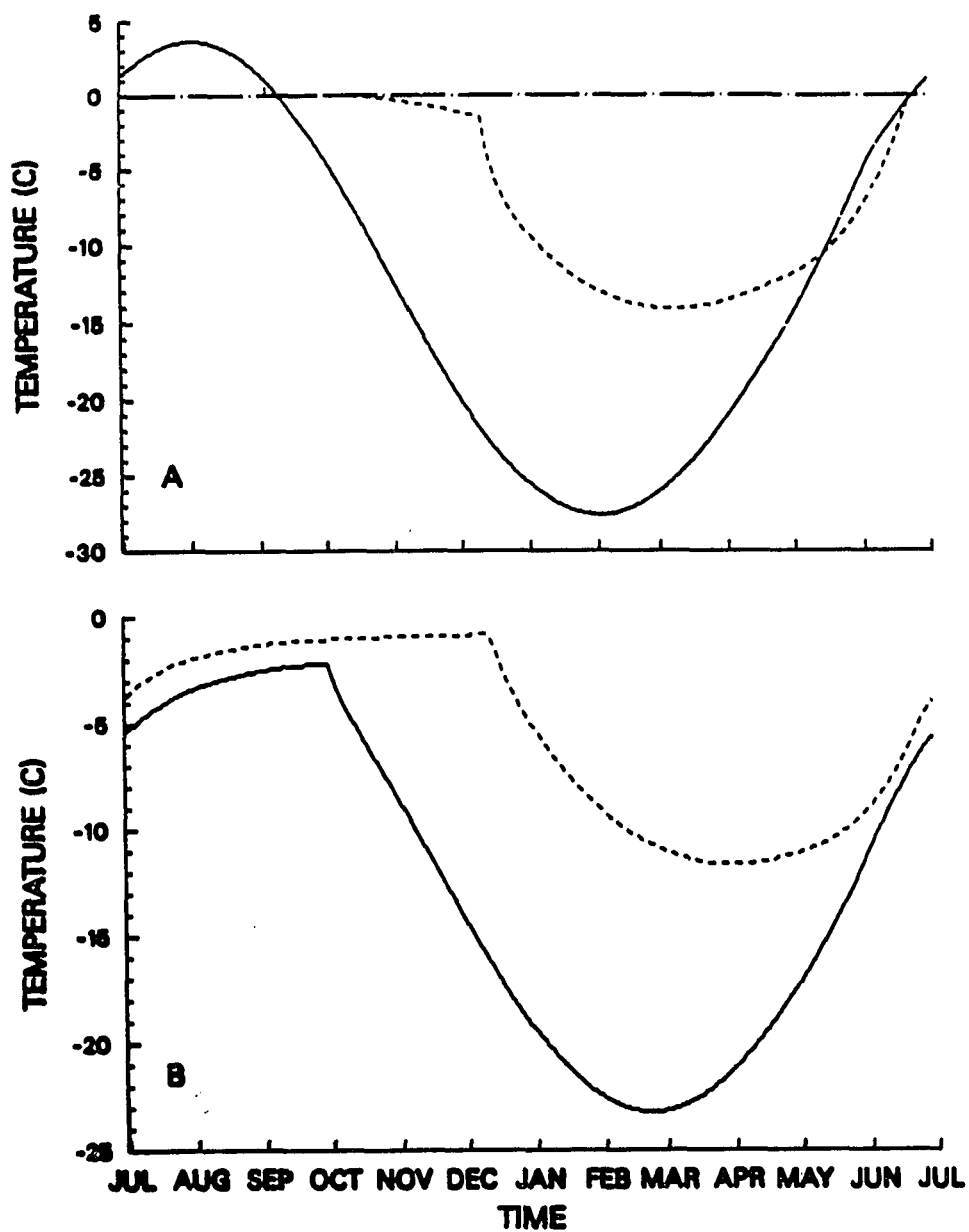


Figure 5.21 Influence of seasonal snow cover on temperatures at the ground surface (A) and at depth of 1.0 m below the ground surface (B) for two extreme cases as summarized in Table 5.9. Dashed lines stand for case 22 and solid lines for case 23.

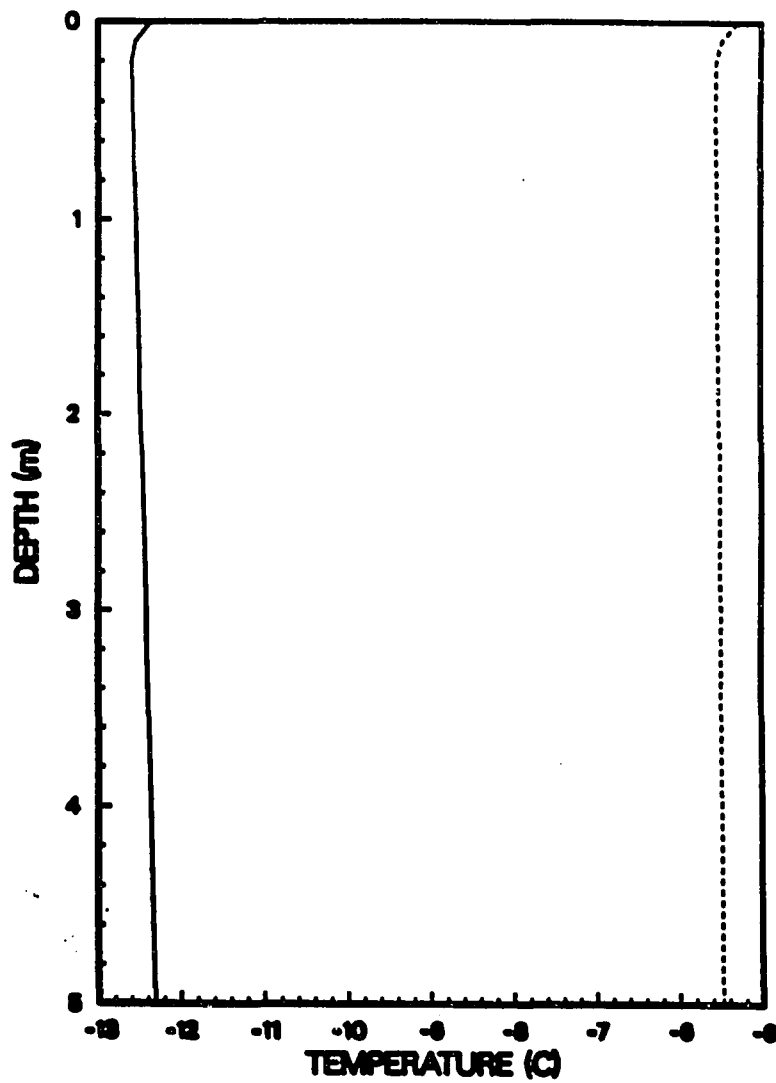


Figure 5.22 Influence of seasonal snow cover on ground temperatures for two extreme cases as summarized in Table 5.9. Dashed line stand for case 22 and solid line for case 23.

Table 5.8 Summary of calculated results for all cases. ΔT represents the difference of mean annual ground surface temperature from the standard calculations, T_{off} is the thermal offset value.

case No.	ΔT ($^{\circ}C$)	T_{off} ($^{\circ}C$)	Comments
1	+0.20	-0.39	<i>Longest duration</i>
3	-0.13	-0.42	<i>Shortest duration</i>
4	-2.03	-0.39	$H_{max} = 0.15m$
5	-1.00	-0.43	$H_{max} = 0.25m$
7	+0.95	-0.45	$H_{max} = 0.45m$
8	+1.42	-0.45	$H_{max} = 0.50m$
9	-2.53	-0.39	$\phi = 0.0$
10	-1.67	-0.41	$\phi = 0.10$
11	-0.82	-0.42	$\phi = 0.20$
12	+0.78	-0.45	$\phi = 0.40$
13	+1.57	-0.45	$\phi = 0.50$
14	+0.18	-0.44	$n = 1$
15	-1.19	-0.40	$n = 2$
16	-1.91	-0.39	$n = 3$
19	+1.10	-0.46	$A_o = 18^{\circ}C$
20	+1.50	-0.67	$A_o = 20^{\circ}C$
21	+1.44	-0.88	$A_o = 22^{\circ}C$

Table 5.8 shows that the effect of the total thickness of seasonal snow cover and depth hoar layer fraction are most important factors for the seasonal snow cover parameters. A change in the maximum snow cover thickness by 0.10 m could vary MAGST by about $1^{\circ}C$. A change in the depth hoar fraction by 10% could vary MAGST by about $0.8^{\circ}C$. Effect of changes in seasonal snow cover parameters on the thermal offset is generally not significant, (less than $0.1^{\circ}C$). However, the combined effect of changes in all these parameters could be very significant. Two extreme cases were calculated to investigate this combined effect. Table 5.9 summarizes the input data for the calculations. For early snowfall and later snowmelt

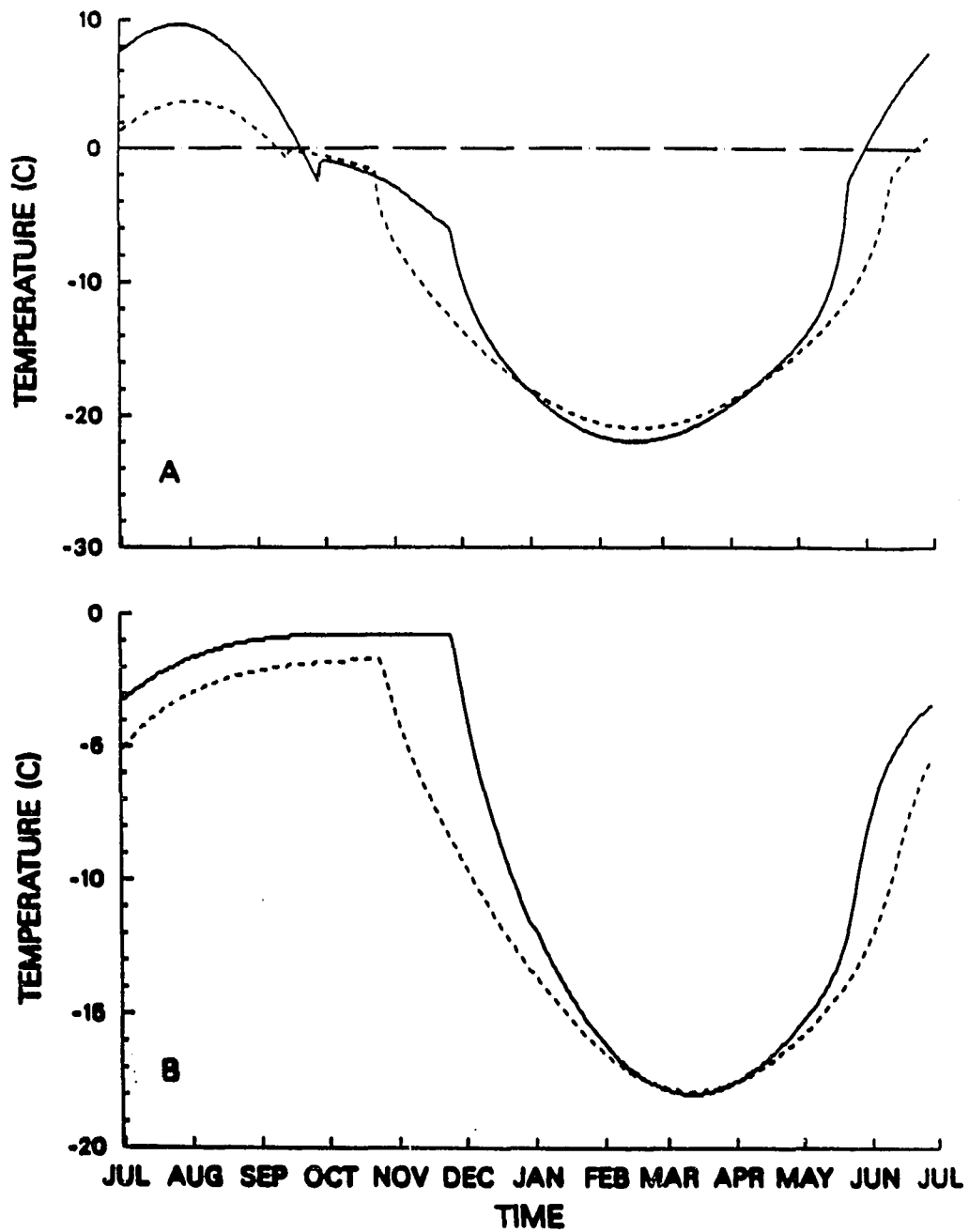


Figure 5.23 Influence of air temperature and seasonal snow cover on temperatures at the ground surface (A) and at depth of 1.0 m below the ground surface (B) along the Arctic Coast (solid line) and inland (dashed line) in Alaska north of the Brooks Range.

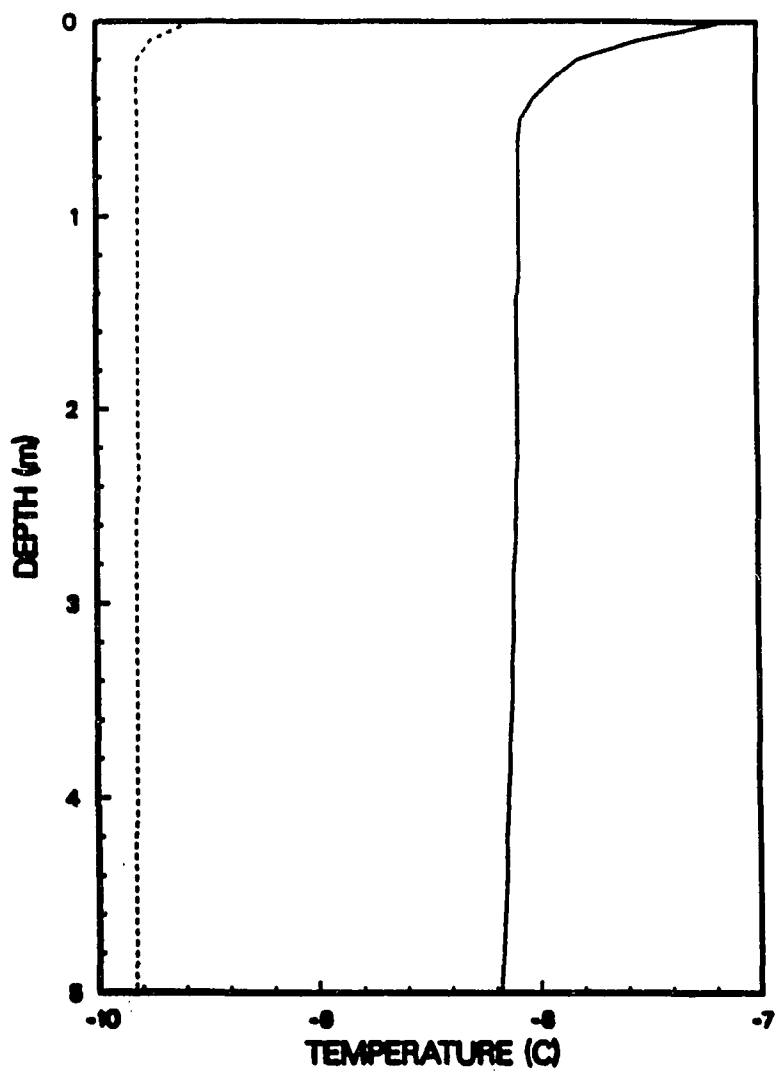


Figure 5.24 Influence of air temperature and seasonal snow cover on ground temperatures along the Arctic coast (solid line) and inland (dashed line) in Alaska north of the Brooks Range.

with the annual maximum snow thickness of about 0.50 m and the depth hoar layer well developed (case 22), the ground surface temperature could increase over 3.1°C from the long-term average condition. On the other hand, if there is a late snowfall and early snowmelt with the maximum snow thickness of 0.15 cm and depth hoar layer poorly developed (case 23), MAGST could decrease as much as 3.8°C . The temperature difference between the two extreme cases is as high as 6.9°C as shown in Figure 5.23. The active layer freezes up over two months earlier for case 23 than that for case 22. In Spring, the late snow melt for case 22 prevents the rapid warming of the ground surface compared with the early snow melt as shown in Figure 24. Temperature at 1.0 m is slightly lower for case 23 than for case 22 due to the extreme cold temperature in the previous winter.

Table 5.9 Summary of input values for two extreme cases

item	case 22	case 23	Unit
P_1	66	88	(day)
P_2	358	338	(day)
H_{max}	50	15	(cm)
ϕ	0.50	0.0	(%)
n	1	3	
A_o	16	16	($^{\circ}\text{C}$)
T_s	-5.2	-12.1	($^{\circ}\text{C}$)
T_g	-5.5	-12.4	($^{\circ}\text{C}$)
T_{off}	0.3	0.3	($^{\circ}\text{C}$)

Micro-climatic conditions can change significantly from place to place. Each location has its own combination of air temperature and snow cover. The combined effect on the ground thermal regime can be very different. Table 5.2 summarizes the average climatic conditions along the coast which includes Barrow, Barter Island, West Dock, Prudhoe Bay

and Deadhorse, and Inland which includes Umiat, Franklin Bluffs and Happy Valley stations. Figure 5.21 shows comparison of snow cover and air temperature effect on the ground thermal regime along the Arctic Coast and inland in Alaska North of the Brooks Range. Although their MAATs are about the same, differences in timing and duration, maximum thickness of seasonal snow cover, and in amplitude of mean annual air temperature results in different patterns of ground temperature variations with time (Figure 5.21) and a MAGT difference of over 1.6°C (Figure 5.22). This can partly explain why permafrost temperatures increase about 4°C from the coast to inland in Alaska north of the Brooks Range. Combined with the difference in vegetation and depth hoar layer development from the coast to inland, the permafrost temperature increase could be well understood in the regions.

5.6 Summary

A finite difference model for one-dimensional heat flow problems with phase change was used to investigate the effect of air temperature and seasonal snow cover on permafrost temperatures. The model was calibrated with the measured physical and thermal properties and temperature data at West Dock, near Prudhoe Bay. The upper boundary was set at the snow surface when seasonal snow cover was present and the boundary condition was represented by the measured daily mean air temperatures. For the remainder of the year, the boundary was set at the base of the living plant layer and the boundary condition was represented by an equation correlating measured daily air and ground surface temperatures.

The thickness of seasonal snow cover was measured by the National Weather Service near Deadhorse airport for the time same period as the soil temperature measurement in this region. A two layer structure (wind-packed layer and depth hoar layer) of the seasonal snow cover was used in the model. Thermal conductivity of the snow cover was calculated based upon an

equation developed using series heat conduction theory. Physical and thermal properties for soils were obtained from Chapter 3 and *Lachenbruch et al. (1982)* .

Two different cases were calculated to verify the numerical model. Case I was calculated with the upper boundary set at the snow surface when snow was present and at the ground surface when snow was absent. The results show good agreement between the measured and calculated values. The standard deviation of the calculated daily mean ground surface temperature from the measured values is within 1°C . Case II was calculated with the upper boundary set at the ground surface and the boundary conditions represented by the measured daily mean ground surface temperatures. Results show that case II provides a better agreement with the measured temperature data than the values calculated by case I. This may be due to errors produced by modeling the effect of seasonal snow cover on the ground temperatures with daily mean air temperature. There is an offset between computed and calculated temperatures in the upper permafrost. Results from cases I and II indicate an excellent agreement between the measured and calculated permafrost temperatures with depth.

Sensitivity analysis of the ground thermal regime to changes in seasonal snow cover parameters such as the timing and duration, thickness, depth hoar layer, accumulation and melting processes, and amplitude of MAAT were conducted using the calibrated numerical model. Twenty one cases were calculated to investigate the effect of changes in seasonal snow cover parameters on the ground thermal regime.

For the same air temperature conditions, the earliest snow cover on the ground keeps the ground from freezing and maintains the ground surface temperature near 0°C for about two weeks longer compared with the results from the average case. The latest snow cover on ground allows ground to freeze before snowfall. Once a snow cover is established on the ground, the surface temperature increases to 0°C due to the heat stored in the active layer. The early snow cover provides more insulating effect, thus the active layer lasts longer and

temperatures at the ground surface and at 1.0 m are higher compared with late snow cover on ground. As winter progresses, the temperature difference between the two cases decreases. Late snow disappearance in Spring prevents the warming of the ground due to the latent heat effect of snow melting. As a whole, the early snow cover and late snow disappearance on ground can raise the MAGST by as much as 0.35°C compared with the results for late snow cover in Fall and early snow disappearance in Spring. Effect of timing and duration of seasonal snow cover on the thermal offset is not significant.

The insulating effect of seasonal snow cover increases with increase of H_{max} . The rate of MAGST increase with H_{max} is around $0.1^{\circ}\text{C}/\text{cm}$, but this rate decreases slightly with increasing H_{max} . The thermal offset value increases slowly with H_{max} and ranges from -0.39°C for $H_{max} = 15 \text{ cm}$ to -0.47°C for $H_{max} = 50 \text{ cm}$.

Due to the low density and low thermal conductivity of the depth hoar layer, the insulating effect of the seasonal snow cover increases with increasing depth hoar fraction, ϕ . The rate of MAGST and MAGT increase with ϕ is about 0.8°C for changes in ϕ by 10%. Development of the depth hoar layer during early winter can have a significant effect on the rate at which the active layer freezes up. However, the effect of the depth hoar layer on the ground thermal regime during Spring is reduced substantially. The effect of the depth hoar layer on the thermal offset is relatively small.

Thicker snow cover in early winter provides the most insulating effect, while thinner snow cover indicates the least effect. A thicker snow cover in early winter can make the active layer freeze up about one month later and MAGST and MAGT become about 2°C higher compared with the effect of a thinner snow cover. The effect of different snow melting processes (e.g. $n=1, n=2$, and $n=3$) on MAGST and MAGT in late Spring is reduced significantly.

The combined effect of changes in seasonal snow cover parameters on MAGST and MAGT can be very significant. For early snowfall and later snowmelt with the maximum snow

thickness of about 0.5 m and the depth hoar layer well developed, MAGST could increase over 3.1°C from the long-term average condition. For late snowfall and early snowmelt with the maximum snow thickness of 15 cm and the depth hoar layer poorly developed, MAGST could decrease as much as 3.8°C from the long-term average condition. The MAGST difference between these two extreme cases could be as high as 6.9°C and the active layer freeze up could be delayed about two months from one case to the other.

The calculated results also show that the combined effect of local seasonal snow cover and air temperature on the ground thermal regime could be very different. Although the MAAT along the Arctic Coast and Inland are about the same, but differences in timing, duration, and maximum thickness of seasonal snow cover and in amplitude of mean annual air temperature can result in different patterns of ground temperature variations with time. The computed results show that permafrost temperature can differ about over 1.6°C from the Coast to inland due simply to variation in timing and maximum thickness of seasonal snow cover. Combined with the difference in vegetation and depth hoar layer development from the Coast to inland, the permafrost temperature increase could be well understood in the regions.

CHAPTER 6

Response of Permafrost Temperature to Changes in Climate

6.1 Introduction

Studies of the interaction between the atmosphere and permafrost can generally be divided into two categories: the forward problem, investigating the effects of climatic change on ground temperatures or the heat flow; and the inverse problem, inferring past climatic variations from ground temperature data. Some of this work was done in the 1920's and the 1930's (*Lane, 1923 ; Hotchkiss and Ingersoll, 1934*). *Beck (1992)* provides a brief review of the history of the forward and inverse studies. *Wang (1992)* summarized the last two decades of research. Recently *Lachenbruch and Marshall (1986)* and *Lachenbruch et al. (1988)* presented geothermal evidence from the Alaskan Arctic for a global warming in the last century. Since then, the use of borehole temperature data to study past climatic change has gained great attention.

It has been established that the long-term mean surface temperature (MST) of the permafrost, obtained by extrapolating the deep linear portions of temperature profiles to the surface, in Alaska's Arctic Region north of the Brooks Range has recently warmed about 2 to 4°C (*Lachenbruch and Marshall, 1986; Lachenbruch et al., 1988; Osterkamp, 1988; Clow and Lachenbruch, 1990*). Estimates for the start of this warming are generally about 40 to 80 years ago. Weather records for the North American Arctic and Alaska show that there was a cooling trend from about 1940 until the mid-1970s (e.g. *Hansen and Lebedeff, 1987*). However, there is no evidence for this colder period, which lasted three and one-half decades,

in the permafrost temperature profiles. This apparent anomaly suggests that the relationships between air and permafrost temperatures require further investigation. *Zhang and Osterkamp* (1993a,b) investigated, through modeling, the response of permafrost temperatures in Alaska north of the Brooks Range to changes in climate using climatological data at Barrow. Their primary results show that changes in air temperature alone could not have produced the permafrost warming and changes in seasonal snow cover could play an important role. Detailed information on the climatic change and permafrost temperatures were included in Chapter 2 and in *Zhang and Osterkamp* (1993a,b) .

This chapter investigates the effects of changes in air temperatures and seasonal snow cover in the past, the active layer, initial temperature conditions, and variations of thermal properties of soils on permafrost temperatures. We will review some of the available information on permafrost temperatures. Numerical modeling results will be presented showing the effects of using past air temperatures as the boundary condition at the permafrost surface, ground surface, and surface of the snow cover when snow cover was present and on the ground surface when snow cover was absent. The effects of initial conditions, the presence or absence of a snow cover and changes in thermal properties of soils on permafrost temperatures will be discussed.

6.2 Model Assumptions and Data

A finite difference model for one-dimensional heat flow problems with phase change (Goodrich 1976, 1977, 1982) was used. This numerical model has a detailed routine for including the effect of snow cover on soil (active layer and permafrost) temperatures. The model has been modified to use weather data input files and for the long-term calculations needed in this research. Comparisons of model predictions with analytical solutions have been

excellent (see Chapter 5). This numerical model has been calibrated using our unpublished data for conditions near the West Dock at Prudhoe Bay, Alaska which is close to site E of Lachenbruch et al. (1982).

Three temperature time series were used as the boundary conditions for various cases. The first temperature time series, named BC1, is the air temperature variations for the period from 1880 through 1985 for the North American quadrant of the Arctic (*Hansen and Lebedeff, 1987*) as shown in Figure 6.1C. Seasonal temperature variations were not included and daily temperatures were generated from mean annual temperatures by linear interpolation. The second temperature time series, named BC2, is the daily air temperatures for the period from July 1, 1923 through December 31, 1991 at Barrow. For the period from January 1, 1949 through December 31, 1988, daily air temperatures were obtained through the Alaska Climate Research Center at the Geophysical Institute, University of Alaska Fairbanks. For periods from July 1, 1947 through December 31, 1948 and from January 1, 1989 through December 31, 1991, daily mean air temperatures were obtained from Local Climatological Data. Daily mean air temperatures for the period from July 1, 1923 through June 30, 1947 at Barrow were obtained from monthly mean air temperatures using the linear interpolation method. The third temperature time series, named BC3, is a combination of BC2 with part of Hansen's data. The daily air temperatures for the period from January 1, 1880 through June 30, 1923 were generated from mean monthly air temperatures (*Hansen and Lebedeff; 1987*) using linear interpolation.

Seasonal snow cover data for the period from January 1, 1949 through December 31, 1988 at Barrow were obtained through the Alaska Climate Research Center at the Geophysical Institute, University of Alaska Fairbanks. For periods from July 1, 1947 through December 31, 1948 and from January 1, 1989 through December 31, 1991, the thicknesses of the seasonal snow cover were obtained from the Alaska Climatological Summary. Continuous snowfall

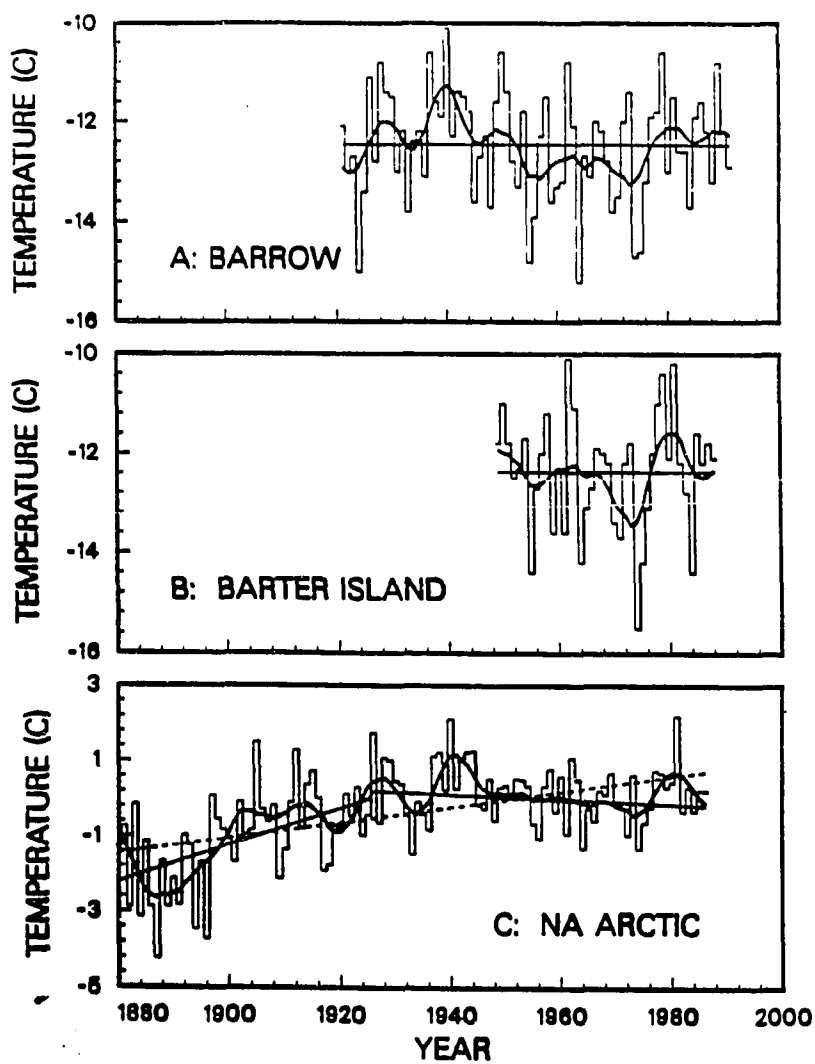


Figure 6.1 MAAT from the U. S. Weather Bureau at Barrow (A) and at Barter Island (B). The data in (C) represent the temperature variations obtained by Hansen and Lebedeff (1987) for the North American quadrant of the Arctic. The record average (thin solid lines in A and B) and selected regression lines (thin solid and dashed lines in C) as used by Lachenbruch et al. (1988) are also shown.

measurements at Barrow started in Fall 1923 but there were no direct measurements of snow cover thickness on the ground surface for the period from 1923 through 1947. However, the thickness of seasonal snow cover on the ground is directly related to the total snowfall, although wind and local microrelief can be important factors which affect the thickness of snow on the ground. Figure 6.2 shows the relationship between annual total snowfall and maximum thickness of snow on ground for the period from 1947 through 1991 at Barrow. The maximum thickness of seasonal snow cover can be expressed as

$$H_{max} = 0.42P_{sf} + 4.70 \quad (6.1)$$

where P_{sf} represents the annual total snowfall in cm, with a correlation coefficient of 0.82 and standard deviation of $\pm 9cm$. Daily thicknesses of snow cover on the ground were generated using (4.1) with H_{max} calculated by (6.1). The other parameters needed in (4.1) are listed in Table 5.1. There were only sporadic measurements of snowfall and snow on ground before 1923.

The choice of initial conditions for modeling the response of permafrost to surface temperature changes is often difficult. A constraint is imposed by the long-term MST (obtained by extrapolating deeper temperatures to the surface) and the time when the equilibrium temperature profile was established. The possibility remains that near surface permafrost temperatures may have been significantly colder or warmer than the long-term mean for periods of several decades. Perturbations in the temperature profiles supporting this idea have not been reported. This problem is inherent in forward modeling of long-term permafrost temperatures.

The soil was represented as a layered system and the lower boundary was set at a depth of 300 m with a constant geothermal heat flux. For each individual layer, the thermal properties were constant but varied from one layer to another with distinct frozen and thawed values.

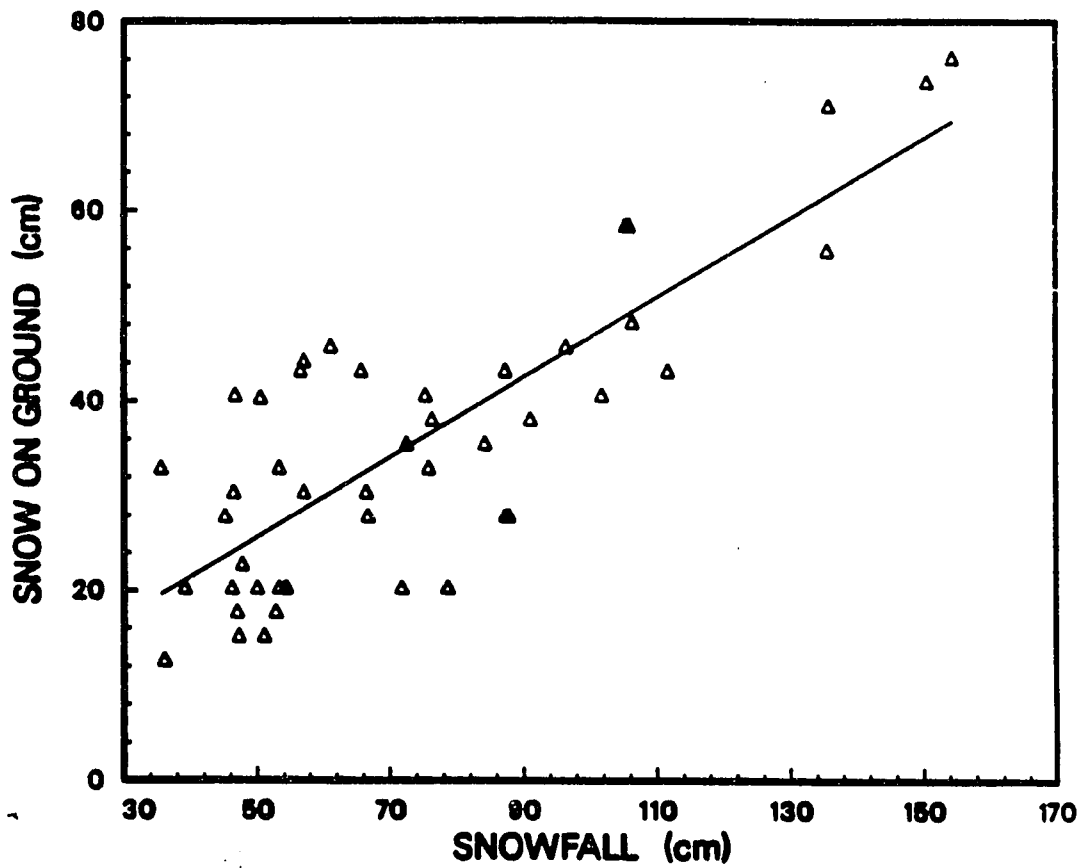


Figure 6.2 Relationship between total annual snowfall and maximum thickness of snow on the ground for the period from 1947 through 1991 at Barrow

The effective thermal conductivity of the seasonal snow cover was calculated by (5.7) with all other parameters defined in Table 5.1.

The calculation was conducted with $\Delta t = 1$ day and Δx ranged from 0.02 m in the seasonal snow cover and near the ground surface to 5 m near the lower boundary.

6.3 Modeling Results

Table 6.1 summarizes brief information for each case. Detailed data for the calculations will be stated specifically for each case.

6.3.1 Effects of Initial Conditions and Air Temperature

The air temperature changes for the North American Arctic (Figure 6.1C) were used for the surface temperature changes of the permafrost (0°C corresponding to a $MST = -12.0^{\circ}\text{C}$). Seasonal temperature variations were not included. Lachenbruch et al. (1988) have made similar calculations for their AWUNA site, about 375 km southwest of Prudhoe Bay. Physical and thermal parameters for the active layer and permafrost were based upon data for Prudhoe Bay conditions such as occur at or near site E (Lachenbruch, et al., 1982; Zhang, 1989) as shown in Table 6.2. Figure 6.3 shows the calculated permafrost temperature changes for different initial conditions. The initial condition in 1880 was assumed to be an equilibrium temperature condition with different long-term MST. In fact, air temperatures were assumed to be constant with the value of the long-term mean until 1880 and then to vary as shown in Figure 1C. For case 1, the $MST = -12^{\circ}\text{C}$ which was changed in increments of -1°C for case 2, case 3, and case 4. This procedure introduces a step change in 1880 ranging between -1°C and 2°C . These curves illustrate the effects of air temperature changes and of different choices of the initial condition on changes in the permafrost temperatures. The results show

Table 6.1 Summary of the calculation conditions, PS represents the permafrost surface, GS the ground surface and SS the snow surface.

case No.	MST ($^{\circ}C$)	T_o ($^{\circ}C$)	Snow	Upper Boundary	BC	Site	Period
1	-12.0	0	NO	PS	BC1	E	1880-1985
2	-13.0	0	NO	PS	BC1	E	1880-1985
3	-14.0	0	NO	PS	BC1	E	1880-1985
4	-15.0	0	NO	PS	BC1	E	1880-1985
5	-12.2	0	NO	GS	BC3	SB3	1880-1991
6	-12.2	-1	NO	GS	BC3	SB3	1880-1991
7	-12.2	-2	NO	GS	BC3	SB3	1880-1991
8	-12.2	-3	NO	GS	BC3	SB3	1880-1991
9	-12.2	-4	NO	GS	BC3	SB3	1880-1991
10	-13.46	0	NO	PS	BC1	E	1880-1985
11	-13.46	0	NO	PS	BC1	E	1880-1985
12	-14.21	0	NO	PS	BC1	E	1880-1985
13	-14.21	0	NO	PS	BC1	E	1880-1985
14	-12.2	0	NO	GS	BC2	SB3	1923-1991
15	-12.2	0	YES	SS	BC2	SB3	1923-1991
16	-12.0	0	NO	GS	BC2	E	1923-1991
17	-12.0	0	YES	SS	BC2	E	1923-1991
18	-12.0	0	YES ⁺	SS	BC3	E	1880-1991
19	-12.0	0	YES ⁺⁺	PS	BC3	E	1880-1991
20	-9.2	0	YES	GS	BC2	E	1923-1991
21	-12.2	0	YES	GS	BC3	SB3	1880-1991
22	-12.2	0	YES	GS	BC3	SB3	1880-1991
23	-12.2	0	YES	GS	BC3	SB3	1880-1991
24	-12.2	0	YES	GS	BC3	SB3	1880-1991
25	-12.2	0	YES	GS	BC3	SB3	1880-1991

+ — $H_{max} = 12.7 \text{ cm}$

++ — $H_{max} = 18.0 \text{ cm}$

that air temperature variations since 1880 are sufficiently large to account for the geothermal

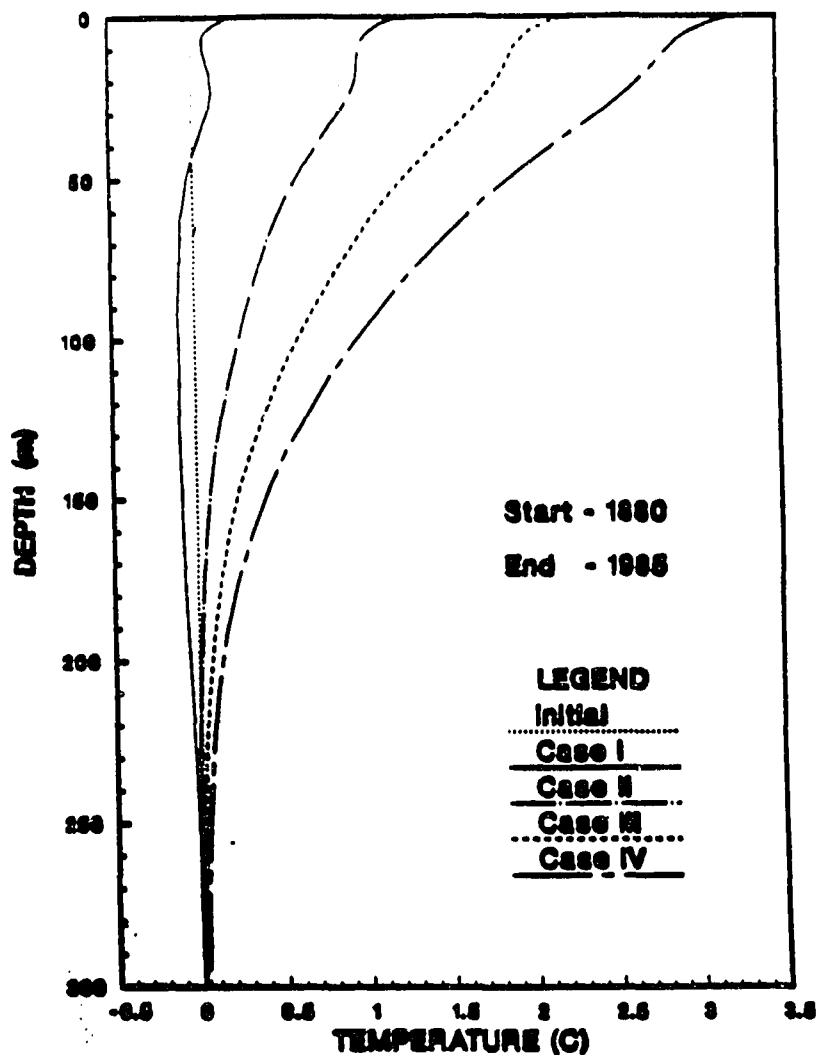


Figure 6.3 Calculated permafrost temperature change in 1985 after removal of the initial linear equilibrium temperature profile, for Prudhoe Bay conditions starting in 1880, using BC1 for the upper boundary condition at the permafrost surface. For case 1 (solid line), the initial equilibrium surface temperature was set at -12°C which was changed in increments of -1°C for case 2 (chain-dotted line), case 3 (dashed line) and case 4 (chain-dashed line).

observations provided that a sufficiently cold MST is assumed initially. Case 3 and case 4 are better matches to the data of Lachenbruch et al. (1986) for the Prudhoe Bay area. Depth of penetration of the calculated curves compared to the data shows that the calculated warming penetrates deeper than observed for these cases.

Table 6.2 Summary of physical and thermal properties of soils at Prudhoe Bay, ρ_b stands for dry bulk density; W for soil water content by mass; D_{th} and D_{fr} for the thawed and frozen soil thermal diffusivities, respectively.

Depth (m)	Soil Type	ρ_b (kg/m ³)	W (%)	D_{th} (m ² /yr)	D_{fr} (m ² /yr)
0.0 - 0.35	peat	330	380	4	30
0.35 - 2.0	silt	1200	37	12	32
2.0 - 30.0	sand	1400	31	18	44
30.0 - 300.0	gravel	1620	24	23	51

Table 6.3 Summary of the physical and thermal properties of soils at Barrow, ρ_b stands for dry bulk density; W soil water content by mass; D_{th} and D_{fr} for the thawed and frozen soil thermal diffusivities, respectively.

Depth (m)	Soil Type	ρ_b (kg/m ³)	W (%)	D_{th} (m ² /yr)	D_{fr} (m ² /yr)
0.0 - 0.2	peat	270	395	5	24
0.2 - 1.0	silt	1100	38	11	30
1.0 - 24.0	silt	1200	30	13	32
24.0 - 300.0	gravel	1440	22	19	35

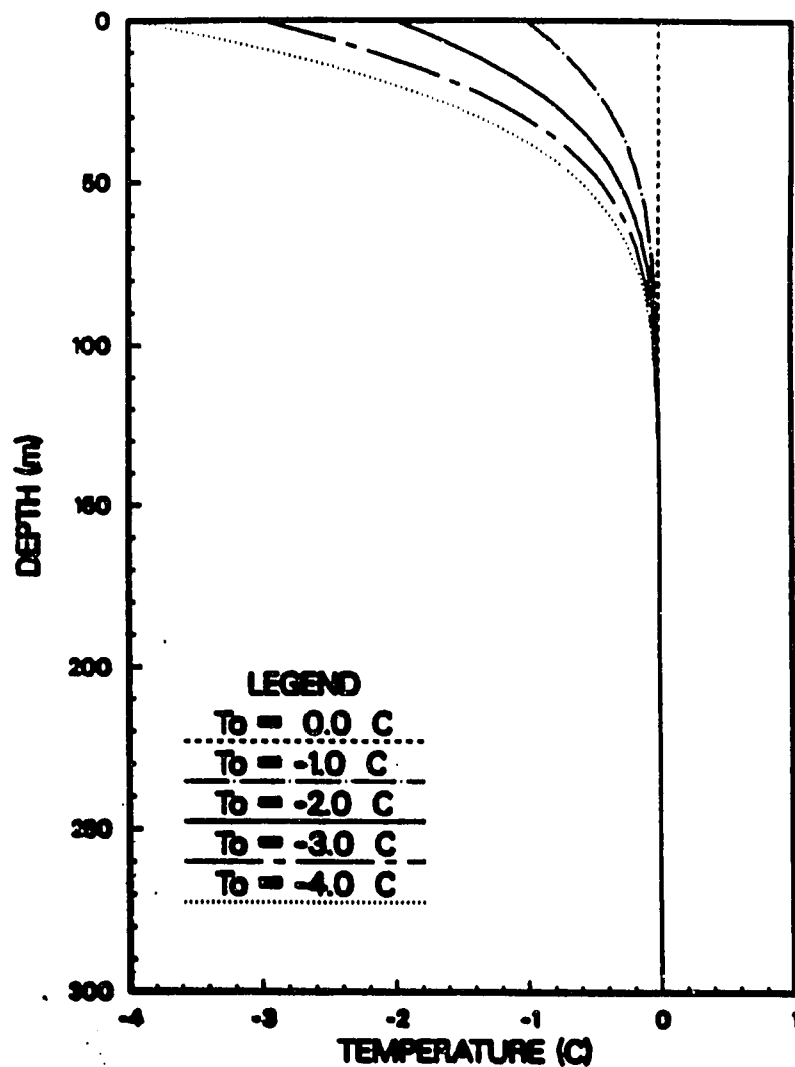


Figure 6.4 Assumed initial permafrost temperatures in 1880 after removal of the equilibrium temperatures with depth. The initial permafrost temperatures were generated by equations (2) and (6) of Lachenbruch et al. (1988) with $n = 2$, $t^* = 35$ years (prior to 1880), for case 5, $T_o = 0.0^\circ\text{C}$ which was changed in increments of -1°C for case 6, case 7, case 8, and case 9 (here T_o represents D in Lachenbruch's paper).

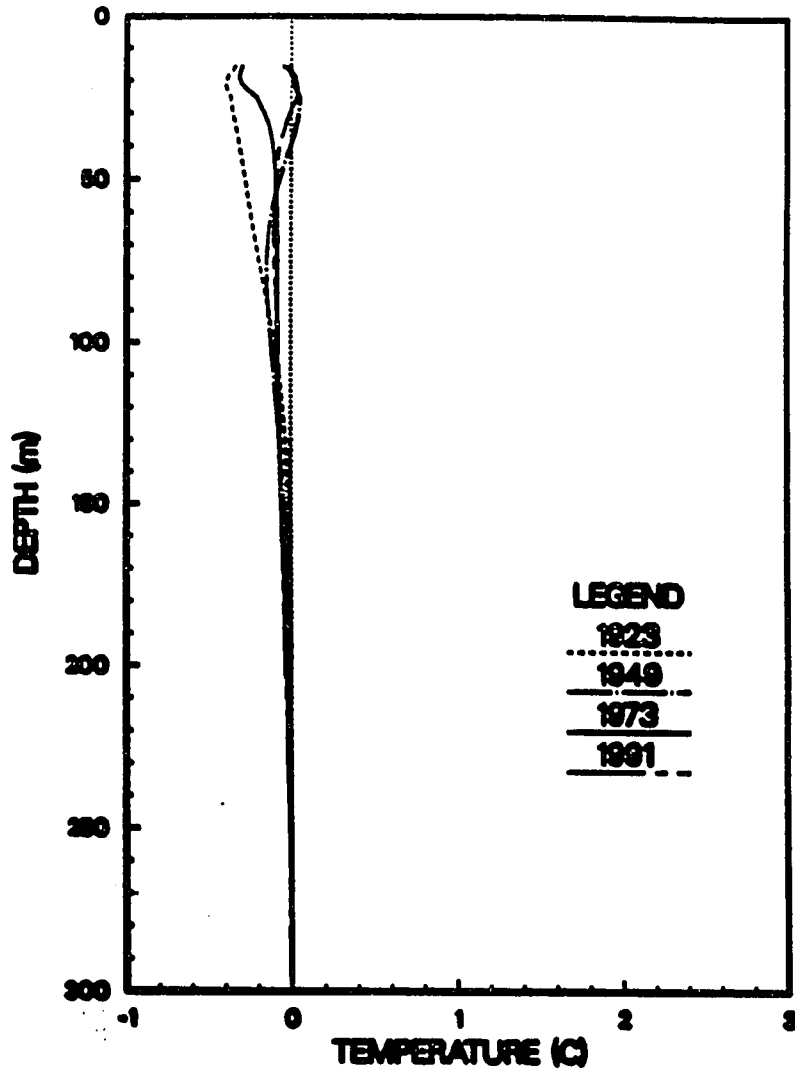


Figure 6.5 Calculated permafrost temperature changes with time for the period from 1880 through 1991 at site SB3 near Barrow, using BC3 for the upper boundary conditions at the ground surface. The initial MST was chosen as -12.2°C with $T_o = 0.0^{\circ}\text{C}$ for case 5.

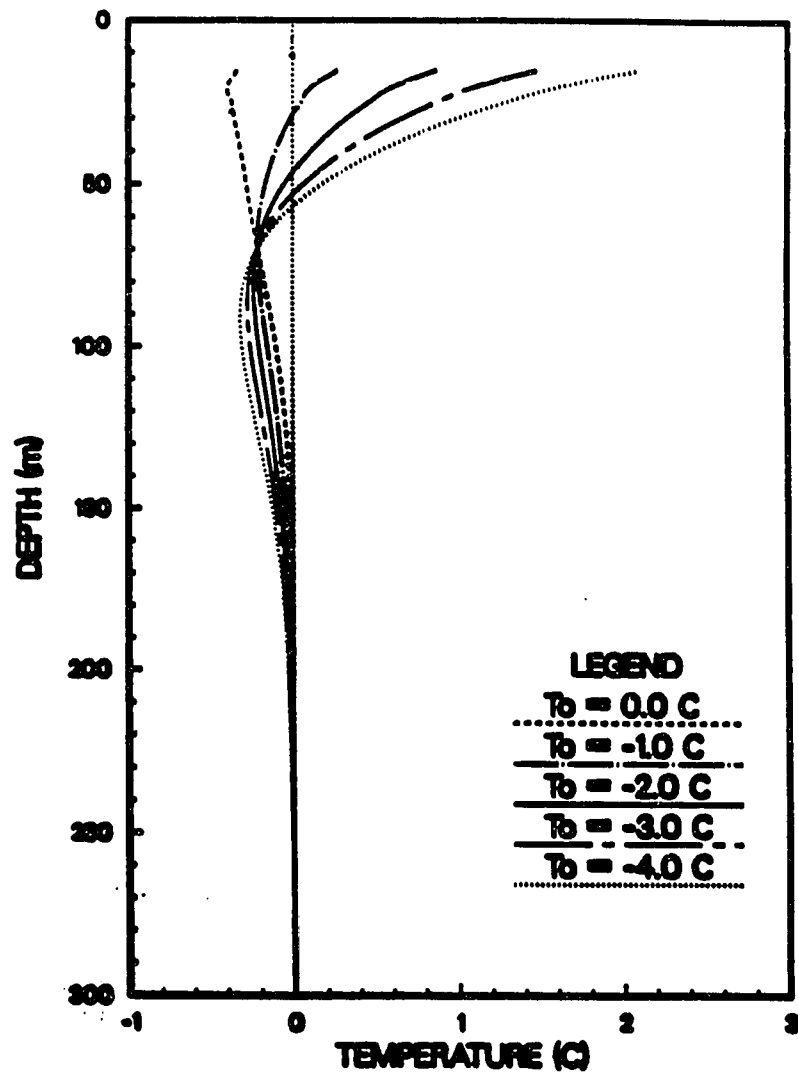


Figure 6.6 Calculated permafrost temperature changes from the assumed initial conditions in 1923 for the conditions at SB3 near Barrow. BC3 was used for the upper boundary conditions at the ground surface. The long term MST was chosen as -12.2°C with different choice of T_0 , as shown.

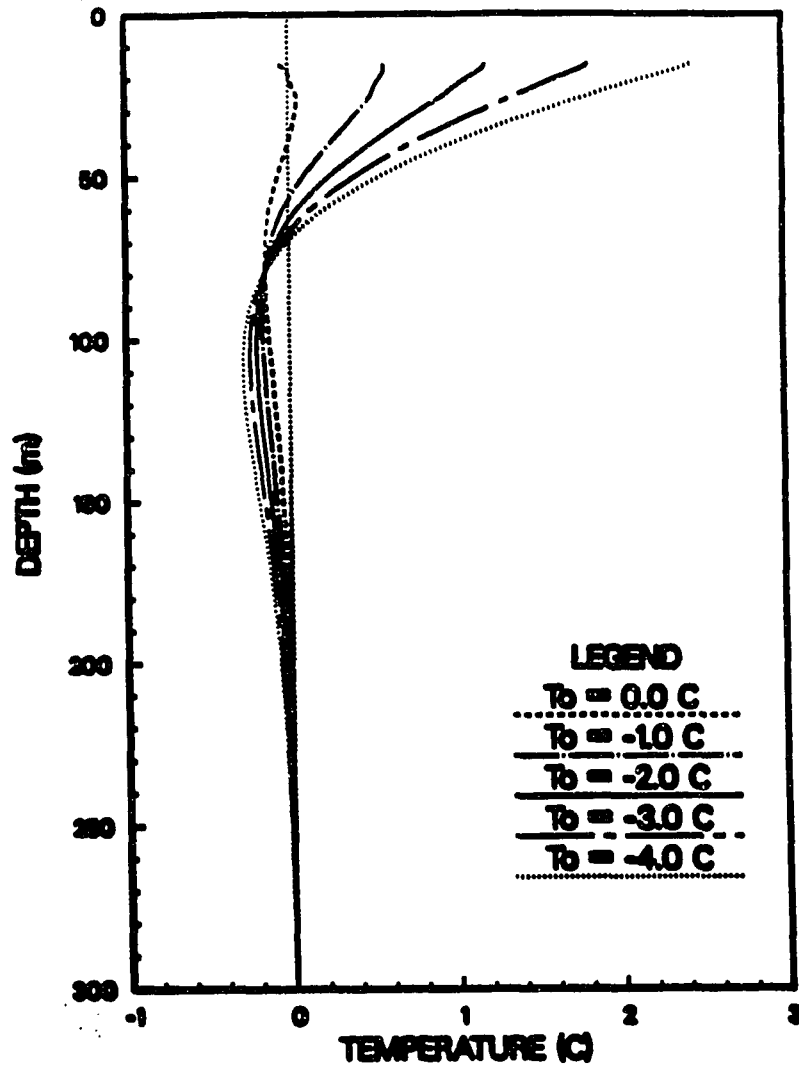


Figure 6.7 Calculated permafrost temperature changes from the assumed initial conditions in 1949 for the conditions at SB3 near Barrow. BC3 was used for the upper boundary conditions at the ground surface. The long term MST was chosen as -12.2°C with different choice of T_0 as shown.

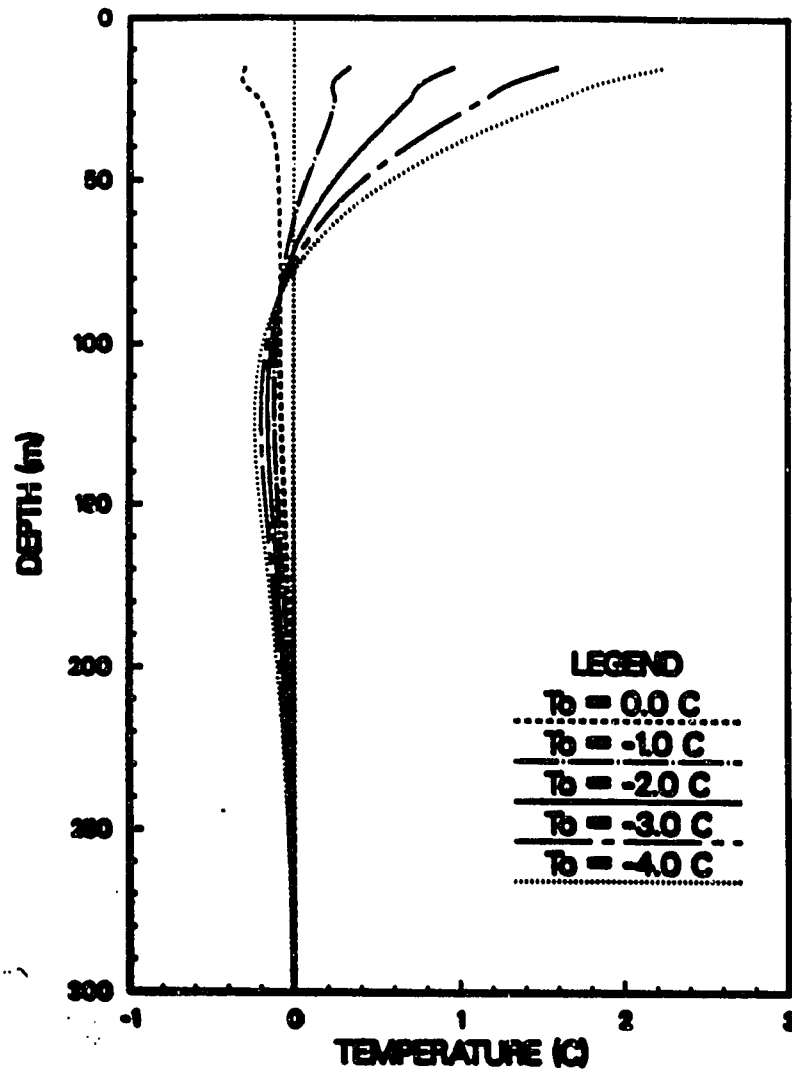


Figure 6.8 Calculated permafrost temperature changes, from the assumed initial conditions, in 1973 for the conditions at SB3 near Barrow. BC3 was used for the upper boundary conditions at the ground surface. The long term MST was chosen as -12.2°C with different choice of T_o as shown.

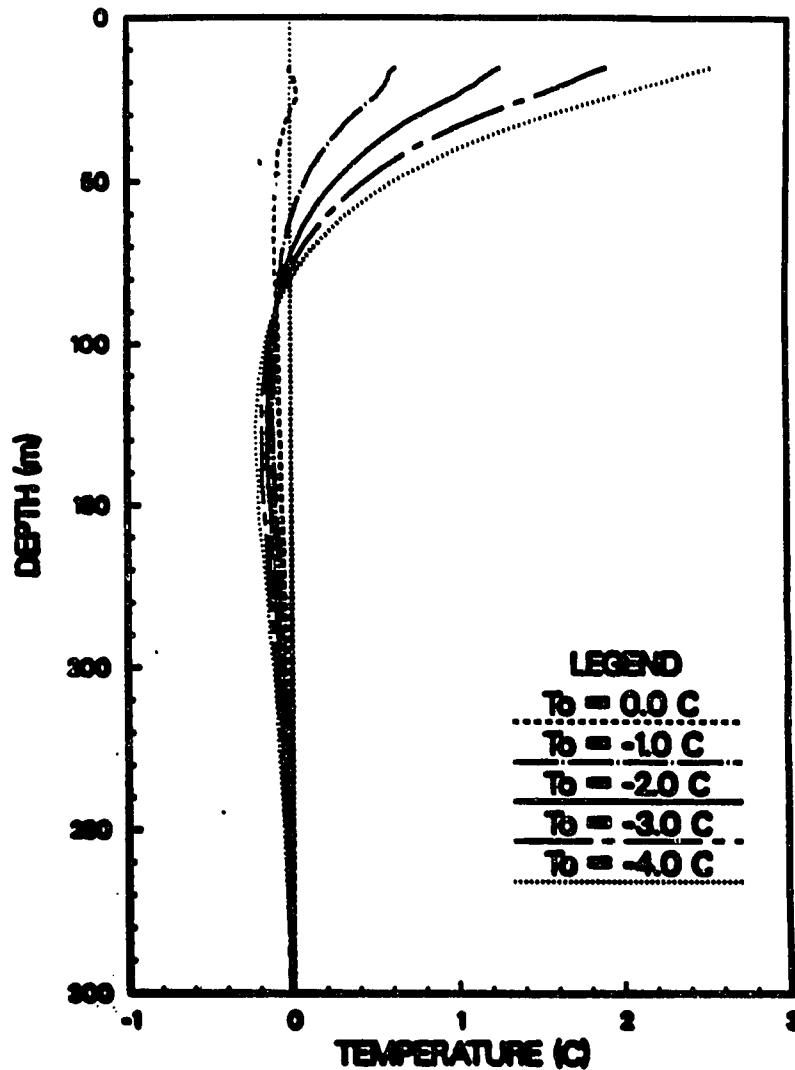


Figure 6.9 Calculated permafrost temperature changes, from the assumed initial conditions, in 1991 for the conditions at SB3 near Barrow. BC3 was used for the upper boundary conditions at the ground surface. The long term MST was chosen as -12.2°C with different choice of T_0 as shown.

Zhang and Osterkamp (1993) reported that another possibility is that the shallow permafrost temperatures were colder than the assumed initial conditions. A few cases were calculated to verify this possibility. The upper boundary was set at the ground surface and the boundary condition was represented by BC3 at site SB3 near Barrow. Physical and thermal properties for the active layer and permafrost were based upon data for Barrow conditions (*Lachenbruch, 1962; Brown, 1969; McGaw et al., 1978; Lachenbruch and Marshall, 1986*) as shown in Table 6.3. The initial long term MST was chosen as -12.2°C and the long term temperature profile in permafrost was generated with the temperature gradient of $0.03^{\circ}\text{C}/\text{m}$. The initial colder temperature profiles for the top layer were generated by equations (2) and (6) of *Lachenbruch et al., (1988)* with $n = 2$, $t^* = 35$ years (prior to 1880), $T_o = 0.0^{\circ}\text{C}$ which was changed in increments of -1°C for cases 5 through 9 (here T_o is the same as D in *Lachenbruch's* paper). These initial cold temperature disturbances were superimposed on the long-term linear equilibrium temperature profiles in the permafrost. Figure 6.4 shows the initial temperature conditions used for the simulation after removal of the long term temperatures with depth. Figures 6.5, 6.6, 6.7, 6.8 and 6.9 show the calculated results. For $T_o = 0.0^{\circ}\text{C}$, all the permafrost temperature profiles show a slight cooling from the long term MST. As T_o decreases, permafrost temperatures increase and at the same time, the cold wave of the initial temperature condition moves downwards. As shown in Figure 6.9, after about 111 years, the temperature profiles at depth (for $T_o < 0^{\circ}\text{C}$) still did not reach their initial equilibrium condition ($T_o = 0^{\circ}\text{C}$). The maximum offset of temperature profiles at depths from their initial equilibrium condition was about -0.3°C in 1923 and about -0.2°C in 1991 for $T_o = -4^{\circ}\text{C}$. For $T_o = -1^{\circ}\text{C}$ or $T_o = -2^{\circ}\text{C}$, the maximum offsets were within -0.2°C . The depth of penetration changes with time and with the magnitude of T_o . If the initial shallow permafrost temperatures were warmer than the assumed initial equilibrium conditions ($T_o > 0^{\circ}\text{C}$), the results would show that current permafrost temperatures would be colder than the assumed

initial conditions and there would be a “warm” wave moving downwards. Obviously, this is not possible for the problem of permafrost warming which is currently dealt with.

These results show that it is possible that the shallow permafrost temperatures were colder than the assumed initial equilibrium conditions, but it will require a long time for the deep permafrost temperatures to reach their initial equilibrium condition. Evidence for an earlier cold temperature wave deeper in the permafrost has not been reported. However, there is a possibility that these changes were small enough to be beyond the range of instrumental sensitivity of the current measurements.

A comparison was also made between cases where the air temperature data were used for the permafrost surface boundary condition and where these data were approximated by a straight line as in Lachenbruch et al. (1988). The initial conditions were taken to be the starting points of regression lines fitted to the data (Lachenbruch et al, 1988). Case 10 in Figure 6.10 used the air temperature data and case 11 used the single regression line from 1880 to 1985 (Figure 6.1C) with the initial MST offset by -1.46°C from the long term MST for both cases. Case 12 used the air temperature data and case 13 used the two regression lines (Figure 6.1C) with an initial offset of -2.21°C from the long term MST for both cases. The results in Figure 6.10 show that the differences between using straight lines to approximate the data and using the actual data are relatively small but generally measurable below about 50 m and may be more significant above this depth.

6.3.2 Effect of Seasonal Snow Cover

A few cases were calculated to evaluate the effects of seasonal snow cover on permafrost temperatures for the period from 1923 through 1991 at site SB3 (see *Lachenbruch and Marshall, 1986 ; Lachenbruch et al., 1988*) near Barrow. The calculations were made using the

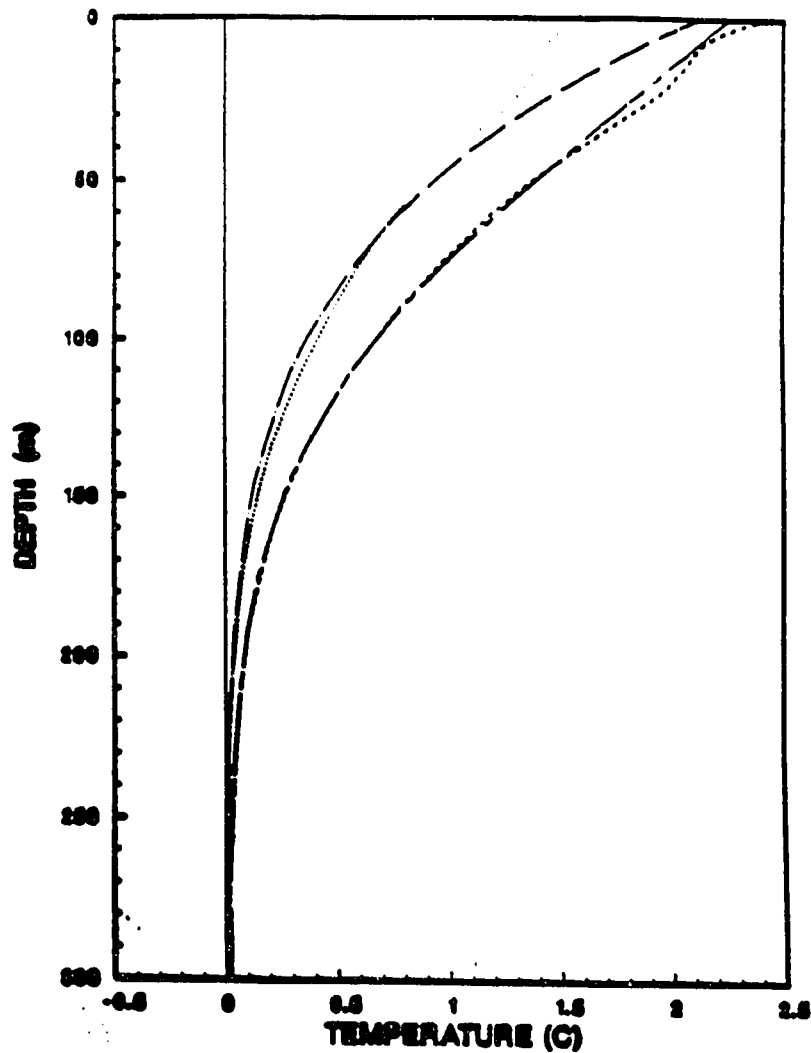


Figure 6.10 Calculated permafrost temperature changes in 1985, for Prudhoe Bay conditions starting in 1980, using BC1 (case 10 dotted line and case 12 dashed line), the single regression line in Figure 6.1C (case 11 chain-dotted line), and the two regression lines in Figure 6.1C (case 13 chain-dashed line), for the upper boundary condition at the permafrost surface.

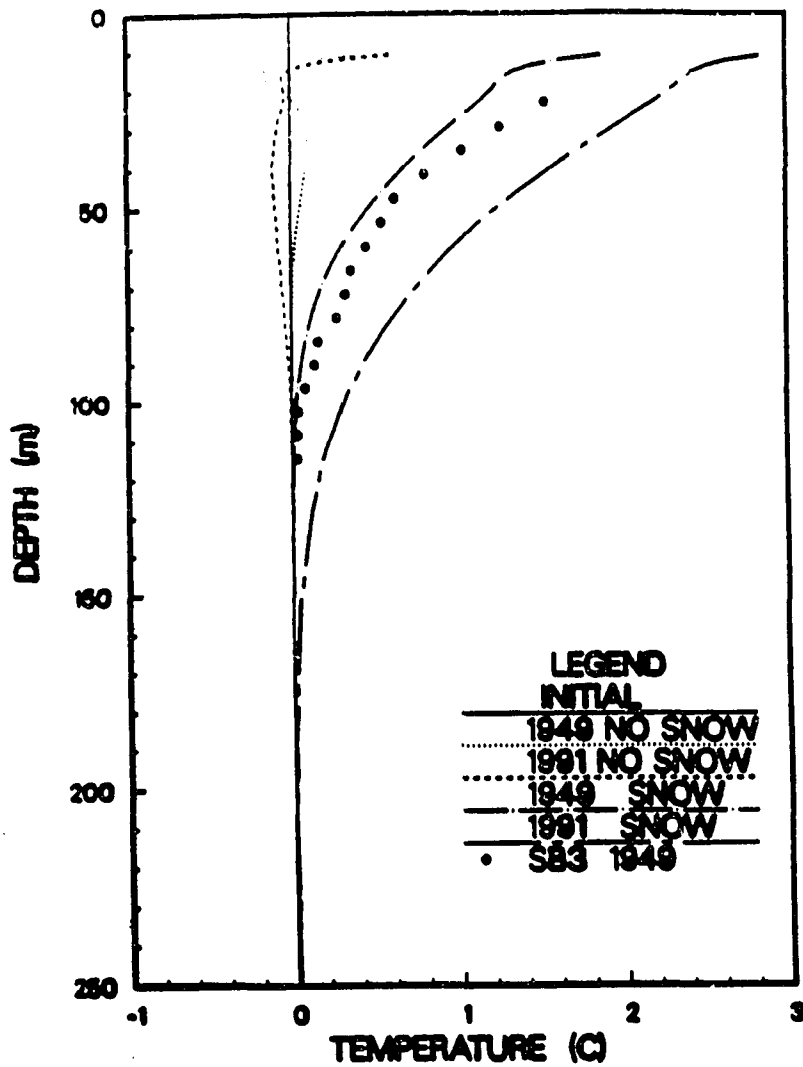


Figure 6.11 Calculated permafrost temperature changes at site SB3 near Barrow using BC2 as the upper boundary condition at the ground or snow surface as approximate. The dotted and dashed lines represent the results of case 14 (without snow cover). The chain-dotted and chain-dashed lines represent the results of case 15 (with snow cover). The dark dots are the approximate permafrost temperature changes at site SB3 in 1949 (Lachenbruch et al., 1962).

air temperatures to drive the ground surface temperatures for cases without (case 14) and with (case 15) a snow cover. Barrow weather data (mean daily air temperature, snowfall and snow cover) for the period from 1923 through 1991 were used in the calculations. Thermal properties of the snow were estimated using (4.1) and the results of Benson (1982) and Sturm (1992). The initial (1923) MST was assumed to be -12.2°C with a thermal gradient of $0.03^{\circ}\text{C}/\text{m}$. The snow surface or ground surface, as appropriate, was taken as the upper boundary. Physical and thermal parameters for the active layer and permafrost were based upon data for Barrow conditions (Brown, 1969; McGaw *et al.*, 1978 ; Lachenbruch and Marshall, 1986) as shown in Table 6.1. Figure 6.11 indicates the calculated results and the dots represent data which were obtained in 1949 at site SB3 (see Lachenbruch *et al.*, 1962).

A similar case was also calculated to evaluate the effects of seasonal snow cover on permafrost temperatures for conditions at site E (see Lachenbruch and Marshall , 1986; Lachenbruch *et al.*, , 1988) near Prudhoe Bay. This case was calculated with the same conditions at site SB3 except that the initial (1923) MST was assumed to be -12.0°C with a thermal gradient of $0.019^{\circ}\text{C}/\text{m}$. Physical and thermal parameters for the active layer and permafrost were based upon data for Prudhoe Bay conditions (Lachenbruch *et al.*, 1982 ; Zhang, 1989 ; Zhang, 1993, chapter 3 in this thesis) as summarized in Table 6.1. Case 16 was calculated without a seasonal snow cover and case 17 with a seasonal snow cover. Figure 6.12 shows the calculated results and the dots represent data which were obtained in 1973 at site E near Prudhoe Bay (Lachenbruch and Marshall, 1986 ; Lachenbruch *et al.*, 1988).

With no snow cover (case 14) at site SB3 near Barrow, the model predicts a slight warming of permafrost temperatures for 1949 and a slight cooling for 1991. For conditions at site E near Prudhoe Bay, the model (case 16) predicts that the permafrost temperatures for 1973 and 1991 cooled slightly from the initial conditions. These results do not agree with the observations at site SB3 near Barrow, at site E near Prudhoe Bay nor at other sites where

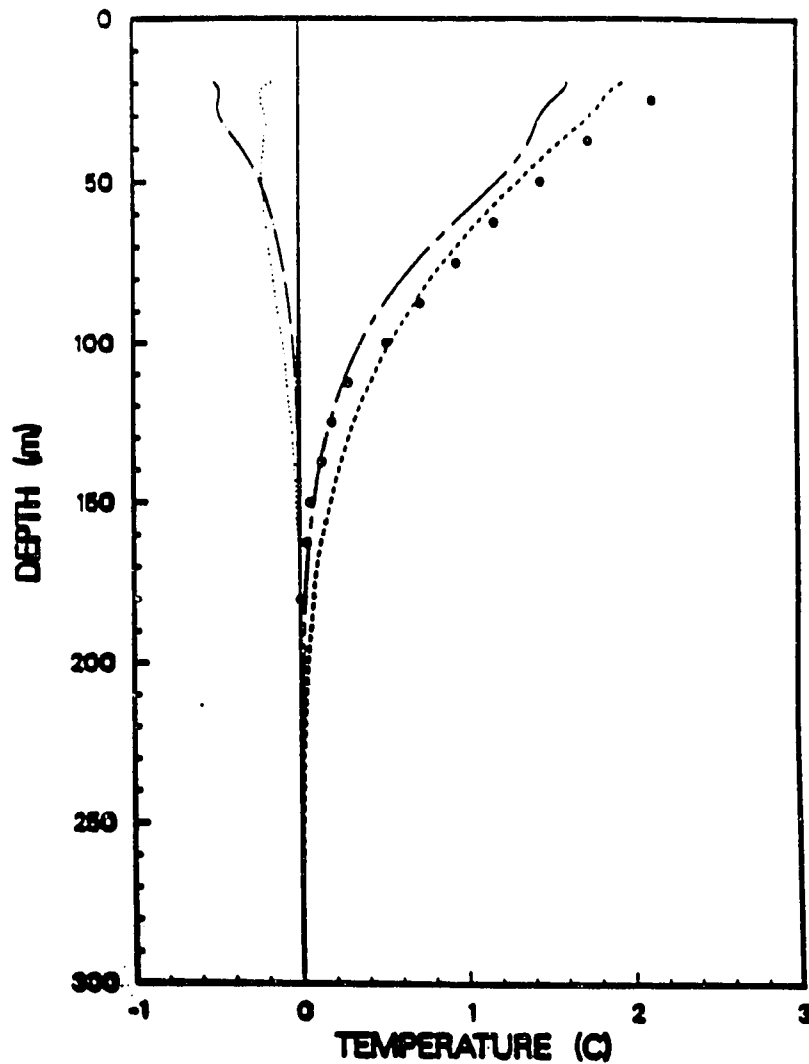


Figure 6.12 Calculated permafrost temperature changes at site E near Prudhoe Bay using BC2 as the upper boundary condition at the ground or snow surface as appropriate. The dot and chain-dotted lines are for cases 14 and 16 with no snow cover. The dash and chain-dashed lines for 15 and 17 with snow cover. The dots are the approximate permafrost temperature changes at site E in 1973 (Lachenbruch et al., 1988).

warming has occurred. Given the assumptions, these calculations show that air temperature variations alone could not have produced the observed permafrost warming.

With the snow cover (case 15 and case 17), the model predicts permafrost temperature changes which compare favorably with the measurements at site SB3 near Barrow and site E near Prudhoe Bay as shown in Figures 6.11 and 6.12. Depths of penetration for the permafrost temperature changes are about the same for both the model and the data at site SB3 near Barrow and site E near Prudhoe Bay.

Temperature variations at the ground surface control the changes of the ground thermal regime. Figure 6.13 shows the temperature history at the ground surface calculated by the model (case 14) with snow cover and measured air temperatures for the period from 1923 through 1991 at site SB3 near Barrow. The maximum thickness of the seasonal snow cover, H_{max} , was obtained for the period from 1923 through 1947 from (4.4) and thickness of the seasonal snow cover was obtained from (5.1). Calculated MAGST for the period was about $-9.1 \pm 1.5^{\circ}C$, while MAAT was about $-12.4 \pm 1.2^{\circ}C$. The difference between the calculated MAGST and observed MAAT for individual year ranges from $1.3^{\circ}C$ to $6.1^{\circ}C$, with an average value of $3.3 \pm 1.1^{\circ}C$. These values are very close to the measured values ($3.0^{\circ}C$ to $6.0^{\circ}C$) as reported by *Zhang and Osterkamp* (1993) in the Prudhoe Bay region. The difference between the calculated MAGST and observed MAAT, in general, is smaller for the period from 1923 through 1947 than for the period from 1947 through 1991. This could be a result of the method used to produce snow cover data before 1947 which was calculated from the annual total snowfall using (4.1). The calculated H_{max} by equation 5.1 has a standard deviation of ± 9 cm from the measured value. As shown in Chapter 5, the change of MAGST with H_{max} is about $0.1^{\circ}C/cm$. Therefore, the calculated MAGST before 1947 may have an error of around $\pm 0.9^{\circ}C$.

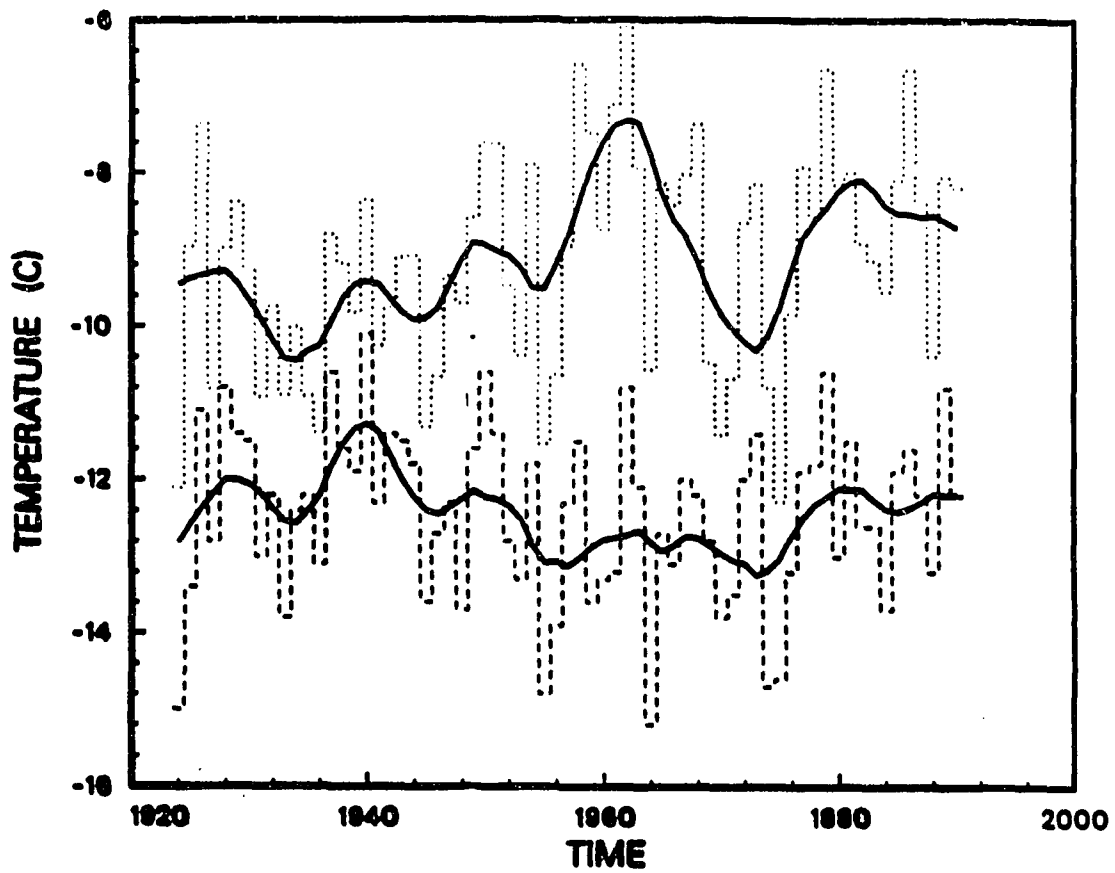


Figure 6.13 Mean annual air temperature (dashed line) and calculated (case 14) ground surface temperature (dotted line) history for the period from 1923 through 1991 at site SB3 near Barrow. These data were smoothed by a low-pass filter with a cut-off frequency of 0.091 year^{-1} .

There is no clear evidence for a cooling of permafrost from 1940 to the mid-1970's for the cases that included a snow cover. As shown in Figure 2.15, there is an anti-correlation between air temperature and total snowfall. While MAGST is directly proportional to changes in total snowfall, MAGST changes in the same direction as annual total snowfall does with a minor modification by MAAT. This indicates that the effect of changes in seasonal snow cover on the ground thermal regime can mask the effect of changes in MAAT.

However, these results, approximately correct predictions for both magnitude and penetration depth of permafrost temperature changes, are fortuitous and misleading. One of the assumptions of the model was that the initial ground surface temperature (-12.2°C) at site SB3 was about the same as the long-term MAAT at Barrow. The difference was about 0.2°C for SB3 near Barrow and about 0.4°C for site E near Prudhoe Bay. If this was the case, an extremely thin seasonal snow cover would have to be assumed prior to 1923 as reported by *Zhang and Osterkamp, (1993)*. A case was calculated to verify this hypothesis. The calculation (case 18) was carried out with conditions at site E near Prudhoe Bay. The initial long term MST was assumed to be -12.0°C . BC3 was used as the upper boundary condition which was set at the ground surface or snow surface when appropriate for the period from 1880 through 1923. For the period from 1923 through 1991, the conditions used in the calculation were the same as case 17. Case 18 was calculated with $H_{max} = 12.7$ cm (compared to an average of 34.5 cm for the period from 1923 through 1991 at Barrow) before 1923. Figure 6.14 shows that the calculated temperature profile (case 18) in 1923 was very close to the initial temperature profile except that temperatures in the top 70 m were slightly higher. The model also calculated the correct magnitude of the permafrost warming and the depth of penetration in 1973. Another case (case 19) was calculated for conditions at site SB3 near Barrow with $H_{max} = 18.0$ cm (average value of 34.5 cm for the period from 1923 through 1991) for the period from 1880 through 1923. The results (Figure 6.15) show that the calculated MST of the

permafrost increased over 1°C by 1923 with the penetration depth over 100 m. Although the model (case 19) calculated the correct magnitude of permafrost warming near the permafrost surface in 1949, the depth of penetration was deeper than the measured values. Therefore, an extremely thin snow cover before 1923 could reduce the difference between MAGST and MAAT and produce a MST of permafrost which was approximately in equilibrium with the deep permafrost temperatures around 1920. The change from an assumed thin snow cover to the thicker recorded snow cover would produce the permafrost warming without the significant increase in MAAT as shown in Figure 6.11 at site SB3 and Figure 6.12 at site E near Prudhoe Bay.

However, from the sporadic snowfall measurements (1902 - 1923) at Barrow, an extremely thin seasonal snow cover or very little snowfall seems unlikely. Table 6.4 summarizes the discontinuous measurements of snowfall before 1923 at Barrow. It suggests that snowfall before 1923 was above the long-term average value of $71 \pm 30\text{cm}$. The difference between MAGST and MAAT prior to 1923 should be at the range from 3°C to 6°C (Zhang and Osterkamp, 1993). Lack of evidence for a thin snow cover implies that (i) MST at the permafrost surface should have been a few degrees warmer than -12.2°C around 1923, and (ii) permafrost could have started warming before 1923 as the atmospheric did.

Figure 6.13 shows that the calculated MAGST was about 2°C to 4°C warmer than MAAT during the 1920's at Barrow. In order to investigate the consequence of the warmer initial MST, a case (case 20) was calculated with an initial MST of -9.2°C , 3°C warmer than the initial MST for case 17 (1923- 1991) and other conditions were the same. Figure 6.16 shows that the depth of penetration is beyond 150 m by 1949, deeper than the measured penetration depth of about 110 m at SB3 near Barrow. Obviously, the calculated results of case 20 do not explain the measured permafrost warming.

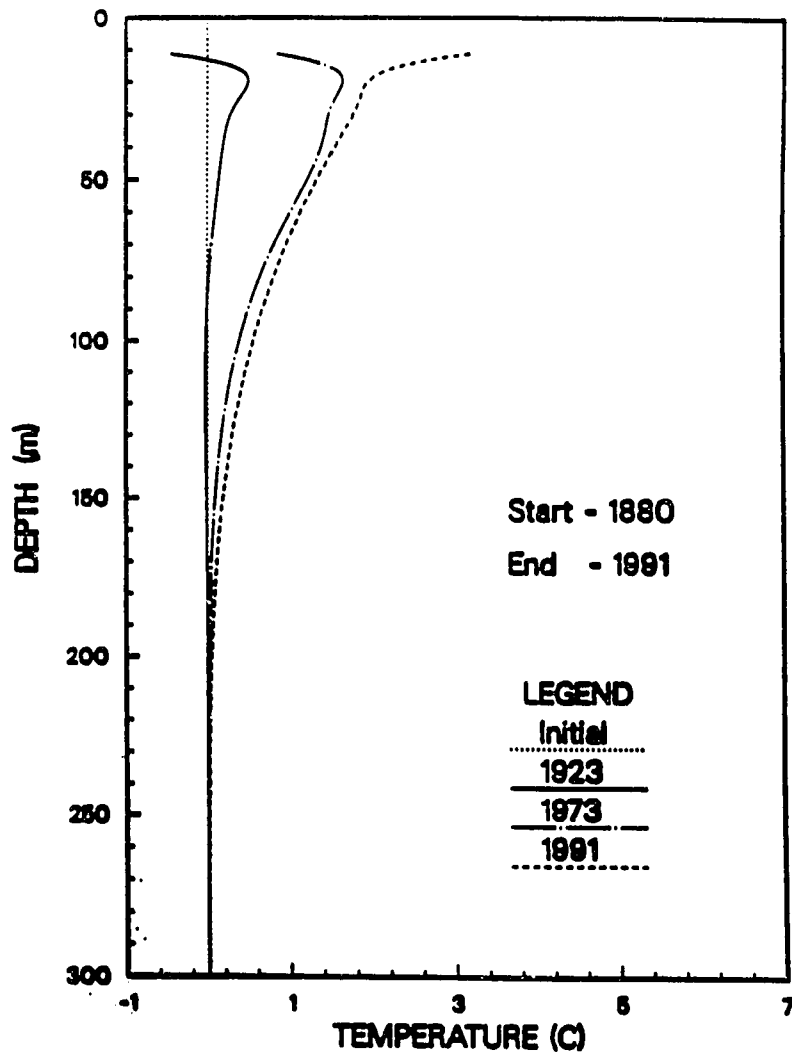


Figure 6.14 Calculated permafrost temperature changes since 1880 for the indicated times at site E near Prudhoe Bay. The maximum thickness of seasonal snow cover was assumed to be 12.7 cm (before 1923) (case 18) and BC3 was used as the upper boundary conditions. The upper boundary was set at the ground or snow surface as appropriate.

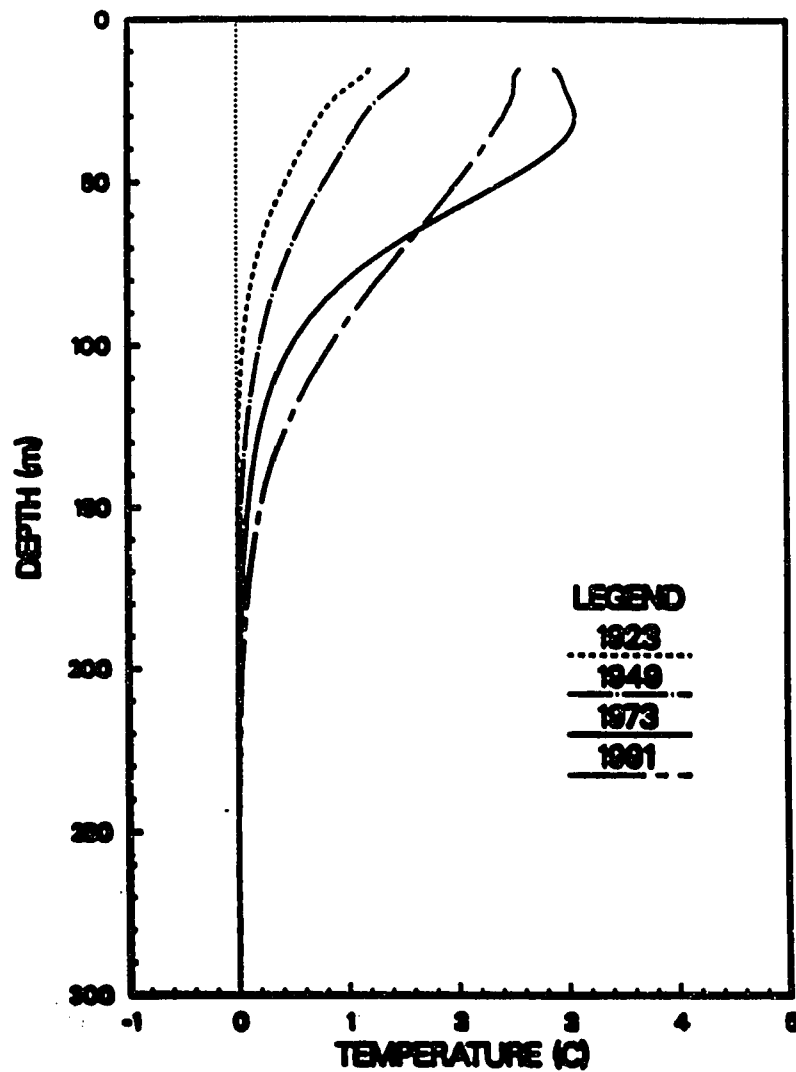


Figure 5.15 Calculated permafrost temperature changes since 1880 for the indicated times at site SB3 near Barrow. The maximum thickness of seasonal snow cover was assumed to be 18.0 cm (before 1923) (case 19) and BC3 was used as the upper boundary condition. The upper boundary was set at the ground or snow surface as appropriate.

Table 6.4 Sporadic snowfall data from 1902 through 1923 at Barrow

Season	Snowfall (cm)	Months measured	Missing months
1902-03	40.6	8	9, 12, 4, 5*
1903-04	27.2	5	9, 10, 11, 12, 1, 5, 6
1915-16	160.0	6	7, 8, 9, 10, 11, 6
1916-17	161.3	7	7, 3, 4, 5, 6
1920-21	87.6	9	7, 8, 9
1921-22	85.6	12	
1922-23	166.1	10	1, 2

* — 1 stands for January, 2 for February, etc.

6.3.3 Effect of Thermal Properties

Variation of the unfrozen water content in the permafrost with temperature changes the thermal properties of permafrost. The existence of salt or brine in the permafrost decreases the freezing point and increases the unfrozen water content. As a result, the apparent heat capacity increases and apparent thermal diffusivity decreases which would decrease the depth of penetration of a climatic warming signal.

A few cases were calculated for conditions at Barrow to illustrate the effect of thermal diffusivity on the penetration depth of temperature changes. For case 21, the calculations were made with the thermal diffusivity $D = 15 \text{ m}^2/\text{yr}$ which was changed in increments of $10 \text{ m}^2/\text{yr}$ for case 22, case 23, case 24 and case 25 for depths ranging from 30 m to 300 m. Previously, a value of $35 \text{ m}^2/\text{yr}$ was used for deeper depths at Barrow. The initial equilibrium MST of the permafrost was chosen as -12.2°C . The upper boundary was set at the snow surface when snow was present and on the ground surface when snow was absent and BC3 was used as the boundary conditions. The snow cover data for the period from 1880

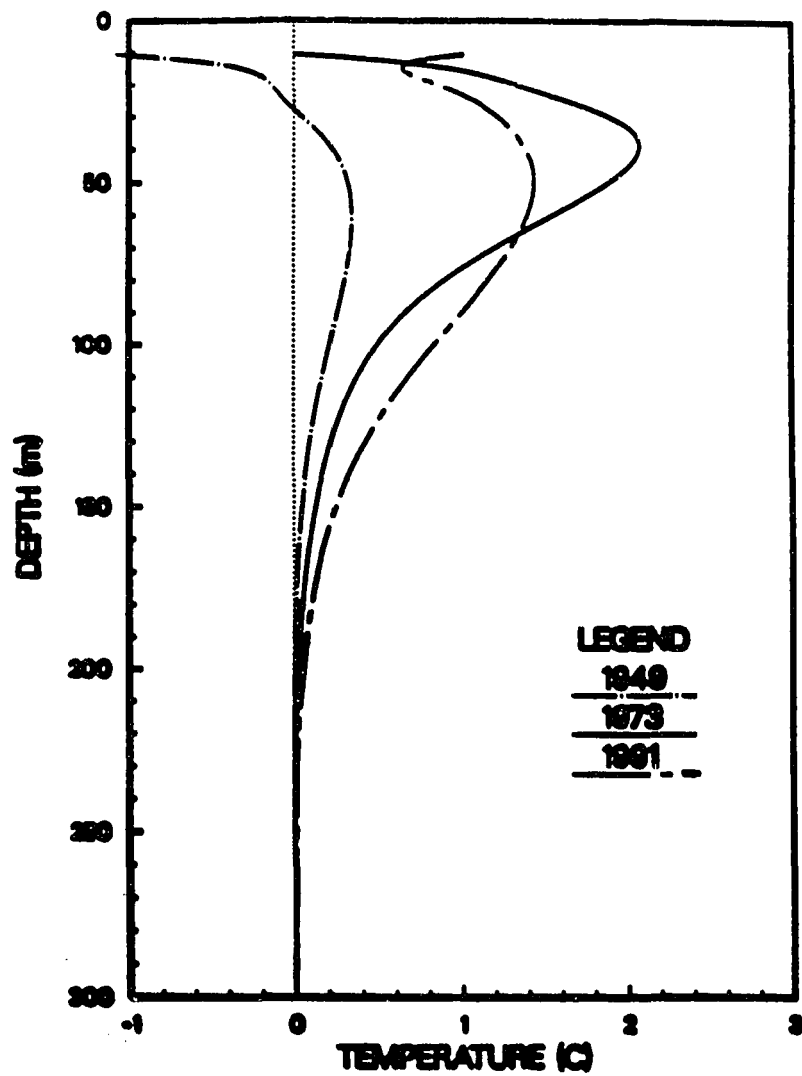


Figure 6.16 Calculated permafrost temperature changes with seasonal snow cover for the period from 1923 through 1991 at site SB3 near Barrow (case 20). The initial long term MST was chosen as -9.2°C , about 3°C warmer than the measured values. All the other conditions are the same as case 17.

through 1923 were generated by (4.1) with $H_{max} = 35$ cm which was the average thickness of seasonal snow cover for the period from 1923 through 1991 at Barrow. The calculated results (Figures 6.17 through 6.20) clearly indicate the penetration depth changes with variations of thermal diffusivity. Interestingly, for $D = 15 \text{ m}^2/\text{yr}$, the model predicts approximately correct penetration depth with the measured values for the main group. For $D = 25 \text{ m}^2/\text{yr}$ at depth and with the near surface conditions at Prudhoe Bay, the model predicts the correct value for the Prudhoe Bay group. Previously, $D = 51 \text{ m}^2/\text{yr}$ was used below 30 m for Prudhoe Bay. With the higher values of D , the calculated penetration depth is much deeper than the measured values. This implies that the values of the thermal diffusivity used in reconstructing the MST history of the permafrost might be too high.

6.4 Application of the Modeling Results to Permafrost Temperature Data

There exist problems with the current analyses and interpretations of the permafrost temperature data which will be explored below. Near Barrow, the measured long term MST of the permafrost constrains the assumed initial MST to -12.5°C which was the coldest measured long term MST of the permafrost. *Lachenbruch et al.*, (1988) and *Zhang and Osterkamp* (1993) concluded that air temperature changes were large enough to account for the permafrost warming in the Alaskan Arctic if reasonable assumptions for the initial MST were made (see Fig. 6.3 and 6.10). Therefore, there is a contradiction between the assumed and the measured long-term MST (extrapolated from deep linear permafrost temperature profiles). However, if the measured long-term MST is used as an initial condition in 1923, the air temperature changes alone (Fig. 6.1; 6.11 and 6.12) since 1923 are not large enough to account for the permafrost warming. On the other hand, if the assumed long term MST was colder than the measured values (Fig. 6.3 and 6.10), it would predict the correct magnitude of the permafrost

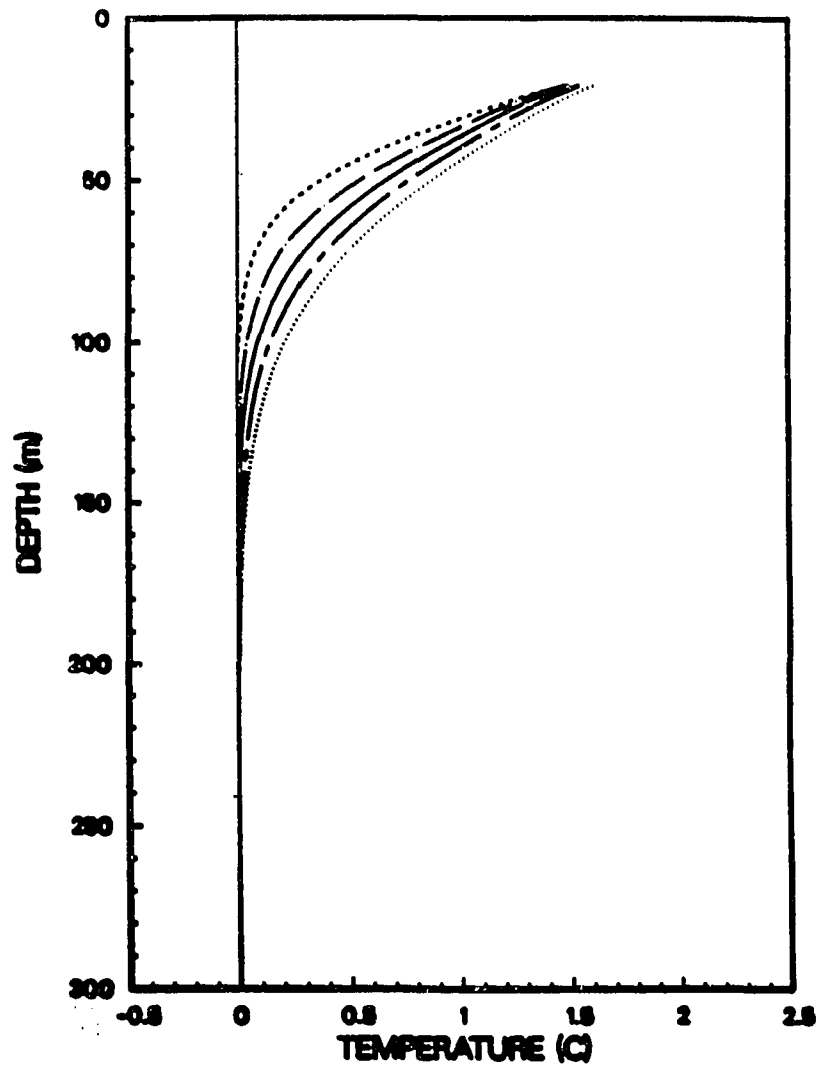


Figure 6.17 Calculated permafrost temperature changes with no seasonal snow cover in 1923 at site SB3 near Barrow. The dashed line represents case 21 with $D=15 \text{ m}^2/\text{yr}$, the chain-dotted line case 22 with $D=25 \text{ m}^2/\text{yr}$, the solid line case 23 with $D = 35 \text{ m}^2/\text{yr}$, the chain-dashed line case 24 with $D = 45 \text{ m}^2/\text{yr}$ and the dotted line case 25 with $D = 55 \text{ m}^2/\text{yr}$.

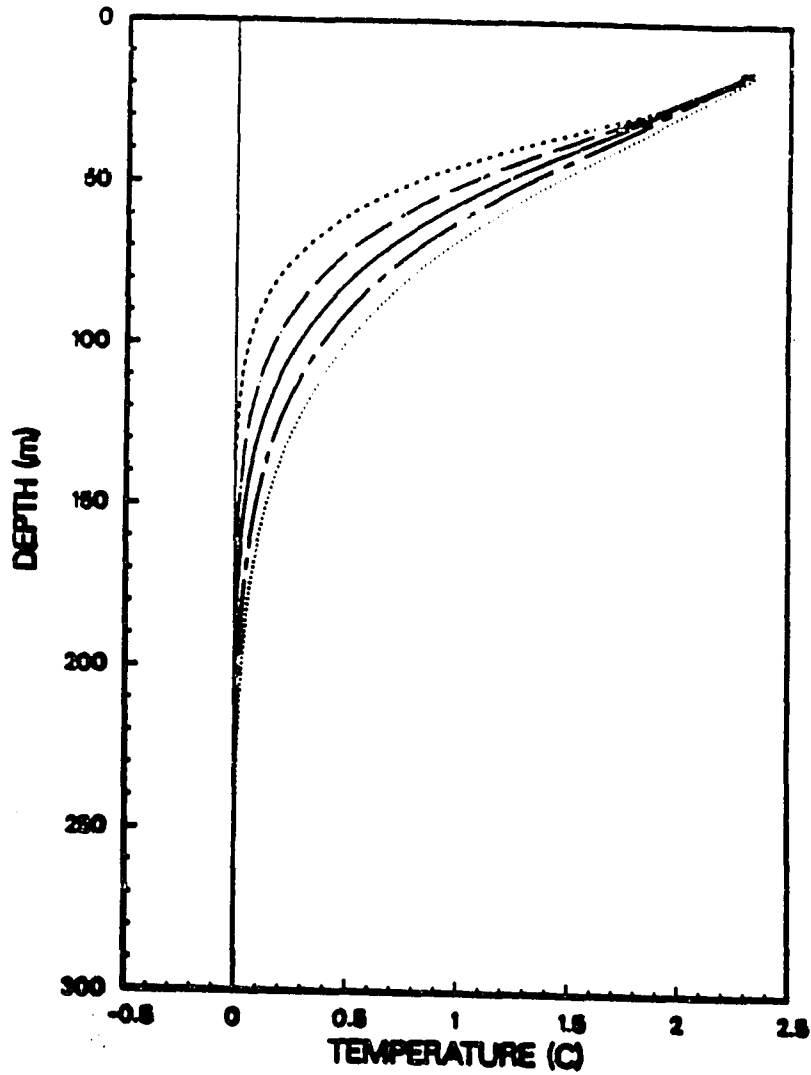


Figure 6.18 Calculated permafrost temperature changes with no seasonal snow cover in 1949 at site SB3 near Barrow. The dashed line represents case 21 with $D=15 \text{ m}^2/\text{yr}$, the chain-dotted line case 22 with $D=25 \text{ m}^2/\text{yr}$, the solid line case 23 with $D = 35 \text{ m}^2/\text{yr}$, the chain-dashed line case 24 with $D = 45 \text{ m}^2/\text{yr}$ and the dotted line case 25 with $D = 55 \text{ m}^2/\text{yr}$.

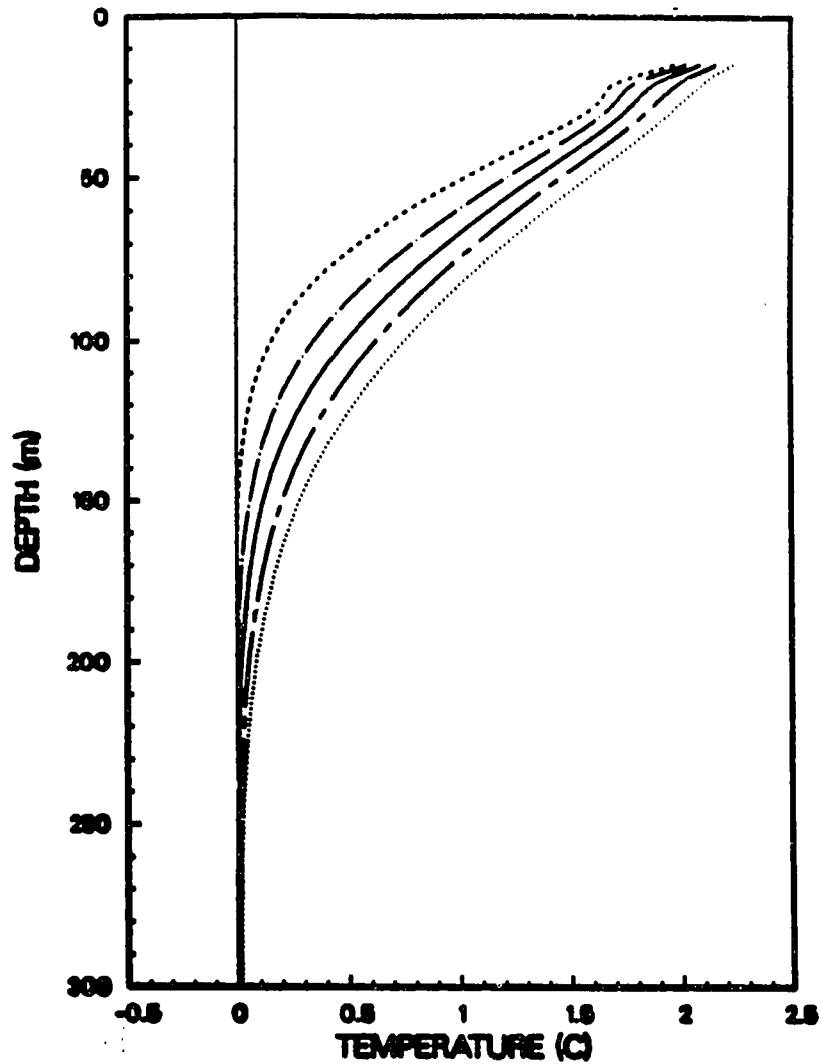


Figure 6.19 Calculated permafrost temperature changes with no seasonal snow cover in 1973 at site SB3 near Barrow. The dashed line represents case 21 with $D=15 \text{ m}^2/\text{yr}$, the chain-dotted line case 22 with $D=25 \text{ m}^2/\text{yr}$, the solid line case 23 with $D = 35 \text{ m}^2/\text{yr}$, the chain-dashed line case 24 with $D = 45 \text{ m}^2/\text{yr}$ and the dotted line case 25 with $D = 55 \text{ m}^2/\text{yr}$.

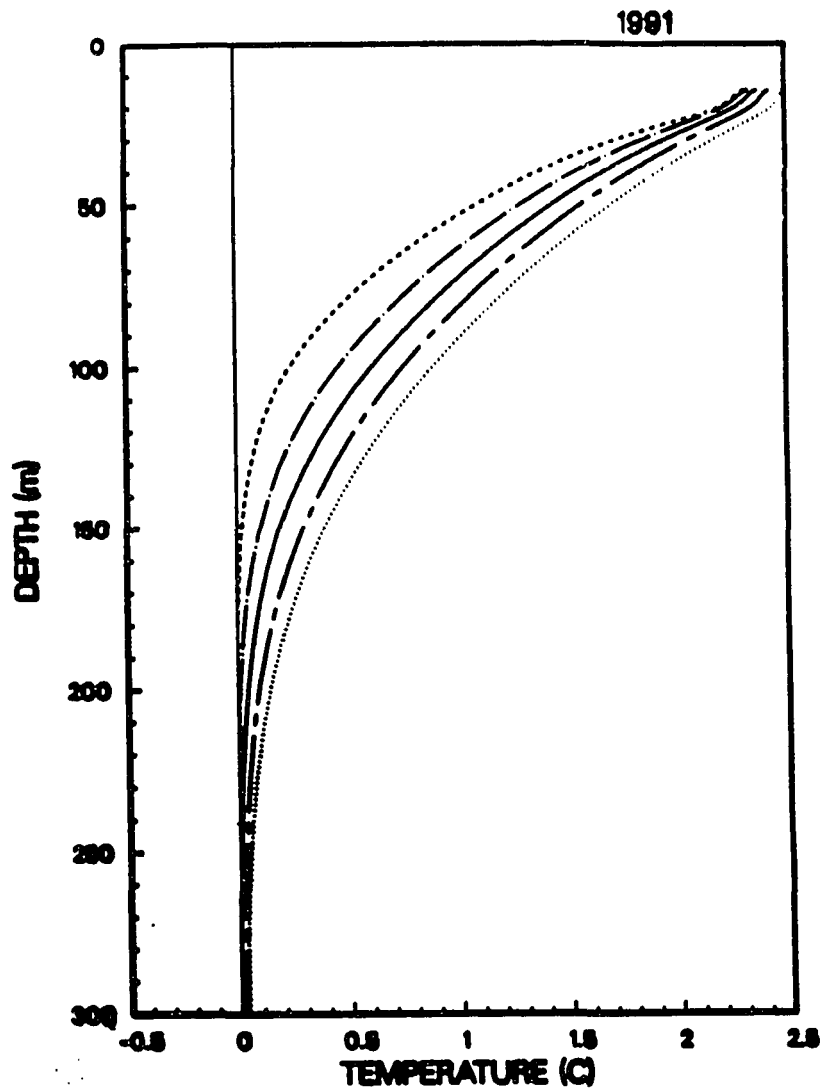


Figure 6.20 Calculated permafrost temperature changes with no seasonal snow cover in 1991 at site SB3 near Barrow. The dashed line represents case 21 with $D=15 \text{ m}^2/\text{yr}$, the chain-dotted line case 22 with $D=25 \text{ m}^2/\text{yr}$, the solid line case 23 with $D = 35 \text{ m}^2/\text{yr}$, the chain-dashed line case 24 with $D = 45 \text{ m}^2/\text{yr}$ and the dotted line case 25 with $D = 55 \text{ m}^2/\text{yr}$.

warming but the depth of penetration would be deeper than the measured values. *Lachenbruch et al.* (1988) claimed that the atmospheric warming started earlier than the permafrost warming. For these calculations, this is true only if the air temperature started warming in the 1880's with an extremely thin snow cover so that the permafrost did not warm as the atmosphere did as illustrated by case 18 prior to 1923. Later (around 1920s), the increase in seasonal snow cover thickness would warm up the permafrost as indicated by cases 15 and 17. However, the sporadic measurements of snowfall before 1923 at Barrow show that this situation seems unlikely. If the long-term MST around or before 1880 was about 1 to 2°C colder than the measured MST, it would require a long time (at least several hundred years) to reach the new equilibrium condition. Even if the long-term MST from deep permafrost temperature profiles show the same value as the measured MST but with a few degree colder for the upper layers as the initial condition (see Figure 6.4), it still requires a long time to reach the original equilibrium temperature profiles (Figures 6.5 through 6.9). In this case, the timing when the long-term MST was established at the permafrost surface is critical to understand the permafrost warming and it is likely that the measured long-term MST was established before or around 1880 with a magnitude of about -12.2 to -12.5°C near Barrow.

Effects of the seasonal snow cover on the ground thermal regime has to be considered in the context of studies of the permafrost temperature response to climatic change. The results from case 15 and 17 can correctly predict both the magnitude of permafrost temperature changes and the penetration depth of these changes. However, suddenly placing a snow cover on the ground would be equivalent to warming the ground surface by several degrees in a step change. For these results and data to be compatible, it would have to be assumed that an extremely thin snow cover existed prior to 1923. The results from case 19 shows that an extremely thin snow cover (about 12.7 cm) can reduce the temperature difference between MAGST and MAAT to about 1°C or less and produce a MST of the permafrost which was

approximately in equilibrium conditions with the deep permafrost temperatures around 1920's. However, from the sporadic snowfall measurements before 1923 at Barrow, an extremely thin snow cover appears to be unlikely since the snowfall was above the long-term average value of $71 \pm 30\text{cm}$. In this case, the temperature difference between MAGST and MAAT should be in the range from 3°C to 6°C . This implies that the MST of permafrost was at least a few degrees warmer than -12.2°C at site SB3 near Barrow and -12.0°C at site E near Prudhoe Bay around 1920's. The calculation (case 20) with warmer initial MST (-9.2°C) shows that the penetration depth (beyond 150 m) is much deeper than the measured values (about 110 m). This conclusion contradicts the result that the temperature difference between MAGST and MAAT was small, probably less than 1°C around the 1920's. However, this conclusion is consistent with the results that the long-term MST of the permafrost was established before or around 1880. The long-term MST of the permafrost (extrapolated from deep permafrost temperature profiles) averaged about $-10.9^{\circ} \pm 0.6^{\circ}\text{C}$ in the region while MAAT was about at least 3 to 4°C colder than the MST of permafrost. This temperature difference could be partially caused by seasonal snow cover as shown in Figure 6.13. Therefore, it is reasonable to conclude at this stage that the long-term MST of permafrost was established around 1880 and permafrost started warming as the same time as the atmosphere starting warming in 1880's. The difference in the magnitude of the permafrost warming from site to site may be caused by local factors such as soil type, microrelief, moisture conditions, but variations in the seasonal snow cover and vegetation may be the most important factors. For example, changes in total thickness and depth hoar layer of seasonal snow cover can result in a change in MAGST several degrees respectively (see chapter 5).

The major factor that controls the rate of temperature change and the depth of penetration is the thermal diffusivity of permafrost although the penetration depth varies with time and the magnitude of the permafrost temperature changes at the surface. The calculated results

in case 21 through 25 show that low thermal diffusivity would reduce the penetration depth significantly. The model predicts an approximately correct penetration depth compared with the measured depth with $D = 15 \text{ m}^2/\text{yr}$ for the main group and $D = 25 \text{ m}^2/\text{yr}$ for the Prudhoe Bay group.

The thermal diffusivity of permafrost varies with soil type, ice and unfrozen water content and the salinity of the pore water in permafrost, through its effect on the unfrozen water content, can reduce the thermal diffusivity dramatically. Osterkamp (1987) calculated that the thermal diffusivity is about $20 \text{ m}^2/\text{yr}$ for subsea permafrost containing sea water brine at about -10°C . Osterkamp (1989) also reported that saline permafrost might be expected in coastal areas as a result of airborne salts, seawater flooding, and variations in ground surface and sea levels over geologic time. He reported that such occurrences have been found at Nome, Kotzebue, Barrow, Prudhoe Bay and at other sites along Alaska's extensive coast. Evidence for extremely high pore water salinities have been found in well logs by Osterkamp and Payne (1981) within continuous permafrost in coastal areas. Collett (1993) has systematically examined those well logs and reported that the ice-bearing permafrost interval is not vertically continuous, but rather it is interrupted by numerous intervals or zones in which the ice content is greatly diminished or absent due to the extremely high salinity of the pore water. The salinity of the pore water could be as high as 130 ppt, more than three times higher than the normal sea water. The most prominent anomaly occurs within 50 m to 250 m of the surface with a range in thickness from 50 m to 100 m, where the permafrost warming has occurred during the last century or so. The high salinity in permafrost would reduce the thermal diffusivity so that the penetration depth would be reduced significantly compared with the results obtained from the current high thermal diffusivity values. The variations of the penetration depth from site to site may be related mainly to the changes in soil type and salinity of the pore water in permafrost.

Based upon the discussions above, the following conclusions can be made: (i) The difference between MAGST and MAAT prior to 1923 near Barrow should average at least 3°C since available measurements suggest that the snowfall may have been above the long term average value. This implies that the MST of the permafrost should have already been a few degrees warmer than -12.2°C around 1923. It suggests that permafrost could have started warming before 1923 as did the atmosphere. (ii) Due to the constraint of the long term MST (extrapolated from linear portion of deep permafrost temperature profiles) which requires a long time (hundreds of years) of relatively stable air temperature and ground surface conditions to be established, it was impossible to assume the initial MST around the 1880's was colder than -12.5°C which was the coldest long term MST of the permafrost near Barrow. (iii) The current thermal diffusivity values used in the calculations may be too high since the high salinity of pore water in permafrost could reduce the thermal diffusivity significantly so that the penetration depth would be reduced dramatically.

From all of these points of view, the general conclusion can be made: the long term MST of the permafrost was established before 1923, probably in the late 1800's. Permafrost started warming at the same time as the atmosphere started warming, about 1890. Variations in the penetration depth may be related to changes in thermal properties of permafrost, variations in the magnitude of the permafrost surface warming may be due to local factors such as soil type, vegetation, microrelief, soil moisture condition, and seasonal snow cover. Changes in seasonal snow cover may be the dominant factor which influences the local ground thermal regime.

6.5 Relation to Climatic Change

A comprehensive review of climatic history in geologic time is far beyond the scope of this thesis, but a general outline of the climatic change for the last few thousand years in the

Arctic, especially in Alaska, is necessary as background information. According to *Maxwell*, (1987), in the Arctic, the climate became increasingly warmer and wetter, reaching a peak about 5000 years B.P., often called the "postglacial climatic optimum warm period". After the climatic optimum, a cooling period or "Neoglaciation" followed for around 3000 years B.P. According to *Williams and Wigley* (1983), there were three recent climatic excursions: a cold period between the 8th and 10th centuries, the medieval little optimum around the 12th century, and the Little Ice Age around the 17th century. The same pattern is reported by *Calkin* (1988) in Alaska. Distinct but generally minor glacier advances occurred in many areas about 1200 years B.P., followed by a warm period until the strong advances of the Little Ice Age between 400 and 100 years B.P.

The long term MST of the permafrost (extrapolated from deep permafrost temperature profiles) may have been established during the last millenium or so. Permafrost temperature might respond to the atmospheric warming in the 1880s. However, compared with 2°C to 4°C warming of the permafrost surface temperature, the increase in MAAT (about 2°C) is not enough to account for the permafrost warming if we consider the early air temperature cooling was a short term fluctuation during the 1880's. One possibility is that during the 1880s vegetation might have been poorly developed due to the cooler MAAT (about 3°C colder than the historic long term mean at Barrow). Poorly developed vegetation would reduce the thickness of the depth hoar layer of seasonal snow cover and the insulation effect of the seasonal snow cover. As the air temperature gradually increased, vegetation may have subsequently recovered. Denser vegetation would increase the insulating effect of the snow cover through its effect on the thickness of the depth hoar layer. This would increase the temperature difference between the MAGST and MAAT so that the increase in of the MST of permafrost would be more than that of MAAT (the interaction of vegetation and seasonal snow cover could have amplified the signal of air temperature changes in the permafrost). This mechanism can

be verified by the current climatic conditions and permafrost temperatures in Alaska north of the Brooks Range (see chapters 2 and 4). The MAAT north of Umiat in the Alaskan Arctic was about $-12.4 \pm 0.3^{\circ}\text{C}$ from 1987 to 1991, while mean annual temperatures near the permafrost surface ranged from -9°C along the coast to about -5°C inland. Although the longer thaw season and higher summer air temperature may play an important role in increasing the permafrost temperature inland, the interaction of local microrelief and vegetation with snow appears to change the insulating effect of seasonal snow cover and may be the major factor which controls the permafrost temperatures during the winter and thus the mean annual temperature near the permafrost surface.

6.6 Summary

A finite difference model for one-dimensional heat flow problems with phase change (Goodrich, 1977) was used to investigate the effects of air temperature, seasonal snow cover, the active layer, initial temperature conditions in permafrost, and variations in the thermal properties of soils on permafrost temperatures. Simulations were carried out using past air temperatures for the boundary conditions at the permafrost surface, ground surface, or surface of the snow cover. The effects of initial conditions, active layer, snow cover, thermal properties, and the use of approximations for the surface temperature history on permafrost temperatures were examined in this investigation.

When air temperature variations in the North American Arctic were applied to the permafrost surface at Prudhoe Bay, it was found that the permafrost temperature variations depended strongly on the choice of initial conditions. If the initial MST near Barrow was chosen close to the measured long term MST of the permafrost near Barrow, the air temperature changes since 1923 would not be large enough to account for the permafrost warming.

Lachenbruch et al. (1988) stated that the air temperature variations since 1880 are large enough to account for the geothermal observations by assuming the initial long term MST of the permafrost was about 1.5 to 2.2°C colder than the measured long term MST of the permafrost. These assumptions are unrealistic since the long term MST of the permafrost requires many centuries to be established. An alternative explanation of the last result is that the shallow permafrost temperatures were colder than the assumed initial conditions. The calculated results show that it is possible that the shallow permafrost temperatures were colder than the assumed initial long term conditions, but it would require a long time for the permafrost temperatures to reach their initial long term MST. The differences between using air temperature data at the permafrost surface compared to using straight line approximations to the data were small but measurable below about 50 m and may be more significant above this depth.

Barrow air temperatures (1923-1991) used for the ground surface boundary condition (active layer but no snow cover) at a site SB3 near Barrow and at site E near Prudhoe Bay produced little change in permafrost temperatures from the initial condition. This result is inconsistent with permafrost temperature observations at site SB3 and at site E and confirms that air temperature variations alone (since 1923) cannot account for warming of the permafrost. When the snow cover was added, the model correctly predicted both the magnitude and penetration depth of permafrost temperature changes. The temperature history at the ground surface calculated by the model with snow cover shows that the difference between MAGST and MAAT ranges from 1.3°C to 6.1°C, with an average value of $3.3 \pm 1.1^\circ\text{C}$. This value is consistent with the measurements in the Prudhoe Bay region. There is no clear evidence for a cooling of permafrost from 1940 to the mid-1970s for cases that included a snow cover. This indicates that the effect of changes in the seasonal snow cover on the ground thermal regime may be significant. For the observations and predictions to be compatible when the snow cover was added, the initial ground surface temperature must have been about

the same as the MAAT. This implies a very thin snow cover prior to 1923. The calculated results show that an extremely thin snow cover prior to 1923 could reduce the temperature difference between MAGST and MAAT significantly, but the sporadic measurements show that snowfall was above the long term average value of 71 ± 30 cm. This implies that (i) MST of permafrost around 1923 was at least a few degrees warmer than the long term MST of permafrost extrapolated from deep permafrost temperature profiles, (ii) permafrost had started warming before 1923 as the atmosphere had.

The model predicts that the penetration depth changes with variations of thermal diffusivity for the same upper boundary conditions. The current values of thermal diffusivity used for the calculations were about $35 \text{ m}^2/\text{yr}$ near Barrow and about $51 \text{ m}^2/\text{yr}$ near Prudhoe Bay. The penetration depth near Prudhoe Bay is about 30% deeper than that near Barrow since 1923. The model predicts correct penetration depth compared with the measured value for $D = 15 \text{ m}^2/\text{yr}$ for the main group and for the Prudhoe Bay group with $D = 25 \text{ m}^2/\text{yr}$ since 1880. With higher values of D , the calculated penetration depth is much deeper than the measured values. This implies that the values of the thermal diffusivity used in re-constructing the MST history of the permafrost might have been too high.

By applying those calculated results to permafrost temperature data, we can conclude that the long term MST of the permafrost may have been established before or around 1880. Permafrost started warming at the same time as the atmosphere did in the middle 1880's. Variations in the penetration depth may be related to changes in the thermal properties of permafrost. Variations in the magnitude of the permafrost surface warming may be due to the effect of local factors such as soil type, microrelief, soil moisture condition, and seasonal snow cover. Changes in seasonal snow cover and vegetation appears to be the dominant factors which influence the local ground thermal regime.

Although the timing of the permafrost warming was the same as the atmospheric warming, the magnitude of the permafrost warming is still greater than that of MAAT. This can be explained by the effect of the interaction of local microrelief and vegetation with snow. The effect of the interaction of vegetation and snow cover may have amplified the signal of air temperature changes in permafrost. This mechanism can be verified by the current climatic conditions and permafrost temperatures in Alaska north of the Brooks Range.

CHAPTER 7

Summary

7.1 Climate and Climatic Change

Air temperatures in Alaska north of the Brooks Range are strongly affected by marine influences. Table 7.1 summarizes the range of climatic parameters. The mean annual air temperature (MAAT) for stations within about 100 km from the Arctic Coast is about $-12.4 \pm 0.4^{\circ}\text{C}$, while the annual amplitude of MAAT ranges from 16.0°C along the coast to 22.0°C inland. The reduction of the annual amplitude along the coast is due not only to the lower summer temperatures but also the relatively warmer winter temperatures. Freeze and thaw indices range from about 4700 and 300 degree-days along the coast to about 5400 and 920 degree-days inland, respectively. The air temperature gradient inland from the coast changes seasonally and its magnitude is greater during the summer (over $6.0^{\circ}\text{C}/100 \text{ km}$ in July) than during the winter (about -3.0 to $-4.0^{\circ}\text{C}/100 \text{ km}$ in January).

Precipitation changes strongly with elevation. The 30-year average indicates precipitation ranges from 180 mm for the Coastal Plain to about 640 mm at Atigun Pass. Over 60% of precipitation falls in the winter (September through May) as snow, and the rest comes as rain. Air temperature between stations and sites are linearly correlated; while correlations of precipitation and snowfall are relatively poor.

Air temperature trends at Barrow follow those for Alaska, the North American Arctic and the Arctic as a whole showing an increasing trend until 1940, a decreasing trend to the mid-1970s and then an increase to warmer temperature during the late 1970s and 1980s. The

Table 7.1 Climate and Permafrost Conditions in Alaska North of the Brooks Range

	Arctic Foothills	Arctic Inland	Arctic Coast
Distance to the ocean (km)	150 - 300	20 - 150	< 20
Elevation (m)	300 - 900	50 - 400	< 50
Air temperature ($^{\circ}C$)			
Mean annual	-8.6	-12.4 ± 0.4	-12.4 ± 0.4
Range of mean annual	-8.0 to -10.0	-10.5 to 14.5	-10.5 to -14.5
Annual amplitude	16.8	21.1 ± 0.5	17.5 ± 1.2
Temperature ($^{\circ}C$)			
Ground surface	-	-6 to -7	-7 to -9
Permafrost Surface	-4 to -6	-6 to -8	-8 to -9
Precipitation (mm)			
Snow	186	117	104
Rain	-	113	108
Annual total	324	230	212
Degree-day ($^{\circ}C - day$)			
Freeze	3995	5283 ± 74	4930 ± 151
Thaw	800	932 ± 165	420 ± 123
Thaw season (days)	-	128 ± 12	94 ± 11
Thickness of the active layer (m)	-	0.6 - 0.8	0.4 - 0.6
Permafrost Thickness (m)	~ 250	$\sim 300 - 500$	~ 600

warming in the North American Arctic and the Arctic could have started as early as during the mid-1880s. The power spectra for air temperature time series at Barrow show that MAAT had a strong signal at $P=10.3$ years which may represent the solar cycle and $P=19.7$ years which is close to the lunar-solar signal. Freeze and thaw indices, precipitation and snowfall also show peaks with similar periods.

Departures of the MAAT, freeze and thaw index from their long-term means at Barrow show that variation of freeze index is over three times greater than the thaw index. The standard

deviation for monthly air temperatures from their long-term means is about two times greater during winter months than during summer months. These results indicate that the change of the MAAT is mainly controlled by the variation of winter temperatures. The variation of summer temperature is not significant to the variation of MAAT. One should be very careful when tree ring data are used to reconstruct the paleoclimate in Alaska north of the Brooks Range, which is mostly related to the summer temperatures.

There was a trend with greater snowfall during colder years and smaller snowfall during warmer years.

7.2 Physical and Thermal Properties of Soils

It was found that the top 0.2 and 0.3 m of the soils consists of live and dead organic materials mixed with wind blown silt. Below the peat layer is silt with a few organic spot. Dry bulk density of the mineral soils ranges from 1350 kg/m^3 to about 1500 kg/m^3 . The soil moisture was also measured by TDR method (Osterkamp, unpublished research) *in situ* and results were very consistent with the measurements in laboratory, with the maximum percent difference less than 10%.

The apparent thermal diffusivity of the active layer and upper permafrost was determined from soil temperature time series using a numerical scheme (Zhang and Osterkamp, 1993, see Appendix A) with uneven space and time intervals. Table 7.2 summarizes the calculated results for temperatures below -8°C for the West Dock site and below -4°C for Franklin Bluffs and Deadhorse sites.

A noteworthy feature shows that the values of D during warming of the soil and permafrost are less than during cooling. It may indicate that there is a larger difference in the rate of change of unfrozen water content during cooling and warming processes (Zhang, 1989). Soil

Table 7.2 Apparent Thermal Diffusivity near Prudhoe Bay

Depth (m)	Franklin Bluffs	Deadhorse	West Dock
0.0 ~ 0.2	-	-	6.5 ± 2
0.4 ~ 0.9	29 ± 3	28 ± 3	8 ± 3
3.0 ~ 25.0	-	-	36 to 44
25.0 ~ 50.0	-	-	45 to 53

temperature data show that the rate of temperature change with time during the cooling process is much greater than during warming process. Another explanation for the difference in D may be due to the unequal water movement during the cooling and warming processes of the upper permafrost. During the cooling and after the freeze-up of the active layer, limited water may move upwards from the upper permafrost to the active layer due to its cold temperatures; while the downwards movement of water in the summer thaw periods takes place in a relatively warm open system. When water moves down from the thawed layer during the warming processes to the upper permafrost and refreezes, the latent heat released will increase the apparent heat capacity which results in the decrease of D.

7.3 Seasonal Snow Cover

The date when the seasonal snow cover first becomes established shows a relatively constant time over the period of record; while, for Barrow, there has been a trend towards earlier snowmelt since about 1953. This trend is not very obvious at Barter Island (1957-1988) and at Umiat (1978-1991). The early snowmelt at Barrow may be related to the local development and population expansion.

Summer snowfall is relatively small, less than 10% of annual total, snow only lasts a few hours or a few days on ground. The maximum monthly snowfall occurs in October and more

than 50% of annual snowfall occurs in September through November, and the thickness of the seasonal snow cover increases rapidly. The temperature gradient across the snowpack is greatest, the density is low, and the depth hoar layer starts to form.

It takes 40 to 50 days for the disappearance of seasonal snow cover along the coast and about 30 days inland.

The evolution of seasonal snow cover can be approximated by

$$H_s(t) = \begin{cases} 0 & 0 \leq t \leq P_1 \\ (A)H_{max} & P_1 \leq t \leq P_2 \\ (1 - B)H_{max} & P_2 \leq t \leq P_3 \\ 0 & P_3 \leq t \leq P \end{cases} \quad (7.1)$$

where H_s is thickness of seasonal snow cover in m at time t in day, P_1 is the first day of steady seasonal snow cover on ground, P_2 is time at which snow thickness is maximum H_{max} in m, P_3 is last day of steady seasonal snow cover on ground, n is a positive integer and

$$A = \left(\frac{t - P_1}{P_2 - P_1} \right)^{n/2}$$

and

$$B = \left(\frac{t - P_2}{P_3 - P_2} \right)^{n/2}.$$

In equation (7.1), the time periods $0 \leq t \leq P_1$ and $P_3 \leq t \leq P$ are generally snow free, where $P=365$ days started at July 1. During these periods, snow may stay on ground for a few hours or a few days. The time period $P_1 \leq t \leq P_2$ is for the accumulating processes and $P_2 \leq t \leq P_3$ for the melting processes. The accumulating and melting processes vary with the choice of n , $n = 1$ for $P_1 \leq t \leq P_2$ and $n = 3$ for $P_2 \leq t \leq P_3$ gives the best fit to data.

7.4 Influence of Seasonal Snow Cover on Ground Thermal Regime

There is a sharp change in the amplitude of daily ground surface temperature at the date when snow disappears in the spring and at the date when snow cover first becomes established in autumn. This sharp change in the amplitude can provide some evidence about the presence or absence of the seasonal snow cover on the ground surface. The date for presence or absence of snowpack on the ground determined by change in daily surface amplitude is consistent with the date measured at the reporting stations when a trace (snow thickness is less than 2.5 cm) is observed.

The average value of ΔT_{ga} (the difference between monthly ground surface and air temperature) for summer is about 1.3°C . After the establishment of continuous seasonal snow cover on ground surface, ΔT_{ga} increases and reaches its maximum value in November due to the rapid decrease of air temperature, low density of snowpack and release of latent heat from the active layer. During the middle of winter (December through March), ΔT_{ga} varies from a few degrees to about 10°C . An extreme value of $\Delta T_{ga} = 35^{\circ}\text{C}$ was recorded in the winter of 1988 at Franklin Bluffs. In a storm event, ΔT_{ga} can be reduced to 0°C or become negative, that is, the snowpack cools the surface. In late April, ΔT_{ga} decreases to the summer average value when the ground surface is snow free. During May, air temperature can be a few degrees higher than the ground surface temperature and ΔT_{ga} becomes negative. This cooling effect continues in early June until the seasonal snow cover is completely removed. After the disappearance of seasonal snow cover, the surface temperature increases substantially, as a whole, ΔT_{ga} in June is very close to the summer average value ΔT_{ga} .

Seasonal snow cover can raise the seasonal and mean annual ground surface temperature by several degrees. The average value of ΔT_{ga} during winter is about 5°C to 8°C higher

than that during snow free period. Seasonal snow cover can increase the mean annual ground surface temperature by 3°C to 6°C .

The response of the permafrost surface temperature to air temperature follows the similar pattern as variation of ΔT_{ga} . The difference, ΔT_{pa} , between the permafrost surface and air temperature from May to August is negative and the magnitude of ΔT_{pa} is greater from October to March than ΔT_{ga} .

7.5 Relation of Current Climatic Conditions with Permafrost Temperatures

Although the MAAT is about $-12.4 \pm 0.4^{\circ}\text{C}$ from West Dock to Happy Valley, the mean annual temperature near the permafrost table increases over 3°C . The longer thaw season and higher summer air temperature are major factors in increasing permafrost temperatures inland during the summer. The combination of microrelief and vegetation with snow may increase the insulating effect of seasonal snow cover and raise the permafrost surface temperature during the winter. The decrease of permafrost thickness inland from the coast is partly associated with the variation of mean annual temperature near the permafrost surface which is largely controlled by the above factors.

Permafrost temperatures at deep levels show a cooling trend from 1983 to 1987 and then warming again until 1992. Over the same time period, average air temperature was about -12.0°C and average maximum thickness of snow on ground was about 12 cm. Cold air temperature (below -12.0°C) and thin snow cover (less than average) during the early years of record are responsible for the permafrost cooling. Higher air temperature and thicker snow cover after 1987 may respond to the warming of permafrost. Obviously, changes in air temperature alone can not drive the change in permafrost temperature although the insulating

effect of seasonal snow cover is controlled by many factors such as timing, duration, structure, and accumulating processes.

Thermal offset in near-surface mean annual ground temperature at West Dock and Franklin Bluffs ranged from 0.3°C to 1.8°C over four years of measurements. The value of thermal offset was greatest with heavy snowfall and thick snow on ground during the year of 1988-1989; by contrast, the value is smallest with light snowfall and less snow on ground during the year of 1989-1990. This is probably because early and thick snow on ground can make the thawed active layer persist longer and the thermal offset value greater; while late and thin snow cover accelerates the freeze-up processes which reduces the thermal offset value.

7.6 Calibration of the Numerical Model

The numerical model was calibrated with the measured physical and thermal properties and temperature data at West Dock, Prudhoe Bay. The upper boundary was set at the snow surface when seasonal snow cover was present and the boundary condition was represented by the measured daily mean air temperatures. For the remainder of the year, the boundary was set at the base of the living plant layer and the boundary condition was represented by an equation correlating daily air and ground surface temperatures.

The thickness of seasonal snow cover was measured by the National Weather Service near Deadhorse airport for the same period of the soil temperature measurement in this region. A two layer structure (wind-packed layer and depth hoar layer) of the seasonal snow cover was used in the model. Thermal conductivity of the snow cover was calculated based upon an equation developed using series heat conduction theory. Physical and thermal properties for soils were obtained from Chapter 3 and *Lachenbruch et al. (1982)*.

Two different cases were calculated to verify the numerical model. Case I was calculated with the upper boundary set at the snow surface when snow was present and at the ground surface when snow was free. The results show a good agreement between the measured and predicted values. The standard deviation of the predicted daily mean ground surface temperature from the measured values is within $1^{\circ}C$. Case II was calculated with the upper boundary set at the ground surface and the boundary conditions represented by the measured daily mean ground surface temperatures. Results show that case II provides a better agreement with the measured temperature data than the values predicted by case I. This may be due to errors produced by modeling the effect of seasonal snow cover on the ground temperatures with daily mean air temperature. There is difference between computed and predicted temperatures in the upper permafrost during warming of the permafrost. This difference may be related to the latent heat effect due to the changes of unfrozen water content with temperature and moisture migration from the upper active layer. Results from cases I and II generally indicate an excellent agreement between the measured and predicted permafrost temperatures with depth, the maximum difference between measured and predicted values is within $0.2^{\circ}C$.

7.7 Sensitivity Analysis of Ground Thermal Regime to Changes in Snow Cover Parameters

Sensitivity analysis of the ground thermal regime to changes in seasonal snow cover parameters such as the timing and duration, thickness, depth hoar layer, accumulating and melting processes were conducted using the calibrated numerical model. Twenty one cases were calculated to investigate the effect of changes in seasonal snow cover parameters on the ground thermal regime. Table 7.3 summarizes the calculated results.

Table 7.3 Sensitivity of surface temperature to snow cover parameters

Run No.	ΔT ($^{\circ}C$)	T_{off} ($^{\circ}C$)	Comments
1	+0.20	-0.39	<i>Longest duration</i>
3	-0.13	-0.42	<i>Shortest duration</i>
4	-2.03	-0.39	$H_{max} = 0.15m$
5	-1.00	-0.43	$H_{max} = 0.25m$
7	+0.95	-0.45	$H_{max} = 0.45m$
8	+1.42	-0.45	$H_{max} = 0.50m$
9	-2.53	-0.39	$\phi = 0.0$
10	-1.67	-0.41	$\phi = 0.10$
11	-0.82	-0.42	$\phi = 0.20$
12	+0.78	-0.45	$\phi = 0.40$
13	+1.57	-0.45	$\phi = 0.50$
14	+0.18	-0.44	$n = 1$
15	-1.19	-0.40	$n = 2$
16	-1.91	-0.39	$n = 3$
19	+1.10	-0.46	$A_o = 18^{\circ}C$
20	+1.50	-0.67	$A_o = 20^{\circ}C$
21	+1.44	-0.88	$A_o = 22^{\circ}C$

The combined effect of changes in seasonal snow cover parameters on MAGST and MAGT can be very significant. For early snowfall and later snowmelt with a maximum snow thickness of about 0.5 m and the depth hoar layer well developed, MAGST could increase over $3.1^{\circ}C$ from the long-term average condition. For late snowfall and early snowmelt with a maximum snow thickness of 15 cm and the depth hoar layer poorly developed, MAGST could decrease as much as $3.8^{\circ}C$ from the long-term average condition. The MAGST difference between these two extreme cases could be as high as $6.9^{\circ}C$ and the time of active layer freeze up could be delayed about two months one from another.

The calculated results also show that the combined effect of local seasonal snow cover and air temperature on the ground thermal regime could be very different. Although the MAAT from the Coast to inland is about the same, variations in timing and duration, maximum thickness of seasonal snow cover and in amplitude of MAAT could result the change in ground surface temperature by several degrees. The calculated results show that permafrost temperature could differ about over 1.6°C from the Coast, inland just from variation in timing and maximum thickness of seasonal snow cover. Combined with the difference in vegetation and depth hoar layer development from the Coast to inland, the observed permafrost temperature increase could be well understood in the regions.

7.8 Response of Permafrost Temperature to Changes in Climate

The calibrated numerical model for one-dimensional heat flow problems with phase change was used to investigate the effects of air temperature, seasonal snow cover, the active layer, initial temperature conditions in permafrost and variations in the thermal properties of soils on permafrost temperatures. Simulations were carried out using past air temperatures for the boundary conditions at the permafrost surface, ground surface, or surface of the snow cover. The effects of initial conditions, use of approximations for the surface temperature history, and of the active layer, snow cover and thermal properties on permafrost temperatures were examined in this continuing investigation.

When air temperature variations in the North American Arctic were applied to the permafrost surface at Prudhoe Bay, it was found that the permafrost temperature variations depended strongly on the choice of initial conditions (long-term MST). If this initial MST was chosen close to the measured long term MST of the permafrost near Barrow, the air temperature change would not be large enough to account for the permafrost warming. An alternative

explanation of the last result is that the shallow permafrost temperatures were colder than the assumed initial conditions. The calculated results show that it is possible that colder shallow permafrost temperatures existed than the assumed initial long term conditions, but it will require a long time for the permafrost temperatures to reach their initial long term MST. The differences between using air temperature data at the permafrost surface compared to using straight line approximations to the data were small but measurable below about 50 m and may be more significant above this depth.

Barrow air temperatures (1923-1991) used for the ground surface boundary condition (active layer but no snow cover) at a site SB3 near Barrow and at site E near Prudhoe Bay produced little change in permafrost temperatures from the initial condition. This result disagrees with permafrost temperature observations at site SB3 and at site E and confirms that air temperature variations alone (since 1923) cannot account for warming of the permafrost. When the snow cover was added, the model correctly predicts both the magnitude and penetration depth of permafrost temperature changes. The temperature history at the ground surface predicted by the model with snow cover shows that the difference between MAGST and MAAT ranges from 1.3°C to 6.1°C , with the average value of $3.3 \pm 1.1^{\circ}\text{C}$. This value is very consistent with the measurements in Prudhoe Bay regions. There is no clear evidence for a cooling of permafrost from 1940 to the mid-1970s for cases that included a snow cover. It indicates that the effect of changes in seasonal snow cover on ground thermal regime masks the effect of changes in MAAT. For the observations and predictions to be compatible when the snow cover was added, the initial ground surface temperature must have been about the same as the MAAT. This implies a very thin snow cover prior to 1923. The calculated results support the idea that an extremely thin snow cover prior to 1923 could reduce the temperature difference between MAGST and MAAT significantly, but sporadic measurements show that snowfall was above the long term average value of $71 \pm 30 \text{ cm}$ for the period from 1923 through 1991.

This implies that (i) MST of permafrost was at least a few degrees warmer than the long term MST of permafrost extrapolated from deep permafrost temperature profiles around 1923. The calculated results indicate that the higher initial MST would produce a penetration depth far deeper than the measured values. (ii) Permafrost had started warming before 1923 as the atmosphere.

The model predicts that the penetration depth changes with variations of thermal diffusivity for the same upper boundary conditions. The current values of thermal diffusivity used for the calculations were about $35 \text{ m}^2/\text{yr}$ near Barrow and about $50 \text{ m}^2/\text{yr}$ near Prudhoe Bay. The penetration depth near Prudhoe Bay is was about 30% deeper than that near Barrow since 1923. The model predicts correct penetration depth compared with the measured value for $D = 15 \text{ m}^2/\text{yr}$ for the main group and $D = 25 \text{ m}^2/\text{yr}$ for the Prudhoe Bay group since 1880. With higher values of D , the predicted penetration depth is much deeper than the measured values. This implies that the values of the thermal diffusivity used in reconstructing the MST history of the permafrost might be too high.

By applying those calculated results to permafrost temperature data, we can conclude that the long term MST of the permafrost was established before or around 1880. Permafrost probably started warming at the same time as the atmosphere did in the 1880s. Variations in the penetration depth may be related to changes in thermal properties of permafrost, variations in the magnitude of the permafrost surface warming may be due to the effect of local factors such as soil type, vegetation, microrelief, soil moisture condition and seasonal snow cover. Changes in seasonal snow cover may be the dominant factor which influences the local ground thermal regime.

Although the timing of the permafrost warming was the same as the atmosphere warming, the magnitude of the permafrost warming is still greater than that of MAAT. This can be explained as the effect of the interaction of local microrelief and vegetation with snow. The

effect of the interaction of vegetation and snow cover may have amplified the air temperature changes in permafrost. This mechanism can be verified by the current climatic conditions and permafrost temperatures in Alaska north of the Brooks Range.

APPENDIX A

Derivation of a Numerical Expression for Uneven Space and Time Intervals

Formulas for the first and second derivatives with uneven increments can be derived through a Taylor series expansion about the point x_o . Suppose we have the points (x_{-2}, f_{2-2}) , ..., (x_2, f_2) , where $f_i = f(x_i)$ and the points are uneven spaced, the expansion about x_o would be

$$f(x_o + t) = f_o + t f'_o + \frac{t^2}{2} f''_o + \frac{t^3}{6} f'''_o + \dots; \quad (A.1)$$

$$f(x_o - s) = f_o - s f'_o + \frac{s^2}{2} f''_o - \frac{s^3}{6} f'''_o + \dots \quad (A.2)$$

Multiplying s^2 to (3A-1) and t^2 to (3A-2), then subtracting we find that

$$f'_o = \frac{\frac{1}{t^2} f(x_o + t) - \frac{1}{s^2} f(x_o - s)}{\frac{1}{t} + \frac{1}{s} - \left(\frac{1}{t} - \frac{1}{s}\right)} + O[(t \times s)]. \quad (A.3)$$

Multiplying s to (A.1) and t to (A.2), then adding we have

$$f''_o = \frac{2s f(x_o + t) + 2t f(x_o - s)}{st(s + t)} - \frac{2}{st} f(x_o) + O[(t - s)]. \quad (A.4)$$

Applying (A.3) and (A.4) to one dimensional heat conduction equation

$$\frac{\partial T}{\partial t} = D \frac{\partial^2 T}{\partial x^2} \quad (A.5)$$

we have

$$\frac{\partial T}{\partial t} = \frac{\frac{1}{(\Delta t_2)^2} T_i^{j+1} - \frac{1}{(\Delta t_1)^2} T_i^{j-1}}{\frac{1}{\Delta t_1} + \frac{1}{\Delta t_2} - \left(\frac{1}{\Delta t_2} - \frac{1}{\Delta t_1} \right) T_i^j} + O\left[(\Delta t_1 \Delta t_2)\right]; \quad (\text{A.6})$$

If only one time step involved, then

$$\frac{\partial T}{\partial t} = \frac{T_i^{j+1} - T_i^j}{\Delta t} + O[(\Delta t)]; \quad (\text{A.7})$$

and

$$\frac{\partial^2 T}{\partial x^2} = \frac{2\Delta x_1 T_{i+1}^j + 2\Delta x_2 T_{i-1}^j}{\Delta x_1 \Delta x_2 (\Delta x_1 + \Delta x_2)} - \frac{2}{\Delta x_1 \Delta x_2} T_i^j + O\left[(\Delta x_2 - \Delta x_1)\right]. \quad (\text{A.8})$$

where the integers i and j reference positions and times for the node of interest, $\Delta x_1 = x_i^j - x_{i-1}^j$, $\Delta x_2 = x_{i+1}^j - x_i^j$, $\Delta t_1 = t_i^j - t_i^{j-1}$, and $\Delta t_2 = t_i^{j+1} - t_i^j$ represent increments of depth and time in the observation mesh.

Equation used to estimate the values of D with uneven space and time increments can be obtained by applying (A.6) and (A.8)

$$D = \frac{\left(\Delta x_1 \Delta x_2 (\Delta x_1 + \Delta x_2) \right) \left(\frac{1}{(\Delta t_2)^2} T_i^{j+1} - \frac{1}{(\Delta t_1)^2} T_i^{j-1} \right)}{2 \left(\Delta x_1 T_{i+1}^j + \Delta x_2 T_{i-1}^j - (\Delta x_1 + \Delta x_2) T_i^j \right) \left(\frac{1}{\Delta t_1} + \frac{1}{\Delta t_2} - \left(\frac{1}{\Delta t_2} - \frac{1}{\Delta t_1} \right) T_i^j \right)}. \quad (\text{A.9})$$

Equation used to estimate the values of D for uneven space increment with even time increment can be obtained by setting $\Delta t = \Delta t_1 = \Delta t_2$ in equation (A.6) and substituting it into equation (A.5) together with (A.7), we have

$$D = \frac{\Delta x_1 \Delta x_2 (\Delta x_1 + \Delta x_2) (T_i^{j+1} - T_i^{j-1})}{4\Delta t (\Delta x_1 T_{i+1}^j - (\Delta x_1 + \Delta x_2) T_i^j + \Delta x_2 T_{i-1}^j)}; \quad (A.10)$$

If only two time step involved, then substitute (A.7) and (A.8) into (A.5), we have

$$D = \frac{\Delta x_1 \Delta x_2 (\Delta x_1 + \Delta x_2) (T_i^{j+1} - T_i^j)}{2\Delta t (\Delta x_1 T_{i+1}^j - (\Delta x_1 + \Delta x_2) T_i^j + \Delta x_2 T_{i-1}^j)}. \quad (A.11)$$

Equation used to estimate the values of D for uneven time increment with even space increment can be obtained by set $\Delta x = \Delta x_1 = \Delta x_2$ in (3.A -5) and then substitute it into (A.5) together with (A.6), we have

$$D = \frac{(\Delta x)^2 ((\Delta t_1)^2 T_i^{j+1} - ((\Delta t_1)^2 - (\Delta t_2)^2) T_i^j - (\Delta t_2)^2 T_i^{j-1})}{\Delta t_1 \Delta t_2 (\Delta t_1 + \Delta t_2) (T_{i+1}^j - 2T_i^j + T_{i-1}^j)}. \quad (A.12)$$

If only two temperature profiles are used, the equation used to estimate values of D with even space and time increment becomes (Zhang, 1989 ; Zhang and Osterkamp, 1993) ,

$$D = \left(\frac{(\Delta x)^2}{\Delta t} \right) \frac{T_i^{j+1} - T_i^j}{T_{i+1}^j - 2T_i^j + T_{i-1}^j}. \quad (A.13)$$

By setting $\Delta x = \Delta x_1 = \Delta x_2$ in (A.6) and $\Delta t = \Delta t_1 = \Delta t_2$ in (A.8), then substitute them into (A.5), equation for even space and time increments is obtained

$$D = \left(\frac{(\Delta x)^2}{2\Delta t} \right) \frac{T_i^{j+1} - T_i^{j-1}}{T_{i+1}^j - 2T_i^j + T_{i-1}^j}. \quad (A.14)$$

APPENDIX B

Considerations in Determining Thermal Diffusivity from Temperature Time Series Using Numerical Methods

T. Zhang and T. E. Osterkamp

Geophysical Institute, University of Alaska Fairbanks, 99775-0800

ABSTRACT

This paper investigates numerical methods for determining the in situ apparent thermal diffusivity, D , of the active layer and permafrost from repeated measurements of vertical temperature profiles. The results can be applied to any soil or rock where heat flow is conductive. An analytical expression was derived for D when unfrozen water is present in frozen soils and permafrost. The usual numerical expression for D (termed model I) was extended to include higher order terms (model II). This substantially reduces truncation errors but increases measurement errors somewhat. Extremely accurate temperature measurements (approaching $\pm 0.01^\circ\text{C}$) are required to apply the method. Synthetic temperature time series were used to evaluate and compare predictions of models I and II. Model I produced spikes (large positive and negative values) in the calculated D at times where the ground temperatures were near a maximum or minimum. Using model II, the spikes disappeared or were substantially reduced in magnitude and duration and errors in D at other times were reduced compared to model I. Application of the method requires acquisition of very precise temperature measurements at appropriate space (Δx) and time (Δt) intervals at a depth where measurable temperature changes occur. Selection of values for Δx and Δt must take into account the accuracy of the temperature measurements,

duration and amplitude of the temperature changes, depth, and the expected values for D . In general, Δx should be much less than the depth of interest and Δt must be less than the period or duration of surface temperature changes. For the active layer, Δx can range from a few centimeters to a tenth of a meter or so and Δt from a few minutes to an hour or so. For the near-surface permafrost within the depth of annual temperature variations, Δx can range from a few tenths meter to about one meter and Δt from one day to several weeks. Below the depth of annual temperature variations in the permafrost, values for Δx of several meters and Δt of a year or more may be appropriate.

B.1 INTRODUCTION

Investigations of the thermal regime of the active layer and permafrost require an understanding of their thermal properties, particularly thermal conductivity, volumetric heat capacity and thermal diffusivity. The thermal diffusivity is of primary importance in natural systems since it controls the rate of thermal response. McGaw *et al.*, (1978) developed a method to determine thermal diffusivity *in situ* for the active layer and permafrost from a temperature time series. This method has also been used by Nelson *et al.* (1985), Outcalt and Hinkel (1989, 1990), Zhang (1989), and Hinkel *et al.* (1990). While it appears that good results can be obtained, reported *in situ* values for thermal diffusivity are sometimes large, contain zero values, may be negative, and have considerable scatter. Using a synthetic thermal profile, Hinkel *et al.* (1990) showed that large positive and negative values ("spikes") were a result of the method and occur when the rate of change of the temperature gradient becomes small.

They attributed other large fluctuations in thermal diffusivity to non-conductive heat flow processes in the active layer; a conclusion which is rendered uncertain by the variable results for D.

This paper investigates further the application of numerical methods for determining the thermal diffusivity of the active layer and permafrost from temperature time series.

B.2 REVIEW OF THEORY

The one-dimensional transient heat conduction equation is

$$\frac{\partial}{\partial x} \left(K \frac{\partial T}{\partial x} \right) = C_v \frac{\partial T}{\partial t} \quad (B.1)$$

where K is the thermal conductivity ($Wm^{-1}^{\circ}C^{-1}$), T is the temperature ($^{\circ}C$), x is the distance coordinate (m), C_v is the volumetric heat capacity ($Jm^{-3}^{\circ}C^{-1}$) and t is the time (sec).

In the application of (1), it is often assumed that K does not depend on position (i.e., the soil is homogeneous). In a thawed active layer and in a frozen active layer and permafrost that does not contain unfrozen water, K and C_v are approximately independent of temperature. With these assumptions, (1) becomes

$$\frac{\partial^2 T}{\partial x^2} = \frac{1}{D} \frac{\partial T}{\partial t} \quad (B.2)$$

where $D = K/C_v$ is the thermal diffusivity (m^2/sec).

Equation (2) has been used in the past to calculate an apparent thermal diffusivity $D = T_t/T_{xx}$, where T_t and T_{xx} are the numerical approximations of $\partial T/\partial t$ and $\partial^2 T/\partial x^2$, respectively. This relation has a singular point at $T_{xx} = 0$ which may create difficulties when using it to calculate D .

If the active layer and permafrost are partially frozen and contain unfrozen water, then K and C_v are functions of temperature. Equation (1) becomes (Guymon, 1984)

$$K \frac{\partial^2 T}{\partial x^2} + \frac{\partial K}{\partial T} \left(\frac{\partial T}{\partial x} \right)^2 = C_v \frac{\partial T}{\partial t} - L \frac{\rho_i}{\rho_u} \frac{\partial \theta_i}{\partial t} \quad (B.3)$$

where L is the volumetric latent heat of fusion (Jm^{-3}), θ_i is the volumetric ice content (m^3/m^3), and ρ_i and ρ_u are the densities of ice and unfrozen water, respectively. Equation (3) can be written

$$K \frac{\partial^2 T}{\partial x^2} + \frac{\partial K}{\partial T} \left(\frac{\partial T}{\partial x} \right)^2 = C_a \frac{\partial T}{\partial t} \quad (B.4)$$

where $C_a = C_v + L(\partial\theta_u/\partial T)$ is the apparent volumetric heat capacity and θ_u is the volumetric unfrozen water content (m^3/m^3) (eg. Osterkamp, 1987). An apparent thermal diffusivity for frozen soils and permafrost containing unfrozen water can be defined as follows. For saturated soils, common in permafrost and the active layer,

$$K = K_s^{(1-\theta_f)} K_i^{\theta_f} \left(\frac{K_u}{K_i} \right)^{\theta_u} \quad (B.5)$$

where K_s , K_i and K_u are the thermal conductivities of the soil, ice and unfrozen water components, and θ_f is the porosity in the frozen state. The temperature dependence of the thermal conductivity of the constituents is ignored over the range of temperatures usually found in the field. Using $\theta_u = \rho_b w_u / \rho_u$ and $w_u = A(-T)^B$, where ρ_b is the bulk density of the soil (kg/m^3), ρ_u is the density of unfrozen water, w_u is the gravimetric water content (kg/kg), and A and B are constants, then

$$\frac{1}{K} \frac{\partial K}{\partial T} = -R(-T)^{B-1} \quad (B.6)$$

where $R = AB\rho_b \ln(K_u/K_i) / \rho_u$. Then, (4) becomes

$$D \left[\frac{\partial^2 T}{\partial x^2} - R(-T)^{B-1} \left(\frac{\partial T}{\partial x} \right)^2 \right] = \frac{\partial T}{\partial t} \quad (B.7)$$

and

$$D = \frac{T_t}{T_{xx} - RT_x^2(-T)^{B-1}} \quad (B.8)$$

where T_x is $\partial T/\partial x$. Application of (8) requires a knowledge of the variation of θ_u and R with temperature.

If the water in the thawed active layer or the unfrozen water in the partially frozen active layer or permafrost moves with a constant velocity, v , then a term of the form $C_w v \partial T/\partial x$ (e.g., Guymon, 1984), where C_w is the volumetric heat capacity of water, would be subtracted from the left hand side of (4). This term, divided by C_a , would then enter into the numerator on the right hand side of (8) and then both v and C_a have to be known in order to evaluate D . Until present, only (2) has been used to evaluate D ; however, when unfrozen water is present, K and C_a are strongly dependent on θ_u and (8) is more suitable.

The application of (2) for evaluating D requires computation of T_t and T_{xx} by numerical methods. Two models will be discussed.

B.2.1 Model I

The numerical approximations of the derivatives T_t and T_{xx} are (Gerald and Wheatley, 1989)

$$T_t = \frac{T_i^{j+1} - T_i^{j-1}}{2\Delta t} + O[(\Delta t)^2] \quad (B.9)$$

and

$$T_{xx} = \frac{T_{i-1}^j - 2T_i^j + T_{i+1}^j}{(\Delta x)^2} + O[(\Delta x)^2] \quad (B.10)$$

where the integers i and j reference positions and times for the node of interest and Δx and Δt represent increments of depth and time in the observation mesh. Equation (9) can also be approximated by (Carnahan et. al., 1969)

$$T'_t = \frac{T_i^{j+1} - T_i^j}{\Delta t} + O[(\Delta t)]. \quad (B.11)$$

Equations (9) and (11) are alternate expressions which can be used for numerical calculations where (9) involves two time steps and (11) involves only one time step. Let $\Delta_t T = T_i^{j+1} - T_i^{j-1}$, $\Delta_{xx} T = T_{i-1}^j - 2T_i^j + T_{i+1}^j$ and $\Delta_t T' = T_i^{j+1} - T_i^j$, then, neglecting the terms $O[(\Delta x)^2]$ and $O[(\Delta t)^2]$, substituting (9) and (10) into (2) and rearranging yields

$$D \cong \left(\frac{(\Delta x)^2}{2\Delta t} \right) \frac{\Delta_t T}{\Delta_{xx} T}. \quad (B.12)$$

Similarly, substituting (10) and (11) into (2) yields

$$D \cong \left(\frac{(\Delta x)^2}{\Delta t} \right) \frac{\Delta_t T'}{\Delta_{xx} T}. \quad (B.13)$$

The application of (12) requires three temperature profiles with two time steps and (13) requires two temperature profiles with only one time step. Equation (12) has been used by McGaw, et al. (1978); Nelson, et al. (1985); Zhang (1989); Hinkel, et al. (1990) and (13) by Zhang (1989) to compute the apparent thermal diffusivity in the active layer and permafrost.

B.2.2 Model II

Numerical approximations (truncation errors) of derivatives can be improved by retaining higher order terms in the interpolating polynomial (Gerald and Wheatley, 1989). A Taylor series expansion with higher order terms was used to obtain

$$T_t = \frac{1}{12\Delta t}(T_i^{j-2} - 8T_i^{j-1} + 8T_i^{j+1} - T_i^{j+2}) + O[(\Delta t)^4] \quad (B.14)$$

and

$$T_{xx} = \frac{1}{12(\Delta x)^2}(-T_{i-2}^j + 16T_{i-1}^j - 30T_i^j + 16T_{i+1}^j - T_{i+2}^j) + O[(\Delta x)^4] \quad (B.15)$$

Let $\Delta'_t T = T_i^{j-2} - 8T_i^{j-1} + 8T_i^{j+1} - T_i^{j+2}$ and $\Delta'_{xx} T = -T_{i-2}^j + 16T_{i-1}^j - 30T_i^j + 16T_{i+1}^j - T_{i+2}^j$, then, neglecting higher order terms and substituting (14) and (15) into (2),

$$D \cong \left(\frac{(\Delta x)^2}{\Delta t} \right) \frac{\Delta'_t T}{\Delta'_{xx} T}. \quad (B.16)$$

While application of (16) requires five temperature profiles with four time steps, it should yield a more accurate estimate of D .

In addition to the obvious requirement that the heat flow must be conductive, there are several general considerations for applying (12), (13), or (16) to field data. First, the heat conduction equation has been derived from continuum theory (Carslaw and Jaeger, 1959) and is valid for an infinitesimally small volume or layer with conductive heat flow while (12), (13), and (16) are for a finite volume. More accurate results using these numerical equations may be expected when Δx and Δt are small; however, both Δx and Δt are restricted by requirements associated with the measuring apparatus. Second, the soil volume in the active layer must be

in either a frozen or a thawed state for the time steps of the calculations and the soil volume should be homogeneous. Third, interpolation errors in the numerical procedure depend upon the degree of the polynomial used to obtain the derivatives so that (16) may be expected to give more accurate results than (12) which is more accurate than (13). Round off errors increase as Δx and Δt are decreased since this requires adding and subtracting temperatures that are more nearly the same value. Generally, round off errors can be reduced by using double precision (Gerald and Wheatley, 1989). Fourth, the accuracy of the field temperature measurements influences the estimate of D . The estimate of $\Delta_i T$, $\Delta'_i T$ and $\Delta''_i T$ are nearly independent of temperature accuracy, since only the temperature change at one sensor is required, while the estimate of $\Delta_{xx} T$ and $\Delta'_{xx} T$ depends upon the accuracy of the sensors. The quantities $\Delta_{xx} T$ and $\Delta'_{xx} T$ at any depth should be greater (preferably much greater) than errors, $\delta(\Delta_{xx} T)$ and $\delta(\Delta'_{xx} T)$, in their determination. Thus, temperature variations at depth should be sufficient to make $\Delta_{xx} T \gg \delta(\Delta_{xx} T)$ or $\Delta'_{xx} T \gg \delta(\Delta'_{xx} T)$. Table 1 shows $\delta(\Delta_{xx} T)$ and $\delta(\Delta'_{xx} T)$ for errors, δT , in the temperature measurements.

Table B.4 Effects of errors, δT , in temperature measurements on $\delta(\Delta_{xx} T)$ and $\delta(\Delta'_{xx} T)$ ($^{\circ}C$)

δT	0.2	0.1	0.05	0.02	0.01
$\delta(\Delta_{xx} T)$	0.5	0.3	0.13	0.05	0.03
$\delta(\Delta'_{xx} T)$	7.5	3.8	1.88	0.75	0.38

Since model II uses higher order terms to calculate the derivatives in the expression for D , it would appear to be superior to model I. An error analysis based upon the accuracy of the temperature measurements required to evaluate (12) and (16) (Table 2) shows that model I produces somewhat more accurate values for D . For the conditions in Table 2, the accuracy of the temperature measurements must approach $\pm 0.01^{\circ}C$ or better to obtain reasonable estimates

of D . Considering the increased complexity and reduced accuracy of model II, because of measurement errors, it may not seem worthwhile to use it. However, the reduction in truncation errors for T_t and T_{xx} in model II is a much greater factor than the measurement errors which ultimately makes model II much more precise than model I. It will also be shown that the use of model II helps to clarify the interpretation of results obtained with model I. In addition, model II can be used in some cases when model I becomes unstable and produces spikes in the values for D .

Table B.5 Measurement errors in calculated values of D using models I and II at a depth of 0.3 m for a daily temperature wave with a surface amplitude of 4°C with $\Delta x = 0.1\text{ m}$ and $\Delta t = 10\text{ min}$.

Temperature accuracy ($^\circ\text{C}$)	Model I Error in D (m^2/yr)	Model II Error in D (m^2/yr)
0.1	78	105
0.05	39	52.5
0.01	7.9	10.5
0.001	0.9	1.2

Synthetic temperature time series were calculated for surface temperatures consisting of daily waves, annual waves with a superimposed daily variation and annual waves with a superimposed multi-year linear trend. Wave parameters were chosen to prevent the possibility of phase change. An input value of $D=25\text{ m}^2\text{ yr}^{-1}$ was used in all of these calculations. Calculated values of D from these synthetic temperature profiles, using model I (Eq. 12) and model II, were then compared to the input value of D . The stated errors are the differences between the calculated and input values divided by the input values (percent difference). The results help to illustrate the general considerations noted above and suggest additional factors that should be taken into account when calculating D from a measured temperature time series.

B.3 RESULTS AND DISCUSSION

B.3.1 Daily Surface Temperature Variations

Under stable weather conditions, the ground surface is subjected to a daily cycle of warming and cooling, which can cause measurable temperature changes to depths of about one to two meters. However, the presence of a thaw or a freeze front shields the underlying ground from these changes. Daily temperature variations can be used to determine D in a thawed or frozen active layer and in the permafrost underlying a frozen active layer. Synthetic temperatures for the daily cycle of warming and cooling were generated with a ground surface temperature

$$T(0, t) = T_d + A_d \cos(\omega_d t) \quad (B.17)$$

where T_d is the mean daily surface temperature, A_d is the amplitude of the daily surface temperature, $\omega_d = 2\pi/P_d$, and the period, $P_d = 1$ day. It was assumed that $T_d = -10^\circ C$ and $A_d = 4^\circ C$. Temperatures were generated at 0.1 m increments from the surface to the 0.5 m depth at 10 minute intervals using the steady-state solution of (2) (Carslaw and Jaeger, 1959). Figure b.1 shows temperature variations at depths of 0.2 m, 0.3 m and 0.4 m, the variations in $\Delta_t T$ and $\Delta_{xx} T$, and the calculated values (using models I and II) for D at the 0.3 m depth with $\Delta t = 10$ minutes. For model I, the calculations were made using the temperatures at 0.2 m, 0.3 m and 0.4 m depths, while for model II the temperatures from 0.1 m to 0.5 m were used.

Figure B.1(C) shows that there are significant errors in values for D calculated with model I. The largest errors occur near times when the temperature vs. time curve at the 0.3 m

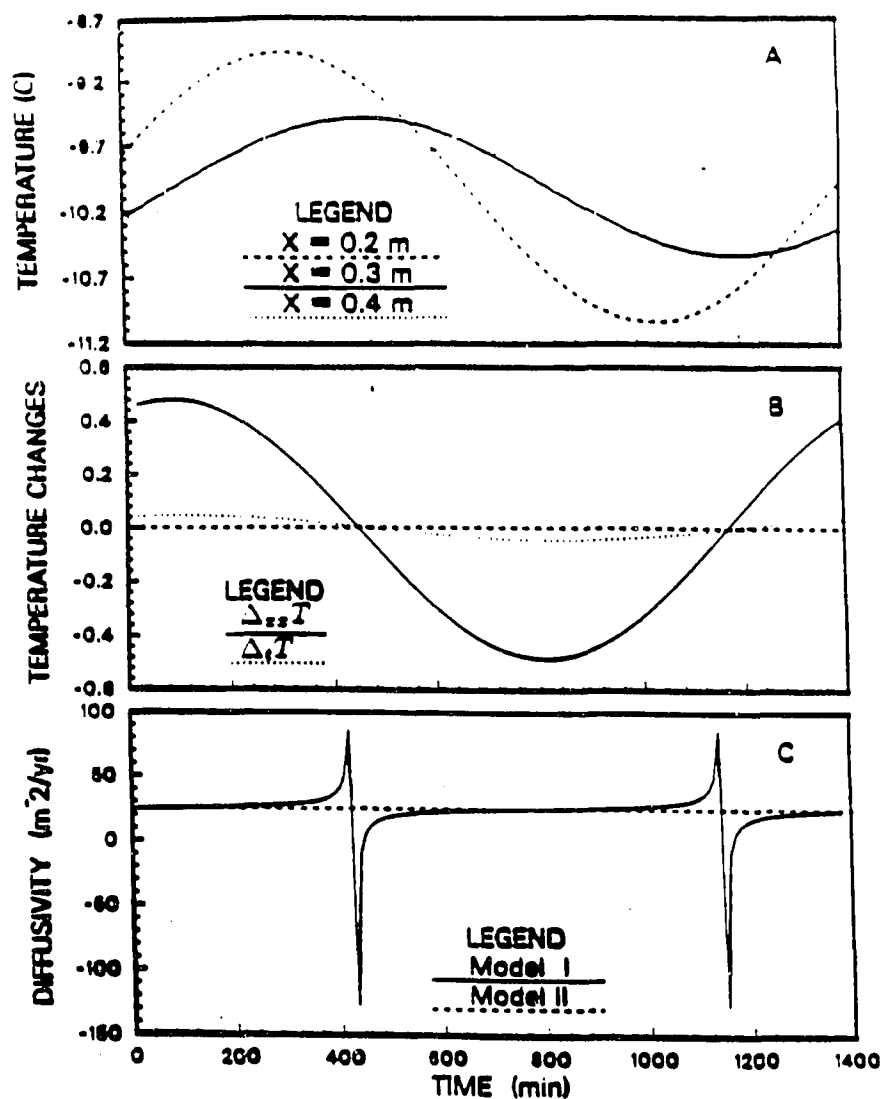


Figure B.1 (A) Synthetic temperature time series at three depths for a daily surface temperature wave with a surface amplitude of 4°C , (B) $\Delta_{xx}T$ and $\Delta_t T$ at the central depth of 0.3 m, and (C) a comparison of the calculated values of the thermal diffusivity at the 0.3 m depth with the input value of $25 \text{ m}^2 \text{ yr}^{-1}$. For these calculations, $\Delta x = 0.1 \text{ m}$, $\Delta t = 10 \text{ min}$.

depth passes through a maximum or minimum (i.e., when the magnitude of $\Delta_t T$ and $\Delta_{xx} T$ become small). Large positive and negative spikes in D are produced at these times. The best agreement of D with the input value occurs (near) where the magnitudes of $\Delta_t T$ and $\Delta_{xx} T$ are largest. Calculations of D at other depths show that the spikes in D change with depth and time due to the time lag as the temperature wave penetrates into the ground from the surface.

The results of calculations using model II (Fig. 1C) are much improved over those of model I. Spikes have been eliminated and the maximum error is only 4%. This reduction in error appears to be due to the more accurate higher order approximations (smaller truncation errors) for the derivatives in (2). Results for calculations using double precision (sixteen significant figures) were almost identical to calculations using single precision suggesting that round off errors were small for both models I and II for the conditions of these calculations. Practical disadvantages of model II are that more data are required and these data need to be very accurate.

Figure B.2 shows some of the effects of truncation errors in D when models I and II are used with different choices for Δx and Δt . In Fig. B.2B and B.2C, Δt is constant (1 min) and Δx changes from 0.1 m to 0.01 m. For model I, the errors in D decrease at all times for this change in Δx including a decrease in the magnitude and duration of the spikes. In Fig. B.2A and B.2C, Δx is constant (0.01 m) and Δt changes from 10 min to 1 min. Errors in D for this change in Δt decrease as Δt decreases except at spikes. The duration of the spikes is the same while their magnitude increases as Δt decreases. The results for model II are similar but the errors in D are much smaller (see Fig. B.2B) and the spikes are almost eliminated. Since the conditions were the same for both models, this suggests that the above errors are primarily truncation errors in $\Delta_t T$ and $\Delta_{xx} T$.

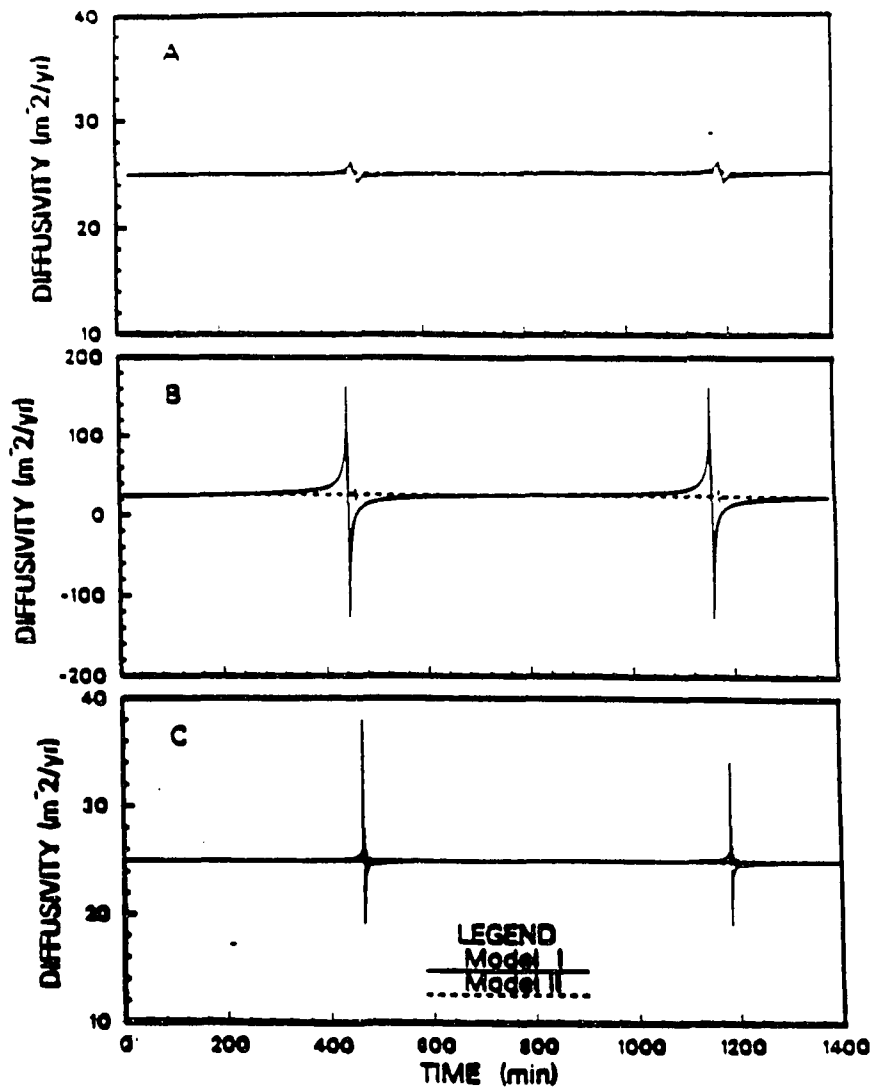


Figure 8.2 Variations of the calculated thermal diffusivity at a depth of 0.3 m for different values of Δx and Δt (A) $\Delta x = 0.01$ m and $\Delta t = 60$ min, (B) $\Delta x = 0.10$ m and $\Delta t = 1$ min, and (C) $\Delta x = 0.01$ m and $\Delta t = 1$ min.

B.3.2 Daily and Seasonal Surface Temperature Variations

The ground surface temperature also varies with changes in the weather and seasonal changes over the year. These changes provide an opportunity to obtain D from depths of about 1 m to 20 m or more. However, daily surface temperature variations are superimposed on these changes and must be considered in the methodology. An annual wave with a superimposed daily wave was used to investigate this problem. Synthetic temperature profiles were generated using

$$T(0, t) = T_y + A_d \cos(\omega_d t) + A_y \cos(\omega_y t) \quad (B.18)$$

where T_y is the mean annual temperature. The second term on the right hand side of (18) is the daily surface temperature wave and the third is the annual surface wave with amplitude, A_y , and $\omega_y = 2\pi/P_y$ where $P_y = 1$ year.

Several sets of calculations of D were made using (18) with A_d ranging from $0^\circ C$ to $4^\circ C$ and Δt from 10 min to 1 day with $A_y = 16^\circ C$, $T_y = -20^\circ C$, and $\Delta x = 0.1$ m. For both models I and II at depths up to 1.2 m where daily temperature variations are significant, using $\Delta t = 1$ day, errors in D were generally large (10 - 30%) and depended on A_d . Using $\Delta t = 10$ min, for depths up to 0.5 m, the errors in D for both models were similar, as expected, to those shown in Fig. B.1C. These results illustrate the requirement at these shallow depths that Δt must be much smaller than the period, P_d , and show that the effect of the annual temperature wave on D is not significant.

Using model I at a depth of 0.8 m with $\Delta t = 1$ hour, the errors in D were small except near the maximum and minimum temperatures at this depth where multiple spikes were produced. These spikes are a result of daily temperature variations which cause both $\Delta_{xx}T$ and $\Delta_t T$ to oscillate with a frequency of one day. The amplitude of the oscillations is such that both $\Delta_{xx}T$

and $\Delta_t T$ repeatedly pass through zero values which produces positive and negative spikes in values for D . Both the magnitude and duration of the spikes were reduced when using model II.

Values for D were calculated using models I and II for depths from 4 m to 20 m with $A_d = 4^\circ C$, $A_y = 16^\circ C$, $T_y = -20^\circ C$, $\Delta x = 1 \text{ m}$ and $\Delta t = 5 \text{ days}$ (Fig. B.3). For model I, the maximum percent difference between the calculated values and the input value in Fig. B.3 was less than 20%. Diffusivity values calculated by model II were almost identical to the input value. Additional calculations show that D can be obtained in the depth range from 1 m to 20 m or more with Δx ranging from a few tenths of a meter to a few meters and Δt from one day to a few weeks, depending upon the depth of interest.

B.3.3 Climatic Fluctuations and Ground Surface Temperature Variations

Fluctuations in climate on a scale of years produce changes in air temperatures and in snow cover which can affect permafrost temperatures. These effects can be monitored at depths below the seasonal changes by measuring the temperatures in a drill hole over several years. While the temperature changes at these depths are small, they can usually be measured with precision equipment, and D can be estimated using temperature recording frequencies from a few months to several years. The method is illustrated using the surface temperature

$$T(0, t) = T_y + A_y \cos(\omega_y t) + C_o t \quad (B.19)$$

where the initial mean ground surface temperature $T_y = -20^\circ C$. The second term on the right side of (19) is the annual temperature wave and the third term is an assumed linear temperature trend at the surface, where C_o is the rate of temperature change at $x = 0$. The initial condition is $T(x, 0) = T_y + G_o x$, where the temperature gradient $G_o = 0.019^\circ C/m$.

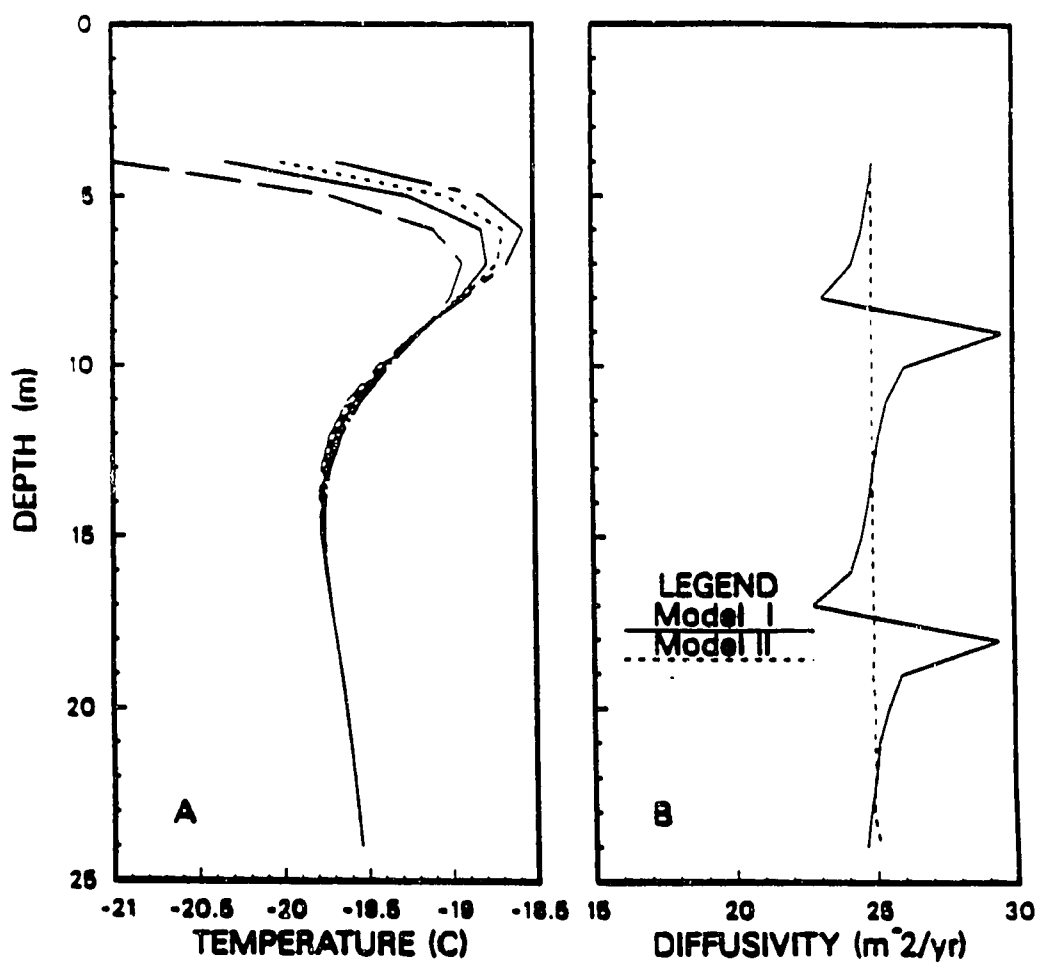


Figure B.3 (A) Five synthetic temperature profiles for depths below the daily zero temperature variations and, (B), a comparison of the calculated values between models I and II. For these calculations, $A_d = 4^\circ\text{C}$, $\Delta x = 1\text{ m}$, and $\Delta t = 5\text{ days}$.

Temperature profiles after 10 years were generated with $A_v = 16^\circ C$, $C_o = 0.2^\circ C yr^{-1}$, for 1 m space and 1 year time intervals. Figure B.4 shows the calculated temperature profiles and values for D predicted by models I and II with $\Delta x = 4$ m and $\Delta t = 1$ year. The errors in D below 35 m were less than 2%. The relatively large errors above 35 m were caused by the annual temperature variations and can be eliminated by choosing $\Delta t \ll 1$ year. At about 64 m, round off errors begin to affect the results for both models. Additional calculations show that relatively good results can be obtained for Δt ranging from less than a year to several years.

B.4 APPLICATIONS

The above methodology suggests that it should be possible to obtain values for the thermal diffusivity from a temperature time series, not only in the active layer and near-surface permafrost, but to any depth where there are measurable temperature changes. However, the above results are largely based on assumed periodic surface temperature variations with fixed amplitudes in soil where there is no freezing or thawing. Additional opportunities for determining D are created by weather patterns and by the presence of a freezing or thawing front in the active layer. For example, Climate in Alaska and other permafrost areas is often dominated by aperiodic temperature fluctuations with varying amplitudes lasting from a few days to a few weeks. Solar radiation at these high latitudes exhibits strong seasonal variations. A seasonal snow cover attenuates air temperature variations reducing the variations in ground surface temperatures. A freezing or thawing front in the active layer shields the underlying active layer and permafrost from ground surface temperature variations since the temperature at a front is generally constrained by the requirement for phase equilibrium to be near $0^\circ C$. As the ground surface warms and the active layer begins to thaw, the remaining frozen active

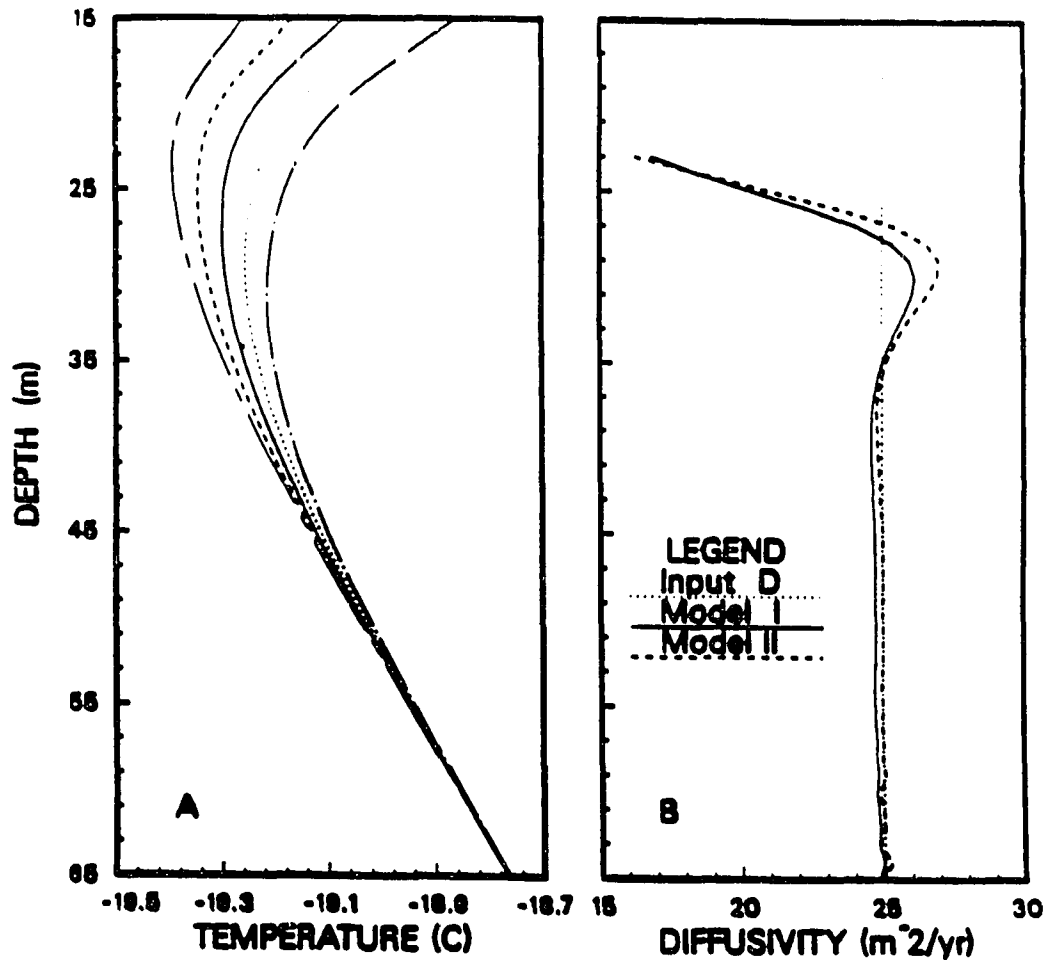


Figure B.4 (A) Five synthetic temperature profiles, calculated after ten years, for a warming trend of ground surface temperature with a superimposed annual surface temperature wave and (B) a comparison of the calculated thermal diffusivities from the temperature profiles. For the temperature calculations, $A_y = 16^\circ C$, $\Delta x = 1 m$, and $\Delta t = 1 year$, and for the thermal diffusivity calculations, $\Delta x = 4 m$ and $\Delta t = 1 year$.

layer and permafrost warm slowly with time. As the ground surface cools and begins to freeze, the remaining thawed active layer becomes isothermal since it is bounded on the top by the freezing front and on the bottom by the permafrost table. Upward freezing at the base of the active layer causes the adjacent permafrost to cool while the deeper permafrost continues to warm. The temperature changes brought about by these thawing and freezing effects generally continue for about six to nine months each year.

Applications of the method require the acquisition of very precise temperature data (preferably $\pm 0.01^\circ C$ or better) at appropriate depth (Δx) and time (Δt) intervals. Selection of values for Δx and Δt must take into account the accuracy of the temperature measurements, duration and amplitude of the temperature changes, depth where D is to be determined, and the diffusivity of the soil. Since the diffusivity of the soil can easily vary from 10 to 50 $m^2 yr^{-1}$, a factor of five or more, it is desirable to have information which allows a rough initial estimate of D to be made. A periodic surface temperature wave can be helpful in making initial estimates for Δx and Δt provided some information is available on the wave parameters. For a periodic surface temperature variation with surface amplitude, A , and frequency, ω , the depth, X , where the amplitude of the temperature variation is A_x can be obtained from (Carslaw and Jaeger, 1959)

$$X = \ln\left(\frac{A}{A_x}\right) / \sqrt{\frac{\omega}{2D}}. \quad (B.20)$$

Table 3 gives the depths for a daily temperature wave (X_d) and an annual wave (X_y) where the amplitude has been reduced to A_x for $D = 25 m^2 yr^{-1}$, $A_d = 4^\circ C$, and $A_y = 16^\circ C$.

Experience with models I and II suggests that, in general, Δx and Δt should be made small with $\Delta x \ll X$, the depth of interest, $\Delta t \ll P$ (period or duration of surface temperature change), $\Delta_{xx}T \gg \delta(\Delta_{xx}T)$ and $\Delta'_{xx}T \gg \delta(\Delta'_{xx}T)$. For the active layer, these

Table B.6 Depths for a daily temperature wave (X_d) and an annual wave (X_y) where the amplitude has been reduced to A_x .

A_x ($^{\circ}C$)	0.200	0.100	0.050	0.020	0.010	0.001
X_d (m)	0.34	0.44	0.54	0.68	0.78	1.12
X_y (m)	12.36	14.32	16.27	18.86	20.81	27.31

considerations and Table 3 suggest that Δx can range from a few centimeters to a tenth of a meter or so and Δt can range from a few minutes to an hour or so. At deeper depths but within the depth of annual temperature variations, Δx can range from a few tenths of a meter to about one meter and Δt from one day to several weeks.

B.5 SUMMARY

The purpose of this paper is to investigate numerical methods for determining the *in situ* thermal diffusivity, D , of the active layer and permafrost from a temperature time series. When the active layer and permafrost contain unfrozen water, the thermal parameters become strongly dependent upon temperature. In this case, it is shown that

$$D = \frac{T_t}{T_{xx} - RT_x^2(-T)^{B-1}} \quad (B.8)$$

where T is the temperature, T_t , T_x and T_{xx} are the numerical approximations of $\partial T/\partial t$, $\partial T/\partial x$, and $\partial^2 T/\partial x^2$, respectively, B is a constant and R is defined in the text. Application of (8) requires a knowledge of the variation of unfrozen water, θ_u , and R with temperature.

Previous investigators have used the first order numerical expression for D for the case of constant thermal parameters, termed model I, which is

$$D \cong \left(\frac{(\Delta x)^2}{2\Delta t} \right) \frac{\Delta_t T}{\Delta_{xx} T} \quad (B.12)$$

where Δx is the space step, Δt is the time step, $\Delta_t T = T_i^{j+1} - T_i^{j-1}$, $\Delta_{xx} T = T_{i-1}^j - 2T_i^j + T_{i+1}^j$, and the integers i and j reference positions and time. A second order approximation of the derivatives T_t and T_{xx} was developed using a Taylor series expansion, termed model II, which yields

$$D \cong \left(\frac{(\Delta x)^2}{\Delta t} \right) \frac{\Delta'_t T}{\Delta'_{xx} T} \quad (B.16)$$

where $\Delta'_t T = T_i^{j-2} - 8T_i^{j-1} + 8T_i^{j+1} - T_i^{j+2}$ and $\Delta'_{xx} T = -T_{i-2}^j + 16T_{i-1}^j - 30T_i^j + 16T_{i+1}^j - T_{i+2}^j$.

In addition to the obvious requirement for conductive heat flow, there are several considerations in applying (12) and (16) to determine D . The spatial separation, Δx , of the temperature measurements (sensors) and the time intervals, Δt , between measurements must be relatively small and the soil in either a frozen or thawed state. Estimates of $\Delta_t T$ and $\Delta'_t T$ are nearly independent of sensor accuracy while $\Delta_{xx} T$ and $\Delta'_{xx} T$ depend on sensor accuracy. Temperature changes at depth should be sufficient to make $\Delta_{xx} T$ and $\Delta'_{xx} T$ much greater than the errors in their determination.

The higher order approximations used for T_t and T_{xx} in model II result in smaller truncation errors which makes model II much more accurate than model I. However, there are also measurement errors associated with the temperatures, positions, and time. An error analysis shows that the measurement errors are dominated by errors in the temperature measurements. For a given level of accuracy in the temperature measurements, the measurement errors for model I are somewhat less than those for model II. The analysis also shows that the accuracy

of the temperature measurements must approach $\pm 0.01^\circ\text{C}$ to obtain reasonable estimates of D .

Additional information on the application of model I and model II was obtained by using surface temperatures consisting of a daily wave, an annual wave with a superimposed daily wave, and an annual wave with a superimposed linear trend to generate synthetic temperature time series in the ground. Calculated values of D using (12) and (16) were then compared to the input value used to calculate the synthetic temperature profiles. The percent difference between the calculated values and the input value is the error in the calculations.

For a daily wave, model I produces large spikes in the calculated values for D . These spikes occur near times where T is a maximum or a minimum and $\Delta_t T$ and $\Delta_{xx} T$ become very small. Using model II, the spikes disappear and the errors are also much smaller at other times. These improved estimates using model II are due to the reduction in truncation errors compared to model I. Round off errors do not appear to be significant for either model for the parameters used in the calculations.

For a daily wave superimposed on an annual wave, the effect of the annual wave is not significant at shallow depths (up to 0.5 m in the example calculation). At these depths, the results for D were similar to those for a daily wave only. As the amplitude of the daily wave increased, the errors in D increased and as the depth increased to 1.2 m and beyond the errors decreased. At a depth of 0.8 m, calculated values for D using model I resulted in a series of spikes near the temperature maximum and minimum and normal values elsewhere. These spikes were produced by the daily temperature variations which caused the temperature dependent quantities on the right sides of (12) and (16) to oscillate about zero for a period of time. The number of spikes, their amplitude, and duration were substantially reduced using model II. At a depth of several meters to 20 m or more, model I produced values for D which

were in error by less than 20%. However, when model II was used, the values for D were nearly identical to the input value.

An annual surface wave with a superimposed linear trend, which could be caused by climatic fluctuations, was used to show that D could be obtained at depths below those of annual variations (about 35 m for this example). The errors in values for both models I and II were less than 2% with model II being more precise.

Values for D can be obtained at any depth where measurable temperature changes occur. Short term weather patterns, the presence of a freezing or thawing front in the active layer, and longer term climatic fluctuations and trends create opportunities for determining D . Application of the method requires the acquisition of very precise temperature data (preferably $\pm 0.01^\circ\text{C}$ or better) at appropriate depth (Δz) and time (Δt) intervals. Selection of values for Δz and Δt must take into account the accuracy of the temperature measurements, duration and amplitude of the temperature changes, depth where D is to be determined, and the diffusivity of the soil. In general, $\Delta z \ll X$ (the depth of interest), $\Delta t \ll P$ (period or duration of surface temperature changes), and $\Delta_{zz}T$ and $\Delta'_{zz}T$ much greater than the errors in their determination. For the active layer, Δz can range from a few centimeters to a tenth of a meter or so and Δt from a few minutes to an hour or so. At deeper depths in the permafrost but within the depth of annual temperature variations, Δz can range from a few tenths of a meter to a meter or more and Δt from one day to several weeks. Below the depth of annual temperature variations, values for Δz of several meters and Δt of a year or more may be appropriate. The method is not limited to permafrost regions and should be applicable to any soil or rock where the heat flow is conductive.

B.6 Acknowledgements

We wish to thank Dr. Z. Kowalik for his helpful discussions. This research was funded by the National Science Foundation grant DPP 91-22928, Army Research Office grant DAAL03-89-K-0106, State of Alaska funds and by the Lanzhou Institute of Glaciology and Geocryology, Chinese Academy of Sciences, People's Republic of China.

REFERENCES

- Alaska Climate Center, News and reviews, Vol. 1 through Vol. 3, 1983 — 1985.
- Ames, W. F., Numerical methods for partial differential equations, 434 pp., Barnes and Noble, Inc., New York, 1969.
- Anderson, D. M. and N. R. Morgenstern, Physics, chemistry, and mechanics of frozen ground: A review, *Proceedings of the Second International Conference on Permafrost*, National Academy of Sciences, p. 257-288, 1973.
- Anderson, D. M., A. R. Tice and H. L. McKim, The unfrozen water and the apparent specific heat capacity of frozen soils, *Proceedings of the Second International Conference on Permafrost*, National Academy of Sciences, p. 289-294, 1973.
- Baker, D. J., The Arctic's role in climate, *Oceanus*, 29, 41-46, 1986.
- Beck, A. E., Interring past climate change from subsurface temperature profiles: some problems and methods, *Palaeogeography, Palaeoclimatology, Palaeoecology, Global and Planetary Change Section*, 98, p. 73-80, 1992.
- Benson, C. S., *The seasonal snow cover of Arctic Alaska*, Final report to The Arctic Institute of North America, p. 47, 1969.
- Benson, C. S., Reassessment of winter precipitation on Alaska's Arctic Slope and measurements on the flux of wind blown snow, *Geophysical Institute Report, Report No. UAG R-288*, Geophysical Institute, University of Alaska Fairbanks, 1982.
- Benson, C. and M. Sturm, Structure and wind transport of seasonal snow on the Arctic Slope of Alaska, *Glaciology*, in press, 1993.
- Black, R. F., Precipitation at Barrow, Alaska, greater than recorded, *Transactions, American Geophysical Union*, 35, pp. 203-206, 1954.
- Blackman, R. B. and J. W. Tukey, 1958, *The Measurements of Power Spectra*, Dover, New York, p. 190.
- Bowling, S. A., The variability of the present climate of interior Alaska, *Proceedings of a Conference on the Potential Effects of Carbon Dioxide-induced Climatic Changes in Alaska*,

- edited by J. H. McBeath, pp. 235 School of Agriculture and Land Resources Management, University of Alaska Fairbanks, 1977.
- Brooks, C. P. E., *Climate through the ages*, Second revised Edition, Dover Publications, Inc. New York, 1970.
- Brown, J. and P. V. Sellmann, Permafrost and coastal plain history of arctic Alaska, *Alaskan Arctic Tundra*, ed. by M. E. Britton, pp. 145, Arctic Institute of North America Technical Paper No. 25, p. 31-47, 1975.
- Brown, R. J. E. and W. O. Kupsch, *Permafrost terminology*, Technical Memorandum No. 111, Associate Committee on Geotechnical Research, National Research Council of Canada, 1974.
- Burg, J. P., Maximum Entropy Spectral Analysis, Paper presented at 37th Meeting, Soc. of Explor. Geophys., Oklahoma City, 1967.
- Burn, C. R. and C. A. S. Smith, Observations of the "thermal offset" in near-surface mean annual ground temperatures at several sites near Mayo, Yukon Territory, Canada, *Arctic*, 41(2), p. 99-104, 1988.
- Calkin, P. E., Holocene glaciation of Alaska (and adjoining Yukon Territory, Canada), *Quaternary Science Reviews*, 7, 159-184, 1988.
- Carnahan, B., H. A. Luther and J. O. Wilkes, *Applied numerical methods*, John and Sons, Inc. New York, 1969.
- Carslaw, H. S. and J. C. Jaeger, *Conduction of heat in solids*, second edition, Oxford University Press, Ely House, London W. 1, 1959.
- Cheng, G. D., The forming process of thick layered ground ice, *Scientia Sinica (Series B)*, 25, pp. 777-788, 1982.
- Cheng, G. D., The mechanism of repeated-segregation for the formation of thick layered ground ice, *Cold Regions Science and Technology*, 8, pp. 57-66, 1983.
- Climatological Data, Alaska, vol. 67 through 74, 1981 — 1988.
- Collett, Timothy S. and Kenneth J. Bird, Unfrozen, high-salinity intervals within ice-bearing permafrost, North Slope of Alaska, in *Proceedings of Sixth International Conference on Permafrost*, Vol. 1, Science Press, Beijing, P. R. China, 1993.

- Committee on the Role of the Polar Regions and Climatic Change (Polar Research Board), *The Polar Regions and Climatic Change*, National Academy Press, 59 pp., Washington, D. C., 1984.
- Crowley, T. J., The Geologic record of climatic change, *Reviews of Geophysics and Space Physics*, 21, 828-877, 1983.
- de Vries, D. A., Thermal properties of soils, in *Physics of Plant Environment*, edited by W. R. Van Wijk, North-Holland, pp. 5-28, Amsterdam, 1963.
- Dingman, S. L., R. G. Barry, G. Weller, C. Benson, E. F. LeDrew, and C. W. Goodwin, Climate, snow cover, microclimate, and hydrology, *An Arctic Ecosystem: The Coastal Tundra at Barrow, Alaska*, edited by J. Brown, P. C. Miller, L. L. Tieszen and F. L. Bunnell, The Institute of Ecology, 1980.
- Dutton, E. G. and D. J. Endres, Snowmelt date at Barrow, Alaska, *Alpine and Arctic Research*, 21(2), 1991.
- Ellsaesser, H. W., M. C. MacCracken, J. Walton, and S. L. Grotch, Global climatic trends as revealed by the recorded data, *J. Geophy. Res.*, 24, 745-792, 1986.
- Everett, K. R., Landforms, in *Geobotanical Atlas of the Prudhoe Bay Region, Alaska*, edited by D. A. Walker, K. R. Everett, P. J. Webber and J. Brown, CRREL Report 80-14, June 1980.
- Foster, J. L., The significance of the date of snow disappearance on the Arctic tundra as a possible indicator of climate change, *Arctic and Alpine Research*, 21, p. 60-70, 1989.
- Foster, J. L., L. W. Winchester and E. G. Dutton, The date of snow disappearance on the Arctic tundra as determined from satellite, meteorological station and radiometric in-situ observations, in *Proceedings of 1991 International Geoscience and Remote Sensing Symposium, Volume IV*, Helsinki University of Technology, Espoo, Finland, 1991.
- Gold, W. and A. H. Lachenbruch, Thermal conditions in permafrost — A review of North American literature, *Proceedings of the Second International Conference on Permafrost*, National Academy of Sciences, pp 3-26, 1973.
- Goodrich, L. E., A numerical model for assessing the influence of snow cover on the ground thermal regime, Ph.D. Thesis, McGill University, Montreal, 1976.

- Goodrich, L. E., Some results of a numerical study of ground thermal regimes, in *Proceedings of the Third International Conference on Permafrost*, vol. 1: 29-34, Ottawa, National Research Council of Canada, 1978.
- Goodrich, L. E., Efficient numerical technique for one-dimensional thermal problems with phase change, *International J. of Heat and Mass Transfer*, 21, pp. 615-621, 1982
- Goodrich, L. E., The influence of snow cover on the ground thermal regime, *Can. Geotech. J.*, 19, pp 421-432, 1982.
- Goodrich, L. E., Field measurements of soil thermal conductivity, *Canadian Geotech. J.*, 23, 51-59, 1986.
- Hall, D. K., Assessment of polar climate change using satellite technology, *Rev. Geophys.*, 26, 26-39, 1988.
- Hamilton, T. D., Alaskan temperature fluctuations and trends: an analysis of recorded data, *Arctic*, 18(2), pp.105-117, 1965.
- Hamilton, T. D., Glaciation of the Brooks Range. *Glaciation in Alaska*, edited by R. M. Thorson and T. D. Hamilton, University of Alaska Fairbanks, pp. 35-41, 1983.
- Hamilton, T. D., Correlation of quaternary glacier deposits in Alaska, *Quaternary Science Reviews*, 5, 171-180, 1986.
- Hansen, J. and S. Lebedeff, Global trends of measured surface air temperature, *J. of Geophys. Res.*, 92, D11, p. 13,345-13,372, 1987.
- Harris, S. A., Effects of climatic change on northern permafrost, *Northern Perspectives*, 15, 7-12, 1987.
- Haugen, R. K. and J. Brown, Coastal-inland distributions of summer air temperature and precipitation in northern Alaska, *Arctic and Alpine Res.*, 12(4), p. 403-412, 1980.
- Haugen, R. K., Climate of remote areas in north-central Alaska 1975-1979 summary, CRREL Report 82-35, 1982.
- Hinkel, K. M., S. I. Outkalt and F. E. Nelson, Temperature variation and apparent thermal diffusivity in the freezing active layer, Toolik Lake, Alaska, *Permafrost and Periglacial Processes*, 1, 265-274, 1990.

- Hinzman, L. D., D. L. Kane, R. E. Gieck and K. R. Everett, Hydrological and thermal properties of the active layer in the Alaskan Arctic, *Cold Regions Science and Technology*, 19, pp 95-110, 1991.
- Hoekstra, P., Delaney, A. and Atkins, R., Measuring the thermal properties of cylindrical specimens by the use of sinusoidal temperature waves, *CRREL Technical Report 244*, U. S. Army Corps of Engineers, Cold Regions Research and Engineering Laboratory, Hanover, New Hampshire, 1973.
- Hoffman, P. A. and T. E. Osterkamp, Bar graphs of climatological data for Alaskan stations: temperature, snowfall, and thawing and freezing degree days for 1949-1982, Geophysical Institute, University of Alaska Fairbanks, Interim report to Alaska Department of Transportation and Public Facilities, 1986.
- Hopkins, D. M., Thaw lakes and thaw sinks in the Imuruk Lake area, Seward Peninsula, Alaska, *Journal of Geology*, vol. 57, p. 119-131, 1949.
- Hopkins, D. M. and W. Hartz, Coastal morphology, coastal erosion, and barrier islands of the Beaufort Sea, Alaska, *U.S. Geological Survey Open File Report 78-1063.*, 1978.
- Hopkins, D. M., Glacial sequence, southwestern Seward Peninsula. *Paleoecology of Beringia*, edited by D. M. Hopkins, pp. 456, Academic Press, New York, 1983.
- Hotchkiss, W. O. and L. R. Ingersoll, Post-glacial time calculations from recent geothermal measurements in the Calumet Copper Mines, *J. Geol.*, 42, p. 113-142, 1934.
- Jaeger, J. C., Application of the theory of heat conduction to geothermal measurements, in *Terrestrial Heat Flow*, edited by W. H. K. Lee, pp. 345, Published by American Geophysical Union, 1965.
- Johnson and Hartman, Environmental atlas of Alaska, Inst. Water Res., University of Alaska Fairbanks, p. 95, 1971.
- Jones, P. D., T. M. L. Wigley and P. B. Wright, Global temperature variations between 1961 and 1984, *Nature*, 322, 430-434, 1986.
- Kane, R. P., Power spectrum analysis of solar and geophysical parameters, *J. Geomag. Geoelect.*, 29, pp 421-495, 1977.
- Kane, R. P., Maximum entropy spectral analysis of some artificial samples, *J. Geophys. Res.*, 84, pp 965-966, 1979.

- Kay, B. D., and J. B. Goit, Temperature-dependent specific heats of dry soil materials, *Can. Geotech. J.*, 12, p. 209-212, 1975.
- Kellogg, W. W., Possible effects of a global warming on Arctic sea ice, precipitation and carbon balance, in *the Potential Effects of Carbon-Dioxide-Induced Climatic Changes in Alaska*, edited by J. H. McBeath, pp. 145, School of Agriculture and Land Resources Management, University of Alaska Fairbanks, 1984.
- Kelly, P. M. and P. D. Jones, Annual temperatures in the Arctic, 1881-1981, *Climate Monitor*, 11(1), 1982.
- Kersten, M. S., Laboratory research for the determination of the thermal properties of soils, Final report, Engineering Experiment Station, University of Minnesota, June, 1949.
- Koppen, W., Das geographische System der Klimate, In *Handbuch der Klimatologie I. C.*, Eds. by W. Koppen and Geiger, pp. 44, Berlin:Borntrager, 1936.
- Koranda, J. J., The plant ecology of the Franklin Bluffs area, Alaska, Ph. D. thesis, University of Tennessee, p. 235, 1960.
- Lachenbruch, A. H., Periodic heat flow in a stratified medium with application to permafrost problems, *U. S. Geol. Surv. Bull.*, 1083-A, 1959.
- Lachenbruch, A. H., M. C. Brewer, G. W. Greene, and B. V. Marshall, Temperatures in permafrost, *Temperature — Its Measurement and Control in Science and Industry*, v. 3, pt 1: New York, Reinhold Publishing Co., p. 791-803, 1962.
- Lachenbruch, A. H., G. W. Greene, and B. V. Marshall, Permafrost and the geothermal regimes, *Environment of the Cape Thompson Region, Alaska*, Chapter 10, Washington D. C., U. S. Atomic Energy Commission, Division of Technical Information, p. 149-165, 1966.
- Lachenbruch, A. H., and B. V. Marshall, Heat flow in the Arctic, *Arctic* v. 22, p. 300-311., 1969.
- Lachenbruch, A. H., J. H. Sass, B. V. Marshall, and T. H. Moses, Permafrost, heat flow, and the geothermal regime at Prudhoe Bay, Alaska, *J. Geophys. Res.*, 87, 9301-9316, 1982.
- Lachenbruch, A. H. and B. V. Marshall, Changing climate: geothermal evidence from permafrost in the Alaskan Arctic, *Science*, 234, pp. 689-696, 1986.

- Lachenbruch, A. H., T. T. Cladouhos, and R. W. Saltus, Permafrost temperature and the changing climate, *Proceeding of the 5th International Conference on Permafrost*, Trondheim, Norway, 1988.
- Lane, A. C., Geotherms of Lake Superior Copper Country, *Bull. Geol. Soc. Am.*, 34, p. 703-720, 1923.
- Liston, G. E., Seasonal snowcover of the foothills region of Alaska's Arctic Slope: A survey of properties and progresses, M. S. thesis, Geophysical Institute, University of Alaska Fairbanks, 1986.
- Local Climatological Data, Barrow, U.S. Department of Commerce, Weather Bureau, 1921 — 1988.
- Local Climatological Data, Barter Island, U. S. Department of Commerce, Weather Bureau, 1948 — 1988.
- Lovell, C. W., Temperature effects on phase composition and strength of partially-frozen soil, *Highway Research Board Bull.* 168, p. 74-95 1957.
- Lunardini, V. J., *Heat transfer in cold climates*, Van Nostrand Reinhold Company, New York, 1981.
- Mackay, J. R. and D. K. MacKAY, Snow cover and ground temperatures, Garry Island, N. W. T., *Canadian J. of Earth Sciences*, 192, 187-296, 1975
- MacKay, J. R., Downward water movement into frozen ground, western arctic coast, Canada. *Canadian J. of Earth Sciences*, 201, 120-134, 1984.
- Maxwell, B., Atmospheric and climatic change in the Canadian Arctic — Causes, Effects, and Impacts. *Northern Perspectives*, 15, 2-6, 1987.
- Maykut, G. A. and P. E. Church, Radiation climate of Barrow, Alaska, 1962-1966, *J. of Applied Meteorology*, 12, pp. 620-628, 1973.
- McGaw, R. W., S. I. Outcalt and E. Ng, Thermal properties and regime of wet tundra soils at Barrow, Alaska, *Proceedings of the Third International Conference on Permafrost*, Ottawa: National Research Council of Canada, 1, pp 47-53, 1978.
- Nakano, Y. and J. Brown, Effect of a freezing zone of finite width on the thermal regime of soils, *Water Resources Research*, 7(5), pp. 1226-1233, 1971.

- Nakano, Y. and J. Brown, Mathematical modeling and validation of the thermal regimes in tundra soils, Barrow, Alaska, *Arctic and Alpine Research*, 4(1), pp. 19-38, 1972.
- Nassar, I. N. and Horton, R., Determination of soil apparent thermal diffusivity from multiharmonic temperature analysis for non uniform soils, *Soil Science*, 149(3), 125-130, 1990.
- National Oceanic and Atmospheric Administration, Local climatological data annual summaries, Alaska, 1951-1988.
- National Oceanic and Atmospheric Administration, Alaska Climatological Data Annual Summaries, 1920-1988.
- Nelson, F. E., S. I. Outcalt, C. W. Goodwin and K. M. Hinkel, Diurnal thermal regime in a peat-covered palsa, Toolik Lake, Alaska, *Arctic* 38(4), pp 300-315, 1985.
- Ng, E. and P. C. Miller, Validation of a model of the effect of tundra vegetation on soil temperatures, *Arctic and Alpine Research*, 9(2), pp. 89-104, 1977.
- Osterkamp, T. E. and M. W. Payne, Estimates of permafrost thickness from well logs in northern Alaska, *Cold Reg. Sci. Technol.*, 5, 13-27, 1981.
- Osterkamp, T. E., Thermal models for estimating the potential impact of a warmer climate on permafrost in Alaska, *Geophysical Institute Report, UAG R-295*, Geophysical Institute, University of Alaska Fairbanks, March, 1983a.
- Osterkamp, T. E., Response of Alaskan permafrost to climate, *Proceeding of Fourth International Conference on Permafrost*, National Academy Press, Washington, D. C., 1983b.
- Osterkamp, T. E., Potential impact of a warming climate on permafrost in Alaska, *The Proceeding of a Conference on The Potential Effects of Carbon Dioxide-induced Climatic Changes in Alaska*, edited by J. H. McBeath, School of Agriculture and Land Resources Management, University of Alaska Fairbanks, 1984a.
- Osterkamp, T. E., Temperature measurements in permafrost, *Report No. FHWA-AK-RD-85-11*, State of Alaska, Department of Transportation and Public Facilities, 1984b.
- Osterkamp, T. E., J. K. Peterson, and T. S. Collett, Permafrost thicknesses in the Oliktok Point, Prudhoe Bay and Mikkelsen Bay areas of Alaska, *Cold Reg. Sci. Technol.*, 11, 99-105, 1985.

- Osterkamp, T. E., Freezing and thawing of soils and permafrost containing unfrozen water or brine, *Water Resources Research*, 23(12), 2279-2285, 1987a.
- Osterkamp, T. E., Things are heating up in Alaska — Permafrost, *The Geophysical Institute Quarterly* 6(3), p.2-3, 1987b.
- Osterkamp, T. E. and G. G. Walker, Temperature variation of the thermal properties of ice, *Geophysical Institute Report, Report No. UAGR-309*, Geophysical Institute, University of Alaska Fairbanks, 1987.
- Osterkamp, T. E., J. P. Gosink, and K. Kawasaki, Measurements of permafrost temperatures to evaluate the consequences of recent climate warming, Final Report, *Report No. AK-RD-88-05*, State of Alaska, Department of Transportation and Public Facilities, 1987.
- Outcalt, S. I., C. Goodwin, G. Weller and J. Brown, A digital computer simulation of the annual snow and soil thermal regimes at Barrow, Alaska, *Water Resources Research*, 11, pp. 709-715, 1975.
- Outcalt, S. I. and K. M. Hinkel, Night frost modulation of the near-surface soil water ion concentration and thermal fields, *Physical Geography*, 10(4), 336-348, 1989.
- Outcalt, S. I. and K. M. Hinkel, The soil electric potential signature of summer drought, *Theoretical and Applied Climatology*, 41(1), 63-68, 1990.
- Panofsky, Hans A. and G. W. Brier, *Some applications of statistics to meteorology*, published by the Pennsylvania State University, 1968.
- Penner, E., Thermal conductivity of frozen soils, *Can. J. of Earth Sci.* 7, 982, 1970.
- Penner, E., G. H. Johnston and L. E. Goodrich, Thermal conductivity laboratory studies of some Mackenzie Highway soils, *Canadian Geotechnical J.*, 12(3), 271-288, 1975.
- Permafrost Subcommittee, *Glossary of Permafrost and Related Ground-Ice Terms*, 156 pp., National Research Council of Canada, Ottawa, Ontario, Canada, 1988.
- Persaud, N. and A. C. Chang, Computing mean apparent soil diffusivity from daily observations of soil temperature at two depths, *Soil Science*, 139(4), 297-304, 1985.
- Pewe, T. L., Quaternary Geology of Alaska, *U. S. Geological Survey Professional Paper 835*, 145 pp., 1975.

- Robock, A., Ice and snow feedbacks and the latitudinal and seasonal distribution of climate sensitivity, *J. Atmos. Sci.*, 40, 986-997, 1983.
- Smith, M. W., Microclimatic influences on ground temperatures and permafrost distribution, Mackenzie Delta, Northwest Territories, *Can. J. Earth Sci.*, 12, 1421-1438, 1975.
- Smith, M. W. and D. W. Riseborough, Permafrost sensitivity to climatic change, *Proceedings of Fourth International Conference on Permafrost*, National Academy Press, Washington, D. C., 1983.
- Soil Conservation Service, Alaska Annual Data Summary, Water Year 1991.
- Squires, G. L., *Practical physics*, third edition, 213 pp., Cambridge University Press, New York, 1985.
- Sturm, M., Natural convection in the subarctic snow cover, *J. Geophys. Res.*, 96(B7), pp. 11657-11671, 1991.
- Sturm, M., Thermal conductivity measurements of depth hoar, *J. Geophys. Res.*, 97(B2), pp. 2129-2139, 1992.
- Tice, A. R., C. M. Burrows and D. M. Anderson, Determination of unfrozen water in frozen soil by pulsed nuclear magnetic resonance. in *Proceedings of the Thirtieth International Conference on Permafrost* Edmonton, Alberta, Canada, National Research Council of Canada, vol. 1, p 149-155, 1978.
- Tice, A. R., P. B. Black and R. L. Berg, Unfrozen water contents of undisturbed and remolded Alaskan silt as determined by Nuclear Magnetic Resonance, *Cold Regions Research & Engineering Laboratory Report 88-19* US Army Corps of Engineers, 1988.
- Ulrych, T. J. and T. N. Bishop, Maximum entropy spectral analysis and auto-regressive decomposition, *Rev. Geophys. Space Phys.*, 13, pp. 183-200, 1975.
- Walker, D. A., Climate, in *Geobotanical Atlas of the Prudhoe Bay Region, Alaska*, edit by D. A. Walker, K.R. Everett, P.J. Webber and J. Brown, United States Army Corps of Engineers, Cold Regions Research and Engineering Laboratory, Hanover, New Hampshire, U. S. A., 1980.
- Walker, D. A. and P. J. Webber, Vegetation, *Geobotanical Atlas of the Prudhoe Bay Region, Alaska*, edited by D. A. Walker, K. R. Everett, P. J. Webber and J. Brown, CRREL Report 80-14, 1982.

- Washburn, A. L., *Geocryology*, John Wiley & Sons, Inc., New York, 1980.
- Weber, F. R., Glacial geology of the Yukon-Tanana Upland — A progress report. in *Glaciation in Alaska — Extended Abstracts from a Workshop*. edited by R. M. Thorson and T. D. Hamilton, pp. 96-100, Fairbanks, University of Alaska Museum Occasional Paper 2, 1983.
- Webster, M. N., Carbon dioxide and world climate, *Scientific American*, 247(2), 36-46, 1982.
- Weller, G., S. Cubley, S. Parker, D. Trabant and C. Benson, The tundra microclimate during snow-melt at Barrow, Alaska, *Arctic*, 25(4), pp. 291-300, 1972.
- Weller, G. and B. Holmgren, The microclimate of the arctic tundra, *J. of Applied Meteorology*, 13, pp. 854-862, 1974a.
- Weller, G. and B. Holmgren, Summer global radiation and albedo - data for three stations in the Arctic Basin, Ice Island T-3, Barrow, Prudhoe Bay, 1971-1973, UAG R-229, Geophysical Institute, University of Alaska Fairbanks, 1974b.
- Wendler, G., C. B. Fahl and S. Corbin, Mass balance on McCall Glacier, Brooks Range, Alaska, *Arctic and Alpine Research*, 4, p. 211-222, 1972.
- Williams, L. D. and T. M. L. Wigley, A comparison of evidence for late Holocene summer temperature variations in the northern hemisphere, *Quat. Res.*, 20, 286-307, 1983.
- Williams, P. J., experimental determination of apparent specific heats of frozen soil, *Geotechnique*, 140, 2, pp.133-142, 1964.
- Woodwell, G., The carbon dioxide problem: A scientific puzzle and political dilemma, in *the Potential Effects of Carbon-Dioxide-Induced Climate Changes in Alaska*, edited by J. H. McBeath, pp. 3-7, School of Agriculture and Land Resources Management, University of Alaska Fairbanks, 1984.
- Zhang, T., B. Tong and S. Li, Influence of snow cover on the lower limit of permafrost in the Altai Mountains, *J. of Glaciology and Geocryology*, in Chinese with English abstract, 7(1), 1985.
- Zhang, T., Thermal regime of permafrost within the depth of annual temperature variation at Prudhoe Bay, Alaska, M. S. Thesis, Geophysical Institute, University of Alaska Fairbanks, p 145, 1989.

- Zhang, T., T. E. Osterkamp and J. Gosink, A model for the thermal regime of permafrost within the depth of annual temperature variations, *Third International Symposium on Cold Regions Heat Transfer*, University of Alaska Fairbanks, Fairbanks, Alaska, June 11-14, 1991.
- Zhang, T. and T. E. Osterkamp, Changing climate and permafrost temperatures in the Alaskan Arctic, *EOS, Trans. Am. Geophys. Union*, Vol. 73, No. 25, 1992.
- Zhang, T. and T. E. Osterkamp, Climate and permafrost temperatures in Alaska north of the Brooks Range, *EOS, Trans. Am. Geophys. Union*, 1993 Spring Meeting, 1993a.
- Zhang, T. and T. E. Osterkamp, Changing climate and permafrost temperatures in the Alaskan Arctic, *Proceedings of the Sixth International Conference on Permafrost, Beijing, China*, Science Press, 1993b.
- Zhou, Y. and D. Guo, Principal characteristics of permafrost in China, *Journal of Glaciology and Cryopedology*, 4(1), pp 1-18, 1982 (in Chinese with English abstract).
- Zhou, Y. and D. Guo, Some features of permafrost in China, in *Proceedings of the Fourth International Conference on Permafrost*, National Academy Press, Washington, D.C., pp 1496-1501, 1983.